Technische Universität München

Lehrstuhl für Systembiologie der Pflanzen

The role of ESCRT-associated AMSH proteins and ALIX in intracellular trafficking in *Arabidopsis thaliana*

Kamila Kalinowska-Brandt

Vollständiger Abdruck der von der Fakultät Wissenschaftszentrum Weihenstephan für Ernährung, Landnutzung und Umwelt der Technischen Universität München zur Erlangung des akademischen Grades eines

Doktors der Naturwissenschaften

genehmigten Dissertation.

Vorsitzender:	Univ.-Prof. Dr. Ralph Hückelhoven
Prüfer der Dissertation:	1. Priv.-Doz. Dr. Erika Isono
	2. Univ.-Prof. Dr. Kay H. Schneitz
	3. apl. Prof. Dr. Ramon A. Torres Ruiz

Die Dissertation wurde am 05.10.2016 bei der Technischen Universität München eingereicht und durch die Fakultät Wissenschaftszentrum Weihenstephan für Ernährung, Landnutzung und Umwelt am 01.12.2016 angenommen.

Acknowledgements

First of all, I would like to thank my supervisor PD Dr. Erika Isono for the possibility to work on this project. I would like to express my gratitude for her contribution to my professional and personal development through teaching me laboratory methods and troubleshooting, preparation of scientific presentations, scientific writing, and for the multiple possibilities that I had during my stay under her supervision to attend highly interesting meetings and courses. Most of all, I would like to thank for her help and advice during writing of this thesis.

Importantly, I would like to express my gratitude to the head of the Chair of Plant Systems Biology, Prof. Claus Schwechheimer, for his constant support as well as his comments and ideas that helped me to pursue this project. Moreover, I would like to thank for his feedback concerning this thesis.

I would like to express my thanks to Prof. Ralph Hückelhoven and Prof. Kay Schneitz who agreed to become members of my thesis committee.

I would like to show my appreciation to my mentor Dr. Stefanie Ranf for her support, comments and ideas concerning my project. I am also thankful to Petra Wick, Rita Kaindl and Daniela Elephand-Dill for their help with administrative issues.

I would like to acknowledge our collaborators who agreed to perform experiments or shared their materials with us, especially M. Otegui, K. Goodman, C. Weis, M. Ostertag, T. Uemura, T. Ueda, A. Nakano, D. Bassham, V. Rubio and L. Cuyas.

Most of all, many thanks to my current and past lab colleagues from the Chair of Plant Systems Biology for their practical and emotional support, as well as for their friendship. I would like to especially acknowledge the fellow PhD students and PostDocs, the students I supervised and our “HiWis” who helped me either with advice or in conducting experiments for this project. This includes Maike, Karin, Franzi, Anthi, Conny, Steffi, Inês, Julia, Benny, Angela, Lilly, Stefan, Quirin, Thomas, Alex, Chris, Aline, Theresia, Tina, Lina, Theresa, Lisa, Vanessa and Bettina.

I would also like to thank the Graduate School of TUM, SFB924 and UnternehmerTUM for giving me the possibility to attend very inspiring courses, meetings and retreats that contributed to the development of my professional qualifications and experience.

Very special thanks go to my husband, my family and friends, as well as the family and friends of my husband for all the support and understanding that I received from them during the past years.

Table of contents

Abstract

Eukaryotic cells respond to external environment by interpreting signal transduction networks and adjusting their protein levels accordingly. These processes are especially evolved in plants that due to the limited ability to use movement to deal with environmental changes had to increase physiological tolerance. Protein levels in plants are controlled among others by degradation rates. This occurs through protein degradation mechanisms such as ubiquitin-proteasome system, endocytic trafficking and autophagy, which are important for plant growth, development and stress responses. These pathways mostly depend on modification of target proteins with ubiquitin, a process regulated by ubiquitinating enzymes and DUBs (deubiquitinating enzymes).

In this study, I have sought to understand the function of two MPN (Mpr1/Pad1 N-terminal)-family DUBs, AMSH1 (ASSOCIATED MOLECULE WITH THE SH3 DOMAIN OF STAM 1) and AMSH3 in *Arabidopsis thaliana*. AMSH3 was previously demonstrated to interact with ESCRT-III (endosomal sorting complex required for transport-III), a highly conserved complex involved in such processes as endocytic sorting and autophagy. Knockout *of AMSH3* causes a number of intracellular trafficking and vacuolar defects, in consequence leading to a seedling lethal phenotype. The function of AMSH1 was poorly understood before this study.

Like many DUBs, AMSH proteins show substrate specificity towards ubiquitin linkages but not towards target proteins. It is therefore essential that their subcellular localization and DUB activity are strictly controlled, which occurs through interaction with other proteins. As the regulators of AMSH function were mostly unknown, I have conducted a Y2H screen using AMSH proteins as bait and identified ALIX (ALG-2-INTERACTING PROTEIN X). ALIX is a conserved eukaryotic adaptor protein and its homologs are implicated in various cellular processes in animals and fungi, though were not yet characterized in plants.

I have shown in this study that the Arabidopsis ALIX interacts with AMSH1, AMSH3 and ESCRT-III, and that *alix* null mutants phenocopy *amsh3* in seedling lethality. Moreover, I have demonstrated that ALIX is required for the endosomal localization of AMSH3 but does not affect its DUB activity. Altogether, my results prove that ALIX function is essential for proper endocytic trafficking, autophagy and vacuole biogenesis in Arabidopsis.

Zusammenfassung

Eukaryotische Zellen reagieren auf ihre äußere Umwelt indem sie Signaltransduktionswege deuten und dementsprechend Anpassungen auf Protein-Ebene vornehmen. Diese Prozesse wurden in Pflanzen hauptsächlich entwickelt, um ihre physiologische Toleranz zu erhöhen, da sie nur eingeschränkt die Möglichkeit haben, sich durch Bewegung an Umweltveränderungen anzupassen. Das Proteinniveau in Pflanzen wird mitunter durch die Abbaurate der Proteine kontrolliert. Dies geschieht durch Proteinabbaumechanismen, wie dem Ubiquitin-Proteasomen-System, dem endozytotischen Transportweg und der Autophagie, welche alle für Pflanzenwachstum und –entwicklung essentiell sind. Diese Wege sind meistens abhängig von der Modifikation von Targetproteinen mit Ubiquitin, einem Prozess, der durch ubiquitinierende und DUBs (deubiquitinierende Enzyme) reguliert wird.

In dieser Studie war mein Ziel die Funktion zweier DUBs in *Arabidopsis thaliana* zu verstehen, AMSH1 (ASSOCIATED MOLECULE OF THE SH3 DOMAIN OF STAM 1) und AMSH3, welche zu der MPN (Mpr1/Pad1 N-terminal)-Familie gehören. Für AMSH3 wurde bereits gezeigt, dass es mit ESCRT-III (endosomal sorting complex required for transport-III) interagiert, einem hoch konservierten Komplex, der in Prozesse wie dem endozytotischen Transport und der Autophagie involviert ist. Null-Mutanten von AMSH3 zeigen eine Vielzahl von Fehlfunktionen im intrazellulären Transport und defekte Vakuolen, welche zu einem keimlingslethalen Phänotyp führen. Über die Funktion von AMSH1 war vor dieser Studie nur wenig bekannt.

Wie viele DUBs, zeigen auch AMSH Proteine Substratspezifität gegenüber Ubiquitinverbindungen, aber nicht gegenüber Targetproteinen. Es ist daher notwendig, dass ihre zelluläre Lokalisation und DUB-Aktivität streng kontrolliert werden, was durch Interaktion mit anderen Proteinen stattfindet. Da die Regulatoren der AMSH-Funktion weitgehend unbekannt waren, habe ich einen Hefe-2-Hybrid-Screen mit AMSH Proteinen als Bait durchgeführt und ALIX (ALG-2-INTERACTING PROTEIN X) als Interaktor identifiziert. ALIX ist ein konserviertes eukaryotisches Adapterprotein und seine Homologe sind involviert in diverse zelluläre Prozesse in Tieren und Pilzen, jedoch war es in Pflanzen noch nicht charakterisiert.

Ich habe in dieser Studie gezeigt, dass ALIX mit AMSH1, AMSH3 und ESCRT-III interagiert und dass *alix* Null-Mutanten einen *amsh3* ähnlichen, keimlingslethalen Phänotyp haben. Außerdem wird ALIX für die endosomale Lokalisation von AMSH3 benötigt, hat aber keinen Einfluss auf dessen DUB-Aktivität. Ich habe insgesamt in dieser Studie gezeigt, dass die ALIX Funktion essentiell für korrekten endozytotischen Transport, Autophagie und Vakuolenbiogenese ist.

Abbreviations

3-AT	3-amino-1,2,4-triazole
AAA ATPase	ATPases ASSOCIATED WITH VARIOUS CELLULAR ACTIVITIES
ALIX	ALG-2-INTERACTING PROTEIN X
AMSH	ASSOCIATED MOLECULE WITH THE SH3 DOMAIN OF STAM
AMSH-LP	AMSH-LIKE PROTEIN
AP-2	adaptor protein complex 2
ARA	ARABIDOPSIS RAB GTPase
ATG	AUTOPHAGY-RELATED GENE / AUTOPHAGY-DEFECTIVE
BCECF-AM	2′,7′-bis-(2-carboxyethyl)-5-(and-6)- carboxyfluorescein-acetoxymethyl ester
BFA	Brefeldin A
Bro1p	Bck1p-like resistance to osmotic shock 1
BROX	BRO1 DOMAIN-CONTAINING PROTEIN WITH A CAAX MOTIF
CaLB	CALCIUM-DEPENDENT LIPID BINDING FAMILY PROTEIN
CCV	clathrin-coated vesicle
CDC2	CELL DIVISION CONTROL PROTEIN 2
CFP	cyan fluorescent protein
CHC	CLATHRIN HEAVY CHAIN
CHMP	CHARGED MULTIVESICULAR BODY PROTEIN
CHX	cycloheximide
CLC	CLATHRIN LIGHT CHAIN
Col-0	Columbia-0
Doa4p	Degradation of alpha2 4
DUB	deubiquitinase
E-64d	2S,3S-trans-(ethoxycarbonyloxirane-2-carbonyl)-L-leucine-(3-methylbutyl) amide
EE	early endosomes
EGFR	EGF receptor
EML2	EMSY-LIKE 2
ER	endoplasmic reticulum
ESCRT	endosomal sorting complex required for transport
EXO70E2	EXOCYST COMPONENT OF 70 kDa E2
FIP1	FH1-INTERACTING PROTEIN 1 / VirF-INTERACTING PROTEIN 1

FYVE1	Fab1, YOTB, Vac1, EEA1 1
GAD	GAL4 activation domain
GBD	GAL4 DNA-binding domain
GFP	green fluorescent protein
GTPase	guanosine triphosphate hydrolase
GST	glutathione S-transferase
HD-PTP	HIS-DOMAIN-CONTAINING PROTEIN TYROSINE PHOSPHATASE
ILV	intraluminal vesicle
K63	lysine 63 of ubiquitin
kDa	kilodaltons
LE	late endosome
L*er*	Landsberg *erecta*
MBP	maltose-binding protein
MDC	monodansylcadaverine
MIM	MIT-interacting motif
MIT	microtubule-interacting and trafficking
mKO	monomeric Kusabira Orange
MPN	Mpr1/Pad1 N-terminal
MVB	multivesicular body
NBR1	NEIGHBOR OF BRCA1 GENE 1
ORF	open reading frame
PI3PK	PHOSPHATIDYLINOSITOL 3-PHOSPHATE-KINASE
PM	plasma membrane
PRD	proline-rich domain
PUB	PLANT U-BOX
PVC	prevacuolar compartment
RAB	Ras-related proteins in brain
RFP	red fluorescent protein
Rim20p	Regulator of IME2 20
RING	really interesting new gene
SH3	Src-homology 3
SKD1	SUPPRESSOR OF K^+ TRANSPORT GROWTH DEFECT 1
SNARE	SNAP receptor
SNF7	SUGAR NON-FERMENTING 7
STAM	STAM SIGNAL TRANSDUCING ADAPTOR MOLECULE
STAMBP	STAM-BINDING PROTEIN

SYP	SYNTAXIN OF PLANTS
TGN	*trans*-Golgi network
TOL	TOM1-LIKE
TSG101	TUMOR SUSCEBILITY GENE 101
Ub	ubiquitin
UBPY	UBIQUITIN ISOPEPTIDASE Y
UBQ10	UBQUITIN 10
UPS	ubiquitin-proteasome system
USP8	UBIQUITIN-SPECIFIC PROTEASE 8
VPS	VACUOLAR PROTEIN SORTING
WM	Wortmannin
WT	wild type
XBAT35	XB3 ORTHOLOG 5 IN ARABIDOPSIS THALIANA
YFP	yellow fluorescent protein
Y2H	yeast two-hybrid

1. Introduction

1.1. Selective protein degradation

Plants cannot use behavior and movement to the same extend as animals to deal with environmental changes or stress, since their sensory and locomotion capacities are less developed. They had to evolve the ability to adapt to and take advantage of changes in climate and environment by adjusting key steps in their growth and development like germination or flowering. The tremendous physiological tolerance and phenotypic plasticity of plants is achieved by complex signaling networks that are triggered at the PM (plasma membrane) through various cell-surface receptors. Beside the signaling receptors, PM-localized channels, transporters, lipids and other key molecules can be used by plant cells to sense external stimuli. Another function of plant cell-surface receptors is to establish communication between cells. In order to coordinate growth and development at the tissue and organ level, plants secrete extracellular signaling molecules to transfer information between cells. The internal and external signals are interpreted via different signal transduction pathways, through which the abundance of various proteins is adjusted. This occurs via different mechanisms that involve changes both in transcription and translation, as well as in protein degradation rates. Many key regulatory proteins have short half-lives and their rapid turnover is important for an immediate answer to specific internal or external stimuli (Vierstra, 2003; Liu et al., 2012a).

Cellular proteins can be degraded through several mechanisms, which are important for plant survival under both advantageous and disadvantageous growth conditions. Membrane-bound proteins such as activated cell-surface receptors can be removed through endocytic degradation, which serves, among others, for signal attenuation in many signal transduction pathways. Downstream of PM receptors, cytosolic and nuclear proteins can be degraded by the UPS (ubiquitin-proteasome system). When plants are subjected to stress, misfolded proteins accumulate to form aggregates that can be efficiently removed through autophagy, ERAD (endoplasmic reticulum-associated protein degradation) or UPS (Figure 1) (Vierstra, 2003; Meusser et al., 2005; Liu et al., 2012a). It is therefore essential to elucidate the molecular mechanisms guaranteeing precise and timely protein degradation in order to understand how plants survive both in favorable and unfavorable growth conditions.

1.1.1. The ubiquitin-proteasome system

Plants put a special emphasis on UPS. In the genome of a model plant thale cress (*Arabidopsis thaliana*), up to 5% of loci are related to this system, which is twice as much as

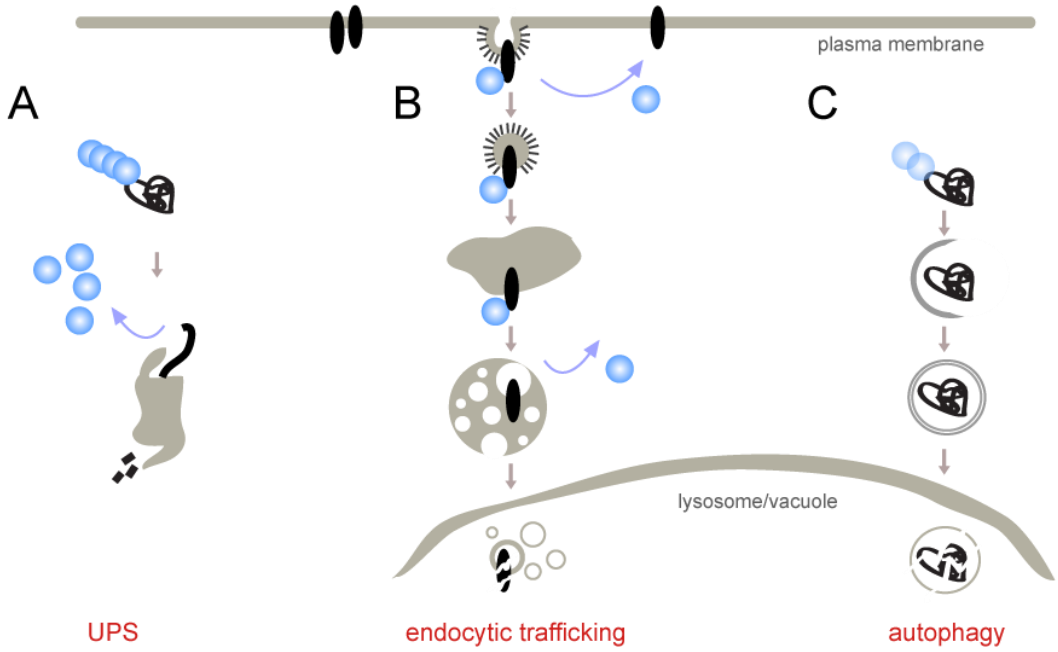

Figure 1. Selective protein degradation pathways.
Three major protein degradation pathways were described in eukaryotes: UPS (ubiquitin-proteasome system), endocytic trafficking and autophagy.
(**A**) In UPS, cytosolic proteins or protein aggregates are modified with ubiquitin. Ubiquitin is recognized and removed by subunits of the regulatory particle of the 26S proteasome. Proteins are unfolded and degraded in the catalytic subunit of the proteasome.
(**B**) In endocytic trafficking, plasma membrane proteins can be ubiquitinated, which could trigger their internalization. Cargo proteins are delivered to the lysosome or vacuole through endosomal compartments. During the final stages, cargo-containing endosomes fuse with the lytic compartment and their content is degraded.
(**C**) In autophagy, protein aggregates or damaged organelles are engulfed within forming autophagosomes and delivered to the lysosome or vacuole. In selective autophagy, the ubiquitinated cargo is recognized by ubiquitin-dependent autophagy receptors. In bulk autophagy, the cargo is enclosed unspecifically within the forming autophagosome.

in animals, yeast or flies (Vierstra, 2003, 2009). The UPS is a selective degradation pathway of cytosolic and nuclear proteins and it also plays a housekeeping role in rapid elimination of misfolded proteins. It is estimated that approximately 10% of total proteins in eukaryotic cells are regulated by this system (Ciechanover, 1998; Hershko and Ciechanover, 1998; Kraft et al., 2010). For the degradation in the 26S proteasome, proteins are marked by the covalent attachment of a small 8.5 kDa (kilodaltons) protein, called ubiquitin (Cook et al., 1994; Beal et al., 1996; Xu et al., 2009). Modified target proteins are recognized and degraded by the 26S proteasome in an ATP-dependent manner (Figure 1A) (Vierstra, 2003; Smalle and Vierstra, 2004).

The disruption of proteasomal function in plants causes lethality during embryogenesis, underlining the essentiality of the UPS already in early stages of growth and development (Brukhin et al., 2005; Book et al., 2009; Gallois et al., 2009; Wang et al., 2009b; Hayashi and Hirayama, 2016). Mutations affecting proteasomal activity were also shown to

block various biological processes such as cell division, hormonal signaling, circadian rhythms, floral development, photomorphogenesis, trichome differentiation, senescence and pathogen responses (Vierstra, 2003; Smalle and Vierstra, 2004; Kraft et al., 2010; Jang et al., 2015; Pogany et al., 2015; Yu et al., 2015).

1.1.2. Endocytic degradation

Endocytic protein degradation plays a crucial role in plant growth and development. Many key processes such as embryo- and tissue differentiation, floral organ development, gravitropism, guard cell movements, metal ion homeostasis, hormone transport and pathogen responses were shown to depend on functional endocytic trafficking (Geldner et al., 2003; Shen et al., 2003; Shope et al., 2003; Silady et al., 2004; Abas et al., 2006; Robatzek et al., 2006; Jaillais et al., 2007; Sutter et al., 2007; Tamura et al., 2007; Tian et al., 2007; Barberon et al., 2011; Tsuchiya and Eulgem, 2011; Kim et al., 2013b; Barberon et al., 2014; Barbosa et al., 2014).

In contrast to UPS that targets mainly cytosolic and nuclear proteins, endocytic cargo consists mostly of integral membrane proteins. As the cells need to constantly adjust their PM composition in response to changing external conditions, proteins located in the plasma membrane are continuously internalized by endocytosis. This is followed either by recycling back to the PM or sorting for endocytic degradation in vacuoles (Figure 1B) (Reyes et al., 2011; Paez Valencia et al., 2016). These processes depend on clathrin, a protein that plays a major role in the formation of coated vesicles. In clathrin-mediated endocytosis, PM proteins are usually ubiquitinated and concentrated in a patch at the plasma membrane prior to their internalization. The endocytic cargo is recognized by AP-2 (adaptor protein complex 2) or other adaptors and accessory proteins that recruit clathrin monomers from the cytosol. Clathrin assembles around the concentrated cargo into triskelia composed of three CHC (CLATHRIN HEAVY CHAIN) and three CLC (CLATHRIN LIGHT CHAIN) molecules and causes the local deformation of the membrane to a pit. The nascent vesicle containing cargo proteins is released from the PM through membrane scission, aided by dynamin and dynamin-interacting proteins. Once the CCV (clathrin-coated vesicle) detaches from the PM, the clathrin starts to disassemble. The uncoating of the vesicle is essential for its fusions with other endosomal compartments (Grabbe et al., 2011; Paez Valencia et al., 2016).

Prior to the delivery to the vacuole for degradation, the cargo is transported through different endosomal compartments. In the final steps of vacuolar trafficking, endosomes fuse to vacuoles assisted by SNAREs (SNAP receptors) and small GTPases (guanosine triphosphate hydrolases). To be able to be degraded in the vacuole, the endocytic cargo needs

to localize not to the limiting membrane of the endosome but to the membranes of ILVs (intraluminal vesicles) carried within it. Compartments that contain ILVs are called MVBs (multivesicular bodies). Upon MVB fusion with the lytic compartment, the limiting membrane fuses with the tonoplast, and the cargo-containing ILVs are released in the vacuolar lumen and degraded by hydrolases.

Yeast and animal endosomes are generally classified based on their main functions into early-, recycling-, intermediate- and late endosomes. The typical mammalian tubule-vesicular EEs (early endosomes) receive recently endocytosed material from the PM, the recycling endosomes recycle endocytosed membrane proteins back to the PM and LEs (late endosomes) sort endocytic cargo into ILVs to form MVBs (Gruenberg and Stenmark, 2004; Otegui and Spitzer, 2008; Reyes et al., 2011). In plants, only two clearly separate endosomal organelles were identified and characterized to date, namely the EE/TGN (*trans*-Golgi network) compartment and LEs (late endosomes)/MVBs/PVCs (prevacuolar compartments) (Otegui and Spitzer, 2008; Reyes et al., 2011). The plant EE/TGN is considered an important hub for both biosynthetic and endocytic pathways. As the typical EEs are not detectable in plants, it is assumed that the EE/TGN receives the endocytosed cargos from PM. On the other hand, similar to the yeast and mammalian TGN, it is also a sorting station for biosynthetic cargo coming from the Golgi apparatus (Reyes et al., 2011; Paez Valencia et al., 2016). Plant late endosomes were shown to be involved in the trafficking not only from PM-, but also from Golgi to the vacuole. MVBs develop in Arabidopsis embryos from Golgi-derived vesicles and carry both vacuolar storage proteins and the proteases that process them. Storage proteins such as 2S albumin can be processed already in MVBs before they reach the vacuole, which shows that plant LEs have more functions than being only passive transporters (Otegui et al., 2006; Otegui and Spitzer, 2008; Gao et al., 2014; Kolb et al., 2015; Teh et al., 2015; Wu et al., 2016). The delivery of the cargo through endosomal compartments to the lysosome/vacuole is supported by the highly conserved multiprotein complexes called the ESCRT (endosomal sorting complex required for transport) machinery (Figure 2) (Winter and Hauser, 2006; Grabbe et al., 2011; Paez Valencia et al., 2016).

1.1.2.1. The ESCRT machinery

ESCRTs are responsible for managing the directional flow and spatial sorting of ubiquitinated cargo along the endocytic route and have been extensively characterized in different eukaryotic kingdoms. ESCRTs are essential in plants and mutations that disrupt the function of core components cause lethality already during embryogenesis or shortly after germination (Haas et al., 2007; Katsiarimpa et al., 2011; Katsiarimpa et al., 2013; Gao et al., 2014). The

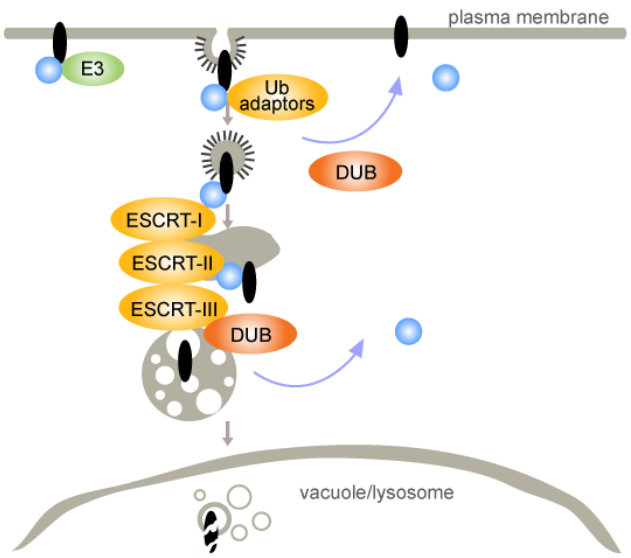

Figure 2. Functions of the ESCRT machinery in endocytic trafficking.
Ubiquitinated plasma membrane proteins can be recognized by Ub (ubiquitin) adaptors or ESCRT-0 and internalized. The cargo is delivered through endosomal compartments to the vacuole or lysososme for degradation, assisted by various adaptor proteins, among others by the ESCRT machinery. If the cargo is deubiquitinated by a DUB (deubiuitinating enzyme) early after internalization, it can be recycled back to the plasma membrane. If not, ESCRT-0/Ub adaptors recruit ESCRT-I to early endosomes. ESCRT-I initiates assembly of ESCRT-II and both complexes are believed to cause invagination of the endosomal membrane. ESCRT-III assembles on the limiting membrane of the endosome, which promotes membrane scission and sorting of the endocytic cargo into the intraluminal vesicles. The late endosome fuses with the vacuole or lysosome and the content is degraded by resident hydrolazes.

animal and yeast ESCRT machinery consists of four complexes, ESCRT-0, -I, -II and –III, while plants lack homologs of ESCRT-0 components (Winter and Hauser, 2006; Grabbe et al., 2011).

ESCRT-0 physically captures and concentrates ubiquitinated cargo at the endosomal membrane. In humans, it consists of HRS (HEPATOCYTE GROWTH FACTOR-REGULATED TYROSINE KINASE SUBSTRATE) and STAM (SIGNAL-TRANSDUCING ADAPTOR MOLECULE), and in yeast of Vps27p (vacuolar protein sorting 27) and Hse1p (has symptoms of class-E mutants 1 or HBP, STAM, EAST 1). Both of the ESCRT-0 components contain an N-terminal VHS (Vps27p, HRS, STAM)-domain that mediates membrane binding. In addition, Vps27p/HRS carries a PI3P (phosphatidylinositol 3-phosphate)-binding FYVE (Fab1p, YOTB, Vac1p, EEA1)-domain that facilitates its association with lipid membranes. ESCRT-0 interacts with ubiquitinated cargo through UIM (ubiquitin-interacting motifs) within Vps27p/HRS and Hse1p/STAM. On top of that, ESCRT-0 can bind to ESCRT-I and clathrin, which contributes to its localization to CCVs (Winter and Hauser, 2006; Grabbe et al., 2011; Pashkova et al., 2013). There are several other ubiquitin binding proteins that function in parallel to ESCRT-0, such as the yeast Tom1p (target of Myb1):Tollip (Toll-interacting protein) complex, GGA3 (Golgi-associated, gamma adaptin ear-containing, ARF-binding protein 3) and Bro1p (Bck1p-like resistance to osmotic shock 1). These ubiquitin adaptor proteins were demonstrated to be able to bind to clathrin and ESCRT-I (Puertollano and Bonifacino, 2004; Puertollano, 2005; Blanc et al., 2009; Pashkova et al., 2013). GGA3s are not conserved in plants, but nine TOL (TOM1-LIKE) proteins were identified that act as ubiquitin adaptors in Arabidopsis (Korbei et al., 2013).

ESCRT-0 and other ubiquitin adaptors contribute to the assembly of ESCRT-I and ESCRT-II. The majority of ESCRT-I is distributed in the cytoplasm as a stable complex that is recruited to endosomes through its interaction with ESCRT-0 and ubiquitin adaptors. Arabidopsis contains three ESCRT-I subunits, each of which is represented by two isoforms: VPS23A/ELCH and VPS23B, VPS28.1 and VPS28.2, VPS37.1 and VPS37.2 (Paez Valencia et al., 2016). VPS23 is a ubiquitin-binding protein that probably interacts with the endocytic cargo (Spitzer et al., 2006; Winter and Hauser, 2006; Paez Valencia et al., 2016). VPS23A/ELCH was also suggested to play role in cytokinesis, especially during trichome morphogenesis (Spitzer et al., 2006).

ESCRT-I recruits ESCRT-II to endosomes. The presence of ESCRT-I and –II induces invagination of the limiting membrane towards the endosomal lumen, which later contributes to the sorting of endocytic cargo into ILVs. ESCRT-II consists of three subunits, VPS22, VPS25 and VPS36. VPS36 contains the GLUE (GRAM-like ubiquitin-binding in Eap45) domain that allows for simultaneous interactions with PI3P-containing membranes, ubiquitin, and ESCRT-I. VPS25 binds to the ESCRT-III subunit VPS20 and thus is responsible for recruitment of ESCRT-III to endosomes (Winter and Hauser, 2006; Grabbe et al., 2011; Richardson et al., 2011; Shahriari et al., 2011; Paez Valencia et al., 2016).

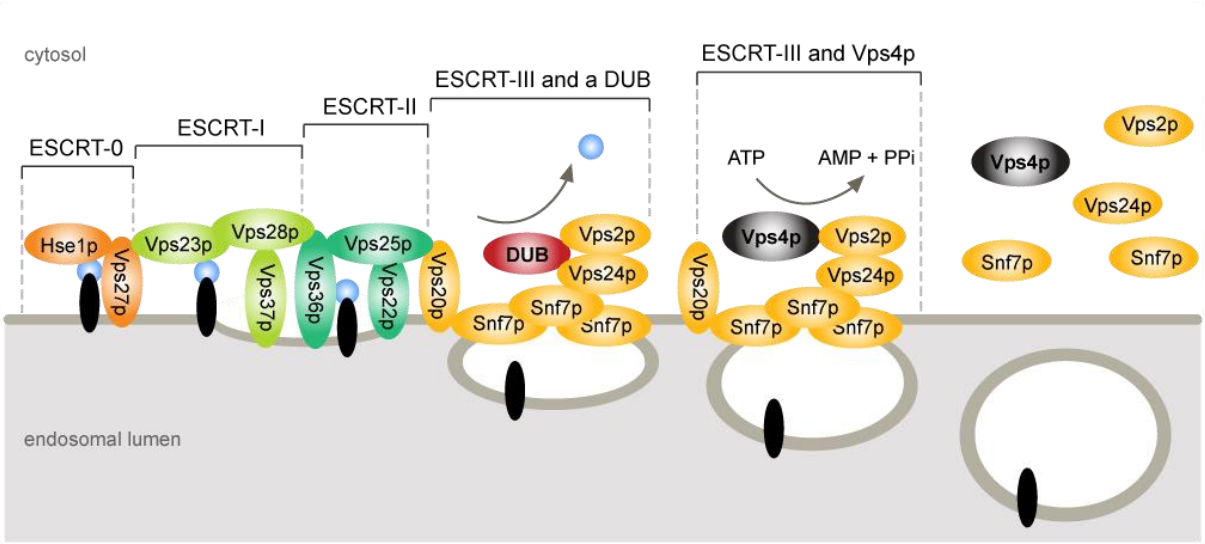

Figure 3. Assembly of ESCRT complexes on endosomal membranes.
In budding yeast, ubiquitinated endocytic cargo is recognized by ESCRT-0. Vps27p recruits ESCRT-I through binding to Vps23p, and ESCRT-I recruits ESCRT-II through interaction with Vps36p. The components of ESCRT-I and -II, Vps37p, Vps36p and Vps22p, bind to the endosomal membrane and cause its invagination. Vps25p recruits the ESCRT-III component Vps20p. Snf7p oligomerizes on the neck of the membrane invagination. Vps24p and Vps2p cap Snf7p filaments and recruit DUBs (deubiquitinating enzymes) that deubiquitinate the cargo. Subsequenty, the AAA ATPase Vps4p binds to Vps2p and catalyzes disassembly of ESCRT-III in an ATP-dependent manner. The disassembly of ESCRT-III completes the membrane scission of the forming ILV (intraluminal vesicle). Cargo is now on the membrane of the ILV inside of the endosome, ready for the fusion with the vacuole.

ESCRT-III is essential for membrane scission during sorting of the endocytic cargo into ILVs. The core ESCRT-III consists of four small highly charged proteins: Vps20p/CHMP6 (CHARGED MULTIVESICULAR BODY PROTEIN 6), Snf7p (sucrose non-fermenting 7)/Vps32p/CHMP4, Vps24p/CHMP3 and Vps2p/CHMP2 (Winter and Hauser, 2006). Although the budding yeast genome codes only for one isoform of each subunit, higher organisms contain several homologs. Arabidopsis encodes two isoforms for Vps20p/CHMP6, called VPS20.1 and VPS20.2, two for Snf7p/CHMP4, called SNF7.1 and SNF7.2, two for Vps24p/CHMP3, called VPS24.1 and VPS24.2, and three for Vps2p/CHMP2, called VPS2.1, VPS2.2 and VPS2.3. Not all isoforms were proven to function in endocytic trafficking and it is expected that different versions of ESCRT-III might have various functions in plants. Moreover, next to the core components, the plant ESCRT-III contains also accessory subunits, such as VPS60 and VPS46/CHMP1 that were shown to affects its function (Muziol et al., 2006; Spitzer et al., 2006; Winter and Hauser, 2006; Katsiarimpa et al., 2011; Richardson et al., 2011; Richardson and Mullen, 2011; Shahriari et al., 2011; Kojima et al., 2016).

All ESCRT-III components share a core domain that facilitates membrane-binding and filament formation, and a C-terminal tail. The C-terminal tail can be either in an open- or closed autoinhibitory state when it is folded back on the core domain. The ESCRT-III subunits exist mainly in the cytosol in an inactive monomeric form and polymerize into oligomeric filaments on endosomal membranes upon activation. This requires a series of conformational changes that relieve autoinhibition, stabilize their membrane association and enable interaction with other molecules by exposing the C-terminal MIM1/2 (MIT-interacting motif 1/2) that can be bound by the accessory proteins. The ordered assembly of ESCRT-III was described in detail in budding yeast. The yeast Vps20p associates with endosomal membranes thorough its myristoylated N-terminus (Teis et al., 2010; Schmidt and Teis, 2012). This triggers the stepwise homo-oligomerization of Snf7p that forms long spiral filamentous polymers around the neck of the curved membrane. These filaments are capped by binding of the Vps24p to the last Snf7p molecule. At the end, Vps24p recruits Vps2p, which completes the complex assembly. While the precise stoichiometry of ESCRT-III has not been determined, the homo-oligomer of Snf7p appears to be its major component (Teis et al., 2010; Schmidt and Teis, 2012; Kojima et al., 2016; Paez Valencia et al., 2016).

The disassembly of ESCRT-III is essential for the completion of the membrane scission and the formation of ILVs. This is catalyzed by the AAA ATPase Vps4p/SKD1 (SUPPRESSOR OF K^+ TRANSPORT GROWTH DEFECT 1). Vps4p/SKD1 is dispersed in the cytosol as monomers in the absence of ATP, while in the presence of ATP it assembles into ring-shaped multimers and in this form can be recruited to ESCRT-III. Vps4p/SKD1 interacts through its N-terminal MIT (microtubule-interacting and trafficking) domain with the MIMs of ESCRT-III

components. After the ESCRT-III disassembly, the sorting of the endocytic cargo into ILVs is completed and the MVB can fuse with the vacuole (Figure 3) (Buono et al., 2016; Kojima et al., 2016; Paez Valencia et al., 2016). A homolog of SKD1 was also isolated in Arabidopsis and implicated in the MVB function, the maintenance of the central vacuole, and indirectly in cell-cycle regulation (Haas et al., 2007; Shahriari et al., 2010).The function of the ESCRT machinery is multilayered and it was shown to be important for not only endocytic degradation but also autophagy.

1.1.3. Autophagic pathway

Autophagy is another mechanism through which proteins can be degraded in eukaryotic cells (Figure 1C). In contrast to UPS and endocytic degradation, the Arabidopsis autophagy-deficient mutants usually lack a major developmental phenotype, suggesting that this pathway does not play crucial housekeeping roles during plant life cycle. However, autophagy becomes essential for the survival of plants under unfavorable growth conditions. Upon nutrient starvation, autophagy-deficient mutants of Arabidopsis show premature leaf senescence and chlorosis, and usually do not survive unless the growth conditions improve (Doelling et al., 2002; Hanaoka et al., 2002). Autophagy is also crucial for plant tolerance to environmental stresses by significantly contributing to the removal of oxidized proteins, protein aggregates and damaged organelles (Bassham, 2009).

Despite the lack of essential roles, autophagy received a great interest from plant biologist due to its impact on the quality and quantity of yield, as well as on plant defense against pathogens. For example, autophagy contributes to the degradation of the leaf starch independently of the classical chloroplast pathway (Wang and Liu, 2013; Wang et al., 2013). Maize (*Zea mays*) autophagy mutants show seedling growth arrest and later enhanced leaf senescence in nitrogen deficiency conditions. This has a severe impact on maize productivity under suboptimal field conditions (Li et al., 2015).

Autophagy can be selective or non-selective. In selective autophagy, protein aggregates, damaged organelles or pathogenic bacteria are modified with ubiquitin. This modification is recognized by specific ubiquitin-dependent autophagy receptors (Figure 4B). Two of them, NBR1 (NEIGHBOR OF BRCA1 GENE 1) and p62 were identified and extensively characterized in humans (Kraft et al., 2010). Plants have only a homolog of NBR1 that was implicated in clearance of peroxisomes through so-called pexophagy, and in consequence in tolerance to abiotic stresses (Svenning et al., 2011; Deosaran et al., 2013; Kim et al., 2013a; Zhou et al., 2013). Selective autophagy specifically targets certain subcellular compartments and proteins, and can regulate cellular processes during both

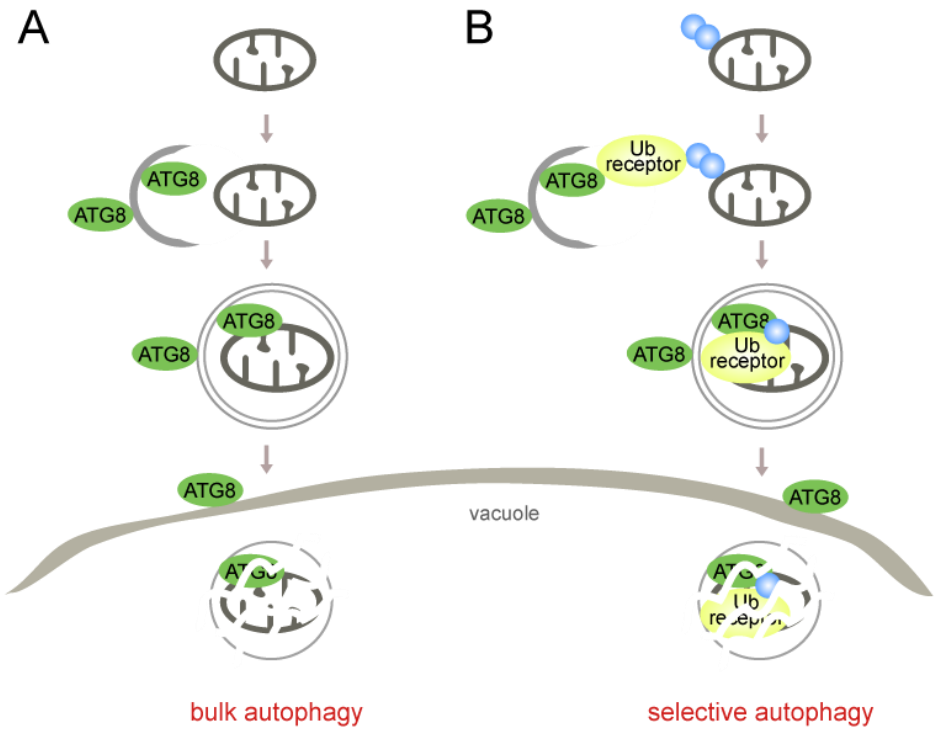

Figure 4. Bulk and selective autophagy.
Two major autophagy pathways function in plant cells, namely bulk autophagy, called also macrophagy, and selective autophagy.
(**A**) In bulk autophagy, damaged organelles or protein aggregates are unspecifically engulfed within the forming vesicle. This vesicle is called autophagosome and is characterized by the presence of a double membrane and the ubiquitin-like modifier, ATG8 (AUTOPHAGY-RELATED GENE 8), associated with the membrane. Upon fusion of the autophagosome with the vacuole, the single-membraned autophagic body is degraded by resident proteases.
(**B**) In selective autophagy, protein aggregates or damaged organelles are modified with ubiquitin. This modification is recognized by autophagy-specific Ub (ubiquitin) receptors, in example NBR1. Through the interacion of the Ub receptors with ubiquitin and with ATG8, the cargo is engulfed within the forming autophagosome. Upon its fusion with the vacuole the content of the autophagosome is degraded. The Ub receptors are also degraded in this process.

severe and favorable growth conditions. Selective autophagy is involved among others in clearance of plastids (Spitzer et al., 2015; Xie et al., 2015), clearance of peroxisomes (Deosaran et al., 2013; Kim et al., 2013a), removal of mitochondria through mitophagy (Li et al., 2014), removal of ER (endoplasmic reticulum) membranes during ER stress (Liu et al., 2012b), degradation of mature ribosomes upon starvation conditions (Kraft et al., 2008) and finally in defense against pathogenic bacteria (Thurston et al., 2009). Even inactive 26S proteasomes are removed in a mechanism called proteaphagy, pointing to a functional link between these two protein degradation pathways (Bartel, 2015; Marshall and Vierstra, 2015).

Bulk autophagy, called also macroautophagy, differs from UPS, endocytic trafficking or selective autophagy in that sense that no modification of target proteins is required. Any part of the cytosol, including organelles or proteins, can be engulfed and delivered for

degradation to the vacuole (Figure 4A) (Bassham, 2009; Michaeli et al., 2016). Bulk autophagy functions at a basal level under normal growth conditions and can be accelerated during senescence or nutrient starvation (Bassham, 2009). In bulk autophagy, *de novo* formation of the vesicle called autophagosome occurs without recognition or interaction with the degradation cargo. At the beginning, the local membranes at the outer face of the cortical ER form a cup-shape called the early phagophore. The phagophore membranes expand and fuse enclosing material for degradation within, causing formation of a double-membraned autophagosome that will be delivered to the vacuole. Upon fusion with the tonoplast, the remaining single-membraned autophagic body is released in the vacuolar lumen and degraded. The breakdown products are probably exported afterwards from the vacuole to cytoplasm for re-use (Le Bars et al., 2014b; Le Bars et al., 2014a).

A number of genes essential for autophagy have been initially identified in yeast through *atg* (*autophagy-defective*) mutant screens (Tsukada and Ohsumi, 1993; Thumm et al., 1994; Harding et al., 1995). Major components are also conserved in plants, including the two ATG conjugation systems (Bassham, 2009). Evidence accumulates that next to the classical autophagy machinery, also compartments and proteins involved in endocytic degradation are essential for the proper autophagic degradation (Rusten et al., 2007; Petiot et al., 2008; Petiot and Sadoul, 2009; Katsiarimpa et al., 2013; Kulich et al., 2013; Jacomin et al., 2015). The interplay between both pathways and the function of the common players are of the high interest.

1.1.4. The role of ubiquitin

All major protein degradation pathways depend, at least partially, on modification of target proteins with ubiquitin. Ubiquitin is a small 76-amino acid polypeptide with a molecular weight of around 8.5 kDa (Figure 5A). It was first discovered over 40 years ago as a posttranslational modifier of proteins that is highly conserved among eukaryotes (Kerscher et al., 2006; Komander, 2009). Ubiquitin can be attached to target proteins through the isopeptide bond between the C-terminal G (glycine) of the ubiquitin molecule and a K (lysine) residue on the surface of the target protein (Figure 5B). It can also form chains through the isopeptide bond between the C-terminal glycine residue of the first ubiquitin molecule and one of seven lysine residues (K6, K11, K27, K29, K33, K48 and K63) of the second ubiquitin molecule (Figure 5A and C). Depending on the internal residue used for the conjugation, the polymers are called for example K6-linked polyubiquitin chains. Additionally, the bond can be formed between the carboxy- and amino-termini of two ubiquitin molecules to generate linear chains. All forms of ubiquitin linkages were identified in eukaryotes, including mixed, forked and branched chains

(Komander et al., 2009; Grabbe et al., 2011; McDowell and Philpott, 2016; Yau and Rape, 2016).

Different types of ubiquitination can affect the modified proteins in various ways. Many proteins functioning as receptors in signaling pathways, as well as histones and other DNA-associated proteins, were shown to be modified by monoubiquitination, which in turn can affect downstream processes such as transcriptional regulation and DNA repair (Figure 5D). Also protein multi-monoubiquitination, or the attachment of monoubiquitin to more than one lysine residue, can have non-proteolytic functions (Figure 5D). Multi-monoubiquitination can cause internalization of certain plasma membrane receptors and was thus implicated in regulating signal transduction pathways and endocytic trafficking (Terrell et al., 1998; Hicke, 2001; Komander et al., 2009; McDowell and Philpott, 2016).

The attachment of ubiquitin chains is called polyubiquitination (Figure 5D). Different forms of polyubiquitin chains were implicated in various cellular processes and new functions are being constantly discovered. In example, attachment of K11- or K48-linked ubiquitin chains leads to protein degradation by the 26S proteasome. K63 linkages were shown to function in

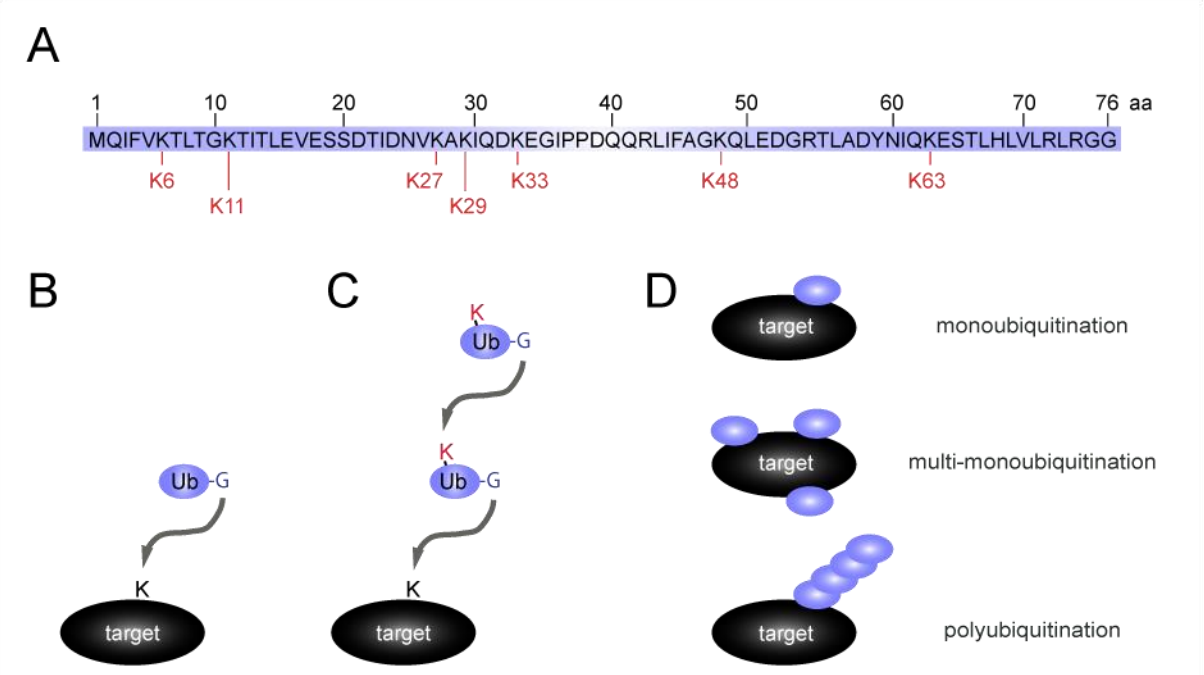

Figure 5. The complexity of ubiquitin modifications.
(**A**) Ubiquitn is a small 76-amino acid molecule. Characteristic for ubiquitin is the presence of seven K (lysine) residues within its sequence. aa: amino acids.
(**B**) Ub (ubiquitin) is attached to the target protein through the isopeptide bond between the carboxy-terminal G (glycine) of the ubiquitin molecule and a K (lysine) residue on the surface of the target protein.
(**C**) Ubiquitin can form chains by an isopeptide bond between the carboxy-terminal G of one Ub and one of seven K residues of another Ub molecule.
(**D**) Target proteins can be modified with one Ub molecule (monoubiquitination), multiple monoubiq-uitins (multi-monoubiquitination) or polyubiqutin chains (polyubiquitination).

receptor endocytosis, and together with K6 also in DNA repair, whereas K29-linked polyubiquitin functions in ubiquitin fusion degradation. In general, different polyubiquitin chains were found to play roles in signal transduction, stress responses, regulation of metabolic processes, regulation of cell cycle, endocytic trafficking, transcriptional regulation and ribosomal function (Galan and Haguenauer-Tsapis, 1997; Hofmann and Pickart, 1999; Deng et al., 2000; Spence et al., 2000; Komander, 2009; Xu et al., 2009; McDowell and Philpott, 2016; Yau and Rape, 2016). Finally, ubiquitin itself can be posttranslationally modified by phosphorylation, acetylation or attachment of ubiquitin-like modifiers such as SUMO (SMALL UBIQUITIN-LIKE MODIFIER) or NEDD8 (NEURAL PRECURSOR CELL EXPRESSED, DEVELOPMENTALLY DOWN-REGULATED 8), further increasing the complexity of the ubiquitin system (Swatek and Komander, 2016; Yau and Rape, 2016).

1.1.4.1. The function of ubiquitinating enzymes

The ubiquitination reaction is catalyzed by a three-step enzyme cascade of ubiquitin-activating- (E1), ubiquitin-conjugating- (E2) and ubiquitin-ligating (E3) enzymes (Komander, 2009). In the first ATP-dependent step, the E1 forms a high energy thioester bond with the C-terminus of ubiquitin. In the next step, activated ubiquitin is transferred to the E2 where it is attached to the catalytic cysteine residue of the E2 via a thioester linkage. Some E2s can directly ubiquitinate substrate proteins but usually a third enzyme, the E3 ligase that recognizes target proteins, is necessary (Pickart, 2001; Komander, 2009) (Figure 6). Three different types of E3 ligases, RING (really interesting new gene), U-box (ubiquitin-box) and HECT (homologous with E6-associated protein C-terminus), act as adaptors that bind both the target protein and the charged conjugating E2 enzyme, and thus facilitate formation of the isopeptide bond (Komander, 2009). Certain E3 ligases also possess elongating activities that support generation of polyubiquitin chains. In some cases, however, efficient polyubiquitination requires additional conjugation factors, called E4s (Koegl et al., 1999; Hoppe, 2005; Grabbe et al., 2011). In Arabidopsis, one E1, 37 E2s and over 1,500 E3 ligases were identified *in silico* (Smalle and Vierstra, 2004; Vierstra, 2012). The large number and diversity of E3 ligases gives specificity to the ubiquitination pathway, as the E3s are responsible for the recognition and recruitment of the target proteins for ubiquitination. The level of specificity is further increased by the E2-E3 combinations, allowing for catalytic attachment of different types of ubiquitin conjugates to a large variety of target proteins (Stone et al., 2005; Mazzucotelli et al., 2006; Komander, 2009).

The ubiquitinating enzymes play key roles in endocytic degradation, since the ubiquitination of PM proteins can trigger their endocytosis (Marmor and Yarden, 2004; Urbe,

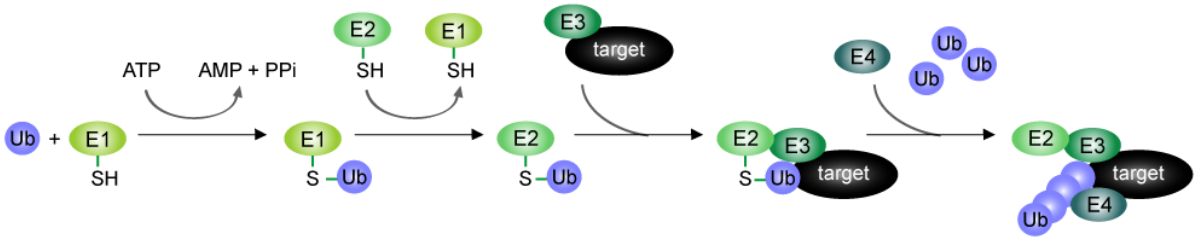

Figure 6. The ubiquitination reaction.
Attachement of Ub (ubiquitin) occurs in a multistep reaction via an enzymatic cascade. In the first step, the ubiquitin-activating enzyme (E1) binds Ub and ATP, catalyzing acyl-adenylation of the carboxy terminus of the ubiquitin molecule. This reaction forms a high energy thioester bond between ubiquitin and the enzyme. In the next step, activated ubiquitin is transferred onto the ubiquitin-conjugating enzyme (E2). The ubiquitin ligase (E3) recognizes the target and facilitates formation of the isopeptide bond between the Ub molecule and the target protein. Elongation of ubiquitin chains requires in some cases additional conjugation factors called E4s.

2005). Numerous plant E3 ligases were reported to function in signaling pathways controlling plant immunity and stress responses (Kirsch et al., 2001; Heise et al., 2002; Kawasaki et al., 2005; Gonzalez-Lamothe et al., 2006; Lee et al., 2009; Lu et al., 2011; Kobayashi et al., 2012). In example, the Arabidopsis FLS2 (FLAGELLIN-SENSING 2), a pattern-recognition receptor that senses bacterial flagellin and mediates plant immune response, was demonstrated to be regulated by ubiquitination (Lu et al., 2011; Robatzek and Wirthmueller, 2013). It was suggested that upon flagellin binding, two closely related U-box E3 ligases PUB12 (PLANT U-BOX 12) and PUB13 are recruited to the FLS2 receptor complex with BAK1 (BRI1-ASSOCIATED RECEPTOR KINASE 1). BAK1 phosphorylates PUB12 and PUB13 that in turn ubiquitinate FLS2. The ubiquitination of FLS2 results in its internalization and degradation in the vacuole, leading to attenuation of immune signaling (Lu et al., 2011). IDF1 (IRT1 DEGRADATION FACTOR 1), another RING E3 ligase, was shown to contribute to iron homeostasis in Arabidopsis by ubiquitinating the ferrous iron transporter IRT1 (IRON-REGULATED TRANSPORTER 1) (Shin et al., 2013). These examples underline the importance of ubiquitination during plant growth and during response to environmental stresses.

1.1.4.2. The function of deubiquitinating enzymes

Enzymes opposing the activity of ubiquitin E3 ligases are called DUBs (deubiquitinating enzymes, deubiquitylating enzymes or deubiquitinases) (Figure 7). Though over 1,500 E3 ligases are predicted in Arabidopsis, only around 50 DUBs were suggested to be encoded by its genome (Smalle and Vierstra, 2004; Vierstra, 2012). The speculated reason for this tremendous difference is the fact that DUBs usually target only ubiquitin linkages, while the E3 ligases show specificity towards target proteins. Moreover, in most of the cases the

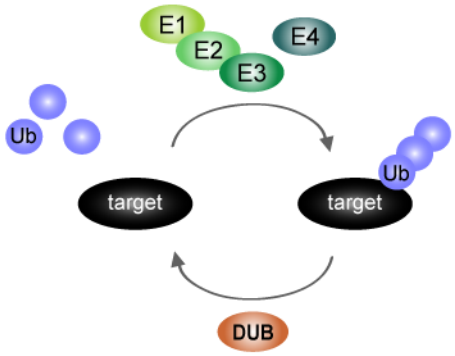

Figure 7. DUBs oppose the activity of ubiquitin ligases.
The ubiquitination occurs via an enzymatic cascade of ubiqutin-activating (E1), ubiqutin-conjugating (E2), ubiquitin-ligating (E3) and sometimes also E4s. Ub (ubiqutin) is removed from target proteins by the activity of DUBs (deubiquitinating enzymes).

interaction of deubiquitinases with their target proteins is mediated by adaptor proteins. In consequence, each DUB can deubiquitinate more than one target protein, which makes it challenging to find proteins deubiquitinated by particular DUBs (Kraft et al., 2005; Stone et al., 2005; Vierstra, 2012; Isono and Nagel, 2014).

In eukaryotes, DUBs are subdivided into five major families based on the differences in catalytic domains. These families include UCHs (ubiquitin C-terminal hydrolases), UBP/USPs (ubiquitin-specific proteases), OTUs (ovarian tumor proteases), Josephins and MPN (Mpr1/Pad1 N-terminal)-family proteins, called also JAMMs (JAB1/MPN/Mov34). With the exception of the MPN domain-containing DUBs that are metalloproteases, most DUBs are cysteine proteases (Komander et al., 2009; Isono and Nagel, 2014).

The MPN proteases contain two zinc ions coordinated within the catalytic domain that activate a water molecule to attack the ubiquitin isopeptide bond. Two DUBs from this family are found in association with large protein complexes. RPN11 is a subunit of the 26S proteasome that deubiquitinates proteins before degradation in order to recycle ubiquitin (Glickman et al., 1998; Verma et al., 2002; Book et al., 2010). Two CSN5 (COP-9 SIGNALOSOME SUBUNIT 5) homologs in Arabidopsis, CSN5A and CSN5B, are the catalytic component of the COP9 (CONSTITUTIVE PHOTOMORPHOGENESIS 9) signalosome. They were shown to specifically remove the ubiquitin-like modifier NEDD8 (Chamovitz et al., 1996; Cope et al., 2002; Cope and Deshaies, 2003). In contrast to RPN11 and CSN5, another MPN-family DUB, AMSH (ASSOCIATED MOLECULE WITH THE SH3 DOMAIN OF STAM)/STAMBP (STAM-BINDING PROTEIN), only transiently associates with the multisubunit complex ESCRT-III and can be active also as a monomer (Agromayor and Martin-Serrano, 2006; Ma et al., 2007; Isono et al., 2010; Katsiarimpa et al., 2011; Solomons et al., 2011).

DUBs display several general functions. One of them is generation of free ubiquitin. Ubiquitin can be transcribed as a linear fusion of multiple ubiquitin molecules and the DUB activity is essential for processing of these fusion genes. Secondly, DUBs can edit the form of

ubiquitin modifications by trimming ubiquitin chains, which can affect the localization or activity of target proteins. In addition to that, the removal of ubiquitin chains from modified proteins can rescue them from degradation. In this way, DUBs can reverse the ubiquitin signaling. DUBs also contribute to ubiquitin homeostasis through recycling ubiquitin prior to degradation of modified proteins (Komander et al., 2009; Grabbe et al., 2011; Isono and Nagel, 2014). Several DUBs were demonstrated to be important in endocytic trafficking, though identification of their target proteins is more challenging than in case of E3 ligases. Deubiquitination thus can affect the fate of endocytosed cargo that can be either recycled back to the PM or degraded in the vacuole.

Two mammalian DUBs, a UBP/USP family cysteine protease UBPY (UBIQUITIN ISOPEPTIDASE Y)/USP8 (UBIQUITIN-SPECIFIC PROTEASE 8) and an MPN-family metalloprotease AMSH/STAMBP were shown to associate with both ESCRT-0 and ESCRT-III, and function in endocytic cargo sorting (Grabbe et al., 2011; Wright et al., 2011). Both DUBs contain a non-canonical SBM (STAM-binding motif) and can regulate the degradation of a model mammalian endocytic substrate EGFR (EGF receptor) (Nakamura et al., 2006). UBPY/USP8 associates with ESCRT-0 through two interactions: a direct binding to the SH3 domain of STAM and an interaction with a BRO1 domain-containing adaptor protein HD-PTP

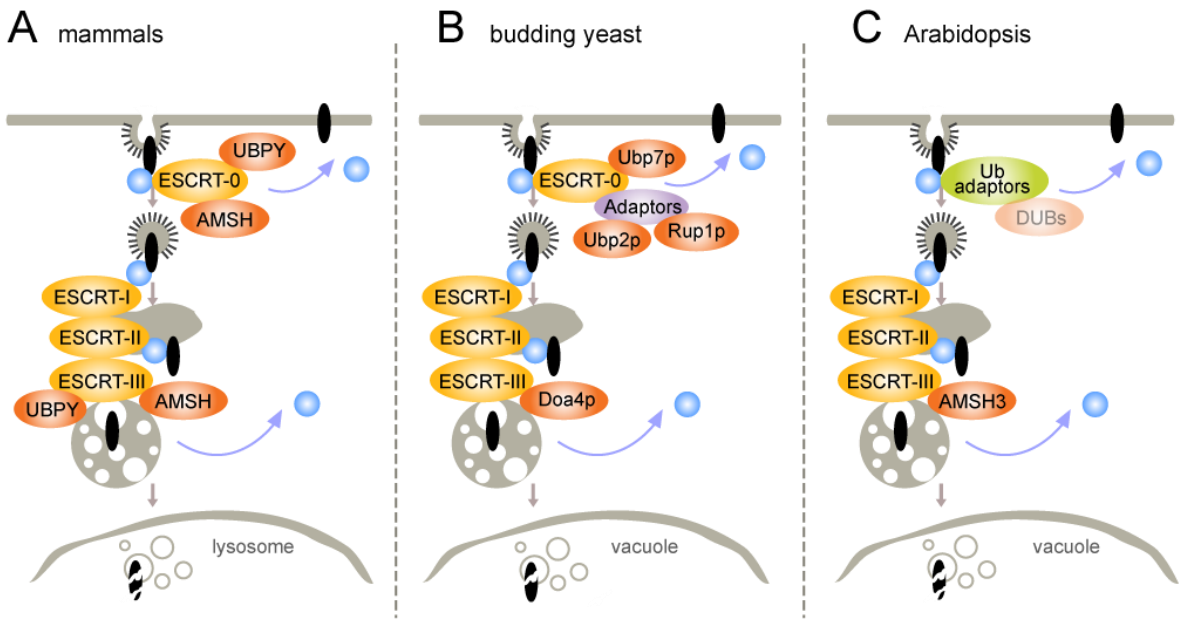

Figure 8. DUBs involved in endocytic trafficking in mammals, budding yeast and Arabidopsis.
(**A**) In mammals, two unrelated DUBs (deubiqutinating enzymes), AMSH/STAMBP and UBPY/USP8, were shown to interact with ESCRT-0 and ESCRT-III, and to regulate ubiquitination status of the endocytic cargo. (**B**) In yeast, DUBs such as Ubp7p, Ubp2p and Rup1p were found to associate directly or indirectly with ESCRT-0, and to affect the ubiquitination status of the cargo. Doa4p is a DUB associated with ESCRT-III that is essential for recycling of Ub (ubiquitin) before sorting of the endocytic cargo into ILVs (intraluminal vesicles). (**C**) Arabidopsis has no obvious homologs of ESCRT-0 and probably other Ub adaptors took over its function. Also the DUBs involved in early stages of endocytic trafficking remain to be discovered. AMSH3 was identified as an ESCRT-III-associated DUB where it probably deubiquitinates the cargo prior to its soring into ILVs.

(HIS-DOMAIN-CONTAINING PROTEIN TYROSINE PHOSPHATASE) (Figure 8A) (Kato et al., 2000; Ali et al., 2013). UBPY/USP8 shows DUB activity towards K48- and K63-linked polyubiquitin chains and monoubiquitin, and its activity is enhanced upon binding to STAM (Kato et al., 2000; McCullough et al., 2004; Row et al., 2006; Row et al., 2007). The N-terminus of UBPY/USP8 contains a MIT domain that binds to the MIM2 of the core ESCRT-III component CHMP4B (Ali et al., 2013). UBPY/USP8 can also interact with the accessory proteins of ESCRT-III, CHMP1B and CHMP7, the latter being important for recruitment of UBPY/USP8 to MVBs (Figure 8A) (Row et al., 2007). In addition to deubiquitinating endocytic cargo, USPY/USP8 is also implicated in removal of ubiquitin from STAM and the adaptor protein EPS15 (EGF RECEPTOR SUBSTRATE 15) (Mizuno et al., 2006; Row et al., 2006; Niendorf et al., 2007; Wright et al., 2011), showing that an ESCRT-associated DUB can control fates of both endocytic cargo and proteins regulating cargo sorting.

The homolog of UBPY/USP8 in budding yeast, Doa4p (degradation of alpha2 4)/Ubp4p (ubiquitin-specific protease 4), does not bind to ESCRT-0, but was shown to associate with ESCRT-III both directly through its interaction with Vps20p and through an adaptor protein Bro1p (Luhtala and Odorizzi, 2004; Richter et al., 2013). Doa4p functions in removal of ubiquitin from cargo prior to its delivery into ILVs and its activity was shown to be essential in sustaining the ubiquitin homeostasis in yeast cells (Amerik et al., 2000; Piper and Katzmann, 2007). Other UBP/USP-family DUBs in budding yeast, Ubp7p, Ubp2p and Rup1p (Rsp5-Ubp2-interacting protein 1) were also implicated in endocytic trafficking. Ubp7p interacts with the ESCRT-0 component Hse1p. It counteracts the Hse1p-interacting E3 ligase Rsp5p and deubiquitinates the endocytic cargo (Ren et al., 2007). Ubp2p and Rup1p were shown to associate with ESCRT-0 through interaction with adaptor proteins and Rsp5p (Figure 8B) (Kee et al., 2005; Ren et al., 2007). In plants, no ortholog of Doa4p/UBPY/USP8 was isolated (Bachmair et al., 2001). *In silico* analysis revealed, however, that the Arabidopsis genome encodes three orthologs of *AMSH/STAMBP*, called *AMSH1, AMSH2* and *AMSH3*. Among three homologs, AMSH3 was demonstrated to be involved in endocytic trafficking in Arabidopsis (Figure 8C) (Isono et al., 2010; Katsiarimpa et al., 2011; Katsiarimpa et al., 2014).

1.2. The roles of AMSH/STAMBP homologs

Multicellular organisms encode several *AMSH* paralogs: the human genome codes for two *AMSH* homologs, *AMSH/STAMBP* and *AMSH-LP (AMSH-LIKE PROTEIN),* and the genomes of higher plants for three (Tanaka et al., 1999; Kikuchi et al., 2003; Isono et al., 2010; Katsiarimpa et al., 2013). AMSH/STAMBP was identified as an interactor of STAM and shown to play a critical role in the cytokine-mediated intracellular signal transduction (Tanaka et al.,

1999). It possesses specificity in hydrolase activity towards K63-linked polyubiquitin (McCullough et al., 2004) and the loss of *AMSH/STAMBP* influences the protein stability of EGFR and other cell surface receptors involved in various essential signaling pathways (McCullough et al., 2004; Herrera-Vigenor et al., 2006; Ma et al., 2007; Reyes-Ibarra et al., 2007; Hasdemir et al., 2009; Hislop et al., 2009; Sierra et al., 2010; Meijer et al., 2012).

AMSH/STAMBP associates with the SH3 domain of the ESCRT-0 subunit STAM through its SBM (Figure 9A) (Sierra et al., 2010). Similarly to another ESCRT-0-associated deubiquitinase, UBPY/USP8, AMSH/STAMBP DUB activity is accelerated upon binding to STAM (McCullough et al., 2006; Sierra et al., 2010). It was shown to localize to early endosomes and CCVs through the interaction with clathrin while the binding to STAM does not influence its localization (Nakamura et al., 2006). AMSH/STAMBP associates with the ESCRT-III component CHMP3/VPS24 through its N-terminal MIT domain, which was shown to be important for recruitment of AMSH/STAMBP to LEs (Solomons et al., 2011). AMSH/STAMBP can also bind to MIM of other ESCRT components, such as the ESCRT-III core subunit CHMP2A/VPS2A and the accessory proteins CHMP1A and CHMP1B (Agromayor and Martin-Serrano, 2006; Solomons et al., 2011).

AMSH-LP shows 54% amino acid sequence identity to AMSH/STAMBP. It contains neither the MIT domain nor the functional STAM-binding motif, and was shown to lack the ability to interact with the ESCRT machinery (Figure 9A). Similar to AMSH/STAMBP, AMSH-LP can cleave K63-linked polyubiquitin and interact with clathrin, though its cellular roles still

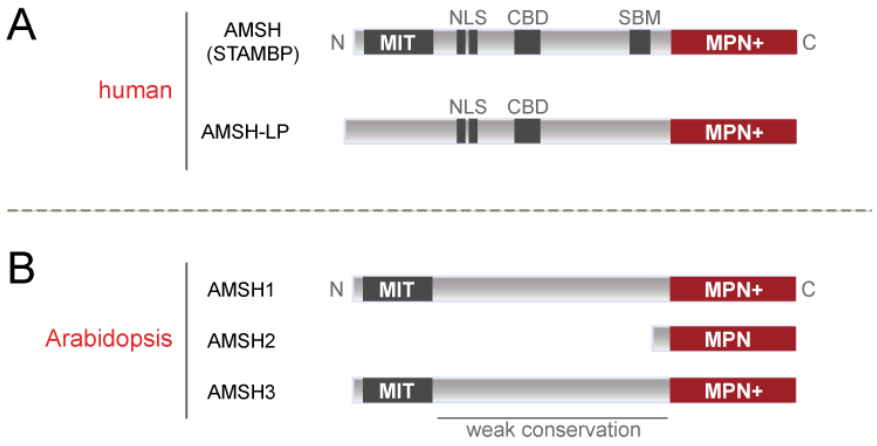

Figure 9. AMSH homologs in humans and Arabidopsis.
(**A**) Humans have two AMSH homologs: AMSH/STAMBP and AMSH-LP. Both proteins contain C (carboxy)-terminal catalytic MPN domain, bipartite NLS (nuclear localization signal) and the CBD (clathrin-binding motif). In addition to that, AMSH/STAMBP, but not AMSH-LP, contains the N (amino)-terminal MIT (microtubule interacting and trafficking) domain for ESCRT-III binding and the SBM (STAM-binding motif) for association with ESCRT-0.
(**B**) The Arabidopsis genome encodes three *AMSH* paralogs: *AMSH1, AMSH2* and *AMSH3*. All AMSH proteins contain the C-terminal catalytic domain. In addition, AMSH1 and AMSH3 have the N-terminal MIT domain that serves for interaction with ESCRT-III. Other motifs present in human AMSH/STAMBP are not conserved in Arabidopsis homologs.

remain to be discovered (Nakamura et al., 2006; Sato et al., 2008). AMSH-LP is expected to have partially different functions than AMSH/STAMBP, as both proteins cannot complement for the loss of each other (Kikuchi et al., 2003; Agromayor and Martin-Serrano, 2006; Clague and Urbe, 2006; Davies et al., 2011; Davies et al., 2013).

Mutations of AMSH/STAMBP affecting its DUB activity or interaction with ESCRT components were shown to cause neurodegenerative diseases, in example MIC-CAP (microcephaly-capillary malformation syndrome) that is associated with severe microcephaly, growth retardation, progressive neuronal loss and vascular malfunction (Carter et al., 1993; McDonell et al., 2013; Pavlovic et al., 2014; Faqeih et al., 2015).

The Arabidopsis genome codes for three *AMSH* homologs, namely *AMSH1*, *AMSH2* and *AMSH3* (Figure 9B). Plants depleted of *AMSH3* are seedling lethal and are defective in multiple trafficking pathways, such as Golgi-to-vacuole- and PM-to-vacuole routes, as well as in autophagic degradation (Isono et al., 2010; Katsiarimpa et al., 2014). In contrast, the anterograde ER-to-Golgi transport and the proteasomal degradation are not affected, suggesting that AMSH3 does not play role in these processes. Moreover, *amsh3* knockout mutants are defective in biogenesis of the central vacuole indicating a close relationship of the intracellular membrane transport pathways and organelle formation (Isono et al., 2010).

AMSH3 is an active DUB that interacts with ESCRT-III core subunits VPS2.1 and VPS24.1, homologs of the mammalian CHMP2 and CHMP3, respectively (Figure 10). The

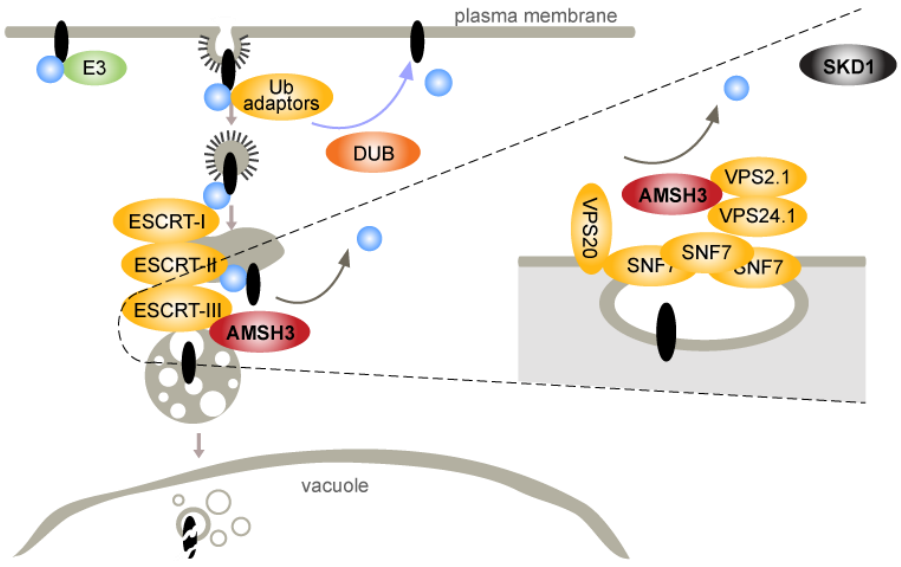

Figure 10. The Arabidopsis AMSH3 interacts with ESCRT-III.
The Arabidopsis AMSH/STAMBP homolog, AMSH3, directly binds through its N (amino)-terminal MIT (microtubule interacting and trafficking) domain to the C (carboxy)-terminal MIM1 (MIT-interacting motif 1) of two core ESCRT-III components, VPS24.1 (VACUOLAR PROTEIN SORTING 24.1) and VPS2.1. The probable function of AMSH3 is to deubiquitinate endocytic cargo before its sorting to the intraluminal vesicles of late endosomes.

association with ESCRT-III is important for AMSH3 function *in planta*, as the AMSH3 variant without the ESCRT-III-interacting MIT domain fails to complement the mutant phenotype (Isono et al., 2010; Katsiarimpa et al., 2011; Katsiarimpa et al., 2014). The probable role of AMSH3 is to deubiquitinate the endocytic cargos before the sorting into ILVs. However, the free ubiquitin is not depleted in *amsh3* knockout mutants suggesting it is not essential for sustaining ubiquitin homeostasis in plants (Isono et al., 2010). Interestingly, AMSH3 DUB activity is required for proper ESCRT-III localization, since the overexpression of its inactive version, AMSH3(AXA), leads to the formation of aberrant cellular compartments containing ESCRT-III components. In addition to that, AMSH3 competes with the ESCRT-III-disassembling factor, the AAA ATPase SKD1, for binding to VPS2.1, suggesting a role of AMSH3 in regulation of ESCRT-III dynamics (Katsiarimpa et al., 2011).

Recently, a homolog of AMSH1 was isolated in *Lotus japonicas. Lj*AMSH1 was demonstrated to be essential for the proper infection and nodule organogenesis during plant infection with rhizobial bacteria (Malolepszy et al., 2015). These findings suggest the role of deubiquitination and properly functioning endocytic trafficking in plant symbiosis with rhizobium and point to a broad physiological role of the AMSH-dependent membrane trafficking routes in plants.

1.3. Aims and objectives of this project

Selective protein degradation through the intracellular trafficking pathway is important for plant growth and development in all environmental conditions. Despite its key role in processes that impact various aspects in plant physiology including yield and yield quality in crop plants, the exact regulation of these processes is still poorly understood. The characterization of these molecular mechanisms is therefore of highest interest in plant biology.

My project aimed at the elucidation of the molecular functions of the MPN-family deubiquitinases AMSH1 and AMSH3 in the model plant *Arabidopsis thaliana*. AMSH homologs can be active as monomers and their subcellular localization is probably controlled through the interaction with other proteins. AMSH-interacting proteins could recruit the DUBs to various subcellular compartments or influence their protease activity. Despite intensive research, the identity of the proteins affecting AMSH function and the mechanisms behind AMSH regulation were mostly unknown before this study.

In order to identify AMSH-interacting proteins in *Arabidopsis thaliana*, I conducted a high-throughput Y2H (yeast-two-hybrid) screen using AMSH as bait. The molecular function of the isolated binding partner(s) together with AMSH proteins was investigated in detail by

applying genetic-, molecular-, biochemical- and cell biological methods. I aimed especially at elucidating the role of AMSH proteins and their newly identified interactor(s) in ubiquitin-dependent selective protein degradation pathways, and the importance of these processes in plant physiology

2. Results

2.1. AMSH1 is an ESCRT-III-associated DUB

Among three homologs of AMSH/STAMBP in Arabidopsis, AMSH1 and AMSH3 carry both the MPN- and MIT domains, whereas AMSH2 consists almost exclusively of the MPN domain (Figure 11A). AMSH3 was previously demonstrated to be an active DUB that is important for the proper intracellular trafficking. In order to examine whether AMSH1 have similar cellular functions to AMSH3, the deubiquitinase activity of AMSH1 was analyzed. Due to challenges in purification of the good quality recombinant full-length AMSH1, a deletion fragment containing the catalytic MPN domain was used for *in vitro* reactions (Figure 11B). K63-, but

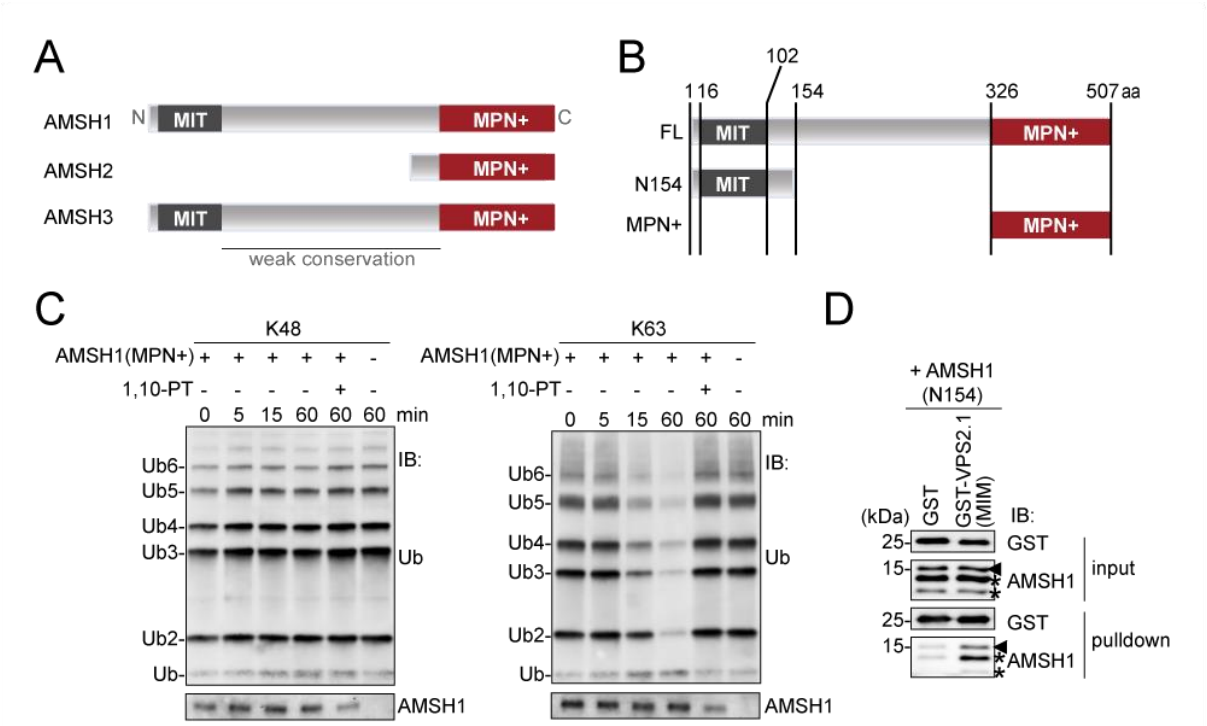

Figure 11. AMSH1 is an ESCRT-III-associated DUB.
(**A**) Scheme of domain organization of Arabidopsis AMSH proteins. N: amino-terminus; C: carboxy-terminus; MIT: MIT domain; MPN+: MPN+ domain.
(**B**) AMSH1 constructs used for experiments shown in **C** and **D**. FL: full-length; MIT: MIT domain; MPN+: MPN+ domain, N154: an N-terminal 154 aa-long fragment; aa: amino acids.
(**C**) DUB assay using K48- and K63-linked polyubiquitin chains. The recombinant MPN+ domain of AMSH1 was incubated with substrates in the presence or absence of the metalloprotease inhibitor 1,10-PT (1,10-phenanthroline). The reactions were terminated at the indicated time points, and the hydrolysis of ubiquitin chains was detected by immunoblotting with an anti-Ub antibody. An anti-AMSH1 immunoblot was conducted to verify the amount of AMSH1 (MPN+) in each reaction.
(**D**) *In vitro* binding assay of AMSH1 and VPS2.1. The fragment containing the MIT domain of AMSH1, N154, was incubated for 45 min either with GST (negative control) or with GST-VPS2.1(MIM). After the GST-pulldown, bead-bound proteins were analyzed by immunoblotting using anti-AMSH1 and anti-GST antibodies. Black arrowheads indicate the positions of AMSH1(N154) and asterisks indicate degradation products. MIM: MIT-interacting motif; N154: the N-terminal 154 aa-long fragment of AMSH1 containing the MIT domain.

not K48-linked polyubiquitin chains were cleaved in the presence of the MPN+ domain of AMSH1 (Figure 11C), indicating that AMSH1 is an active DUB and its domain alone possesses specificity towards K63-linked substrates. Moreover, the activity of AMSH1(MPN+) was inhibited by the metalloprotease inhibitor 1,10-PT (1,10-phenanthroline) (Figure 11C), supporting that similar to other members of the MPN-family, AMSH1 DUB activity also depends on metal ions coordinated within its catalytic domain.

AMSH3 was previously shown to interact through the MIT domain directly with the MIM of two core ESCRT-III subunits, VPS2.1 and VPS24.1 (Katsiarimpa et al., 2011; Katsiarimpa et al., 2014). As AMSH1 also carries an N-terminal MIT domain, a systematic Y2H analysis was previously conducted to test whether it binds to the ESCRT machinery. The analysis revealed that the full-length AMSH1 interacts with one of ESCRT-III subunits, VPS2.1 (Katsiarimpa et al., 2011; Katsiarimpa et al., 2013) (Figure 11A and B). To confirm whether the expected domains mediate the binding between AMSH1 and VPS2.1, a GST-pulldown assay was conducted. The recombinant N-terminal fragment of AMSH1 containing the MIT domain, N154 (Figure 11B), was incubated with GST (negative control) or with GST-tagged MIM of VPS2.1. AMSH1(N154) bound to GST-VPS2.1(MIM) but not to GST (Figure 11D), indicating that similarly to AMSH3, AMSH1 associates with ESCRT-III through its interaction with the MIM of VPS2.1. Altogether, the results suggest that AMSH1 might play similar roles to AMSH3, as it also associates with ESCRT-III and can cleave polyubiquitin chains.

2.2. *amsh1-1* mutant shows defects in autophagic degradation

amsh3 knockout mutants were previously shown to be seedling lethal and have a number of defects in intracellular trafficking (Isono et al., 2010). To better understand the functions of AMSH1 in Arabidopsis, the available T-DNA insertion line (CSHL ET8678; Landsberg *erecta* ecotype) was analyzed. *amsh1-1* was found to be a knock-down mutant that shows no phenotype when grown under normal conditions, suggesting that AMSH1 is either not essential in Arabidopsis or the low protein amounts are sufficient for its function (Katsiarimpa et al., 2013). To test whether the wild-type levels of AMSH1 are important, plants were placed for 5 days in the dark to induce nutrient-deficient conditions. Interestingly, *amsh1-1* knock-down mutants showed stronger leaf chlorosis than the WT (wild-type) plants (Katsiarimpa et al., 2013). Such hypersensitivity to the dark treatment was previously described for a number of autophagy mutants, which have deficiencies in nutrient recycling (Hofius et al., 2009).

To verify whether *amsh1-1* mutant is defective in autophagic degradation, levels of the autophagy-specific marker ATG8 (AUTOPHAGY-RELATED GENE 8) were tested. One of the cell biological methods to measure the rates of autophagic degradation is to analyze the

autophagic body aggregates within the vacuole (Contento et al., 2005). Under the normal conditions, ATG8-positive double-membraned autophagosomes fuse with the vacuole and their content is degraded by vacuolar proteases (Figure 12A). However, upon application of

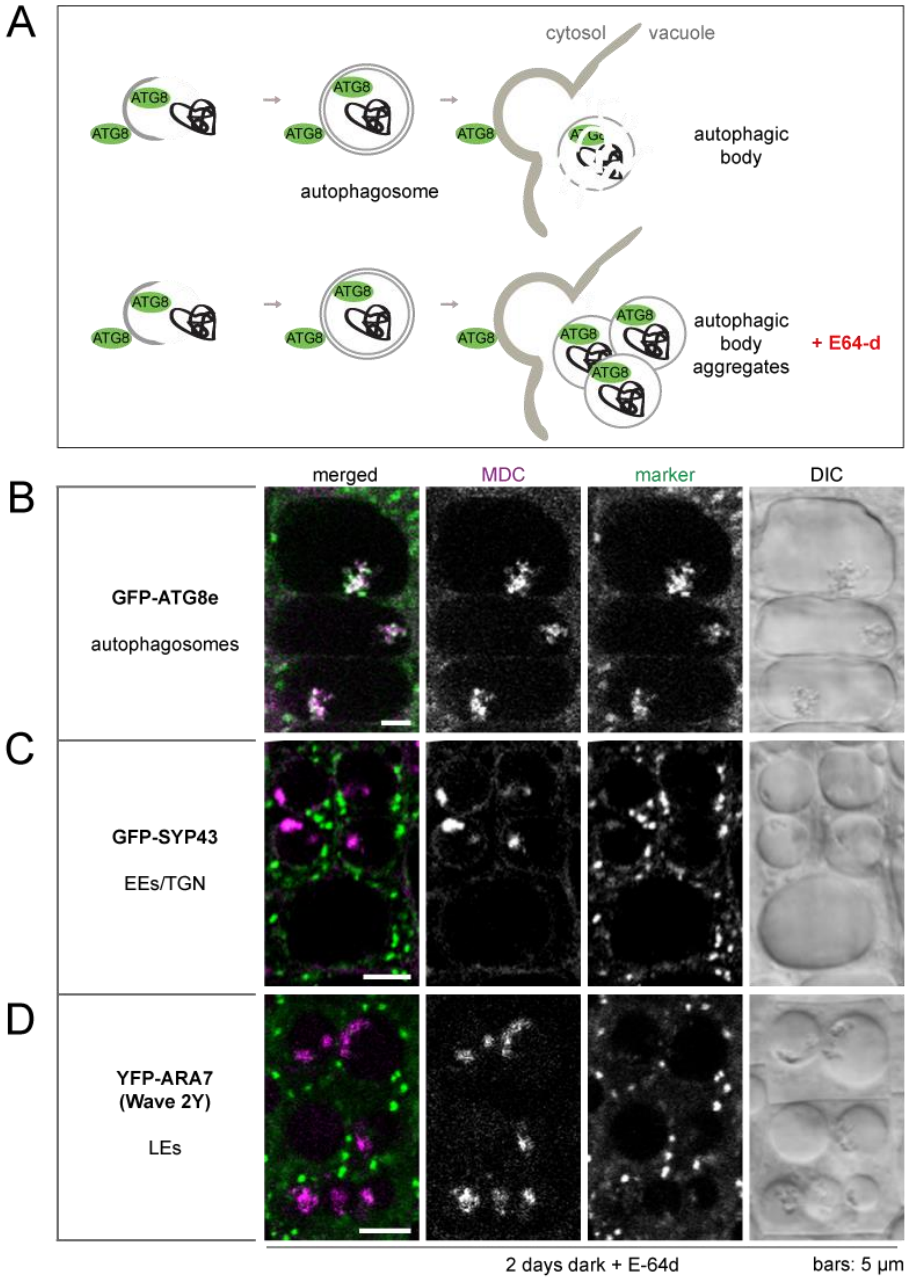

Figure 12. MDC specifically stains autophagic body aggregates.
(**A**) A scheme illustrating the origin of autophagic bodies and autophagic body aggregates. Upon the fusion of the autophagosome with the vacuole, a single-membraned autophagic body is degraded by resident hydrolases. After blocking the activity of vacuolar proteases with E64-d [2S,3S-trans-(ethoxycarbonyloxirane-2-carbonyl)-L-leucine-(3-methylbutyl) amide], autophagic bodies aggregate within the vacuolar lumen.
(**B** to **D**) Confocal images of MDC-stained root epidermis cells expressing either GFP-ATG8e (**B**), GFP-SYP43 (**C**) or YFP-ARA7 (**D**). Seedlings were grown for 7 days on half-strength MS medium under long-day conditions and afterwards were transferred to the dark for 5 days. Seedlings were treated for 6 h with E-64d before staining with MDC. Note that GFP-ATG8e colocalized with MDC on autophagic body aggregates, whereas the EE/TGN (early endosome/*trans*-Golgi network) marker GFP-SYP43 and the LE (late endosomal) marker YFP-ARA7 did not. Scale bars: 5 µm.

protease inhibitors such as E-64d [2S,3S-trans-(ethoxycarbonyloxirane-2-carbonyl)-L-leucine-(3-methylbutyl) amide], undigested autophagic bodies accumulate in vacuolar lumen in a form of large aggregates (Inoue et al., 2006) (Figure 12A). These aggregates can be visualized by staining with an autofluorescent dye MDC (monodansylcadaverine) (Contento et al., 2005).

35Spro(cauliflower mosaic virus 35S-promoter):GFP(green fluorescent protein)-ATG8e was used as a marker to test the specificity of MDC staining. GFP-ATG8e-expressing

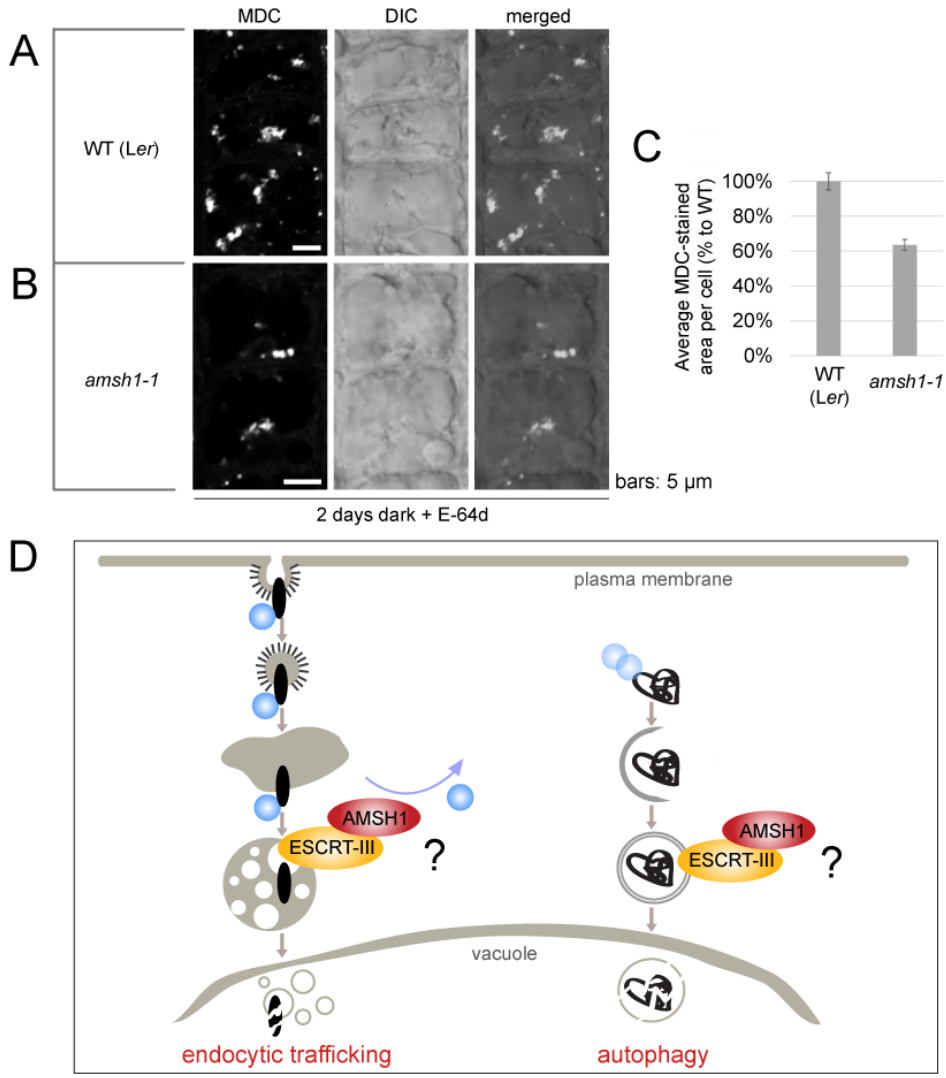

Figure 13. *amsh1-1* is deficient in autophagic degradation.
(**A** and **B**) WT (wild-type) and *amsh1-1* seedlings were grown for 7 days on half-strength MS medium under long-day conditions and afterwards were transferred to the dark for 2 days. Seedlings were treated for 1 h with E-64d before staining with MDC. Confocal images of MDC-stained root epidermal cells of the wild type (**A**) and *amsh1-1* (**B**) are shown. Scale bars: 5 µm. L*er*: Landsberg *erecta*.
(**C**) Quantification of MDC-staining-positive area per cell in the WT (wild type) and *amsh1-1* (n = 435 for L*er* and n = 438 for *amsh1-1*). Photographs taken in **A** and **B** were analyzed by the FluoView software, and the values of the wild type were set to 100%. Error bars indicate standard error.
(**D**) Scheme illustrating probable functions of AMSH1. AMSH1 was shown to interact with ESCRT-III, which might imply its role in endocytic trafficking. On the other hand, *amsh1-1* mutants show defects in autophagic degradation. It is possible that AMSH1 and ESCRT-III either function together directly in autophagic pathway or the proper autophagy requires intact endocytic trafficking.

plants were treated with E-64d and stained with MDC. As expected, GFP-ATG8e signals were observed in large aggregates within vacuolar lumen, where they colocalized with MDC (Figure 12B). MDC was previously reported in mammals not only to stain autophagosomes, but also to partially colocalize with early- and late endosomal markers (Tasdemir et al., 2008). In order to verify the specificity of the MDC staining in Arabidopsis, seedlings expressing the EE/TGN marker *35Spro:GFP-SYP43(SYNTAXIN OF PLANTS 43)* and the LE marker *UBQ10pro(UBIQUITIN 10-promoter):YFP(yellow fluorescent protein)-ARA7(ARABIDOPSIS RAB 7; Wave 2Y)* (Geldner et al., 2009) were subjected to the dark treatment. Accumulation of autophagic bodies was induced by incubation with E-64d and the MDC staining was applied. MDC stained the aggregates within the vacuole lumen, whereas the GFP-SYP43- and YFP-ARA7-positive signals were observed in the cytosol (Figure 12C and D). These results support that MDC is a specific dye for autophagic body aggregates under the tested conditions and can be used for further analyses.

Autophagy mutants like *atg7-2* are impaired in autophagosome formation and no autophagic body aggregates can be observed upon E-64d treatment (Hofius et al., 2009). I wanted to test whether the dark-hypersensitive phenotype of *amsh1-1* is a result of defects in autophagosome formation or in later stages of the autophagosome delivery to the vacuole. For this, *amsh1-1* mutants and wild-type seedlings (L*er*; Landsberg *erecta*) were transferred for 2 days to the dark and subjected to E-64d treatment to induce accumulation of autophagic bodies. After staining with MDC, the area of autophagic body aggregates per cell in wild type and *amsh1-1* was quantified (Figure 13A, B and C). Aggregates of autophagic bodies were forming in *amsh1-1*, suggesting that they are not completely impaired in autophagosome formation like the classical autophagy mutants (Figure 13B). The quantification of the area of autophagic body aggregates revealed that *amsh1-1* seedlings accumulated 36.5% less aggregates than the wild type (n = 435 for WT, n = 438 for *amsh1-1*) (Figure 13C). These results suggest that either less autophagosomes are formed or that they are less efficiently targeted to the vacuole in *amsh1-1*, resulting in the partial deficiency of *amsh1-1* in autophagic degradation.

The decreased area of autophagic body aggregates contrasts with the other results where *amsh1-1* was demonstrated to accumulate the autophagy marker ATG8 on immunoblot (Katsiarimpa et al., 2013). ATG8 associates with autophagosome membranes and its accumulation would rather point to increased amount of autophagosomes in cells. It is possible that the autophagosomes accumulate in *amsh1-1* mutants but do not reach the vacuole due to not properly functioning intracellular trafficking or membrane fusions. Interestingly, a dominant-negative version of ESCRT-III component VPS2.1 showed a similar autophagic degradation defect like *amsh1-1* (Katsiarimpa et al., 2013), pointing to the possibility that

AMSH1 and ESCRT-III play role in autophagic pathway. Alternatively, AMSH1 could function together with ESCRT-III in endocytic trafficking and hence influence the autophagic degradation indirectly (Figure 13D).

2.3. Novel interaction candidates were found in a Y2H screen using AMSH

AMSH1 and AMSH3 can be active as monomers and show specificity towards ubiquitin linkages rather than target proteins. It is therefore essential that the function of AMSH is tightly controlled by other proteins, recruiting them to specific subcellular compartments and regulating their DUB activity. In order to identify novel proteins that could affect AMSH function, I conducted a Y2H screen against 12,000 Arabidopsis sequence-verified ORFs (open reading frames) (Dreze et al., 2010; Arabidopsis Interactome Mapping, 2011; Wessling et al., 2014).

For use in the Y2H screen, full-length wild-type AMSH proteins were fused with the GBD (Gal4 DNA-binding domain) and named GBD-AMSH1, GBD-AMSH2 and GBD-AMSH3. Constructs were transformed into yeast and tested for autoactivation on SC-LWH (synthetic

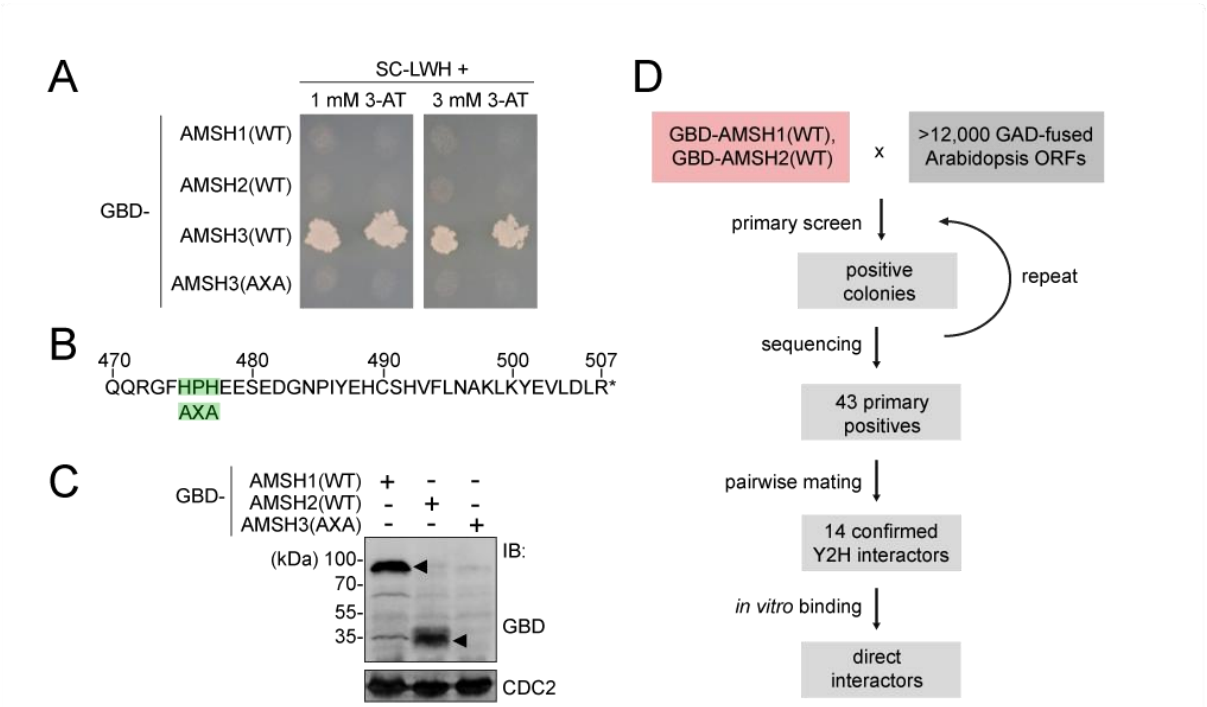

Figure 14. Novel interaction candidates were found in a Y2H screen using AMSH.
(**A**) GBD-AMSH1(WT), -AMSH2(WT), -AMSH3(WT) and AMSH3(AXA) were transformed into yeast and tested for their autoactivation on SC-LWH (synthetic complete medium lacking leucine, tryptophan, and histidine) supplemented with 1- and 3 mM 3-AT (3-amino-1,2,4-triazole). GBD: Gal4 binding domain, WT: wild-type, AXA: mutation.
(**B**) Sequence of the carboxy-terminal part of the MPN+ domain of AMSH3. The region mutated in AMSH3(AXA) is highlighted.
(**C**) Yeast extracts were subjected to immunoblot analysis using anti-GBD antibody. CDC2 was used as loading control. Arrowheads indicate GBD-AMSH1 and GBD-AMSH2.
(**D**) Scheme illustrating steps of the Y2H screen. ORF: open reading frame.

complete medium lacking leucine, tryptophan and histidine), supplemented with 1- or 3 mM 3-AT (3-amino-1,2,4-triazole) prior to their use in the screen. In contrast to AMSH1 and AMSH2 that did not show autoactivation, the wild-type AMSH3 was clearly autoactivating in the tested conditions (Figure 14A). To circumvent this problem, an inactive version of AMSH3, AMSH3(AXA), in which two histidines H475 and H477 were changed to alanines (H475A and H477A) was cloned (Figure 14B). This construct did not show autoactivation (Figure 14A). To verify the expression of GBD-fused proteins, an immunoblot was conducted using anti-GBD antibody. Protein bands were observed at the height of GBD-fused AMSH1 and AMSH2, confirming both constructs were expressing (Figure 14C). No expression could be verified for GBD-AMSH3(AXA), it was thus excluded from further experiments (Figure 14C).

The Y2H screen was carried out twice in order to ensure its reproducibility (Figure 14D). Yeast from the strain Y8930 *MATα* carrying GBD-fused AMSH1 and AMSH2 were

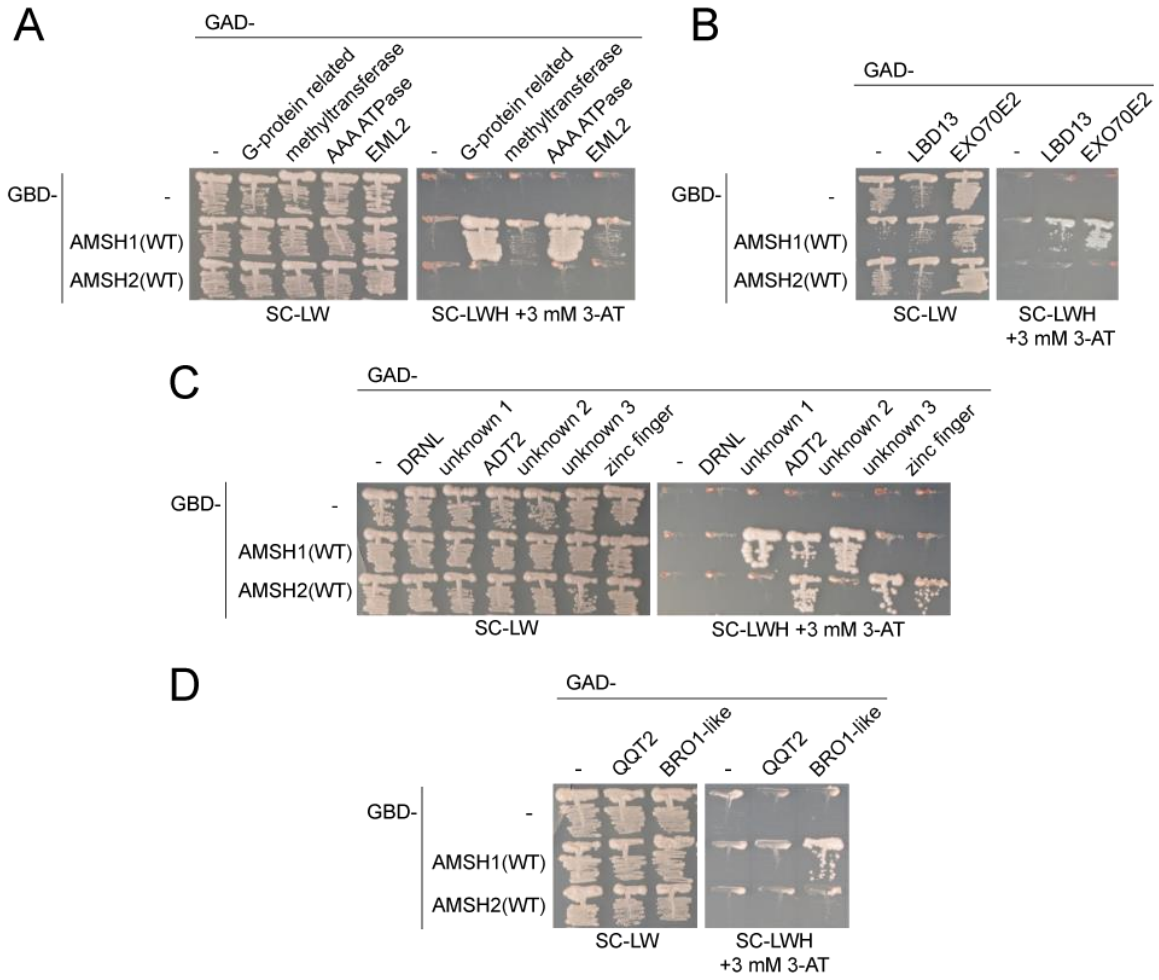

Figure 15. Several interaction candidiates found in the Y2H screen were positively verified.
(**A** to **D**) GBD-AMSH1(WT), GBD-AMSH2(WT), and GAD-fused interaction candidates were transformed in yeast. After mating, transformants were tested for the auxotrophic growth on SC-LW (synthetic complete medium lacking leucine and tryptophan) and SC-LWH (synthetic complete medium lacking leucine, tryptophan and histidine) supplemented with 3 mM 3-AT. GAD: Gal4 activation domain; GBD: Gal4 binding domain.

spotted on YPD (yeast extract, peptone, dextrose) medium. Yeast from the strain Y8800 *MATa* were transformed with GAD (Gal4 activation domain)-fused collection of Arabidopsis ORFs compiled into pools of 188 and spotted on top of GBD-AMSH proteins. After mating, yeast were tested for their auxotrophic growth on SC-LW (synthetic complete medium lacking leucine and tryptophan), SC-LWH (synthetic complete medium lacking leucine, tryptophan and histidine) supplemented with 3 mM 3-AT, and on SC-LWA (synthetic complete medium lacking leucine, tryptophan and adenine). SC-LH (synthetic complete medium lacking leucine and histidine) supplemented with 3 mM 3-AT and 3.6 mM CHX (cycloheximide), and SC-LA (synthetic complete medium lacking leucine and adenine) supplemented with 3.6 mM CHX were used to identify GAD-pools showing unspecific growth. The colonies growing on selection plates were picked, grown in liquid SC-LW medium and subjected to so-called phenotyping (Dreze et al., 2010). In phenotyping, yeast were grown again on selection plates as described above to confirm the results of the screen and discard new autoactivators. The whole procedure was repeated twice.

DNA was extracted from yeast colonies that were positive on selection plates and did not show autoactivation. Purified DNA was used as template for PCR with vector-specific primers (Appendix Table 7 and 8) (Dreze et al., 2010) and the PCR products were submitted for sequencing and the ORFs they encoded were identified using BLAST (Basic Local Alignment Search Tool, TAIR). The sequencing results revealed 43 candidates that interacted with at least one of AMSH proteins (Figure 14D), which are listed in the Appendix Table 2. A high number of candidates was found for GBD-AMSH1, which might suggest that through interacting with a wide variety of proteins, AMSH1 plays multiple roles in Arabidopsis cells. Only several candidates could be identified for GBD-AMSH2, probably due to the fact that AMSH2 is a very small protein consisting almost exclusively of the catalytic domain (Figure 11A).

The interaction candidates found in the Y2H screen were used for verification in targeted Y2H assays against GBD-AMSH1 and GBD-AMSH2. GBD-AMSH3(AXA) was excluded from verification due to the lack of expression on immunoblot. Yeast carrying single GAD-fused candidates were obtained from the Arabidopsis ORF collection (Dreze et al., 2010; Arabidopsis Interactome Mapping, 2011; Wessling et al., 2014). GBD-fused AMSH proteins and GAD-fused candidates were transformed into yeast strains Y8930 and Y8800, respectively. To analyze interactions, single colonies were picked and mixed for mating on YPD plates. Mated yeast were streaked on SC-LW and SC-LWH supplemented with 3 mM 3-AT, and analyzed after a 3-day growth at 30°C. The presence of GAD- and GBD-fusion plasmids was verified by PCR and immunoblot (data not shown). In Figure 15A to D examples of tested candidates are presented.

Y2H results showed that GBD-AMSH1 but not GBD-AMSH2 interacted with GAD-fused extra-large G-protein related protein ("G-protein related") (Figure 15A). G-proteins are highly conserved GDP (guanosine diphosphate)/GTP (guanosine triphosphate)-binding proteins that function in signal transduction. They form heterotrimers on the plasma membrane and are important for plant resistance against *Pseudomonas syringae* and *Fusarium oxysporum* (Zhu et al., 2009; Chakravorty et al., 2015; Maruta et al., 2015). GBD-AMSH1 interacted also with EML2 (EMSY-LIKE 2) (Figure 15A), an ENT (EMSY N-terminal)- and Tudor-like domain-containing protein. Plant proteins carrying ENT domain are nucleoside transporters essential for proper development and metabolism in Arabidopsis. Interstingly, EML2 was previously implicated in RPP7 (RECOGNITION OF PERONOSPORA PARASITICA 7)-mediated disease resistance against *Hyaloperonospora arabidopsidis* and in proper floral transition (Wormit et al., 2004; Tsuchiya and Eulgem, 2011). These results might point to a possible function of AMSH1 in plant immune responses.

The AAA ATPase (ATPases ASSOCIATED WITH DIVERSE CELLULAR ACTIVITIES) of unknown function also showed interaction with GBD-AMSH1 in targeted Y2H assays

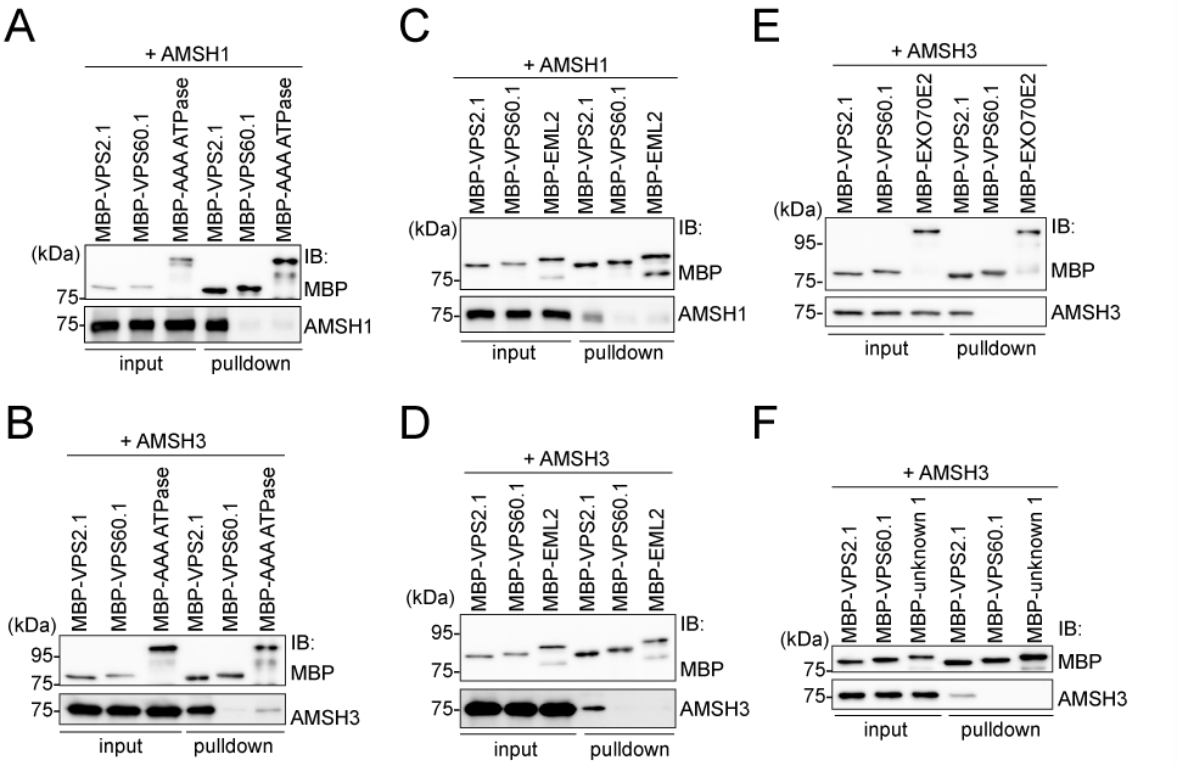

Figure 16. AAA ATPase interacts directly with AMSH3 but not with AMSH1.
(**A** to **F**) Recombinant AMSH1 (**A** and **C**) or AMSH3 (**B**, **D** to **F**) were incubated with either MBP-VPS60.1 (negative control), MBP-VPS2.1 (positive control) or with MBP-tagged proteins: AAA ATPase (**A** and **B**), EML2 (**C** and **D**), EXO70E2 (**E**) or unknown protein no. 1 ("unknown 1") (**F**). After a 2-h incubation at 4°C and extensive washing, samples were subjected to immunoblotting. Anti-AMSH1, anti-AMSH3 and anti-MBP antibodies were used to detect beads-retained material.

(Figure 15A). The AAA superfamily is a large and functionally diverse superfamily of nucleotide triphosphatases that are characterized by a conserved nucleotide-binding and catalytic module, called the AAA module. AAA ATPases display their function by unfolding proteins, remodeling small molecules, remodeling chromatin and disassembling protein complexes. Members of this superfamily are thus involved in a wide range of different cellular processes such as protein degradation, endocytic trafficking, DNA replication, DNA repair and transcriptional regulation (Snider et al., 2008). AMSH1 and AAA ATPase could potentially function together in a complex, affecting the ubiquitination status and structure of target proteins.

In targeted Y2H assays, two proteins with a probable function in endocytic trafficking were verified positively for GBD-AMSH1, EXO70E2 (EXOCYST COMPONENT OF 70 kDa E2) and a BRO1 (Bck1-like resistance to osmotic shock 1)-like domain-containing protein ("BRO1-like") (Figure 15B and D). EXO70E2 is a component of exocyst, an evolutionarily conserved multisubunit protein complex implicated in tethering secretory vesicles to the PM (Heider and Munson, 2012). AMSH1 could associate with exocyst and function together in membrane fusions, in example by regulating the ubiquitination status of other adaptor proteins. BRO1 domain-containing proteins are conserved adaptor proteins implicated in various cellular pathways. They were shown to associate and recruit other proteins to endosomes, and to function in membrane remodeling. Their role is thus important not only for endocytic trafficking, but also for other processes requiring a transient endosomal association of proteins

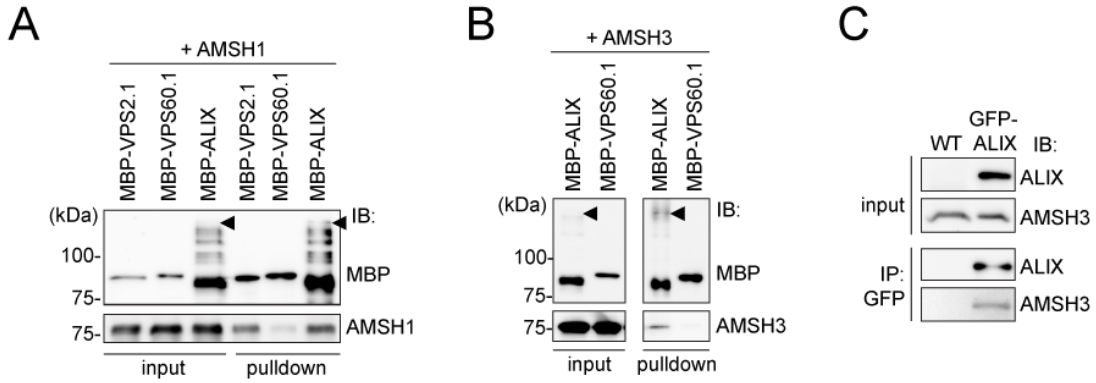

Figure 17. ALIX interacts with AMSH3 *in vitro* and *in planta*.
(**A**) Recombinant AMSH1 was incubated with either MBP-VPS60.1 (negative control), MBP-VPS2.1 (positive control) or with MBP-ALIX ("BRO1-like"). After a 2-h incubation at 4°C and extensive washing, samples were subjected to immunoblotting. Anti-AMSH1 and anti-MBP antibodies were used to detect beads-retained material. Arrowheads indicate MBP-ALIX.
(**B**) Recombinant AMSH3 was incubated with either MBP-VPS60.1 (negative control) or with MBP-ALIX. Anti-AMSH3 and anti-MBP antibodies were used to detect beads-retained material. Arrowheads indicate MBP-ALIX.
(**C**) ALIX and AMSH3 interact *in planta*. IP (immunoprecipitation) was performed from total extracts of wild-type and GFP-ALIX-expressing seedlings using anti-GFP immobilized matrix. Immunoprecipitated material was subjected to immunoblot analysis. GFP-ALIX and endogenous AMSH3 were detected using anti-ALIX and anti-AMSH3 antibodies, respectively.

or membrane scission events (Odorizzi, 2006; Bissig and Gruenberg, 2014). AMSH1 could also participate in these processes through its interaction with the BRO1-like domain-containing protein.

Other proteins, such as dimethylmenaquinone methyltransferase ("methyltransferase"), LBD13 (LOB DOMAIN-CONTAINING PROTEIN 13), unknown protein no. 1 (AT3G19895, "unknown 1") and unknown protein no. 2 (AT3G44940, "unknown 2") were also verified as interactors of GBD-AMSH1 but not GBD-AMSH2 in Y2H assays (Figure 15A, B and C). ADT2 (AROGENATE DEHYDRATASE 2), an enzyme functioning in biosynthesis of phenylalanine, interacted with both GBD-AMSH1 and GBD-AMSH2 (Figure 15C). As AMSH2 consist almost exclusively of the MPN domain, it is possible that it served as the interaction domain for both AMSH proteins with ADT2 (Figure 11A). The unknown protein no. 3 (AT4G16447, "unknown 3") and a zinc-finger (C2H2-type)-family protein ("zinc finger") bound only to GBD-AMSH2, probably to a specific motif not present in AMSH1. It is possible that the small deubiquitinase AMSH2 has specific cellular functions independently of other AMSH paralogs.

The full results of targeted Y2H assays are listed in the Appendix Table 2. Altogether, these results suggest that previously uncharacterized AMSH3 homologs, AMSH1 and AMSH2, might play diverse roles in plant cells requiring their interactions with different proteins.

2.4. ALIX interacts directly with AMSH1 and AMSH3

Interaction candidates that were positive for GBD-AMSH1 in Y2H were tested in *in vitro* pulldown assays to verify whether the binding between these proteins is direct. Due to the sequence similarity, both AMSH1 and AMSH3 were used in these assays. The interaction candidates were fused with the MBP (maltose binding protein) tag and expressed in the *Escherichia coli* DE3 strain Rosetta (EMD Millipore, USA). Proteins were purified together with the MBP-fused ESCRT-III core subunit VPS2.1, the accessory protein VPS60.1 and with the untagged AMSH1 or AMSH3. VPS2.1 was previously shown to be a direct- and VPS60.1 an indirect interactor of AMSH (Katsiarimpa et al., 2011; Katsiarimpa et al., 2013), and were therefore used in these assay as a positive and a negative control, respectively.

The AAA ATPase was selected for verification. Though it interacted with GBD-AMSH1 in Y2H assays, the binding could not be confirmed by *in vitro* pulldown assays (Figure 16A), suggesting that both proteins are probably not direct interactors. Alternatively, eukaryote-specific posttranslational modifications missing in *E. coli*-purified recombinant proteins could

be essential for their interaction. Interestingly, the AAA ATPase bound directly to AMSH3 (Figure 16B), opening the possibility that both proteins function together in Arabidopsis.

The ENT domain-containing EML2, which was implicated in plant development and pathogen defense, proved not to be a direct interactor of either of AMSH proteins (Figure 16C and D). Also the exocyst component EXO70E2 was verified negatively in *in vitro* binding assays, suggesting that AMSH3 does not associate directly with exocyst (Figure 16E). The results obtained with AMSH1 were inconclusive and the assay needs to be repeated and optimized for AMSH1.

Another interaction candidate, the unknown protein no. 1 (“unknown 1”), contains a conserved uncharacterized plant-specific domain, DUF1635 (Finn et al., 2014). The BLAST analysis revealed a great number of homologs in Arabidopsis and other plant species with a high conservation of amino acid sequence, though all of them are uncharacterized proteins. The high conservation within plants and the absence in other kingdoms suggest that the unknown protein no. 1 plays an important yet unknown plant-specific function. It was therefore chosen for testing in *in vitro* pulldown assays. The interaction with AMSH3 was, however, negatively verified, suggesting that AMSH3 does not function together with this conserved plant-specific protein (Figure 16F).

The adaptor BRO1-like domain-containing protein (“ALIX”) (Figure 17A and B) was verified as a direct interactor of both AMSH1 and AMSH3. The BRO1-like domain-containing protein (AT1G15130) was chosen for further experiments due to its high conservation in eukaryotes and multiple layers of function reported in homologs from other kingdoms. *In silico* analysis has revealed that it shows the highest homology to the human ALIX (ALG-2-INTERACTING PROTEIN X; 26.0% amino acid identities) (Figure 18) and slightly lower to the BRO1 domain-containing proteins in *Saccharomyces cereviae* Bro1p (15.8%) and Rim20p (Regulator of IME2 20, 18.0%). Due to the highest similarity to the human homolog, it was named the Arabidopsis ALIX.

Proteins binding to each other in *in vitro* conditions might not necessary function together *in vivo* (Xing et al., 2016). To verify that the interaction between ALIX and AMSH proteins is true also *in planta*, plants expressing a functional fusion protein GFP-ALIX driven by a native *ALIX* promoter were used (mutant complementation is shown in Figure 31H). The construct was generated by L. Cuyas (Cardona-Lopez et al., 2015) and kindly shared. Immunoprecipitation of GFP-ALIX was conducted on total protein extracts from wild-type and GFP-ALIX-expressing seedlings. Subsequent immunoblotting revealed coimmunoprecipitation of endogenous AMSH3 together with GFP-ALIX (Figure 17C). This result confirms that AMSH3 and ALIX associate with each other *in vivo*.

Protein alignment of 2 sequences: AT1G15130 and human ALIX
Identities: 244/907 (26%), positives: 415/907 (45%), gaps: 94/907 (10%)

```
AT1G15130      1 MASSSLSNLMLAIHEKKTSSVDLYRPLRNYVTFTYS---EREAQLIDDDLETLKQLRSDI  57
                 MA+       +++  KKTS VDL +PL  ++  TY    E +AQ      E  K  R+ +
Human ALIX     1 MAT------FISMQLKKTSEVDLAKPLVKFIQQTYPSGGEEQAQYCRAAEELSKLRRAAV  54

AT1G15130     58 ERVSDPSPAARRDLLISYYKVLCLVETRFPISPDKDHVNAVSFVWYDAFKQKH------K 111
                  R  D    A  + L+ YY  +C +E +FP S ++     ++F W DAF +        K
Human ALIX    55 GRPLDKHEGA-LETLLRYYDQICSIEPKFPFSENQ---ICLTFTWKDAFDKGSLFGGSVK 110

AT1G15130    112 ATQQNIHLEKAAVLFNLGASYSQIGLGHDRTTVDGRRQASHAFMAAAGAFAHLRDNESIK 171
                     ++  EK+ VLFN  A  SQI    +    +G + A+  +  A+GAF H++  E++
Human ALIX   111 LALASLGYEKSCVLFNCAALASQIAAEQNLDNDEGLKIAAKHYQFASGAFLHIK--ETVL 168

AT1G15130    172 ATIGPSTTVDVSVECVGMLERLMVAQAQECVFENTIAKGSTPGVSAKIARQVGIFYEEAL 231
                 + +    TVD+S + VG L  +M+AQAQE  F           + AK+A Q   ++ +A
Human ALIX   169 SALSREPTVDISPDTVGTLSLIMLAQAQEVFFLKATRDKMKDAIIAKLANQAADYFGDAF 228

AT1G15130    232 SALIISPLKDHFDKGWISHVQLKAALFYGEACFRYGKELHEKEEIAEEIARLRSGASRLA 291
                        KD   K +  + Q    +   + C       + +  +A++  +     +RL
Human ALIX   229 KQ---CQYKDTLPKYF--YFQEVFPVLAAKHCIMQANAEYHQSILAKQQKKFGEEIARLQ 283

AT1G15130    292 EAKKSSRGAPAQLIEAMNT--LESSINGNLDRAVKENDRVYLMRVPSPSSLSPLPAFSMV 349
                  A +  +   ++  E +N       IN  L  A K+ND +Y  RVP    L P+   ++V
Human ALIX   284 HAAELIKTVASRYDEYVNVKDFSDKINRALAAAKKDNDFIYHDRVPDLKDLDPIGKATLV 343

AT1G15130    350 KPMNMTDILDASKEKMFSILVPDSSAKALSRYTEMVDDVIRTQAERLQQASELTRVRLKE 409
                 K   +   +      +F  +VP S  ++L+ Y +   D+I     ++++A+ L    L
Human ALIX   344 KSTPVNVPISQKFTDLFEKMVPVSVQQSLAAYNQRKADLINRSIAQMREATTLANGVLAS 403

AT1G15130    410 MDLPDSILAVDGNSALPVDLKEDVEAVQISGGPAGLEAELQQLRDLKRVNQELLVHTEEL 469
                 ++LP +I  V G++ +P  +     +V   GG   ++  +++L +L + N+E+L  +  L
Human ALIX   404 LNLPAAIEDVSGDT-VPQSILTKSRSVIEQGGIQTVDQLIKELPELLQRNREILDESLRL 462

AT1G15130    470 LQKEATEDSQFRSQFGTRWTRPQSSTLTKNLQDRLNRFAANLKQAGESDVKIERSVRDNS 529
                 L +E   D+  R++F  RW R  S+ L K L+     F   L +A ++D +++   + +
Human ALIX   463 LDEEEATDNDLRAKFKERWQRTPSNELYKPLRAEGTNFRTVLDKAVQADGQVKECYQSHR 522

AT1G15130    530 ALMSILDR--RPIESAVPTLARPIMSLDATEDAIVGTLKQSLRQLENLGAQRAGLEDMLK 587
                   + +L +    + +A+P+ A P  ++  +E  +V  LK  L  L+ +  +R GLE+ LK
Human ALIX   523 DTIVLLCKPEPELNAAIPS-ANPAKTMQGSE--VVNVLKSLLSNLDEVKKEREGLENDLK 579

AT1G15130    588 EMKRKDDILPKLMTITG-----SYEDMFRKEISK-YDHICEDISQNIEVQEQLLMQIQAQ 641
                  +    D+  K +T        + E +   E+ + Y  +   + ++++ QE LL  IQ
Human ALIX   580 SVNF--DMTSKFLTALAQDGVINEEALSVTELDRVYGGLTTKVQESLKKQEGLLKNIQVS 637

AT1G15130    642 NEEFSTIFNLEDYKASKEKCYKQIQAAIMKYREIKENINEGLKFYVTLQDAITNVKQQCS 701
                 ++EFS +    +    +E+  K +  A   + E+  N+ EG KFY  L + +   + +CS
Human ALIX   638 HQEFSKMKQSNNEANLREEVLKNLATAYDNFVELVANLKEGTKFYNELTEILVRFQNKCS 697

AT1G15130    702 DFVMTRSIQCRDMIEDVQRQMSGLSFQDHRSSGPYPSV----HQPTASSPPPPPETQNPS 757
                 D V  R  +  ++++D+Q+ ++          +  Y S     H PT   P P P T  P+
Human ALIX   698 DIVFARKTERDELLKDLQQSIAREPSAPSIPTPAYQSSPAGGHAPT--PPTPAPRTMPPT 755

AT1G15130    758 HPHPHAPYYRPPEQM----SRPGYSIP-PYG----PPPPYHTPHGQAPQPYPPQAQQQPH 808
                  P P A   RPP  +      P  + P P G     P P  TP G AP   PPQAQ  P+
Human ALIX   756 KPQPPA---RPPPPVLPANRAPSATAPSPVGAGTAAPAPSQTP-GSAP---PPQAQGPPY 808

AT1G15130    809 PSWQQ-GSY--------YDP----QGQQPRPP----YPGQSPY-----------QPPHQG 840
                 P++     Y        Y+P    Q   P PP     PGQ+PY           QPP Q
Human ALIX   809 PTYPGYPGYCQMPMPMGYNPYAYGQYNMPYPPVYHQSPGQAPYPGPQQPSYPFPQPPQQ- 867

AT1G15130    841 GGYYRQ* 847
                   YY Q
Human ALIX   868 -SYYPQQ 873
```

Figure 18. Human and Arabidopsis ALIX show 26.0% amino acid sequence identity.
Protein alignment of the human ALIX with the Arabidopsis BRO1-like domain-containing protein AT1G15130 was performed using Geneious Pro 5.3.6. Muscle alignment was applied with maximum 8 iterations.

2.5. ALIX is an ESCRT-associated protein

ALIX is a direct interactor of AMSH3 and both proteins associate together *in vivo*. To elucidate the interaction network surrounding AMSH3 and ALIX, another Y2H screen was performed, using GBD-ALIX as bait. The full list of interaction candidates identified in the screen is in Appendix Table 2. Two homologs of the ESCRT-III subunit SNF7, a well-known interactor of ALIX (Richardson et al., 2011; Cardona-Lopez et al., 2015), were found in the Y2H screen, strengthening the biological relevance of these results (Appendix Table 2). No common interaction partners with AMSH proteins were identified. Three novel ALIX interactors were chosen for verification in targeted Y2H assays and two of them could be confirmed, FIP1 (FH1-INTERACTING PROTEIN 1 or VirF-INTERACTING PROTEIN 1) (Figure 19A and D) and a CaLB (calcium-dependent lipid binding)-family protein ("CaLB") (Figure 19B and E). The interaction of ALIX with a RING E3 ligase XBAT35 (XB3 ORTHOLOG 5 IN ARABIDOPSIS THALIANA) could not be verified (Figure 19C and F). These results suggest that ALIX might play additional roles in Arabidopsis beyond its interaction with AMSH proteins.

The human ALIX and the yeast Bro1p interact with ESCRT-III (Odorizzi et al., 2003; McCullough et al., 2008; Pires et al., 2009). As mentioned above, also the Arabidopsis ALIX was shown to associate with ESCRT-III through SNF7.1 and SNF7.2 in Y2H assays by others (Richardson et al., 2011; Cardona-Lopez et al., 2015), as well as in this study. The core components and accessory proteins of ESCRT-III are known to accumulate in aberrant endosomal structures upon inhibition of ESCRT-III disassembly. One of the methods to block the disassembly of ESCRT-III is to inactivate the AAA ATPase SKD1, a homolog of the yeast Vps4p (Babst et al., 1998; Haas et al., 2007; Katsiarimpa et al., 2011). In Arabidopsis plants and Arabidopsis cell culture-derived protoplasts, the overexpression of ATPase-inactive SKD1(E232Q), called also SKD1(EQ), was shown to induce the presence of enlarged endosomes with a reduced number of ILVs. These aberrant structures contain components of the ESCRT machinery, ESCRT-associated proteins and late endosomal markers (Haas et al., 2007; Katsiarimpa et al., 2011; Kolb et al., 2015).

If ALIX associates with ESCRT-III *in vivo*, it should relocalize to the aberrant endosomal structures upon the inhibition of the complex disassembly. To verify it, Arabidopsis cell culture-derived protoplasts were cotransformed with *ALIXpro:GFP-ALIX* (Cardona-Lopez et al., 2015), the ESCRT-III core subunit *UBQ10pro:mCherry-VPS2.1*, and either *35Spro:HA-SKD1(WT, wild type)* or enzymatically inactive *35Spro:HA-SKD1(EQ)*. mCherry-VPS2.1 was previously shown to localize to cytosol in wild-type *SKD1* conditions, whereas transient coexpression with HA-SKD1(EQ) causes VPS2.1 to relocalize to aberrant endosomes (Katsiarimpa et al., 2011). Coexpression experiments in Arabidopsis protoplasts revealed that

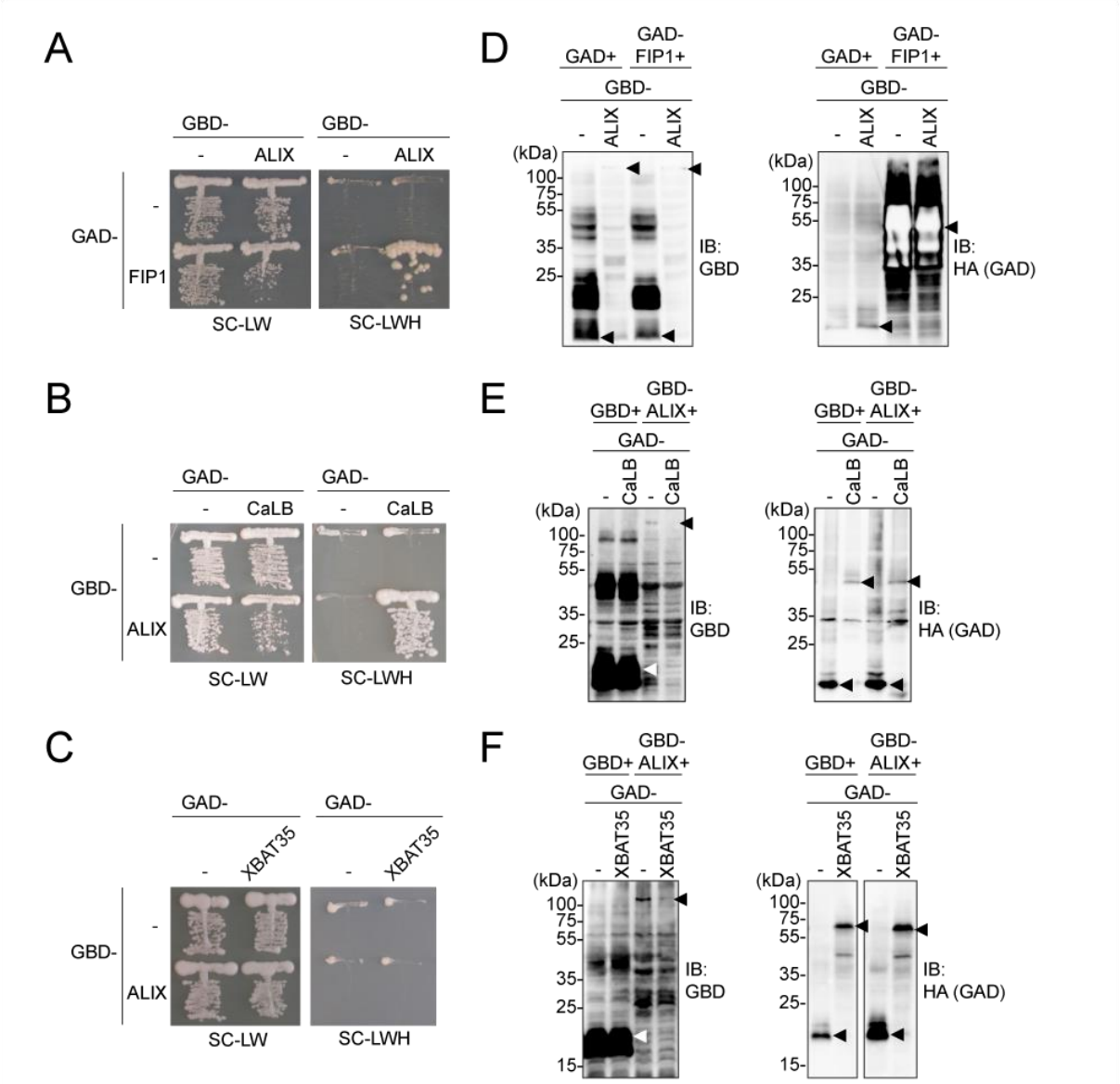

Figure 19. Several interaction candidates for ALIX were verified in targeted Y2H assays.
(**A** to **C**) GBD-fused ALIX was cotransformed in yeast with GAD-FIP1 (**A**), GAD-CaLB (**B**) or GAD-XBAT35 (**C**). Transformants were tested for the auxotrophic growth on SC-LW (synthetic complete medium lacking leucine and tryptophan) and SC-LWH (synthetic complete medium lacking leucine, tryptophan, and histidine). GAD: Gal4-activation domain; GBD: Gal4-binding domain.
(**D** to **F**) Expression of the Y2H clones shown in **A** to **C**, respectively. Yeast total extracts were prepared from transformants and subjected to immunoblotting using an anti-GBD antibody to detect GBD-fusion proteins and an anti-HA antibody to detect the GAD-HA-fusion proteins.

upon cotransformation with HA-SKD1(WT), both GFP-ALIX (75.0%; n = 20) and mCherry-VPS2.1 (80.0%; n = 20) showed mainly cytosolic localization (Figure 20A and B). However, when the HA-SKD1(EQ) was expressed in cells, both mCherry-VPS2.1 (96.3%; n = 27) and GFP-ALIX (96.3%; n = 27) relocalized to enlarged endosomal compartments (Figure 20A and B). These results support the hypothesis that the Arabidopsis ALIX associates with ESCRT machinery *in vivo*.

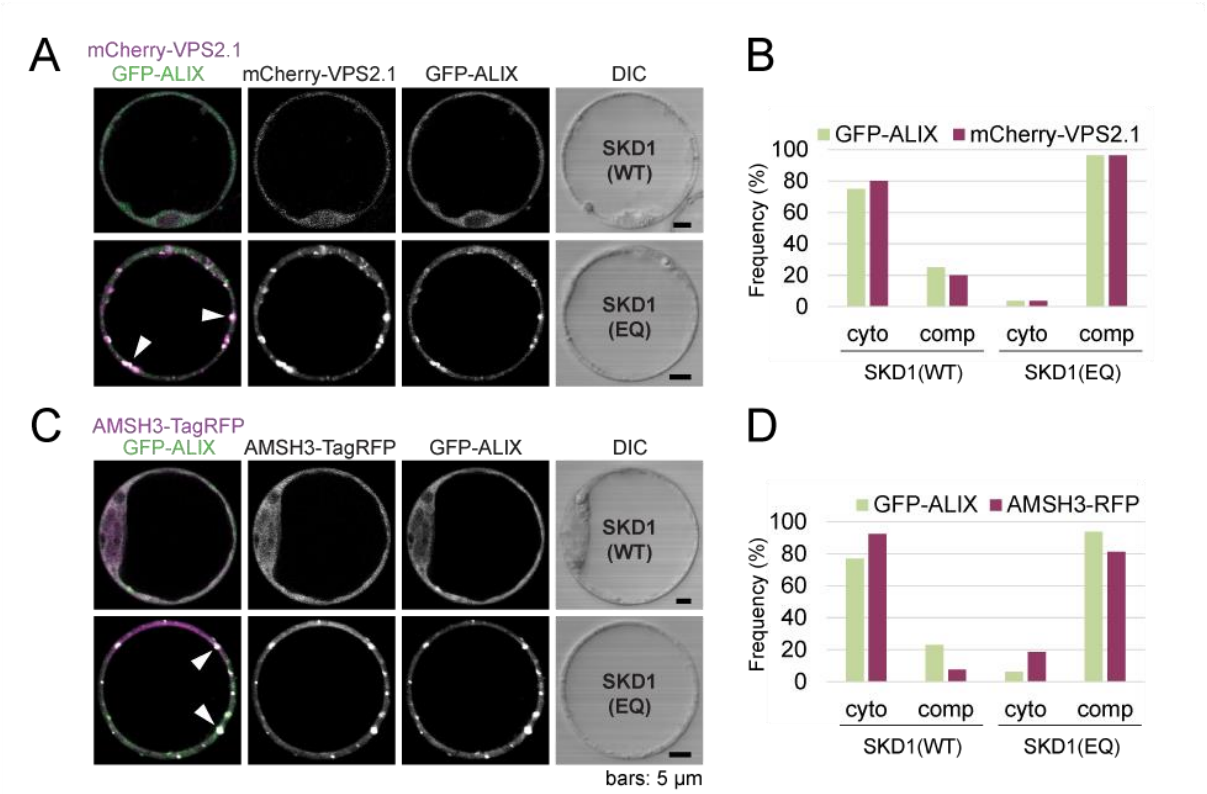

Figure 20. ALIX localizes to SKD1(EQ)-induced aberrant endosomes.
(**A**) and (**B**) ALIX localizes to SKD1(EQ)-induced compartments.
(**A**) *ALIXpro:GFP-ALIX* was cotransformed with *UBQ10pro:mCherry-VPS2.1* and either *35Spro:HA-SKD1(WT)* or *35Spro:HA-SKD1(EQ)* in Arabidopsis root epidermis cell culture-derived protoplasts. Representative cells are shown. Note that upon the coexpression with SKD1(EQ), both mCherry-VPS2.1 and GFP-ALIX relocalized to enlarged endosomal compartments (arrowheads). Scale bars: 5 µm.
(**B**) Percentages of cells with cytosolic localization (cyto) (n = 20) or SKD1(EQ)-induced compartments (comp) (n = 27) of GFP-ALIX and mCherry-VPS2.1 are indicated.
(**C**) and (**D**) AMSH3 and ALIX colocalize in SKD(EQ)-induced compartments.
(**C**) *ALIXpro:GFP-ALIX* and *35Spro:AMSH3-TagRFP* were cotransformed with either *35Spro:HA-SKD1(WT)* or *35Spro:HA-SKD1(EQ)*. Representative cells are shown. Note that upon coexpression with SKD1(EQ), both AMSH3-TagRFP and GFP-ALIX relocalized to enlarged endosomal compartments (arrowheads). Scale bars: 5 µm.
(**D**) Percentages of cells with cytosolic localization (cyto) (n = 13) or SKD1(EQ)-induced compartments (comp) (n = 16) of GFP-ALIX and AMSH3-TagRFP are indicated.

Fluorophore-tagged AMSH3 was previously found to localize to SKD1(EQ)-induced compartments in protoplasts (Katsiarimpa et al., 2011). In order to test whether ALIX and AMSH3 would colocalize on aberrant endosomes, Arabidopsis protoplasts were cotransformed with *ALIXpro:GFP-ALIX* and *35Spro:AMSH3-TagRFP(red fluorescent protein)*, and with either *35Spro:HA-SKD1(WT)* or *35Spro:HA-SKD1(EQ)*. When coexpressed with HA-SKD1(WT), both AMSH3-TagRFP (92.3%; n = 13) and GFP-ALIX (76.9%; n = 13) remained cytosolic (Figure 20C and D). As expected, upon coexpression with the inactive HA-SKD1(EQ), both AMSH3-TagRFP (81.3%; n = 16) and GFP-ALIX (93.8%; n = 16) relocalized to enlarged endosomal compartments (Figure 20C and D). These results confirm that both AMSH3 and ALIX are proteins associated with ESCRT function.

Previous work has shown that AMSH3 binds to two core subunits of ESCRT-III, VPS2.1 and VPS24.1 (Katsiarimpa et al., 2011). Moreover, subcellular fractionation studies showed that the endogenous AMSH3 is present in both soluble and membranous fractions (Isono et al., 2010). These results suggest that AMSH3 might localize on endosomes in plants. As Arabidopsis ALIX was found to interact with SNF7 and localize to SKD1(EQ)-induced aberrant endosomes, it is possible that it also shows an endosomal localization. AMSH3 and ALIX could localize on the same or distinct subcellular compartments.

2.6. AMSH3 partially colocalizes with early endosomal markers

The protoplasts are a transient expression system and do not always fully represent the situation *in planta*. In order to verify the results of the localization experiments obtained in cell culture-derived protoplasts, AMSH3 was fused at the C-terminus with YFP and expressed in *Arabidopsis thaliana* plants under its own promoter (F. Anzenberger). The AMSH3-YFP fusion protein showed dual localization in root epidermis, being present in both cytosol and small punctuate structures (Figure 21A to D). To test whether the foci represent endosomal compartments, AMSH3-YFP-expressing plants were crossed with plants expressing own promoter-driven endocytic markers (Ueda et al., 2004; Uemura et al., 2004; Ebine et al., 2011) and so-called Wave markers. Wave markers are fluorophore-tagged membrane proteins expressed under the weak constitutive *UBQ10* promoter. Wave markers have distinct subcellular localization patterns and are widely used in rapid combinatorial analysis of plant membranous compartments (Geldner et al., 2009).

In plants, two clearly separate endosomal organelles were previously identified, the EE/TGN compartment and the LE/MVB/PVC (Otegui and Spitzer, 2008; Reyes et al., 2011). The EE/TGN was demonstrated to play dual roles. On one hand, it receives recently endocytosed material from plasma membrane like early endosomes in opisthokonta. On the other hand, similar to the yeast and mammalian TGN, it is also involved in sorting of biosynthetic cargo coming from Golgi (Figure 21E) (Reyes et al., 2011; Paez Valencia et al., 2016).

AMSH3-YFP-expressing plants were crossed with two EE/TGN markers *SYP43pro:mRFP(monomeric red fluorescent protein)-SYP43* and *CLCpro:CLC-mKO(monomeric Kusabira Orange)* (Uemura et al., 2004; Fujimoto et al., 2010; Ito et al., 2012; Uemura et al., 2012). SYP43 belongs to SNAREs, proteins that generate a driving force for fusions between lipid membranes (Chen and Scheller, 2001), and was previously shown to localize to EE/TGN in plants (Uemura et al., 2004; Uemura et al., 2012; Uemura et al., 2014).

CLC together with CHC polymerizes into a curved lattice around vesicles budding from the PM, TGN or endosomes (Royle, 2006). CLC is therefore a marker for CCVs and was

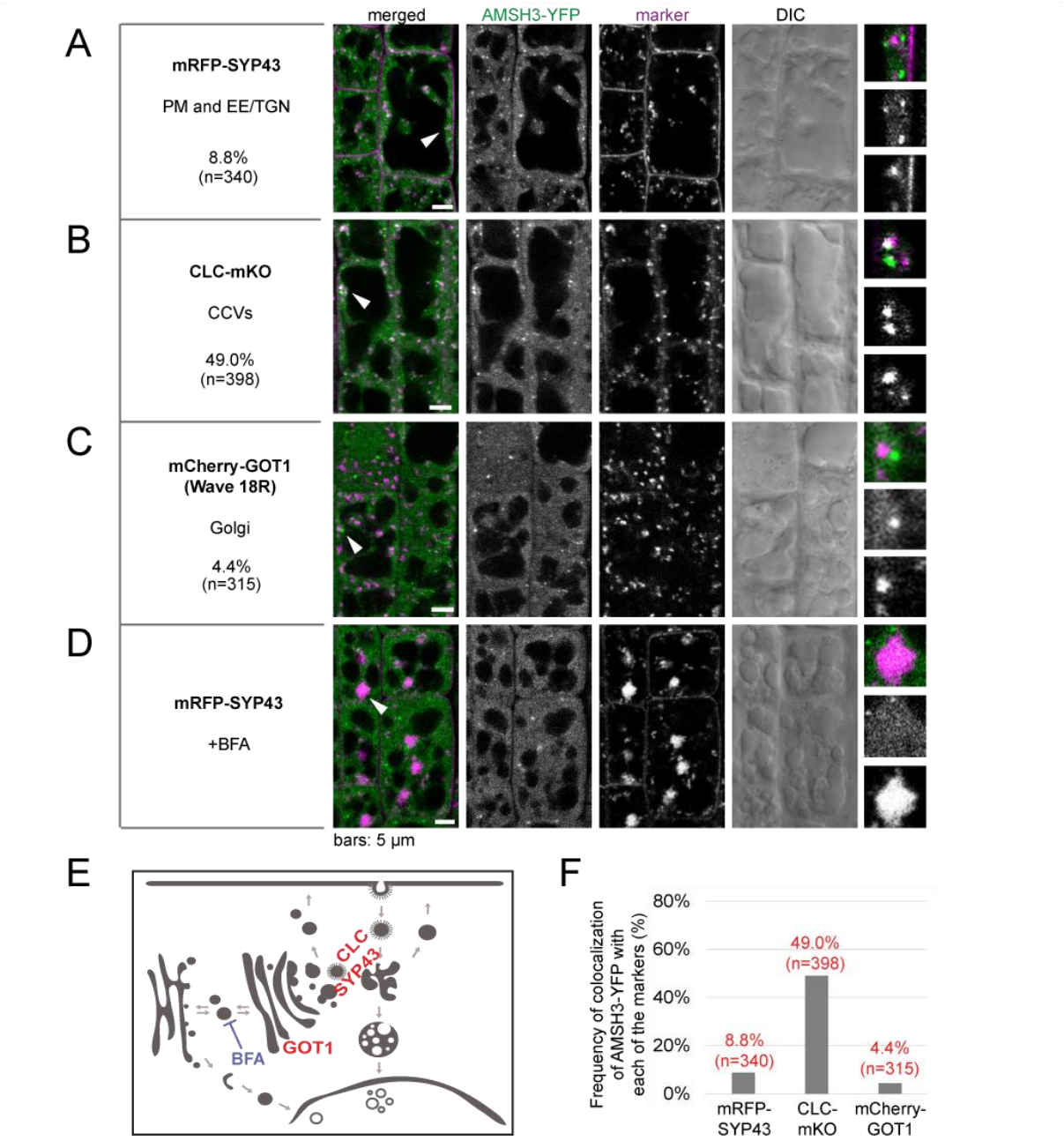

Figure 21. AMSH3-YFP partially localizes to early endosomes.
(**A** to **D**) Seedlings expressing *AMSH3pro:AMSH3-YFP* were crossed with either *SYP43pro:mRFP-SYP43* (**A** and **D**), *CLCpro:CLC-mKO* (**B**) or *UBQ10pro:mCherry-GOT1* (**C**). Plants coexpressing both fusion proteins were examined under a confocal microscope. PM: plasma membrane, EE/TGN: early endosomes/*trans*-Golgi network, CCVs: clathrin-coated vesicles. Scale bars: 5 µm.
(**D**) An AMSH3-YFP/mRFP-SYP43-coexpressing seedling was treated with 50 µM BFA (Brefeldin A) for 60 min. Note that although mRFP-SYP43 relocalized to the BFA bodies, AMSH3-YFP did not. Scale bar: 5 µm.
Magnifications of the areas indicated with white arrowheads are shown on the right side of panels **A** to **D** (from top to bottom: merged, AMSH3-YFP, marker).
(**D**) Scheme presenting the localization of markers used in **A** to **D** and the pathways affected by the BFA treatment.
(**E**) Numbers of AMSH3-YFP-positive vesicles that colocalized with the mRFP- or mKO-tagged markers in **A** to **C** were counted to calculate the colocalization frequency.

previously demonstrated to strongly colocalize with markers for EE/TGN (Ito et al., 2012).

AMSH3-YFP signals did not show strong colocalization rates with the mRFP-SYP43, only 8.8% (n = 340) (Figure 21A and F). Interestingly, 49.0% (n = 398) of the AMSH3-YFP-positive compartments contained CLC-mKO signals (Figure 21B and F). Both results suggest that AMSH3 does partially localize to EE/TGN, but the frequency is uncertain. The discrepancy in colocalization rates between AMSH-YFP and EE/TGN markers might be due to the fact that EE/TGN can originate from both PM and mature Golgi cisternae (Reyes et al., 2011; Paez Valencia et al., 2016). To test whether AMSH3-YFP associates with EE/TGN originating from Golgi stacks, AMSH3-YFP plants were crossed with the Golgi marker mCherry-GOT1 (Wave 18R) (Geldner et al., 2009). The colocalization frequency between AMSH3-YFP and mCherry-GOT1 was very low, 4.4% (n = 315) (Figure 21C and F), suggesting that AMSH3-YFP probably does not localize to vesicles budding off from Golgi or TGN.

To further establish the EE/TGN fraction to which AMSH3 localizes, AMSH3-YFP/mRFP-SYP43-coexpressing lines were treated with BFA (Brefeldin A). BFA is an inhibitor of guanine nucleotide exchange factors ARF-GEFs (ADP RIBOSYLATION FACTOR-GTP EXCHANGE FACTORS) and was found to inhibit GNOM. GNOM is an ARF-GEF that was recently shown to localize to the Golgi apparatus and play role in recycling from ER to Golgi (Naramoto et al., 2014; Doyle et al., 2015). Through the inhibition of GNOM function, BFA indirectly affects EE/TGN, especially the part that arises from the maturation of Golgi cisternae (Doyle et al., 2015; Paez Valencia et al., 2016). Upon the 60-min BFA treatment, the EE/TGN marker mRFP-SYP43 relocalized to so-called BFA bodies. In contrast, AMSH3-YFP signals were not found in the BFA-induced compartments (Figure 21D), suggesting AMSH3 localization does not depend on GNOM or properly functioning ER-to-Golgi trafficking.

Altogether, these results indicate that AMSH3-YFP partially localizes to early endosomes/*trans*-Golgi network, however, AMSH3-YFP-positive compartments probably originate rather from PM than from Golgi.

2.7. AMSH3 shows a strong localization to late endosomes

According to the theory of endosome maturation, EEs/TGN could maturate to LEs/MVBs/PVCs. The maturation of endosomes depends on a variety of protein- and lipid-based remodeling events. In yeast and animals, a switch from a small GTPase family RAB5/Ypt51p to RAB7/Ypt7p and a change in the lipid composition, in example the conversion from PI3P to PI(3,5)P2 are essential in this process. These changes are believed to prepare

the endosomes for fusion with other endosomes and finally with the lysosome or vacuole (Huotari and Helenius, 2011; Scott et al., 2014).

AMSH3-YFP shows a partial localization to EE/TGN. To verify whether AMSH3 localizes also on LEs, *AMSH3pro:AMSH3-YFP*-expressing plants were crossed with plants expressing late endosomal markers *ARA7pro:mRFP-ARA7*, *ARA6pro:ARA6-mRFP* and *UBQ10pro:mCherry-RABG3c(RAB GTPase HOMOLOG G3c; Wave 11R)* (Figure 22E) (Ueda et al., 2001; Ueda et al., 2004; Geldner et al., 2009; Ebine et al., 2011). ARA7, known also as RABF2b, and ARA6, known also as RABF1, belong to *At*RABF subfamily that shows the highest similarity to the human Rab5 and yeast Ypt51p subfamilies (Ueda et al., 2001; Vernoud et al., 2003). In Arabidopsis, ARA6 and ARA7 were shown to localize on partially overlapping populations of late endosomes with reciprocal gradients. Additionally, a small fraction of ARA7 localizes on EE/TGN (Ueda et al., 2004; Otegui and Spitzer, 2008). The third marker used in this study, RABG3c, belongs to the *At*RABG subfamily homologous to the human Rab7 and yeast Ypt7p (Vernoud et al., 2003). In Arabidopsis cells, RABG3c localizes to MVBs and the tonoplast, and is considered a marker for mature late endosomes (Bozkurt et al., 2015).

The confocal analysis revealed that AMSH3-YFP showed a very high colocalization frequency with RABFs mRFP-ARA7 (74.8%; n = 306) (Figure 22A and F) and ARA6-mRFP (62.8%; n = 368) (Figure 22B and F). The lowest colocalization rate was observed with the RABG mCherry-RABG3c, 43.2% (n = 287) (Figure 22C and F). This was a strong indication that the majority of AMSH3-YFP localizes to MVBs, which fits to its function with ESCRT-III. The late endosomal localization of AMSH3-YFP was further confirmed by treating AMSH3-YFP/ARA6-mRFP-coexpressing lines with the PI3K (PHOSPHOINOSITIDE 3-KINASE)/PI4K inhibitor WM (Wortmannin). WM was shown to cause swelling of late endosomes in plants and formation of so-called Wortmannin compartments (Wang et al., 2009a; Takac et al., 2012). Upon treatment with WM, both ARA6-mRFP and AMSH3-YFP localized to the surface of the swollen endosomes that appeared as ring-like structures (Figure 22D). These results corroborate that AMSH3-YFP associates together with LE markers on WM-sensitive compartments.

As mentioned above, endosome maturation is connected to a switch from the small GTPase family Rab5/Ypt51p/RABF to the Rab7/Ypt7p/RABG family (Huotari and Helenius, 2011; Scott et al., 2014). AMSH3-YFP shows the highest colocalization frequency with mRFP-ARA7 and slightly lower with ARA6-mRFP. ARA6 was previously suggested to represent more mature endosomes than ARA7, as ARA7-positive compartments colocalize earlier with an endocytosis tracker FM4-64 [N-(3-triethylammoniumpropyl)-4-(6-(4-(diethylamino) phenyl)

hexatrienyl) pyridinium dibromide] (Ueda et al., 2004; Otegui and Spitzer, 2008). This points to the conclusion that AMSH3-YFP localizes stronger to less mature MVBs. This theory

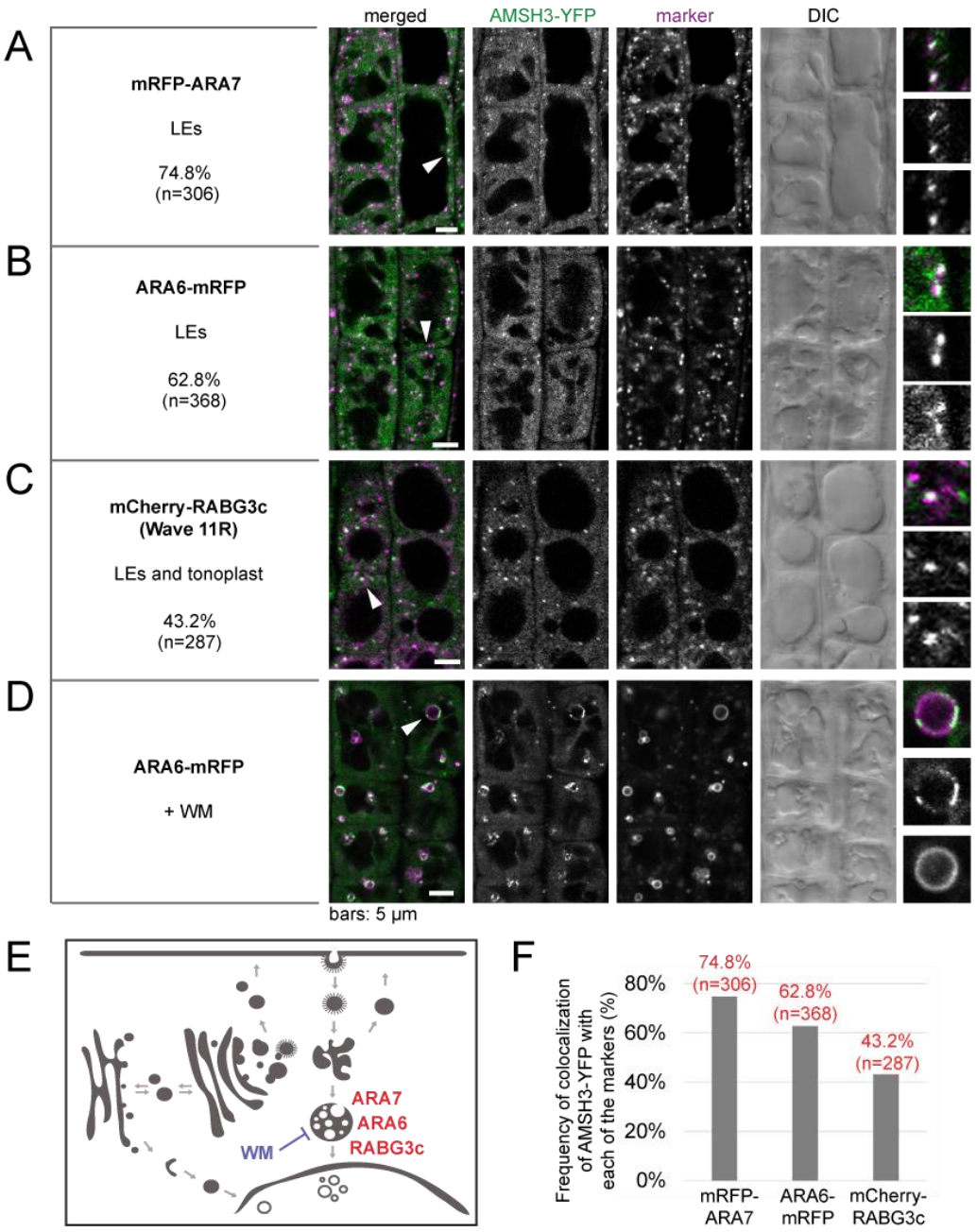

Figure 22. AMSH3-YFP partially localizes to late endosomes.
(**A** to **D**) Seedlings expressing *AMSH3pro:AMSH3-YFP* were crossed with either *ARA7pro:mRFP-ARA7* (**A**), *ARA6pro:ARA6-mRFP* (**B**) or *UBQ10pro:mCherry-RABG3c* (**C**). Plants coexpressing fusion proteins were examined under a confocal microscope. Scale bars: 5 µm.
(**D**) An AMSH3-YFP/ARA6-mRFP-coexpressing seedling was treated with 33 µM WM (Wortmannin) for 120 min. Note that both AMSH3-YFP and ARA6-mRFP relocalized to WM-induced compartments. Scale bar: 5 µm.
Magnifications of the areas indicated with white arrowheads are shown on the right side of panels **A** to **D** (from top to bottom: merged, AMSH3-YFP, marker).
(**E**) Scheme presenting the localization of markers used in **A** to **D** and the compartments affected by WM treatment.
(**F**) The numbers of AMSH3-YFP-positive vesicles that colocalized with the mRFP- or mCherry-tagged markers in **A** to **D** were counted to calculate the colocalization frequency.

corresponds also with the result that the colocalization frequency of AMSH3-YFP with the marker for mature LEs and tonoplast RABG mCherry-RABG3c was the lowest of all tested.

Altogether, these results indicate that AMSH3-YFP-positive foci visible under the confocal microscope are endosomal compartments. Moreover, these compartments seem to represent mostly late endosomes or intermediate compartments of EE/TGN maturing to MVBs.

2.8. AMSH3, CLC and ARA7 partially colocalize with each other

Colocalization analyses suggest that AMSH3 is mainly a late endosomal protein. The colocalization frequency with the EE/TGN marker mRFP-SYP43 was only 8.8%, which rather excludes a significant association with early endosomes. It is therefore surprising that AMSH3-YFP showed 49% colocalization rate with CLC-mKO. CLC is a marker for clathrin-coated vesicles that was previously demonstrated to strongly colocalize with the EE/TGN marker SYP43 and very poorly with the LE marker ARA6 (Ito et al., 2012). It was therefore challenging to find the explanation for the high colocalization rates of AMSH3-YFP with both CLC and late endosomal proteins. In order to better understand the inconsistency in localization studies, AMSH3-YFP/CLC-mKO-coexpressing lines were crossed with plants expressing *UBQ10pro:CFP(cyan fluorescent protein)-ARA7* (Figure 23C).

Analysis of colocalization frequencies in plants expressing AMSH3-YFP, CLC-mKO and CFP-ARA7 revealed that the AMSH3-YFP-positive compartments colocalized in 14.5% (n = 654) with both CLC-mKO and CFP-ARA7 (Figure 23A and D), suggesting a partial overlap between both endosomal markers. 40.4% of AMSH3-YFP signals colocalized only with CFP-ARA7, supporting the strong LE localization of AMSH3. 28.3% of AMSH3-YFP colocalized only with CLC-mKO and 16.8% with neither of the markers (Figure 23A and D). To verify the identity of the compartments on which AMSH3-YFP, CFP-ARA7 and CLC-mKO colocalize with each other, plants were treated with Wortmannin. As expected, CFP-ARA7 and AMSH3-YFP were present on ring-like WM compartments representing swollen MVBs. In some cases, also CLC-mKO signals appeared on these structures (Figure 23B), leading to the conclusion that CLC-mKO at least partially localizes on LEs, possibly as clathrin pits. Importantly, not all AMSH3-YFP signals relocalized to WM-induced compartments (Figure 23B), which suggests that AMSH3 is not exclusively a late endosomal protein and it also localizes to a smaller degree to CCVs, EE/TGN and other unknown compartments. Localization on different endosomal pools could suggest that AMSH3 plays multiple roles in intracellular trafficking.

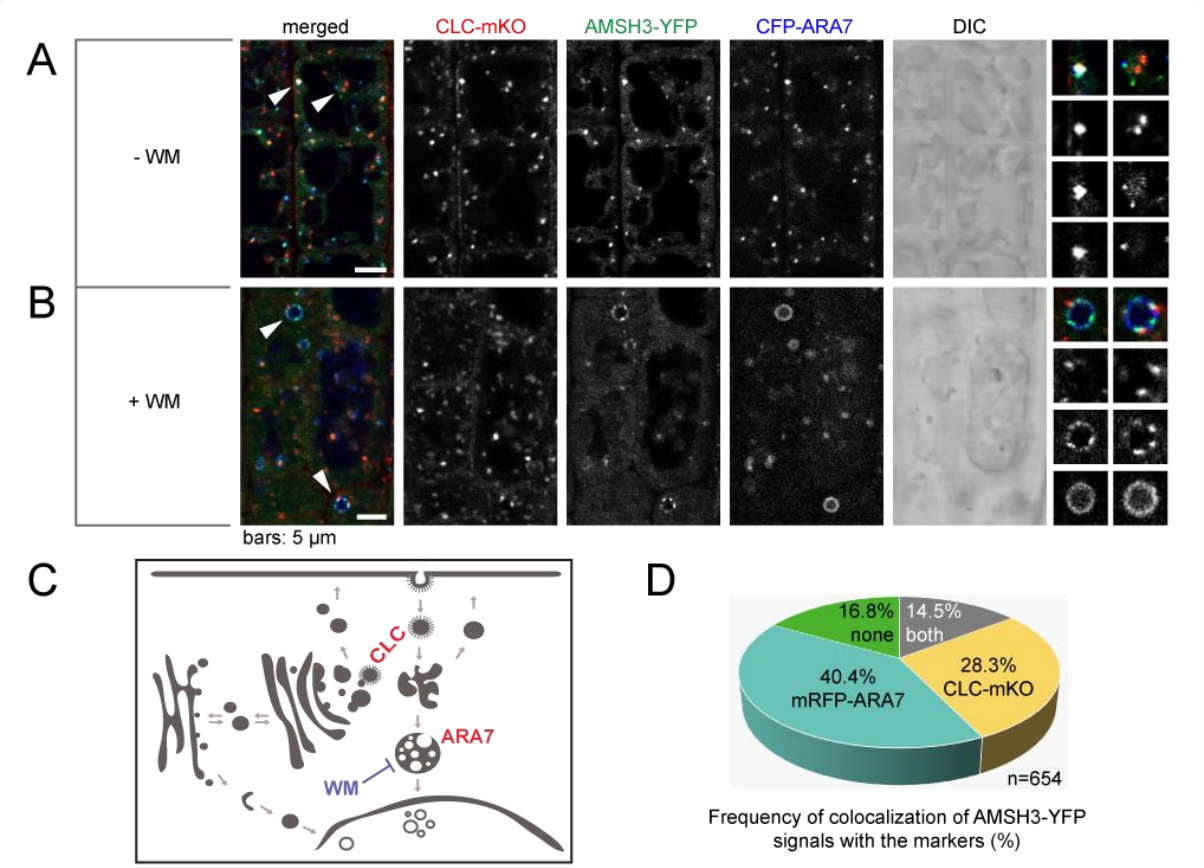

Figure 23. AMSH3, ARA7 and CLC partially colocalize on the same compartments.
(**A** and **B**) Seedlings coexpressing *AMSH3pro:AMSH3-YFP* and *CLCpro:CLC-mKO* were crossed with *UBQ10pro:CFP-ARA7*. Plants coexpressing all three fusion proteins were examined under the confocal microscope. Scale bar: 5 µm.
(**B**) Seedling coexpressing *AMSH3pro:AMSH3-YFP*, *CLCpro:CLC-mKO* and *UBQ10pro:CFP-ARA7* was treated with 33 µM WM (Wortmannin) for 120 min. Note that AMSH3-YFP and CFP-ARA7 clearly relocalized to WM-induced compartments. A few CLC-mKO-positive compartments were associated with WM-induced structures. Scale bar: 5 µm.
Magnifications of the areas indicated with white arrowheads are shown on the right side of panels **A** and **B** (from top to bottom: merged, CLC-mKO, AMSH3-YFP, CFP-ARA7).
(**E**) Scheme presenting the localization of CLC and ARA7, and the compartments affected by the WM treatment.
(**F**) Numbers of AMSH3-YFP-positive vesicles that colocalized with CFP-ARA7, CLC-mKO, with both, or with none of the markers were counted to calculate the colocalization frequency.

2.9. AMSH3 and ALIX colocalize on late endosomes

If ALIX functions together with AMSH3, both protein should at least partially localize on the same subcellular compartments. As described above, upon coexpression with enzymatically inactive SKD1(EQ), GFP-ALIX colocalized with AMSH3-TagRFP on aberrant endosomes in Arabidopsis protoplasts. Since the artificially induced conditions do not fully represent the situation in wild-type plants, the localization of GFP-ALIX *in planta* was examined. Lines expressing *ALIXpro:GFP-ALIX* (Cardona-Lopez et al., 2015) were crossed with plants expressing EE/TGN marker mRFP-SYP43, the CCV marker CLC-mKO and the LE marker mRFP-ARA7 (schemes in Figure 24D and 25E).

Similar to AMSH3-YFP, GFP-ALIX showed both the cytosolic distribution and localized on punctuate structures. 10.0% (n = 311) of the foci colocalized with mRFP-SYP43 (Figure 24A and E), suggesting a poor EE/TGN localization of GFP-ALIX. In addition, mRFP-SYP43 but not GFP-ALIX relocalized to BFA bodies upon the treatment with BFA (Figure 24B), supporting that GFP-ALIX does not localize to the EE/TGN pool sensitive to the inhibition of ER-to-Golgi trafficking. Interestingly, GFP-ALIX showed a very high colocalization rate with

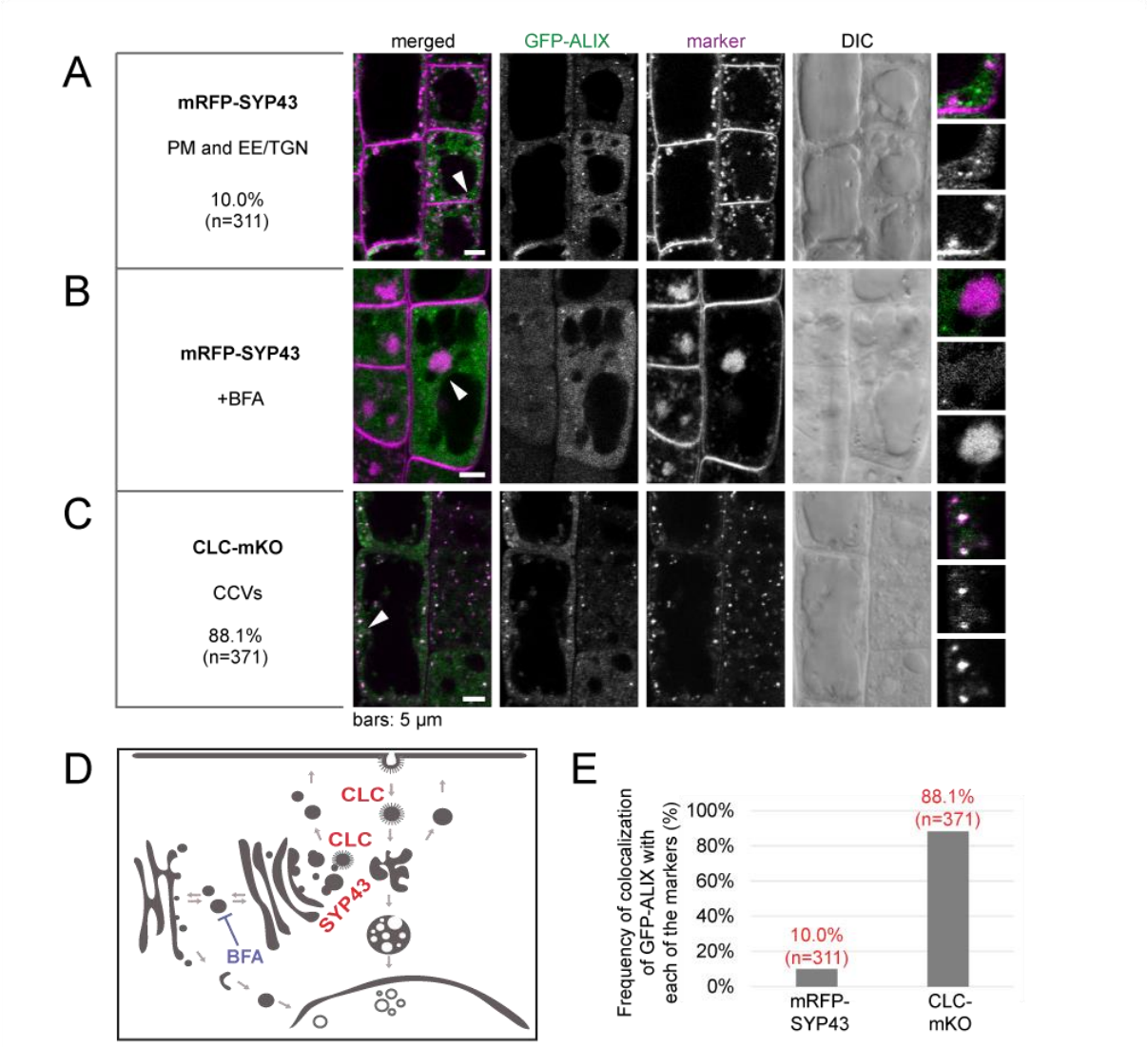

Figure 24. GFP-ALIX strongly localizes to clathrin-coated vesicles.
(**A** to **C**) Seedlings expressing *ALIXpro:GFP-ALIX* were crossed with either *SYP43pro:mRFP-SYP43* (**A**) or *CLCpro:CLC-mKO* (**C**). Plants coexpressing both fusion proteins were examined under the confocal microscope. PM: plasma membrane, EE/TGN: early endosomes/*trans*-Golgi network, CCVs: clathrin-coated vesicles. Scale bars: 5 µm.
(**C**) A GFP-ALIX/mRFP-SYP43-coexpressing seedling was treated with 50 µM BFA (Brefeldin A) for 60 min. Note that mRFP-SYP43 relocalized to BFA-induced bodies, whereas GFP-ALIX did not. Scale bar: 5 µm.
Magnifications of the areas indicated with white arrowheads are shown on the right side of panels **A** to **C** (from top to bottom: merged, GFP-ALIX, marker).
(**D**) Scheme presenting the localization of markers used in **A** to **C** and the compartments affected by BFA treatment.
(**E**) Numbers of GFP-ALIX-positive vesicles that colocalized with the mRFP- or mKO-tagged markers in **A** to **C** were counted to calculate the colocalization frequency.

CLC-mKO, 88.1% (n = 371) (Figure 24C and E). It can be therefore concluded that ALIX localizes mainly on CCVs.

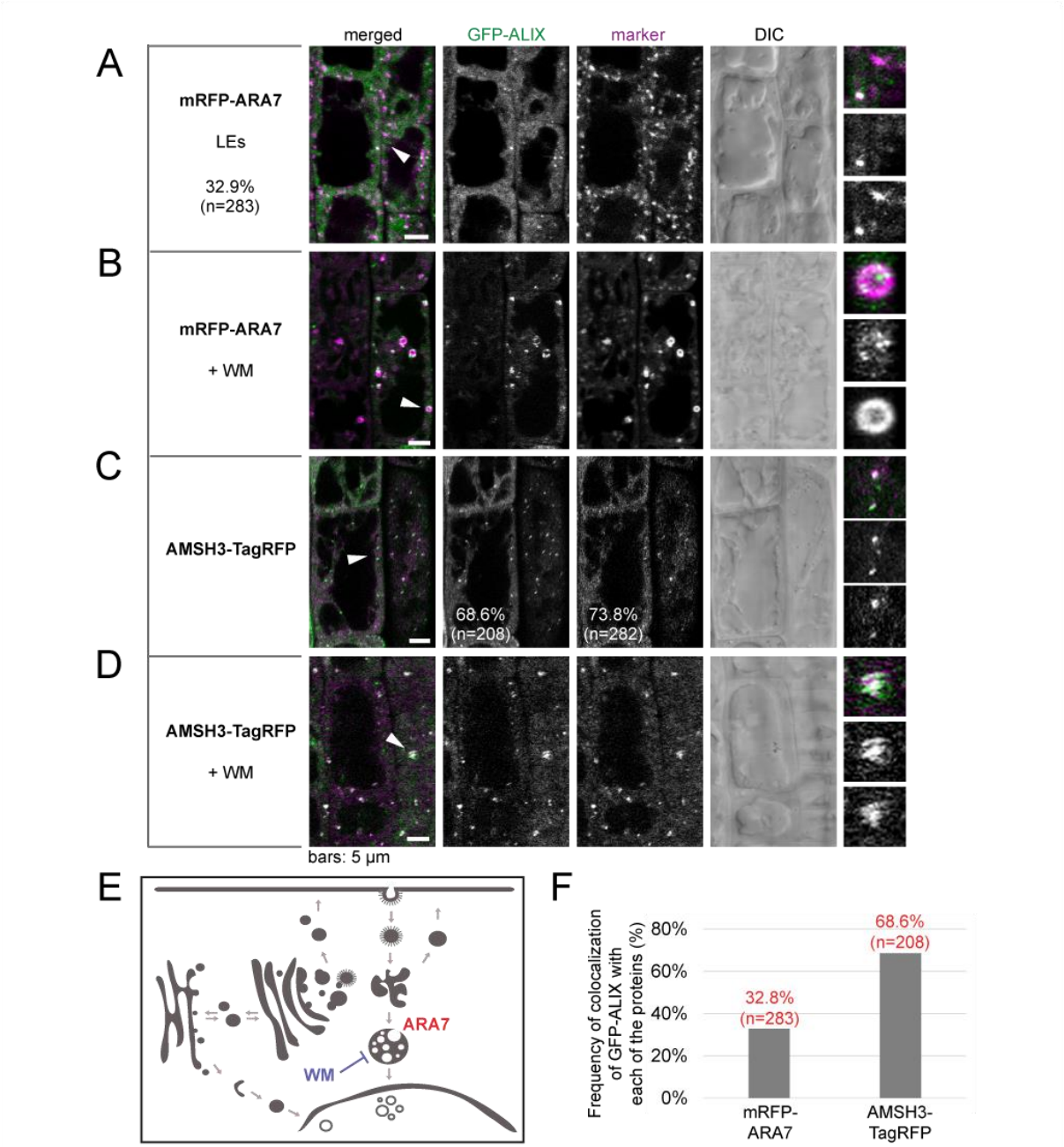

Figure 25. GFP-ALIX colocalizes with AMSH3-TagRFP on late endosomes.
(**A** to **D**) Seedlings expressing *ALIXpro:GFP-ALIX* were either crossed with *ARA7pro:mRFP-ARA7* (**A** and **B**) or transformed with *AMSH3pro:AMSH3-TagRFP* (**C** and **D**). Plants coexpressing the fusion proteins were examined under the confocal microscope. Scale bars: 5 µm.
(**B**) A GFP-ALIX/mRFP-ARA7-coexpressing seedling was treated with 33 µM WM (Wortmannin) for 120 min. Note that both GFP-ALIX and mRFP-ARA7 relocalized to WM-induced compartments.
Scale bar: 5 µm.
(**D**) A GFP-ALIX/AMSH3-TagRFP-coexpressing seedling was treated with 33 µM WM for 120 min. Note that both GFP-ALIX and AMSH3-TagRFP colocalize on WM-induced compartments. Scale bar: 5 µm.
Magnifications of the areas indicated with white arrowheads are shown on the right side of panels **A** to **D** [from top to bottom: merged, GFP-ALIX, mRFP-ARA7 (**A** and **B**) or AMSH3-TagRFP (**C** and **D**)].
(**E**) Scheme presenting the localization of ARA7 and the compartments affected by WM treatment.
(**F**) Numbers of GFP-ALIX-positive vesicles that colocalized with the mRFP- or TagRFP-tagged proteins in **A** to **D** were counted to calculate the colocalization frequency.

AMSH3-YFP was found to be mostly a late endosomal protein. It was therefore investigated whether GFP-ALIX would also localize to MVBs. 32.9% of GFP-ALIX-labelled vesicles (n = 283) showed colocalization with the LE marker mRFP-ARA7 (Figure 25A and F), which was nearly twice less than the colocalization rate between mRFP-ARA7 and AMSH3-YFP. After the Wortmannin treatment of GFP-ALIX/mRFP-ARA7-coexpressing lines, both fusion proteins relocalized to WM-induced compartments (Figure 25B). This confirms that a fraction of ALIX localizes to late endosomes, though smaller than of AMSH3-YFP. In conclusion, ALIX indeed seems to have a partially overlapping subcellular localization with AMSH3.

In order to test to which extend the localization of ALIX and AMSH3 overlap, GFP-ALIX-expressing plants were transformed with *AMSH3pro:AMSH3-TagRFP* (M.-K. Nagel). Similar to the YFP-tagged version, AMSH3-TagRFP showed both cytosolic and endosomal localization. 73.8% (n = 282) of AMSH3-TagRFP-positive compartments colocalized with GFP-ALIX and 68.6% (n = 208) of GFP-ALIX signals colocalized with AMSH3-TagRFP (Figure 25C and F). Both AMSH3 and ALIX were demonstrated to partially localize to EE/TGN, CCVs and LEs. To establish on which of these compartments both proteins colocalize, GFP-ALIX/AMSH3-TagRFP-coexpressing plants were treated with WM. Endosomes containing signals of both proteins swelled after the Wortmannin treatment (Figure 25D), corroborating that both proteins colocalize mainly on LEs.

In conclusion, the colocalization analyses of AMSH3-YFP and GFP-ALIX with endosomal markers revealed that both proteins show partially overlapping localization patterns. AMSH3 was demonstrated to localize mainly to late endosomes (Figure 22) and to compartments that contain clathrin (Figure 21B and F). Analysis of plants coexpressing AMSH3-YFP, CLC-mKO and the LE marker CFP-ARA7 revealed that 14.5% compartments contained all three fusion proteins (Figure 23A and D). In addition, CLC showed a moderate localization to Wortmannin-induced compartments, which suggests that a small fraction of clathrin resides on LEs (Figure 23B). On the other hand, a significant fraction of AMSH3-YFP colocalized with CLC and not with ARA7, pointing to the CCV localization of AMSH3 (Figure 23D). AMSH3-YFP colocalized very poorly with the EE/TGN marker mRFP-SYP43, suggesting that AMSH3 localizes very poorly to Golgi-derived EE/TGN (Figure 21A and F).

In contrast to AMSH3-YFP, GFP-ALIX colocalized only moderately with a late endosomal marker mRFP-ARA7 (Figure 25A and F). Instead, the majority of GFP-ALIX-positive compartments contained clathrin, pointing to a strong localization to CCVs (Figure 24C and E). Similar to AMSH3-YFP, the low colocalization rate with mRFP-SYP43 (10.0%) suggests a poor EE/TGN localization of GFP-ALIX (Figure 24A and E). Despite the differences

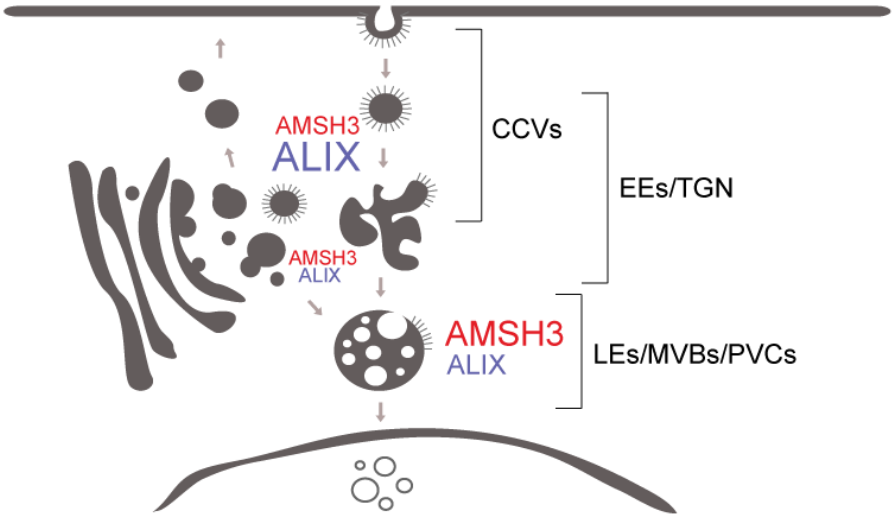

Figure 26. AMSH3 and ALIX show partially overlapping localization.
Colocalization analyses of AMSH3-YFP and GFP-ALIX with endosomal markers revealed that both proteins showed partially overlapping localization patterns. AMSH3 localized mainly to LEs/MVBs/PVCs (late endosomes/multivesicular bodies/prevacuolar compartments). It showed also a partial colocalization with a marker for CCVs (clathrin-coated vesicles) but localized very poorly to EEs/TGN (early endosomes/*trans*-Golgi network).
In contrast to AMSH3-YFP, GFP-ALIX colocalized only moderately with the LE marker mRFP-ARA7. On the other hand, most of GFP-ALIX-positive compartments contained clathrin, suggesting a strong localization to CCVs. Only a low colocalization frequency with EEs/TGN could be observed.
The font size of "AMSH3" and "ALIX" used in the scheme corresponds with colocalization rates with markers for specific compartments.

in localization patterns, AMSH3-TagRFP and GFP-ALIX showed around 70% colocalization frequency with each other (Figure 25C and F). The compartments positive for both proteins were sensitive to Wortmannin, which suggests that a significant fraction of them represents LEs (Figure 25D). The overall localization of AMSH3 and ALIX is summed up in Figure 26.

Endosomal localization of proteins often correlates with their function in endocytic trafficking. AMSH3 was previously demonstrated to be essential for proper endocytic degradation and the *amsh3* knockout mutants are deficient in several intracellular trafficking pathways (Isono et al., 2010; Katsiarimpa et al., 2014). The endosomal localization of ALIX and its interaction with the ESCRT-III subunit SNF7 and AMSH3 might suggest that it also functions in endocytic trafficking in Arabidopsis.

2.10. ALIX and AMSH3 interact with each other through middle domains

ALIX and AMSH3 interact with each other directly and colocalize on endosomal compartments. Both were also demonstrated to bind to ESCRT-III, but to other core subunits. I was therefore interested whether there is an overlap between the domains within AMSH3 and ALIX serving for binding to ESCRTs and to each other. Both proteins could in example

compete with ESCRT-III for binding to each other, thus regulating each other's function. Alternatively, ALIX might bind to the catalytic domain of AMSH3 and affect its activity.

A targeted Y2H analysis was conducted to identify the ALIX-binding domain within AMSH3 sequence. The N-terminus of AMSH3 contains the MIT domain that serves for interaction with subunits of ESCRT-III (Katsiarimpa et al., 2011). The middle region of AMSH3 is poorly conserved and its function is still unknown. AMSH3 lacks three functional domains reported for human AMSH/STAMBP, namely the nuclear localization signal, STAM-binding motif and clathrin-binding domain. The C-terminus carries the catalytic MPN+ domain that provides AMSH3 with a zinc-dependent protease activity (Figure 9) (Isono et al., 2010).

In order to verify which of these motifs interacts with ALIX, different deletion constructs of GAD-fused AMSH3 were generated and used for Y2H interaction studies against ALIX (Figure 27A). The results of Y2H analysis implicated that neither the MIT- nor the MPN+ domain of AMSH3 were required for the interaction with ALIX (Figure 27B and C). This suggests that ALIX probably does not compete with ESCRT-III subunits for binding to the MIT domain of AMSH3 nor does it directly interfere with the catalytic domain of AMSH3. The uncharacterized middle region of AMSH3 did not interact with ALIX, and neither did smaller fragments of this region (data not shown). However, an extended middle region, containing

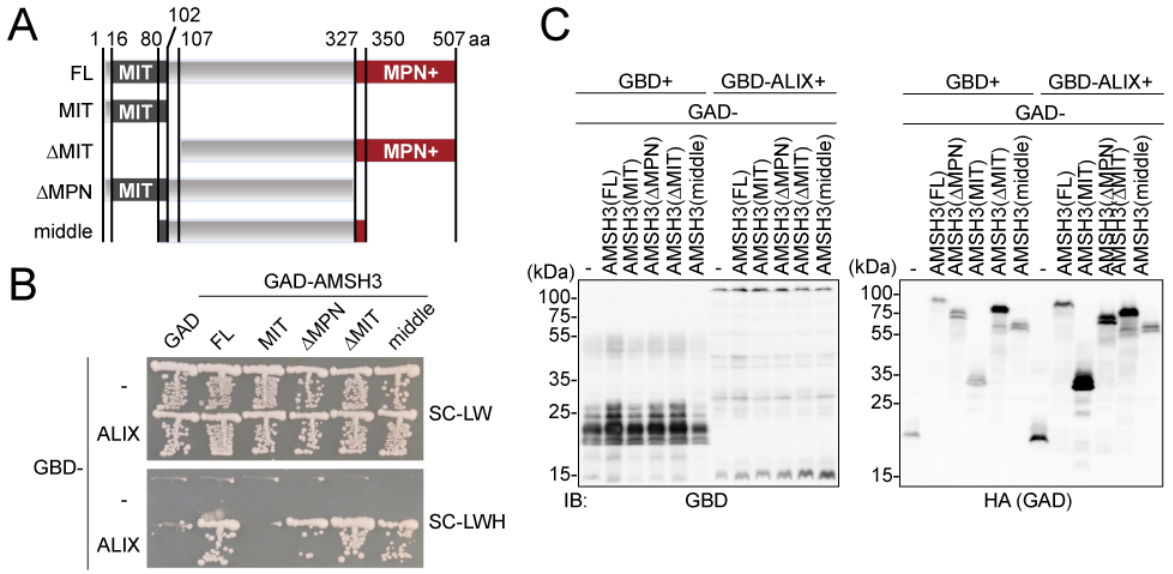

Figure 27. The middle region of AMSH3 interacts with ALIX.
(**A**) AMSH3 constructs used for domain analysis in Y2H interaction studies shown in **B**. FL: full-length; MIT: MIT domain; MPN+: MPN+ domain; aa: amino acid.
(**B**) GAD-fused full-length- or fragments of AMSH3 were cotransformed in yeast with either GBD or GBD-ALIX. Transformants were tested for the auxotrophic growth on SC-LW (synthetic complete medium lacking leucine and tryptophan) and SC-LWH (synthetic complete medium lacking leucine, tryptophan, and histidine). GAD: Gal4 activation domain; GBD: Gal4 binding domain.
(**C**) Expression of the Y2H clones shown in **B**. Yeast total extracts were prepared from transformants and subjected to immunoblotting using an anti-GBD antibody to detect GBD-fusion proteins and an anti-HA antibody to detect the GAD-HA-fusion proteins.

ca. 20 additional amino acids of both N- and C-terminal domains (“middle”), was sufficient and essential for the interaction with ALIX (Figure 27B and C). This result could imply that multiple motifs within AMSH3 interact with ALIX, situated mainly within its middle part, but probably also within MIT and MPN+ domains.

A Pfam database search (Finn et al., 2014) showed that ALIX contains an N-terminal BRO1 (BCK1-like resistance to osmotic shock 1)-like domain followed by a V-domain (V-shaped domain) and a C-terminal PRD (proline-rich domain) (Figure 28A). To identify the region in ALIX that is responsible for binding to AMSH3, Y2H interactions between GDB-fused ALIX fragments and the full-length wild-type GAD-AMSH3 were tested. Both the BRO1-like domain and the C-terminal region of ALIX turned out dispensable for the interaction, suggesting that the V-domain could function in AMSH3-binding (Figure 28B and C). A further

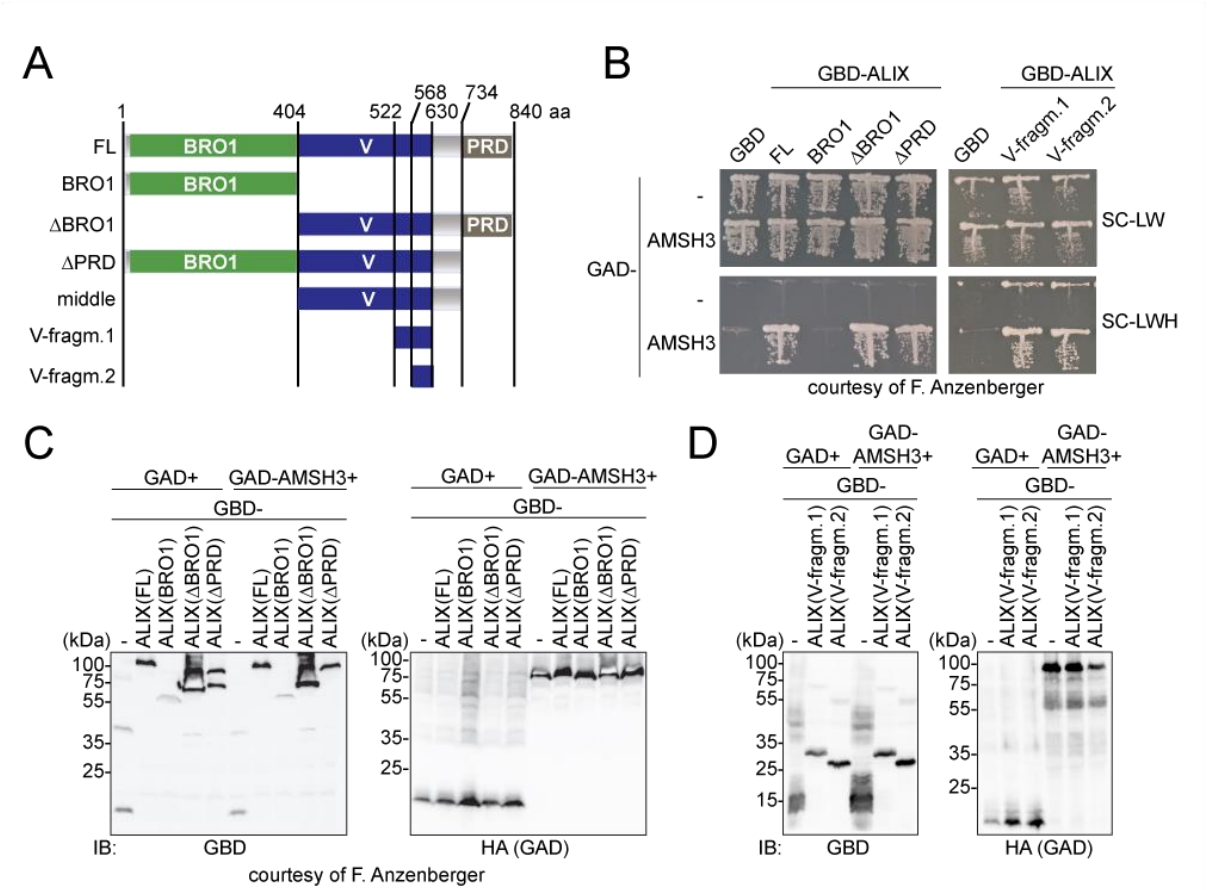

Figure 28. ALIX interacts with AMSH3 through the V-domain in Y2H assays.
(A) ALIX constructs used for domain analysis in Y2H interaction studies and in further assays. FL: full-length; BRO1: BRO1 domain; PRD: Proline-rich domain; V: V-shaped domain; V-fragm. 1/2: V-domain fragment 1/2; aa: amino acid.
(**B**) GBD-fused FL or fragments of ALIX were cotransformed in yeast with either GAD or GAD-AMSH3. Transformants were tested for the auxotrophic growth on SC-LW (synthetic complete medium lacking leucine and tryptophan) and SC-LWH (synthetic complete medium lacking leucine, tryptophan, and histidine). GAD: Gal4 activation domain; GBD: Gal4 binding domain.
(**C** and **D**) Expression of the Y2H clones shown in **B**. Yeast total extracts were prepared from transformants and subjected to immunoblotting using an anti-GBD antibody to detect GBD-fusion proteins and an anti-HA antibody to detect the GAD-HA-fusion proteins.

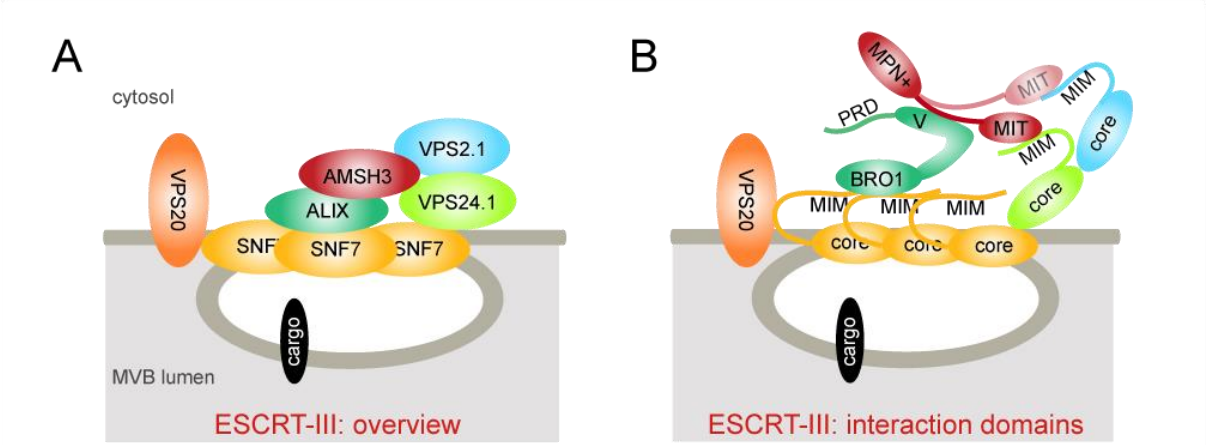

Figure 29. AMSH3 and ALIX interact with ESCRT-III and each other through distinct binding motifs. **(A)** A general scheme scheme presenting interactions between ESCRT-III core subunits and ESCRT-associated proteins AMSH3 and ALIX. ALIX binds to SNF7 and AMSH3, whereas AMSH3 can interact with VPS2.1, VPS24.1 and ALIX. MVB: multivesicular body.
(**B**) A scheme presenting interaction domains between ESCRT-III subunits and the ESCRT-III-associated proteins AMSH3 and ALIX. The N-terminal BRO1 (Bck1p-like resistance to osmotic shock 1) domain of ALIX binds to the carboxy-terminal MIM (MIT-interacting motif) of SNF7. AMSH3 interacts with the carboxy-terminal part of the V-domain (V-shaped domain) of ALIX through its middle region. The amino-terminal MIT (microtubule-interacting and trafficking) domain of AMSH3 can bind to the MIMs of either VPS24.1 or VPS2.1.

analysis using deletion fragments of the V-domain of ALIX revealed that the small 62-aa fragment within the C-terminal part of the V-domain ("V-fragm.2") is essential and sufficient for the interaction with AMSH3 (Figure 28B and D).

The Arabidopsis ALIX was previously demonstrated to interact with ESCRT-III subunits SNF7.1 and SNF7.2 through its N-terminal BRO1 domain (Cardona-Lopez et al., 2015). It is therefore possible that ALIX interacts with ESCRT through the BRO1 domain and with AMSH3 through the V-domain at the same time (Figure 29A and B). Similarly, AMSH3 could bind to ESCRT-III subunits VPS2.1 and VPS24.1 through its N-terminal MIT domain and to ALIX through its middle region (Figure 29A and B). Both AMSH3 and ALIX bind to distinct ESCRT-III core subunits, so they probably do not compete or block each other from interaction with ESCRT-III. However, it cannot be excluded that binding to one another induces structural changes that facilitate or decrease their affinity towards ESCRT-III, or opposite, interaction with ESCRT components could affect the binding between AMSH3 and ALIX.

2.11. The V-domain of ALIX interacts with AMSH3 and monoubiquitin

The results obtained in the Y2H interaction analysis were further verified by the *in vitro* pulldown assay. The full-length AMSH3 bound to the MBP-tagged middle domain of ALIX and not to MBP-VPS60.1 (negative control) (Figure 30A), proving that the V-domain of ALIX is the

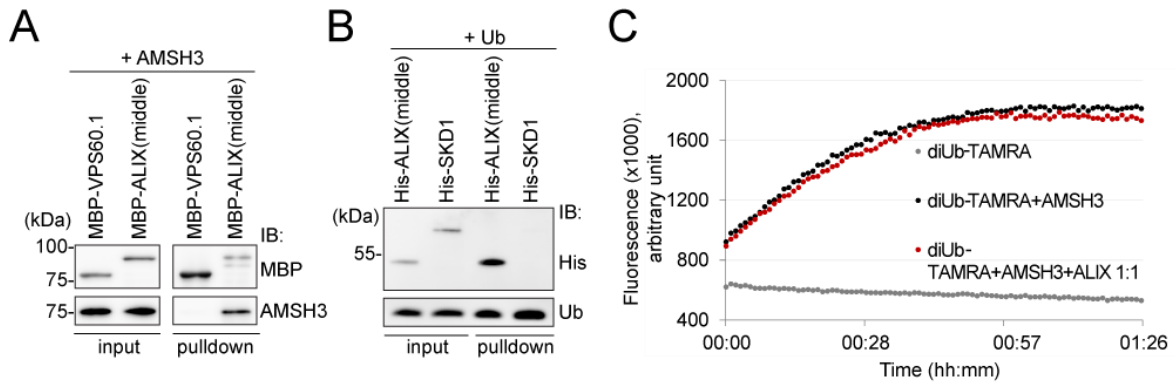

Figure 30. ALIX binds to AMSH3 and monoubiquitin through the V-domain.
(**A**) ALIX interacts directly with AMSH3 through the V-domain. Recombinant AMSH3 was incubated with either MBP-ALIX(middle) or MBP-VPS60.1 (negative control) for 1 h at 4°C, and was subjected to immunoblot analysis after extensive washing. Anti-AMSH3 and anti-MBP antibodies were used to detect bead-retained material.
(**B**) ALIX binds to monoubiquitin through the V-domain. A recombinant His-ALIX(middle) fragment containing the V-domain or His-SKD1 (negative control) were incubated with monoubiquitin agarose. After extensive washing, the eluate was analyzed by immunoblotting using anti-His and anti-Ub (ubiquitin) antibodies.
(**C**) ALIX does not affect AMSH3 DUB activity. Fluorescence-based DUB assay using K63-linked diUb-TAMRA (diubiquitin-TAMRA). Recombinant AMSH3 was incubated with diUb-TAMRA with or without preincubation with an equimolar amount of His-ALIX(middle). Reaction was run for 90 minutes and the fluorescence was measured every minute. Black: diubiquitin-TAMRA with AMSH3; red: diubiquitin-TAMRA with AMSH3 and His-ALIX(middle); gray: diubiquitin-TAMRA alone.

interaction motif for AMSH3. *In vitro* binding assays with the smallest interacting region of the V-domain of ALIX could not be conducted due to the lack of expression of the recombinant "V-fragment 2" in *E. coli* strains (data not shown).

The V-domain of the yeast Bro1p and human ALIX was shown to mediate their interaction with ubiquitin (Joshi et al., 2008; Dowlatshahi et al., 2012; Keren-Kaplan et al., 2013; Pashkova et al., 2013). The amino acid sequence homology of the Arabidopsis ALIX V-domain is rather low in comparison to other kingdoms (25% amino acid identity with the human ALIX and 17% with Bro1p). Moreover, the amino acid residues that were shown to be essential in either Bro1p (Pashkova et al., 2013) or human ALIX (Keren-Kaplan et al., 2013) for interaction with ubiquitin are very poorly conserved in the Arabidopsis ALIX. It was therefore interesting to test whether it can also bind to ubiquitin. For this purpose, an *in vitro* ubiquitin-binding assay was conducted using ubiquitin agarose and a recombinant His-ALIX(middle). His-SKD1 served as a negative control in this assay. His-ALIX(middle), but not the His-SKD1, interacted with monoubiquitin (Figure 30B), suggesting that the ability of the ALIX V-domain to bind ubiquitin is conserved also in Arabidopsis. These results demonstrate that despite low sequence homology, different Bro1p/ALIX homologs retained similar properties in different kingdoms.

The activity of DUBs can be affected by their interaction with other proteins. The human homolog of AMSH3, AMSH/STAMBP, was shown to be activated upon binding to the ESCRT-

0 subunit STAM (Kim et al., 2006; McCullough et al., 2006). As plants do not have an obvious homolog of STAM, ALIX might be the protein that can regulate AMSH3 activity in Arabidopsis. To test this hypothesis, DUB assays using the recombinant untagged full-length AMSH3 in the presence or absence of His-ALIX(middle) were conducted. The K63-linked diUb-TAMRA (lysine 63-linked diubiquitin-5-carboxytetramethylrhodamine) was used as substrate. In fluorescence-based DUB assays, the cleavage of diubiquitin to monoubiquitin separates the quencher from the fluorophore resulting in the increase in fluorescence of the sample. The recombinant AMSH3 readily catalyzed this reaction, however, preincubation with the equimolar amount of His-ALIX(middle) did not affect the AMSH3 enzyme kinetics (Figure 30C) and neither did other amounts of ALIX (data not shown). These results suggest that despite binding to AMSH3 and to ubiquitin, ALIX does not influence the DUB activity of AMSH3 towards K63-linked diubiquitin. Hence, ALIX association with ESCRT-III probably does not serve to regulate AMSH3 activity during endocytic sorting.

2.12. *alix* null mutants are seedling lethal

AMSH proteins were previously demonstrated to be essential for proper plant growth and development. *amsh3-1* knockout mutants are seedling lethal and show a number of defects in intracellular trafficking pathways, whereas *amsh1-1* knockdown mutants are impaired in autophagic degradation (Isono et al., 2010; Katsiarimpa et al., 2013; Katsiarimpa et al., 2014). To investigate whether the same biological pathways are affected in *alix*, available T-DNA insertion lines of *ALIX* were analyzed. Two lines, GABI 837H11 and SALK 063124 (Columbia-0 ecotype), which were named *alix-2* and *alix-4*, respectively, carried T-DNA insertions within exons (Figure 31A). Homozygous *alix-2* and *alix-4* mutants showed reduced germination

Table 1. *alix-2* and *alix-4* show seedling lethality in the germination assay.

	Phenotype of the progeny				
Genotype of the parental line	**WT-looking**	**Seedling lethal**	**Ungerminated**	**Seedling lethal and ungerminated**	**n**
WT (Col-0)	100.0%	0.0%	0.0%	0.0%	424
alix-2 (het)	83.2%	11.9%	4.9%	16.8%	405
alix-4 (het)	77.0%	9.5%	13.5%	23.0%	400

The germination assay using het (heterozygous) *alix-2* and *alix-4* parental lines. Arabidopsis seeds were sterilized using calcium hypochlorite and plated on growth medium containing 1% (w/v) sucrose. Seeds were stratified at 4°C in the dark for 5 days and placed to 21°C and long day for 7 days. WT (wild type) Col-0 (Columbia-0) was used as control.

compared to the wild type (Col-0, Columbia-0) (Table 1), and even if germinated, did not develop beyond the seedling stage (Table 1 and Figure 31B and C). The seedling growth arrest phenotype of *alix-2* and *alix-4* suggests that ALIX is essential in Arabidopsis. Moreover, the previously characterized *amsh3* mutants were also seedling lethal (Figure 32C) (Isono et al., 2010), further proving that AMSH3 and ALIX function in the same biological processes leading to identical defects in growth and development.

To establish whether *alix-2* and *alix-4* are knock-down or knockout mutants, an anti-ALIX antibody was raised in rabbits using the recombinant His-ALIX(middle) as antigen. An immunoblot on wild-type and homozygous *alix-2* and *alix-4* seedlings was conducted. In wild type, a band at the height of ~100 kDa was detected, probably corresponding to the endogenous ALIX. No such band could be observed for *alix-2* and *alix-4* homozygous mutants, suggesting they are null mutants (Figure 31D).

To verify that the seedling lethal phenotype is caused by the loss of ALIX function, heterozygous *alix-2* and *alix-4* plants were crossed with each other and the F1 progeny was analyzed. The transheterozygous (*alix-2*/*alix-4*) F1 progenies showed the same seedling growth arrest phenotype as homozygous *alix-2* and *alix-4* mutants (Figure 31E and F), indicating that *alix-2* is allelic to *alix-4*. To further establish that the phenotype of *alix* null mutants is a result of the lack of *ALIX* expression, *alix-2* was crossed with *ALIXpro:GFP-ALIX*. The seedling lethality of homozygous *alix-2* could be complemented by the *ALIXpro:GFP-ALIX* construct (Figure 31G and H), confirming that *ALIX* is the causative gene for the *alix* mutant phenotype. Altogether, these results indicate that ALIX is essential in Arabidopsis and that depletion of *ALIX* causes seedling growth arrest.

2.13. *alix* shows defects in endocytic degradation and vacuole morphology

AMSH3 was previously implicated in the degradation of ubiquitinated membrane proteins, which depends on its interaction with ESCRT-III (Isono et al., 2010; Katsiarimpa et al., 2011; Katsiarimpa et al., 2014). ALIX is a direct interactor of AMSH3, it colocalizes with AMSH3 on endosomes and associates with ESCRT-III. To verify whether ALIX is also important for ubiquitin-dependent endocytic degradation, total extracts from wild-type, *alix-4* and *alix-2* seedlings were analyzed on immunoblot using an anti-ubiquitin antibody. *alix* mutants showed high levels of ubiquitinated proteins in comparison to the wild type (Figure 32A), confirming that ALIX plays role in ubiquitin-dependent degradation.

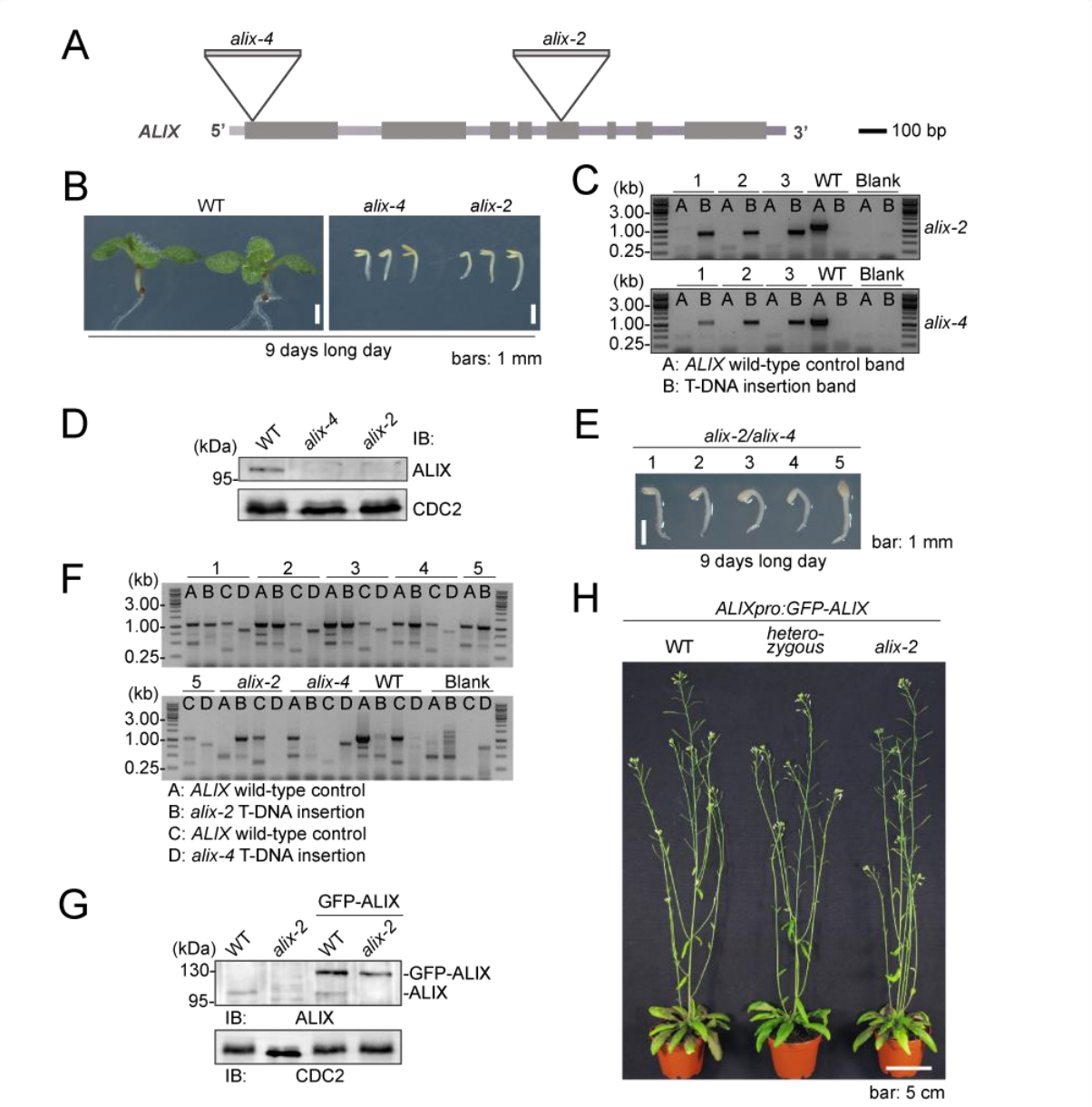

Figure 31. *alix* null mutants show seedling lethality.
(**A**) Schematic presentation of the T-DNA insertion sites of *alix-2* and *alix-4*. Lines indicate introns and gray boxes indicate exons. Scale bar: 100 bp.
(**B**) Phenotypes of 9-day-old WT (wild-type), *alix-4* and *alix-2* seedlings. Scale bars: 1 mm.
(**C**) Genotyping PCR of *alix-2* and *alix-4* mutants. A: *ALIX* wild-type control band; B: T-DNA insertion band.
(**D**) *alix-2* and *alix-4* are null mutants. Total extracts from seedlings shown in **B** were subjected to immunoblot analysis, using an anti-ALIX antibody. CDC2 was used as loading control.
(**E**) *alix-2* and *alix-4* are allelic to each other. Phenotypes of 9-day-old *alix-2/alix-4* transheterozygous seedlings are shown. Scale bar: 1 mm.
(**F**) Genotyping PCR of *alix-2/alix-4* transheterozygous seedlings. A: *ALIX* wild-type control band; B: *alix-2* T-DNA insertion band; C: *ALIX* wild-type control band; D: *alix-4* T-DNA insertion band.
(**G** and **H**) Complementation of *alix-2* with *ALIXpro:GFP-ALIX.*
(**G**) Immunoblot analysis of total extracts from WT (wild type) and *alix-2*, with and without the *ALIXpro:GFP-ALIX* construct using an anti-ALIX antibody. Positions of endogenous ALIX and GFP-ALIX are indicated on the right side of the panel. CDC2 was used as loading control.
(**H**) *ALIXpro:GFP-ALIX* complements seedling lethality of *alix-2*. WT (wild-type), heterozygous and homozygous *alix-2* plants expressing GFP-ALIX were grown for 6 weeks in long-day conditions. Note that the GFP-ALIX/*alix-2* plants show normal growth. Scale bar: 5 cm.

amsh1-1 knock-down mutants are impaired in autophagic degradation (Katsiarimpa et al., 2013). Also *amsh3-1* mutants show increased levels of the autophagy marker ATG8 and accumulate autophagosomes within cytosol (Isono et al., 2010). ALIX is an interactor of AMSH1 and AMSH3, and *alix* null mutants phenocopy *amsh3* in seedling morphology and defects in intracellular trafficking. To test whether *alix-4* and *alix-2* are impaired in autophagic degradation in a similar way to *amsh3-1* and *amsh1-1*, an immunoblot using antibodies against autophagy-related markers ATG8 and NBR1 was conducted. The immunoblot analysis revealed that ATG8 accumulated in *alix-4* and *alix-2*, similarly to the autophagy-defective mutant *atg7-2* (Figure 32B) and *amsh* mutants (Isono et al., 2010; Katsiarimpa et al., 2013), suggesting that *alix* mutants are also impaired in autophagic degradation. NBR1 is a marker specific for selective autophagy that acts as a cargo adaptor protein (Svenning et al., 2011). To test whether *alix* mutants are defective also in selective autophagy, an immunoblot using anti-NBR1 antibody was conducted. Similar to ATG8, NBR1 accumulated at high levels in *alix* mutants and in the autophagy-defective *atg7-2* (Figure 32B), suggesting that ALIX might be important for both selective and nonselective autophagy pathways in Arabidopsis.

Many components of the ESCRT machinery and ESCRT-associated proteins were identified in yeast genetic screens for mutants with aberrant vacuoles (Banta et al., 1988; Raymond et al., 1992), proving that defects in vacuolar protein sorting are often accompanied by abnormal vacuolar morphology. Also in plants, overexpression of the dominant-negative AAA ATPase SKD1 was found to lead to fragmentation and disappearance of vacuoles during trichome development (Shahriari et al., 2010). Moreover, *amsh3* null mutants were previously reported to lack large central vacuoles typical for plant tissues and to contain instead numerous small vacuole-like structures filling the cytosol (Isono et al., 2010).

To examine if *alix* null mutants show the same phenotype, wild-type, *alix-4* and *amsh3-1* seedlings were incubated with BCECF-AM [2′,7′-bis-(2-carboxyethyl)-5-(and-6)-carboxyfluorescein-acetoxymethyl ester], a dye staining vacuolar lumen in a pH-dependent manner. As the vacuole phenotype depends on the developmental stage of the plant, 2-day-old wild-type seedlings were chosen as control for these experiments, due to their similar morphology to *alix* and *amsh3* null mutants (Figure 32C). The confocal analysis of BCECF-AM-stained wild-type and mutant vacuoles revealed that *alix* mutants similar to *amsh3* lack the central vacuole and instead contain multiple small structures, indicating that ALIX together with AMSH3 is necessary for the proper vacuole biogenesis (Figure 32D).

To analyze the vacuolar structure in *alix* and *amsh3* in more detail, a 3D reconstruction analyses on Z-stack images of BCECF-AM-stained wild-type and mutant vacuoles were conducted. Surface rendering revealed that instead of many small vacuoles filling the cytosol,

both mutants had one vacuole of an abnormal shape, consisting of tubular interconnected structures (Figure 32E). These results further confirmed that ALIX and AMSH3 function in the

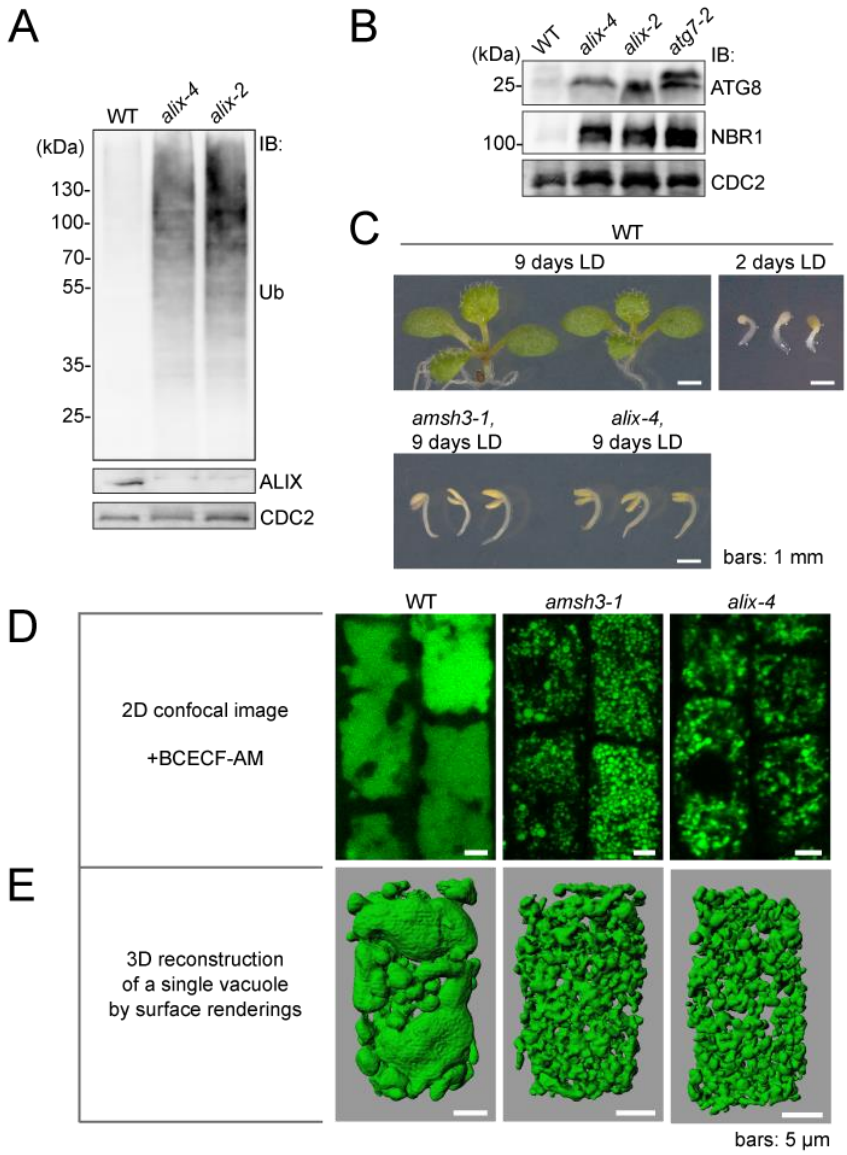

Figure 32. *alix* is impaired in endocytic and autophagic degradation, and shows an aberrant vacuole morphology.

(**A**) *alix* mutants accumulate Ub (ubiquitin) conjugates. Total extracts from WT (wild-type), *alix-4* and *alix-2* seedlings were subjected to immunoblot using an anti-Ub antibody. CDC2 was used as loading control.

(**B**) *alix* accumulates autophagy markers. Total extracts from wild-type (WT), *alix-4*, *alix-2* and *atg7-2* seedlings grown under long-day conditions were subjected to immunoblot analysis using anti-NBR1 and anti-ATG8 antibodies. CDC2 was used as loading control.

(**C**) Phenotypes of 9-day-old WT (wild-type), *alix-4*, *amsh3-1* and 2-day-old WT seedlings. Note the resemblance of the developmental stage of the 2-day-old wild type to the 9-day-old *alix-4* and *amsh3-1*. Scale bars: 1 mm. LD: long day.

(**D** and **E**) Vacuole morphology of wild type, *amsh3-1* and *alix-4* mutants.

(**D**) Vacuoles of 2-day-old WT, and 9-day-old *alix-4* and *amsh3-1* seedlings shown in (**C**) were stained with BCECF-AM and analyzed under the confocal laser scanning microscope. Vacuoles in the root epidermis cells are shown. Scale bars: 5 µm.

(**E**) 3D surface renderings of vacuoles from a representative root epidermal cell of 2-day-old WT and 9-day-old *alix-4* and *amsh3-1* seedlings. Z-stack images were processed to generate the 3D reconstruction pictures of vacuoles. Views from the front are shown. Note the tubular appearance of vacuoles in *alix-4* and *amsh3-1*. Scale bars: 5 µm.

same pathway that controls vacuole phenotype, either through vacuole biogenesis or the maintenance of its structure. It is possible that the disruption of vacuolar function in these mutants causes accumulation of ubiquitinated proteins and autophagosome markers. On the other hand, defective endocytic or autophagic trafficking might also lead to aberrant vacuolar biogenesis or maintenance. It would be interesting for the future to elucidate which phenotypes observed in *amsh3* and *alix* are primary- and which are secondary defects.

2.14. Depletion of *ALIX* leads to aberrant root morphology and leaf chlorosis

alix knockout mutants resemble *amsh3-1* in seedling lethality, defects in endocytic and autophagic degradation, as well as in aberrant vacuole morphology. Interestingly, observation under the confocal microscope revealed the presence of irregularities in root tip morphology in *alix*, a phenotype never observed in *amsh3-1* mutants. To better characterize the root morphology of *alix*, 2-day-old wild-type seedlings together with *alix-2* and *amsh3-1* were analyzed under the SEM (scanning electron micrograph). *alix-2* mutants, but not *amsh3-1* or wild type, showed disorganized root cell files as seen in Figure 33A. These results might point to a possible role of ALIX in cell divisions during the root development, which could be independent of AMSH3 function.

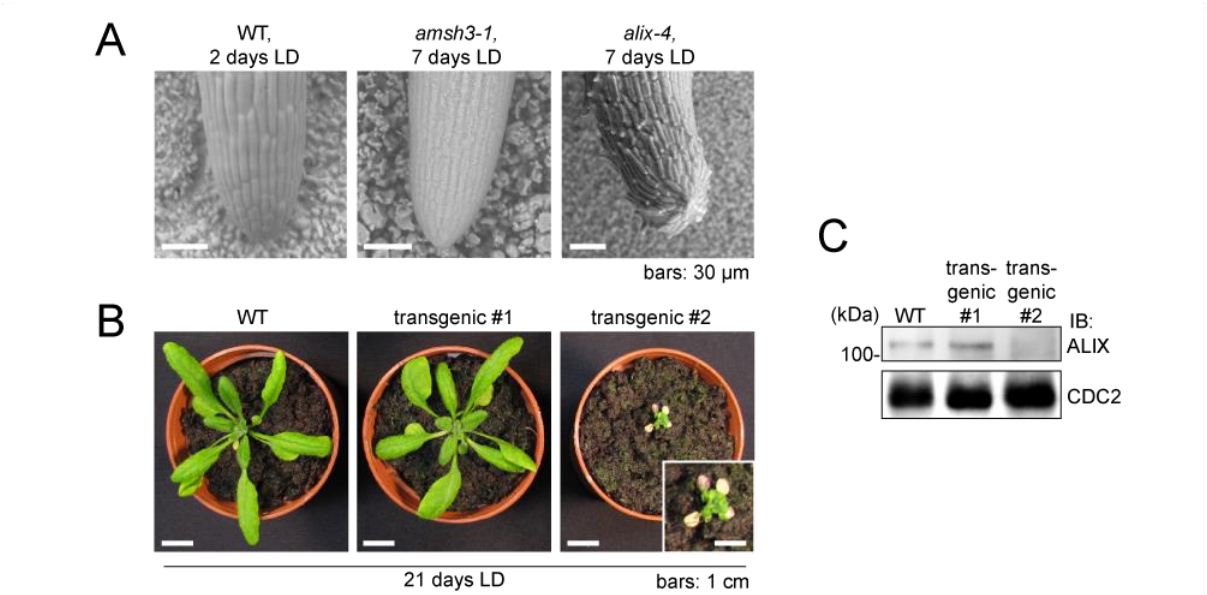

Figure 33. Loss of *ALIX* causes aberrant root tip phenotype and leaf chlorosis.
(**A**) Root morphology of WT (wild type), *amsh3-1* and *alix-4*. Seedlings were grown in LD (long day) for 2- (WT) or 7 days (*amsh3-1* and *alix-4*). Scanning electron micrographs were obtained of WT, *amsh3-1* and *alix-4* root tips. Scale bars: 30 µm.
(**B**) Pictures of 3-week-old WT and two transgenic plants (transgenic #1 and transgenic #2) harboring *35Spro:ALIX*. Note that transgenic #2 shows severe growth defects and leaf chlorosis (magnification in inset). Scale bars: 1 cm. LD: long day.
(**C**) Total extracts from rosetta leaves of plants shown in **B** were subjected to immunoblot analysis using an anti-ALIX antibody. CDC2 was used as loading control. Note that transgenic #2 shows dramatically reduced levels of ALIX.

To further understand the involvement of *ALIX* in Arabidopsis growth and development, the effect of ectopic expression of *ALIX* on plants was investigated. For this, plants harboring the untagged *35Spro:ALIX* were generated. Surprisingly, transgenic T1 plants showed no overexpression of the transgene, but instead had similar or dramatically decreased protein levels of ALIX in comparison to wild-type plants (Figure 33C). Transgenic plants with normal ALIX levels had wild-type phenotype, whereas the plants with strongly reduced amounts of ALIX were dwarfish and displayed leaf chlorosis (Figure 33B). Such phenotypes are often linked to defects in autophagy, hormonal deregulation or reaction to stress (Hanaoka et al., 2002; Yoshimoto, 2010; Vogelmann et al., 2012; Xie et al., 2015), suggesting a possible function of ALIX in some of these processes.

The analysis of plants depleted of *ALIX* suggests that ALIX is indispensable for proper plant growth and development not only in early stages during seedling development, but also in adult plants, controlling their vegetative growth.

2.15. The localization of AMSH3 on ARA7-labeled vesicles is affected in *alix*

ALIX is an ESCRT-III associated adaptor protein that is required for proper plant growth and development. ALIX can interact with AMSH3 but does not affect its enzyme activity. The homolog of ALIX in budding yeast, Bro1p, can bind to Doa4p, a UBP/USP-family deubiquitinase unrelated to AMSH. It was demonstrated that though Doa4p can interact with the ESCRT-III subunit Vps20p, Bro1p is indispensable for the recruitment of Doa4p to MVBs (Luhtala and Odorizzi, 2004; Nikko and Andre, 2007; Richter et al., 2013). The Arabidopsis MPN-family DUB AMSH3 interacts with ESCRT-III core components VPS2.1 and VPS24.1 (Katsiarimpa et al., 2011). As ALIX can bind to both AMSH3 and ESCRT-III, it is possible that ALIX could regulate the association of AMSH3 with endosomes.

To test this hypothesis, the colocalization of AMSH3-YFP with the LE marker mRFP-ARA7 was analyzed in *alix-2* mutant background. As shown in this study, in wild-type seedlings AMSH3-YFP localized to cytosol and to endosomes that contained mRFP-ARA7. Interestingly, in *alix* mutant background, AMSH3-YFP signals became almost completely cytosolic, whereas mRFP-ARA7 still localized on punctuate structures. To confirm this observation, the number of vesicles per area for mRFP-ARA7- and AMSH3-YFP was scored. mRFP-ARA7-containing endosomes did not show a big difference in frequency between the wild-type and the mutant background (Figure 34A, C and E). In contrast, there were over 25 times less AMSH3-YFP-positive compartments in *alix* than in the wild type (Figure 34A, C and E).

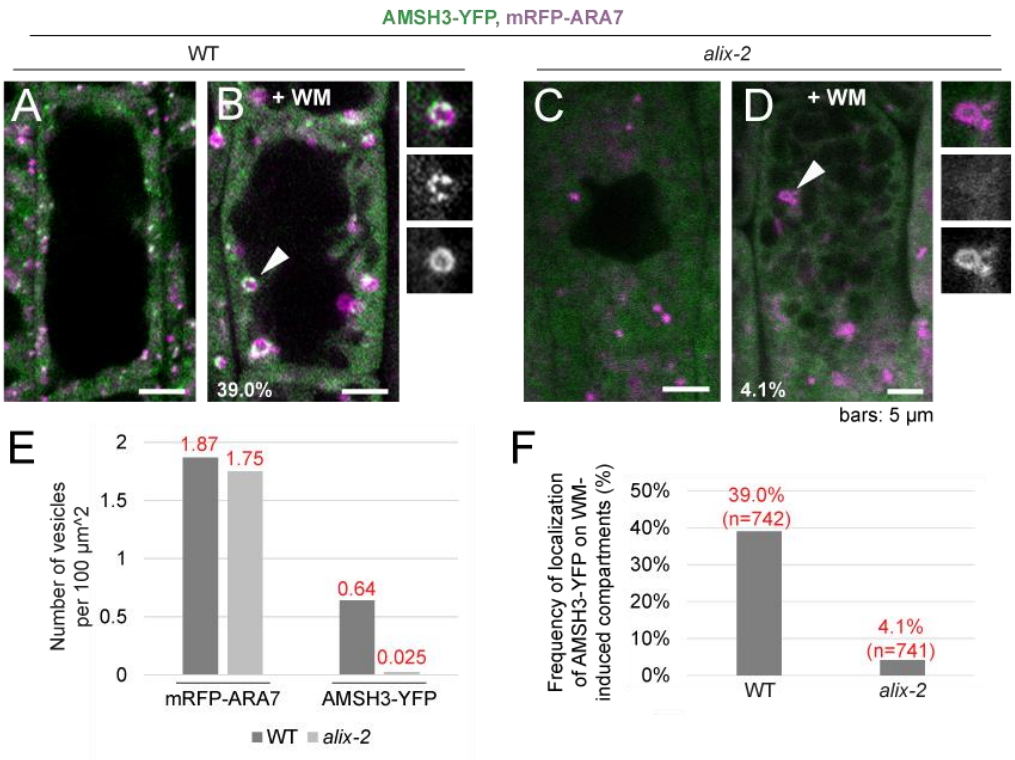

Figure 34. AMSH3-YFP does not localize on ARA7-labeled late endosomes in *alix*.
(**A** to **D**) Localization of AMSH3-YFP and mRFP-ARA7 in root epidermis cells of 7-day-old WT (wild-type) or *alix-2* seedlings without (**A** and **C**) or with (**B** and **D**) 120-min 33 µM-WM (Wortmannin) treatment. Note that in contrast to the wild type, in *alix-2* AMSH3-YFP localized neither on mRFP-ARA7-labeled late endosomes nor on WM-induced compartments. Magnifications of the areas indicated by white arrowheads are shown on the right side of the panels (from top to bottom: merged, AMSH3-YFP and mRFP-ARA7). Scale bars: 5 µm.
(**E**) The number of mRFP-ARA7 and AMSH3-YFP vesicles per 100 µm^2 in WT and *alix-2*. Note that the reduction of the number of AMSH3-YFP vesicles per area in *alix-2* was stronger than of mRFP-ARA7 vesicles.
(**F**) The number of WM-induced mRFP-ARA7 compartments containing AMSH3-YFP signals in WT and *alix-2* seedlings. Note the dramatic reduction of AMSH3-YFP sensitivity to WM treatment in *alix-2*.

The mRFP-ARA7-positive compartments visible in *alix* could represent either functional MVBs or aberrant endosomal structures that were observed in mutants of *ALIX* orthologs in other kingdoms (Raymond et al., 1992; Luhtala and Odorizzi, 2004; Ali et al., 2013). To test the functionality of mRFP-ARA7-containing compartments in *alix*, wild-type and mutant seedlings were treated with Wortmannin. In both wild type and mutants, mRFP-ARA7 appeared on swollen ring-like structures (Figure 34B and D), suggesting that ARA7 in both cases localizes to LEs that at least partially sustained their sensitivity to WM. Finally, to confirm the loss of the late endosomal localization of AMSH3-YFP in *alix*, frequency of the appearance of AMSH3-YFP signals on WM-induced compartments was scored. In wild type, 39% (n = 742) of mRFP-ARA7-positive Wortmannin-induced enlarged structures contained also AMSH3-YFP signals, whereas in *alix* only 4.1% (n = 741) (Figure 34B, D and F). Together, these results indicate that ALIX is required for the localization of AMSH3-YFP to mRFP-ARA7-

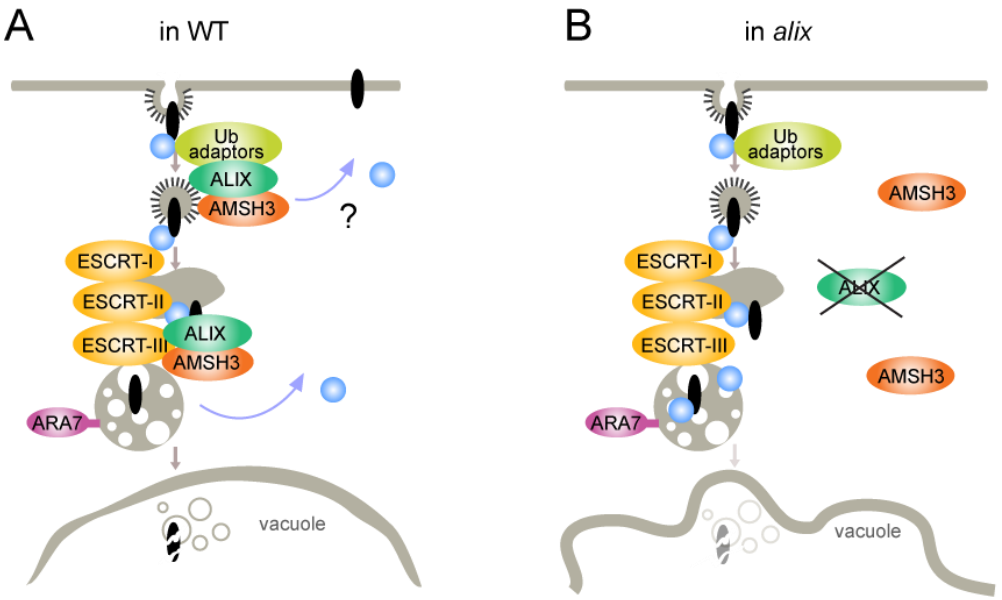

Figure 35. ALIX is essential for the endosomal localization of AMSH3.
(**A**) In WT (wild type), both AMSH3 and ALIX interact with ESCRT-III and localize to LEs (late endosomes). ARA7 is also associated with the membranes of LEs. AMSH3 and ALIX localize also on CCVs (clathrin-coated vesicles), probably through the interaction with clathrin or adaptor proteins. ALIX either recruits or stabilizes AMSH3 interaction with ESCRT-III on LEs and probably with other proteins on CCVs.
(**B**) In the absence of ALIX, ARA7 remains associated with LEs. In contrast, the endosomal localization of AMSH3 is almost completely abolished. AMSH3 cannot fulfill its function as a DUB and ubiquitinated endocytic cargo accumulates in *alix* mutants.

labeled late endosomes *in planta*. The ALIX function together with ESCRT-III and AMSH3 is probably to either help recruiting AMSH3 to ESCRT-III and LEs, or to stabilize this association.

In conclusion, both AMSH3 and ALIX interact with ESCRT-III and localize to late endosomes in the wild type. The RABF ARA7 is also associated with LEs through membrane binding. A significant fraction of AMSH3 and ALIX can be also found on CCVs, possibly due to their interaction with clathrin or CCV-localized proteins. ALIX probably stabilizes AMSH3 interaction with ESCRT-III on LEs and possibly also on CCVs. As ALIX homologs from other kingdoms were shown to bind to clathrin (Pashkova et al., 2013), the Arabidopsis homolog might have a similar ability (Figure 35A). In the absence of ALIX, ARA7 still associates with MVBs, whereas the endosomal localization of AMSH3 is almost completely abolished. Upon the loss of *ALIX*, AMSH3 cannot fulfill its role properly and ubiquitinated cargo proteins accumulate in a similar manner as in *AMSH3*-depleted seedlings (Figure 35B). All results suggest that ALIX is necessary for the proper function of AMSH3 and that both proteins are essential in Arabidopsis.

Altogether, the data collected during this study suggest that ESCRT-III and the proteins associated with ESCRT-III, namely AMSH1, AMSH3 and ALIX, are essential for the proper plant growth and development through regulating ubiquitin-dependent protein degradation pathways such as endocytic trafficking and autophagy in *Arabidopsis thaliana*.

3. Discussion

3.1. Mechanisms that regulate AMSH proteins

In this study, I have sought to understand the mechanisms laying behind the selective protein degradation in *Arabidopsis thaliana*. The centre of my interest were two pathways, endocytic trafficking and autophagy. A special emphasis was put on the role of ubiquitin and MPN-family deubiquitinating enzymes AMSH in these processes.

AMSH proteins can be found in mammals and plants, but not in budding yeast. AMSH are active as monomers and like in case of other DUBs, it is essential that their activity and subcellular localization are strictly controlled. In this study, I have shown that the adaptor protein ALIX interacts with both AMSH1 and AMSH3, and is important for the endosomal localization of AMSH3.

The *in vivo* function of AMSH3 was previously shown to depend on its MIT domain-mediated interaction with ESCRT-III, as the DEX-inducible AMSH3(ΔMIT) constructs failed to complement the *amsh3* seedling lethal phenotype (Isono et al., 2010; Katsiarimpa et al., 2011; Katsiarimpa et al., 2014). In this study, however, I have proven that the MIT-MIM-mediated interaction with ESCRT-III is not sufficient for the endosomal localization of AMSH3 and that ALIX, a novel interaction partner of AMSH3, is indispensable for this. ALIX does not seems to be essential for the ESCRT-III-mediated ILV formation. Since the *alix* mutants contain MVBs, the function of ESCRT-III is probably at least partially sustained in the absence of *ALIX* (Haas et al., 2007; Kalinowska et al., 2015). Considering that ESCRT-III is probably still assembled and disassembled in *alix* mutants, it is possible that the interaction with ESCRT-III is not sufficient for the recruitment of AMSH3 to endosomes.

In conclusion, binding to both ESCRT-III and ALIX is essential for AMSH3 function. It is possible that the combination of both interactions is required, binding to ALIX being necessary for AMSH3 localization and to ESCRTs for other reasons. AMSH3 might regulate ESCRT-III disassembly, as it was previously demonstrated to compete with SKD1 for VPS2.1 binding (Katsiarimpa et al., 2011). An interesting mechanism of ESCRT-III association was shown for the DUB unrelated to AMSH3 in budding yeast, Doa4p. Doa4p can interacts with ESCRT-III through binding to its core component Vps20p. This interaction is indispensable for the role of Doa4p in ILV formation but does not influence its endosomal localization. It is the ALIX homolog Bro1p that recruits Doa4p to late endosomes (Luhtala and Odorizzi, 2004; Richter et al., 2013). Another example is AMSH/STAMBP, for which the interaction with clathrin was shown to be essential for the early endosomal localization. AMSH/STAMBP can

also bind to the ESCRT-0 component STAM, which is indifferent for the localization of AMSH/STAMBP but important for the induction of its DUB activity (Kim et al., 2006; Nakamura et al., 2006). It would be highly intriguing to understand the exact role of AMSH3 interactions with ESCRT-III components and ALIX in Arabidopsis.

AMSH1 is another MPN-family protein in Arabidopsis. In this study I have shown that AMSH1 is an active deubiquitinase that can interact both with the ESCRT-III subunit VPS2.1 and with ALIX. As AMSH3 can interact with two- and AMSH1 with one ESCRT-III component, the affinity of AMSH1 towards ESCRT-III might partially differ from AMSH3. Due to challenges in generation of AMSH1 fluorophore-tagged constructs (such constructs show either no expression or are not functional in Arabidopsis), it is not yet clear whether AMSH1 can localize to endosomes. It might associate with endosomal compartments through its interaction with ESCRT-III and ALIX. On the other hand, as ALIX and VPS2.1 are also cytosolic, the interaction between both proteins and AMSH1 could occur in the cytosol.

The function of Arabidopsis AMSH proteins could be controlled not only upon binding to their interaction partners, but also by posttranslational modifications. Mass spectral analysis revealed that AMSH3 contains a phosphorylation site within its poorly characterized middle domain, S207 (cysteine 207) (PhosPhAt 4.0 database). S207 is not conserved between human AMSH/STAMBP and AMSH3, nor between AMSH3 and AMSH1, suggesting that it might have an AMSH3-specific role. The phosphorylation of S207 could regulate AMSH3 activity, localization or binding to its interaction partners. Mutant versions of AMSH3 that cannot be phosphorylated (S207A) or containing a phosphomimic (S207D or S207E) could be generated and tested for complementation of the *amsh3* mutant phenotype to verify its importance. AMSH1 might also be regulated by posttranslational modifications. It contains multiple predicted phosphorylation sites, among these two phosphorylation hot spots, however, no data from mass spectrometry currently exists (PhosPhAt 4.0 database).

ALIX also could be regulated by posttranslational modifications that might affect its binding to AMSH. In Xenopus, the homolog of ALIX, Xp95, was shown to interact with the homolog of AMSH. This binding depends on the phosphorylation status of Xp95, pointing to the relevance of posttranslational modifications in protein-protein interactions. This was also the first time that the interaction between the homologs of AMSH and ALIX was ever demonstrated before this study (Dejournett et al., 2007).

Human AMSH/STAMBP was shown to be regulated by ubiquitination. It interacts with the RNF11 (RING-FINGER PROTEIN 11) that acts as an adaptor for recruitment of the HECT E3-ligase SMURF2 (SMAD-UBIQUITINATION REGULATORY FACTOR 2). Ubiquitination of AMSH/STAMBP was demonstrated to lead to its degradation by the 26S proteasome (Li and

Seth, 2004). It could be interesting to analyze which mechanisms are regulating the abundance of Arabidopsis AMSH proteins.

The activity of DUBs and ATPases often depend on each other. Occupancy of a DUB by a ubiquitin conjugate can lead to stimulation of the associated ATPase, thereby coupling deubiquitination and ATP hydrolysis. Such a mechanism of stimulating each other's activity was shown for DUBs Ubp6/Usp14 and Uch37, and proteasomal AAA ATPases (Peth et al., 2013; Wauer and Komander, 2014). During this study I have found that AMSH3 interacts directly with the AAA ATPase of unknown cellular function. To date, no protein modulating AMSH3 activity was characterized. It is possible that the AAA ATPase can stimulate ubiquitin cleavage by AMSH3 in an ATP-dependent manner, thus regulating its cellular functions. Alternatively, AMSH3 and the AAA ATPase could function together as a heterodimer or transiently as parts of a larger protein complex. AAA ATPases are known to induce remodeling or unfolding of proteins and small molecules. A complex containing AMSH3 and ATPase could therefore affect both the ubiquitination status and structure of target proteins.

Though a number of potential interaction partners of AMSH1 was isolated in this study, to date none of these interactors, except for ALIX, could be verified by *in vitro* binding assays. The future studies should focus on testing the binding to other interesting candidates isolated in the Y2H screen, such as extra-large G-protein related protein or GEF4 (GDP/GTP EXCHANGE FACTOR 4) that might play roles in intracellular trafficking and pathogen response. Further assays could help to solve the question to which extend the functions of AMSH1 and AMSH3 are overlapping in Arabidopsis.

3.2 The role of ESCRT in autophagy

In this study, I have analyzed the knock-down mutants of *AMSH1* and have shown that they are partially impaired in autophagic degradation. A similar phenotype was observed in plants overexpressing a dominant-negative version of the ESCRT-III subunit VPS2.1 (Katsiarimpa et al., 2013). Previous studies in mammals, flies and nematodes have revealed that the ESCRT machinery plays role in autophagy. Though the core ESCRT components failed to be identified in screens for the *atg* mutants in yeast, the mutant of the homolog of *SKD1*, *Vps4p*, was demonstrated to induce autophagy under non-starved conditions (Shirahama et al., 1997; Rusten and Stenmark, 2009).

The ESCRT machinery could be involved in one or more key steps during autophagy. Inhibition of ESCRT function could cause cellular stress that results in proautophagic signaling, in addition to preventing MVB biogenesis and endocytic degradation of PM

receptors. Alternatively, ESCRTs might be important for closure of the phagophore during autophagosome formation, which is topologically similar to the abscission of ILVs from the limiting membrane of the MVB. Another possibility is that the ESCRT machinery is required for the fusion of autophagosomes with late endosomes or vacuoles. Finally, ESCRTs might be required for lysosome or vacuole biogenesis (Rusten et al., 2007; Tamai et al., 2007; Petiot et al., 2008; Petiot and Sadoul, 2009; Rusten and Stenmark, 2009). In addition to ESCRT machinery and ESCRT-associated proteins, also other factors functioning in intracellular trafficking such as RAB GTPases were demonstrated to be essential for the proper autophagosome maturation (Jager et al., 2004)

There are several reports of ESCRT components functioning in autophagy in Arabidopsis. Beside the dominant-negative effect of the overexpression of VPS2.1 demonstrated in our lab (Katsiarimpa et al., 2013), the ESCRT-III accessory proteins CHMP1A and CHMP1B were shown to regulate the autophagic turnover of plastids in Arabidopsis (Spitzer et al., 2015). Also other players in intracellular trafficking were reported to affect autophagy, such as the exocyst complex (Kulich et al., 2013) or the RABG GTPase RABG3c (Kwon et al., 2010). It is possible that AMSH proteins and ESCRT-III function together in autophagic pathway in Arabidopsis. Alternatively, AMSHs might play role together with ESCRT-III in endocytic trafficking and influence the autophagic degradation indirectly.

Previous studies have shown that AMSH proteins are important not only for the proper development, growth and autophagic degradation but also for defense against pathogens (Isono et al., 2010; Katsiarimpa et al., 2013). The involvement of AMSHs in pathogen defense could be explained by the link of AMSH to autophagy, which is known to regulate the salicylic acid pathway. However, since vesicle trafficking was also shown to play direct roles in this pathway, it cannot be excluded that AMSH proteins might as well. In example, ARA6 and ARA7 were demonstrated to be important for biogenesis and development of the haustorium formed by powdery mildew fungus *Golovinomyces orontii.* Both RABs relocalize to the host-derived membrane surrounding the haustorium (Inada et al., 2016). As AMSH3 strongly colocalizes with these RABs, it could also localize on the extrahaustorial membrane and affect its biogenesis.

alix null mutants accumulate the autophagosome marker ATG8 and the autophagy receptor NBR1 at high levels. Moreover, adult plants with strongly reduced ALIX levels are dwarfish and display leaf chlorosis and senescence, phenotypes linked to autophagy defects. These results suggest that ALIX might be involved in both selective and nonselective autophagy pathway. Moreover, ALIX interacts with AMSH1 and ESCRT-III that were shown to be essential for proper autophagic degradation in Arabidopsis. It is, however, not obvious

that ALIX plays a similar role. Though the human ESCRTs were implicated in autophagy, ALIX was not (Petiot et al., 2008; Petiot and Sadoul, 2009). Depletion of the human *ALIX* does not lead to the accumulation of LC3 (MICROTUBULE-ASSOCIATED PROTEIN 1A/1B LIGHT CHAIN 3), the homolog of the autophagosome marker ATG8, nor does it influence autophagosome maturation. Human ALIX was instead demonstrated to block caspase-dependent and -independent cell death without directly influencing autophagy (Petiot et al., 2008). On the other hand, the homolog of ALIX in budding yeast, Bro1p, seems to be important for nutrient recycling. The Δ*bro1* mutants were demonstrated to grow normally under nutrient-rich conditions, but show aberrant growth patterns upon nutrient deficiency (Nickas and Yaffe, 1996). It is therefore interesting to verify whether the plant homolog is really required for autophagic responses. The accumulation of ATG8 and NBR1 could be an indirect effect of the general defect in intracellular trafficking in Arabidopsis *alix* mutants. Also the leaf chlorosis in adult plants depleted of ALIX might be a result of cell death accelerated independently of autophagy.

3.3. Other potential functions of ALIX

Beside the role in endocytic trafficking and autophagy, mammalian ESCRT machinery was also implicated in cytokinesis. The interaction between the human ALIX and ESCRTs was shown to be essential in this process (Fabbro et al., 2005; Martinez-Garay et al., 2006; Zhao et al., 2006). The human ALIX was found to function as an adaptor protein, recruiting the ESCRT-I component TSG101 and ESCRT-III to the midbody to complete the membrane scission during cytokinesis (Carlton et al., 2008). Both TSG101 and ALIX were shown to interact with a hinge region of CEP55 (CENTROSOME PROTEIN 55 kDa), a protein involved in controlling the midbody integrity and cell abscission during cytokinesis (Fabbro et al., 2005; Sakai et al., 2006; Morita et al., 2007; Carlton et al., 2008). BLAST search using the full-length and hinge region of CEP55 did not reveal any homolog in Arabidopsis. Moreover, the C-terminal GPP-based region used for interaction with CEP55 cannot be found in *At*ALIX, suggesting that this interaction is not conserved in Arabidopsis.

On the other hand, other results suggest that *ALIX* might play some role in cytokinesis in Arabidopsis. During this study, I have shown in SEM analysis that the root tip of *alix* contains disorganized root cell files. Moreover, a low frequency of cytokinesis defects such as aberrant cell shape and oblique cell walls was observed (data not shown), phenotypes described previously in such mutants as *tonneau2*, *tangled* and *RanGAP*^{RNAi} (Walker and Smith, 2002; Xu et al., 2008; Kirik et al., 2012). The nature of these defects suggests that the function of Arabidopsis *ALIX* might be important for determination of division plane during cytokinesis.

In humans, ALIX and ESCRTs can be hijacked by various human pathogenic viruses. These viruses use them either for membrane scission during budding from host cells, or for protection from the host proteasomal machinery (Bissig and Gruenberg, 2014). The enveloped RNA viruses contain so-called late domains, consisting of short conserved motifs with the sequence of $YP(x)_nL$ (where *x* is any residue and *n* is any length). ALIX can associate with these motifs through its middle V-domain and subsequently recruit TSG101 through its PRD motif and the ESCRT-III subunit CHMP4 through its BRO1 domain. Assembly of ESCRTs on PM results in membrane scission and virus release from the cell (Gottlinger, 2007). This mechanism is used by such viruses as HIV1 (human immunodeficiency virus 1), EBOV (Ebola virus), MLV (murine leukemia virus), EIAV (equine infectious anemia virus) and HPIV1 (human parainfluenza virus type I) (Strack et al., 2003; Segura-Morales et al., 2005; Boonyaratanakornkit et al., 2013; Han et al., 2015).The respiratory pathogen HPIV1 exploits ALIX also in a different way. The BRO1 domain of ALIX interacts with accessory C proteins of HPIV1, protecting them from ubiquitination and degradation by the host proteasomal machinery (Boonyaratanakornkit et al., 2013).

In this study, I have shown that the Arabidopsis ALIX interacts with FIP1, a small 28.0 kDa protein that according to annotations might interact with VirF (virulence protein F), an F-box protein, functioning as a crucial virulence factor for the plant pathogen *Agrobacterium tumefaciens*. During infection with Agrobacterium, a single-strand copy of bacterial DNA (T-DNA, transferred-DNA) is exported into the plant host cell. The T-DNA is coated by the bacterial VirE2 (virulence protein E2) but the coat must be removed by VirF before the insertion of bacterial DNA into the host genome. For this, VirF is integrated into the host SCF (SKP1-CUL1-F-BOX PROTEIN) ubiquitin E3 ligase complex. VirF targets the VirE2 coat, as well as a nuclear import facilitator VIP1 (VirE2-interacting protein 1), which leads to their ubiquitination and degradation by the host 26S proteasome (Magori and Citovsky, 2011a, b). It is possible that *Agrobacterium* hijacks FIP1 and ALIX, causing both proteins to recruit the SCF complex or to stabilize the interaction of VirF with the ligase complex (Figure 37A). This could be a mechanism through which plant pathogens evolved to use the plant ALIX as an adaptor protein during infection.

The RING E3 ligase XBAT35 was another protein isolated as a novel interactor of ALIX in a Y2H screen. XBAT35 is a homolog of the rice XB3 (XA21-BINDING PROTEIN 3), a ligase necessary for internalization of the receptor XA21 during the defense reaction against the bacterial blight disease pathogen *Xanthomonas oryzae* pv *oryzae* (Wang et al., 2006). The Arabidopsis XBAT35 was demonstrated to function in ethylene signaling and negatively regulate the apical hook curvature (Carvalho et al., 2012), though its potential role in pathogen defense in Arabidopsis was not studied. XBAT35 contains a YPSI motif. $YP(x)_{1-3}L/I$ is a typical

motif serving for ALIX binding, highly conserved through different kingdoms. In budding yeast, Bro1p binds through its PRD to the YPFL sequence of Doa4p and this was shown to stimulate the activity of Doa4p (Richter et al., 2007). In *Caenorhabditis elegans*, ALX-1 (ALIX-1) interacts with the YPSL motif of EH (EPS15 homology) domain-containing protein RME-1 (RECEPTOR-MEDIATED ENDOCYTOSIS 1) (Shi et al., 2007). Moreover, the human ALIX interacts with such motifs within the substrates of ubiquitin-independent endocytosis (Dores et al., 2012b; Dores et al., 2012a) and, as mentioned above, within the late domains of pathogen viruses (Zhai et al., 2008). Though the interaction between ALIX and XBAT35 was negatively verified in targeted Y2H assays, a positive control was missing. The assays could be repeated including a positive control to exclude potential technical mistakes. If the interaction is true, it would be interesting to test whether the E3 ligase activity of XBAT35 is affected upon ALIX binding and whether both proteins function together in pathogen defense in Arabidopsis.

3.4. BRO1 domain-containing proteins

The Arabidopsis ALIX contains a BRO1-like domain, which can be found in almost all eukaryotes and was characterized in proteins playing adaptor and scaffolding roles in cells. The first crystal structure of the BRO1 domain was resolved over a decade ago (Kim et al., 2005). BRO1 domain serves for interaction with ESCRTs and proteins that contain it play roles in regulation of endocytic trafficking and processes topologically similar to ILV formation, such as cytokinesis and virus budding. BRO1 domain-containing proteins function also in autophagy, cytoskeleton remodeling and response to pH changes (Odorizzi, 2006; Bissig and Gruenberg, 2014). Most of BRO1 domain-containing proteins are modular and often carry two other major domains: the V-domain and the PRD. There are, however, several cases of proteins containing additional motifs or of very small proteins that except for the BRO1 domain do not carry any conserved annotated domains (Figure 36A) (Odorizzi, 2006; Ichioka et al., 2008; Bissig and Gruenberg, 2014; Kalinowska et al., 2015).

The yeast BRO1 domain-containing protein Bro1p was isolated in a mutant screen for factors functioning in cargo endocytosis. Mutants were divided into six classes (from A to F) based on defects in cargo sorting and vacuole morphology. The *vps31/bro1* mutant was assigned to class E that carried aberrant prevacuolar structures that were named the class-E compartments (Raymond et al., 1992). As mentioned above, Bro1p was later demonstrated to bind to the protease Doa4p, to recruit it to LEs and to regulate its DUB activity (Luhtala and Odorizzi, 2004; Richter et al., 2007). More recent research revealed that Bro1p plays role also early in endocytic cargo sorting, as a ubiquitin adaptor functioning in parallel with ESCRT-0.

This role is independent of Doa4p that functions exclusively on late endosomes. Similar to ESCRT-0, Bro1p binds ubiquitin, clathrin, E3 ligases, DUBs and ESCRT-I (Nikko and Andre, 2007; Pashkova et al., 2013). Considering the high CCV localization of the Arabidopsis ALIX, it is possible that it functions together or in parallel with TOL proteins in endocytic cargo recognition, replacing the missing ESCRT-0 in plants. This new potential role of ALIX in endocytic cargo sorting could be dependent or independent of AMSH function.

Another homolog characterized in budding yeast, Rim20p,contains the BRO1 domain and the middle coiled-coil region resembling the V-domain, but lacks the C-terminal proline-rich region (Figure 36A) (Xu and Mitchell, 2001). Rim20p does not play role in endocytic

Figure 36. BRO1 domain-containing proteins in budding yeast, human and Arabidopsis.
(**A**) Budding yeast contain two BRO1 (Bck1p-like resistance to osmotic shock 1) domain-containing proteins: Bro1p and Rim20p. Both can associate with ESCRT-III, but only Bro1p was demonstrated to function in endocytic trafficking. Both proteins contain the middle V-domain (V-shaped domain), but Rim20p lacks the C (carboxy)-terminal PRD (proline-rich domain).
(**B**) Humans have at least five BRO1-domain proteins and all were shown to interact with ESCRT-III through their N (amino)-terminal BRO1 domains. HD-PTP contains two additional motifs: PTP (protein tyrosine phosphatase) and the sequence for degradation PEST (proline-, glutamic acid-, serine- and threonine-rich). RHPN1 and -2 (rhophilin-1 and -2) carry an additional N-terminal HR1 (helical Rho-binding repeat 1) and instead of the V-domain, the PDZ (PSD-95, DISC-LARGE, ZO-1) motif for protein-protein interactions. BROX is a small protein that except for the BRO1 domain carries only the CAAX motif for prenylation.
(**C**) The Arabidopsis genome encodes five BRO1 domain-containg proteins. Only one of them has other motifs found in yeast Bro1p and human ALIX: the V-domain and the PRD. Other four are small uncharacterized proteins devoid of other conserved motifs.

trafficking, but was shown to be essential in responses to changing environmental pH. Rim20p is cytosolic in acidic conditions but it relocalizes to endosomes under alkaline conditions. This results in the cleavage and activation of the transcription factor Rim101p, and in consequence in regulation of activity of pH signaling genes (Xu and Mitchell, 2001; Boysen and Mitchell, 2006). A very similar mechanism was proposed for PalA and PalC, homologs of Rim20p in filamentous fungus *Aspergillus nidulans* (Negrete-Urtasun et al., 1997; Galindo et al., 2007; Lucena-Agell et al., 2015).

In mammals, there are several BRO1 domain-containing proteins and their domain organization is more variable than in other clades. The human ALIX is a typical Bro1p-like protein characterized by the N-terminal BRO1 domain, middle V-domain and the C-terminal PRD (Figure 36B). It interacts not only with ESCRT-III, but also with the ESCRT-I subunit TSG101 (Martin-Serrano et al., 2003; Strack et al., 2003; von Schwedler et al., 2003). On top of that, ALIX was shown to bind to the SH3 domains of the endocytic adaptor proteins SETA/CIN85 (Chen et al., 2000), CMS/CD2AP (Usami et al., 2007), endophilin (Chatellard-Causse et al., 2002) and Src family kinases Src (Schmidt et al., 2005; Dejournett et al., 2007; Zhou et al., 2009) and Hck (Shi et al., 2010). Similar to Bro1p, ALIX can bind directly to monoubiquitin and K63-linked polyubiquitin chains (Keren-Kaplan et al., 2013; Pashkova et al., 2013), yet, despite interactions with ubiquitin and endocytic sorting machinery, the loss of *ALIX* does not block ubiquitin-dependent endocytic sorting (Odorizzi, 2006). ALIX is therefore believed to play role in other cellular processes than endocytic trafficking that involve ESCRT machinery, such as cytokinesis and ubiquitin-independent endocytosis (Morita et al., 2007; Dores et al., 2012b).

HD-PTP is another mammalian BRO1 domain-containing protein and a non-receptor type PTP (protein tyrosine phosphatase). In addition to the BRO1 domain, V-domain and PRD, it contains the PTP domain and the signal for degradation PEST (proline-, glutamic acid-, serine- and threonine-rich) (Figure 36B) (Castiglioni and Maier, 2012). In contrast to the mammalian ALIX, HD-PTP is essential for ubiquitin-dependent endocytic cargo sorting and for the proper MVB biogenesis (Ali et al., 2013). Intriguingly, the *hd-ptp* mutants contain clustered MVBs filled with normally-looking ILVs, similar to Arabidopsis *alix* mutants. Both HD-PTP and the Arabidopsis ALIX therefore seem to be dispensable for ILV formation, in contrast to the yeast Bro1p (Matsuo et al., 2004; Richter et al., 2007; Wemmer et al., 2011; Ali et al., 2013; Kalinowska et al., 2015). HD-PTP can binds to the ESCRT-0 subunit STAM through its BRO1 domain and PRD (Ali et al., 2013; Lee et al., 2016), and to the ESCRT-III core subunit CHMP4B via its BRO1 domain (Ichioka et al., 2007; Ali et al., 2013). Moreover, HD-PTP can interacts with other proteins involved in endocytic sorting, such as endophilin A1 and ALG-2 (APOPTOSIS-LINKED GENE 2) (Ichioka et al., 2007). To date, it is not clear whether HD-PTP

is an active PTP and opinions are divided (Gingras et al., 2009; Mariotti et al., 2009; Lin et al., 2011).

A highly interesting mechanism of the ESCRT exchange and the recruitment of the DUB UBPY/USP8 by HD-PTP and was proposed. HD-PTP binds to the core domain of STAM through its BRO1 domain and to the SH3 domain of STAM through its middle PRD region. STAM is competed out from the BRO1 domain of HD-PTP by the ESCRT-III subunit CHMP4B. This recruits the DUB UBPY/USP8 that binds to the MIM of CHMP4B through its N-terminal MIT domain. UBPY/USP8 contains also a PRD that competes HD-PTP out from the SH3 domain of STA2. This causes the detachment of HD-PTP from ESCRT-0 and the association with ESCRT-III in a route omitting ESCRT-I and ESCRT-II. UBPY/USP8 interacts also with the cargo and deubiquitinates it. It was suggested that in this way, by interacting with UBPY/USP8 and HD-PTP, cargo can be sorted directly from ESCRT-0 to ESCRT-III (Ali et al., 2013). A very similar function together with *Dm*UBPY was suggested for the homolog of HD-PTP in *Drosophila melanogaster*, Mop (Myopic) (Miura et al., 2008; Pradhan-Sundd and Verheyen, 2014, 2015).

In humans, several other BRO1 domain-containing proteins were described, including rhophilins and BROX (BRO1 DOMAIN-CONTAINING PROTEIN WITH A CAAX MOTIF). Rhophilins are effectors of the Rho GTPases, molecular switches that play key role in regulating the actin cytoskeleton (Peck et al., 2002; Steuve et al., 2006). RHPN1 (rhophilin-1) and RHPN2 contain the HR-1 (helical Rho-binding repeat 1) for interaction with Rho and the BRO1 domain that they can use to associate with endosomes. Another motif characteristic for rhophilins, the PDZ (PSD-95, DISC-LARGE, ZO-1) domain, serves for multiple protein-protein interactions and thus formation of multimeric protein complexes (Figure 36B). Mammalian rhophilins are implicated together with Rho GTPases in actin disassembly (Peck et al., 2002; Steuve et al., 2006). BROX is a small BRO1 domain-containing protein characterized by the C-terminal tetrapeptide CAAX that is a site for prenylation (Figure 36B). BROX was found to associate with membranes, interact with the ESCRT-III component CHMP4B, and to colocalize with *cis*- and *trans*-Golgi markers (Ichioka et al., 2008). The cellular function of BROX, however, still needs to be elucidated.

The Arabidopsis genome codes for four additional hypothetical BRO1 domain-containing proteins (*AT1G13310, AT1G17940, AT1G73990,* and *AT5g14020*) (Figure 36C). These proteins are shorter than ALIX and lack other recognizable functional domains. In contrast to BROX, the Arabidopsis BRO1 domain-containing proteins do not have the CAAX box for prenylation. On the other hand, since the human ALIX was shown to bind to the mammalian-specific lipid LBPA (lysobisphosphatidic acid) through the BRO1 domain (Matsuo

et al., 2004), it cannot be excluded that the Arabidopsis BRO1 domain-containing proteins also can interact with lipids. In addition, it still remains to be elucidated whether *AT1G13310*, *AT1G17940*, *AT1G73990*, and *AT5G14020* are expressed and what functions their protein products might have. It was demonstrated in budding yeast that the overexpression of the BRO1 domain of Bro1p leads to the inhibition of ESCRT-III disassembly. It is possible that the other BRO1 domain-containing proteins are regulating ESCRT-III dynamics and deubiquitination of endocytic cargo in Arabidopsis. By interaction with SNF7 and blocking its accessibility for ALIX, other BRO1 domain-containing proteins could affect binding of AMSH and probably also of SKD1 to ESCRT-III. It is tempting to consider the possibility that the regulation of ESCRT-III disassembly and the binding of ESCRT-associated proteins could be a more complex and fine-tuned process than we currently think.

3.5. The role of AMSH3 and ALIX in vacuole biogenesis

Two of the major protein degradation pathways, endocytic trafficking and autophagy, deliver cargo proteins to vacuoles. Plant vacuoles are, however, not only degradation stations. Serving as storage organelles in seeds, fruits and rhizomes, vacuoles are important for establishing and regulating multiple agronomically important traits in plants. Vacuoles can hence determine quality and quantity of the harvest of crop plants. They are essential in biotic and abiotic stress responses, helping plants to sequester toxic ions and release antimicrobial compounds during defense against pathogens. In addition, bursting of vacuoles is important for the programmed cell death, which in turn is used in other defense responses (Frigerio et al., 2008; Zouhar and Rojo, 2009).

In this study, I have shown that *alix* null mutants, similar to the previously characterized *amsh3*, show an aberrant vacuole morphology, suggesting the function of both proteins in vacuole biogenesis or maintenance. This phenotype was never reported for mutants of any BRO1 domain-containing protein in other kingdoms nor for any other DUB than AMSH3. The mutant of the yeast *bro1/vps31* showed no aberrant vacuolar phenotype but instead contained aberrant endosomes, the so-called class-E compartments (Raymond et al., 1992). Structures resembling class-E compartments can be induced in plants or protoplasts upon overexpression of the ATPase-inactive SKD1(EQ), or the ΔMIT- and AXA-constructs of AMSH3 (Haas et al., 2007; Isono et al., 2010; Katsiarimpa et al., 2011; Katsiarimpa et al., 2014). Such effect was not observed in Arabidopsis *alix* mutants, suggesting that ALIX has different roles in regulating ESCRT-III than its yeast homolog Bro1p or other ESCRT-III-associated proteins in Arabidopsis, AMSH3 and SKD1.

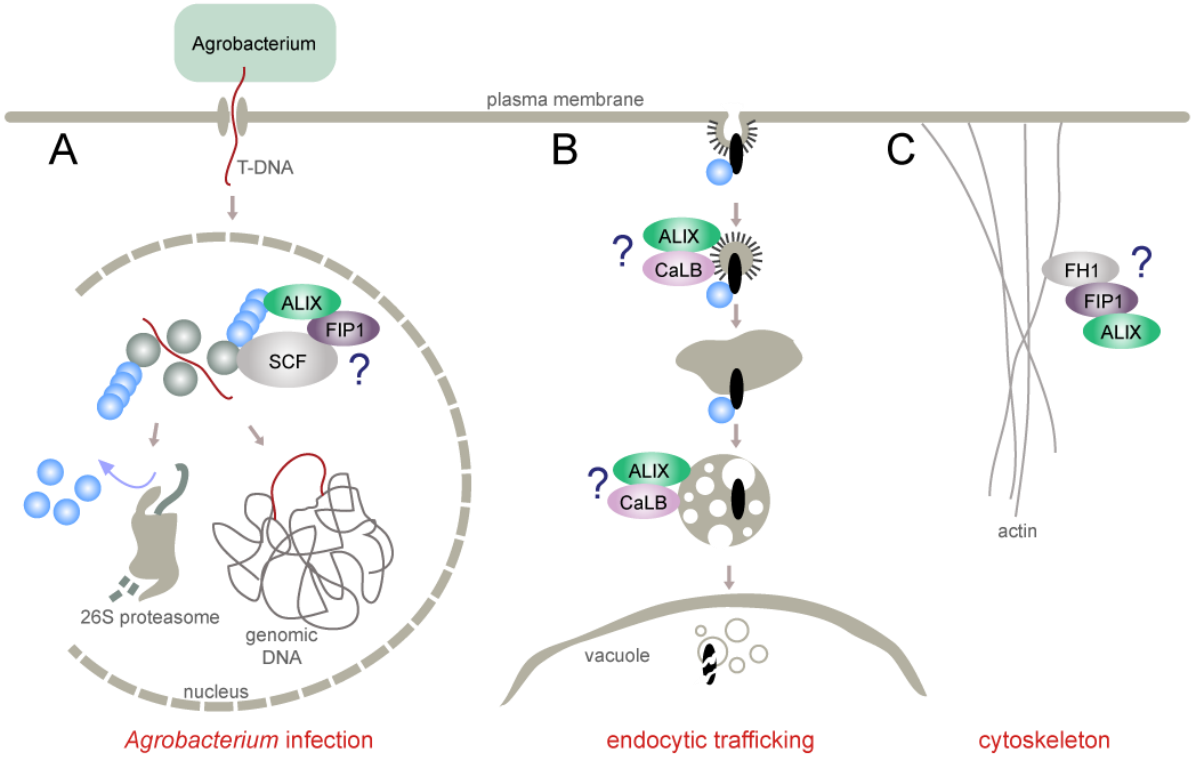

Figure 37. Novel interactors of ALIX could function together with ALIX in various processes.
(**A**) FIP1 (FH1-INTERACTING PROTEIN 1 or VirF-INTERACTING PROTEIN 1) was suggested to interact with VirF, an F-box *Agrobacterium* protein that hijacks the host SCF (SKP1-CUL1-F-BOX PROTEIN) machinery. During transformation, *Agrobacterium* exports a single-strand copy of T-DNA (transferred-DNA) into the host cell. The T-DNA is coated by the bacterial VirE2. Removal of the coat is mediated by VirF and is essential for insertion of the T-DNA into the host genome. VirF integrates into the host SCF ubiquitin E3 ligase complex and recruits it to VirE2 coat, which causes its polyubiquitination and degradation by the host 26S proteasome.
(**B**) ALIX interacts with a CaLB-family protein that can bind to membranes in a calcium-dependent manner. Both proteins might therefore associate with endosomes, autophagosomes or other intracellular organelles. ALIX and CaLB-family protein could be important for membrane fusion events, and could function in endocytic trafficking, vacuole biogenesis, calcium signaling or cell death.
(**C**) FIP1, next to its potential role in *Agrobacterium* infection, was shown to bind to formin FH1. FH1 is an actin nucleator controlling cytoskeleton dynamics. It is possible that FIP1 and ALIX function together with FH1 in cytoskeleton regulation.

Although in contrast to yeast plant vacuoles are essential for survival (Raymond et al., 1992; Rojo et al., 2001), much less is known about the vacuole biogenesis in plants. The vacuole formation and maintenance seem to strongly depend on properly functioning intracellular trafficking, as mutants of many factors functioning in this pathway show defects in vacuole morphology. Apparent VPS homologs in Arabidopsis, such as VPS16/VCL1, VPS29, VPS35 and VPS45, were implicated in vacuole biogenesis (Rojo et al., 2001; Shimada et al., 2006; Sanmartin et al., 2007; Yamazaki et al., 2008; Zouhar et al., 2009). Also the AP-3 (adaptor protein complex 3) functioning in sorting proteins from EE/TGN to the vacuole via an MVB-independent trafficking route was implicated in vacuole biogenesis (Feraru et al., 2010). Vacuole fragmentation or fusion defects were also shown for *rabg3* quintuple mutants (Ebine et al., 2014). Finally, null mutants of the late endosomal protein FYVE1 (FYVE-

DOMAIN PROTEIN 1) phenocopy *amsh3* and *alix* mutants in vacuole morphology (Gao et al., 2014; Kolb et al., 2015).

The vacuole morphology of *amsh3* and *alix* mutants could be a result of a defective ESCRT-dependent trafficking from PM to vacuole. Alternatively, distortion of other routes might lead to the defects in vacuole biogenesis. It was shown that the trafficking of tonoplast proteins and lipids essential for vacuole biogenesis can occur directly from ER omitting Golgi (Viotti et al., 2013). Essential sterols and major vacuolar pumps, V-PPase (VACUOLAR-TYPE INORGANIC PYROPHOSPHATASE) and V-ATPase (VACUOLAR H+-ATPase), are delivered during vacuole biogenesis in double-membraned vesicles resembling autophagosomes, though formed independently of autophagy machinery (Viotti et al., 2013). *amsh3-1* mutants were previously shown to accumulate double-membraned structures that could be autophagosomes (Isono et al., 2010). It is possible that at least a fraction of the structures accumulating in *amsh3-1* mutants represent ER-derived vesicles that due to membrane fusion defects cannot form a proper vacuole. Thus, ER-to-vacuole delivery of tonoplast proteins might be the pathway which distortion in *amsh3* and *alix* causes the aberrant vacuole morphology of these mutants.

Alternatively, the fusion of membranes could be impaired in *amsh3* and *alix*, resulting in tubular vacuoles similar to these found in mesodermal cells. Fusion events of lipid bilayers depend on many cellular components like SNAREs, small GTPases and such factors as calcium (Hay, 2007; Jena, 2009). Interestingly, a small 27.1 kDa CaLB (calcium-dependent lipid binding)-family protein was isolated in a Y2H screen as a novel interactor of ALIX. The CaLB motif, called also C2 domain, binds phospholipids in a calcium-dependent manner and can be found in a wide variety of proteins, involved in signal transduction and membrane fusion events. Also the involvement of CaLB domain proteins in transcription regulation and plant stress responses was previously reported (Hinderliter et al., 1998; de Silva et al., 2011). It is possible that CaLB-family protein and ALIX function together in membrane fusion. Alternatively, both proteins might play role in endocytic trafficking, calcium signaling or in cell death (Figure 37B). AAA ATPases such as NSF (N-ETHYLMALEIMIDE-SENSITIVE FACTOR) were also described to be important for fusions of lipid bilayers (Rowe and Balch, 1997; Martens and McMahon, 2008). The AAA ATPase identified in this study as a direct interactor of AMSH3 could functions together with AMSH3 in regulating membrane fusion events that affect the vacuole formation and maintenance.

Finally, vacuole morphology depends on actin cytoskeleton. It was previously shown that the depolymerization of actin filaments causes changes in vacuole morphology. Upon auxin treatment, actin filaments reorganize and vacuoles become more tubular-like than in

untreated plants, though also solitary fragmented vacuoles can be observed (Scheuring et al., 2016). Due to the striking resemblance of the vacuole morphology of *amsh3* and *alix* mutants to the plants with affected actin cytoskeleton, actin is a strong candidate for the cause of the vacuolar phenotype of these mutants. Importantly, the ALIX interactor isolated in Y2H assays, FIP1, was previously identified also as an interactor of FH1 (FORMIN HOMOLOGY 1) (Banno and Chua, 2000), though its function was not further characterized. FH1 belongs to formins, an evolutionary ancient family of regulators of cytoskeleton assembly and organization. *fh1-1* mutants show increased microtubule dynamics, resulting in impaired endocytic trafficking and cell morphogenesis (Martiniere et al., 2011; Rosero et al., 2013; Rosero et al., 2016). FIP1 contains a C-terminal GRAM (glucosyltransferases, RAB-like GTPase activators and myotubularins) domain that is implicated in interactions with proteins and lipids (Finn et al., 2014). It is possible that FIP1 and the adaptor protein ALIX together with FH1 regulate the cytoskeleton dynamics and in consequence also the vacuole morphology in Arabidopsis (Figure 37C).

Vacuoles are essential for plants (Raymond et al., 1992; Rojo et al., 2001; Isono et al., 2010). The properly functioning vacuoles decide not only on plant survival but also on its agronomically important traits. There seems to be a direct link between the state of the vacuole and the fitness of the plant. The lack of vacuoles or drastically affected vacuole morphology have very severe consequences, usually resulting in death during the embryo or seedling stage (Rojo et al., 2001; Isono et al., 2010; Shahriari et al., 2010; Kalinowska et al., 2015; Kolb et al., 2015). A slightly affected vacuole morphology seems to have a relatively moderate negative effect on plant growth and development. In example, another group has recently shown that a weak mutant of the Arabidopsis *ALIX* carrying a point mutation within its BRO1 domain, called *alix-1,* shows a mildly affected vacuole morphology. Vacuoles in *alix-1* are suggested to be smaller than in the wild type when observed under the confocal microscope. The weak *alix-1* mutants show reduced growth of petioles and rosette leaves, serrated rosette leaves, and late flowering under long-day conditions (Cardona-Lopez et al., 2015). It is possible that there is a strict correlation between the extent to which the vacuole morphology and probably its function is affected, and the general viability of the plant.

In conclusion, in this study, I aimed to understand the function and regulation of AMSH proteins in the context of ubiquitin-dependent endocytic degradation, autophagy and vacuole biogenesis. I have identified a novel interactor of AMSH proteins, ALIX, and by applying biochemical-, cell biological- and genetic methods, I have showed that it regulates the AMSH function. I have also demonstrated that AMSH proteins and ALIX play role together with the ESCRT machinery in Arabidopsis. Due to the tremendous role of such processes as endocytic trafficking, autophagy and vacuole biogenesis in plant growth and development, as well as in

controlling the yield of crop plants, these mechanisms should be studied in detail. Only a deep understanding of the mechanisms behind these pathways in a model plant will allow for the future translation of the knowledge to industrially relevant plants and field-based solutions.

4. Materials and methods

4.1. Materials used in this study

Chemicals and reagents used in this study are listed in Appendix Table 3. Antibodies used for detection of specific proteins are listed in Appendix Table 4. Vectors and plasmids used for cloning and subcloning are listed in Appendix Table 5, and the generated DNA constructs are listed in Appendix Table 6. Sequences of all primers used for cloning and sequencing are listed in Appendix Table 7 and -8, primers used for genotyping are listed in Appendix Table 9. Genotypes of bacteria and yeast strains, as well as Arabidopsis accessions are described in Appendix Table 10. A list of transgenic plants generated in this study is shown in Appendix Table 11.

4.2. Methods

4.2.1. Methods for plant analysis

4.2.1.1. Sterilization of seeds and growth conditions

For growth under sterile conditions, *Arabidopsis thaliana* seeds were sterilized by incubation for 10 min with saturated calcium hypochlorite supplemented with 0.1% (v/v) Silwet L-77. Seeds were subsequently washed once with 80% (v/v) ethanol and further four times with sterile water containing 0.05% (v/v) Silwet L-77. Stratification was typically carried out overnight at 4°C. Seeds were plated on GM (growth medium) [0.43% (w/v) Murashige & Skoog, 1% (w/v) sucrose, 0.05% (w/v) MES, 0.55% (w/v) plant agar, pH 5.8] and grown under continuous light or long day (110 to 150 µmol m^{-2} s^{-1}) at 21°C. For autophagy experiments, seeds were plated on ½ MS medium [0.215% (w/v) Murashige & Skoog, 0.05% (w/v) MES, 0.65% (w/v) plant agar, pH 5.8] and grown under long- or short-day conditions (16 hours light and 8 hours dark or 8 hours light and 16 hours dark, respectively). To grow plants on soil, 7-day-old seedlings were transferred on soil and grown under continuous light, short- or long-day conditions.

4.2.1.2. Plant transformation

The transformation of *Arabidopsis thaliana* was performed using the standard floral dip method (Clough and Bent, 1998). Plasmid DNA was transformed into appropriate *Agrobacterium tumefaciens* strain, GV3101::pMP90, GV3101::pMP90RK or GV3101::pMP90 pSoup.

Transformants were selected on LB medium [1% (w/v) tryptone, 0.5% (w/v) yeast extract, 1% (w/v) NaCl, pH 7.0] supplemented with appropriate antibiotics. The concentrations of 50 µg/ml of rifampicin and 25 µg/ml of gentamycin were used for all Agrobacterium strains. 5 µg/ml of tetracycline was added when pSoup-containing strain and 50 µg/ml of kanamycin when RK strain was used. After the transformation, cells were grown for 24 h at 30°C in a 500 ml liquid culture. After harvesting, cells were resuspended in up to 200 ml of Transformation Buffer [0.22% (w/v) Murashige & Skoog, 5% (w/v) glucose, 0.05% (w/v) MES, 44 µM 6-Benzylaminopurine, 0.05% (v/v) Silwet L-77]. Inflorescences from Col-0 or L*er* plants were submerged in the cell suspension for 1 min. Plants were kept at RT (room temperature) under a plastic cover overnight before return to the growth chamber.

4.2.1.3. Selection of transgenic plants

For antibiotic selection, seeds collected from transformed Arabidopsis plants were selected on ½ MS medium containing antibiotics (50 ng/µl for kanamycin selection or 15 ng/µl for hygromycin B selection). 7-day-old seedling that survived selection were transferred to soil.

For ppt-resistant lines, seeds were planted directly on soil and sprayed twice with 1:1000 Basta (Bayer CropScience, Germany) solution, both 3- and 5 days after germination. 7-day-old seedlings that survived selection were transferred to new pots.

For plants transformed with a plasmid based on pFAST-R05, transformants were selected under the Olympus BZX16 stereomicroscope (Olympus Europa, Germany) by identifying seeds that expressed the RFP reporter gene. Seeds were sterilized and plated on GM plates. 7-day-old seedlings were analyzed and transferred to soil. Plants that positively passed selection were genotyped using specific primers to confirm the presence of the transgene.

4.2.1.4. Establishment of T-DNA insertion lines

The T-DNA insertion lines of *AMSH1* were obtained from the collection of Cold Spring Harbor Laboratory and designated *amsh1-1* (CSHL_ET8678; L*er* ecotype). The T-DNA insertion lines of *ALIX* were designated *alix-2* (GABI-Kat 83711; Col-0 ecotype) and *alix-4* (SALK 063124; Col-0 ecotype). Both lines were obtained through NASC from the collection of the Bielefeld University and Salk Institute, respectively. Primers used for verification of mutant phenotypes are listed in Appendix Table 9.

4.2.1.5. PEG-mediated transformation of Arabidopsis protoplasts

In the first method, 3 to 4 days after subculturing, Arabidopsis suspension-cultured root epidermis cells were collected by centrifugation at 300 *g* and washed once with 10 ml of WD Solution (8 mM $CaCl_2$-$2H_20$, 0.4 M mannitol). The pellet was then resuspended in 10 ml of WD Solution containing 1% (w/v) cellulase “Onozuka R-10” (Serva, Germany) and 0.25% (w/v) macerozyme R-10 (Serva, Germany), and incubated under gentle agitation at RT in the dark. The formation of protoplasts was verified under a light microscope Bx61 (Olympus Europa, Germany). After 2 to 3 hours of incubation, cells were collected by centrifugation at 100 *g* for 2 min. Cells were washed once with 10 ml of WD- and once with 2 ml of W5 Solution (154 mM NaCl, 125 mM $CaCl_2$, 5 mM KCl, 5 mM Glucose). The pellet was dissolved in 2 ml of W5 Solution and incubated on ice for 30 min. Protoplasts were collected by centrifugation at 100 *g* for 1 min and the pellet was carefully resuspended in 1 ml of MMM Solution (15 mM $MgCl_2$, 0.1 % MES, 0.5 M Mannitol). 20 µg of plasmid DNA was mixed with 200 µl of the protoplast suspension and 200 µl of PEG Solution [40% (w/v) PEG4000, 0.4 M Mannitol, 0.1 M $CaCl_2$]. The suspension was incubated on ice for 30 min. Protoplasts were subsequently washed twice with 2 ml of W5 Solution and resuspended in 100 µl of K3 Medium (composition in Appendix Table 12). Transformed protoplasts were incubated for 16 to 20 hours at RT in the dark and analyzed under the FV-1000/IX81 confocal scanning microscope (Olympus Europa, Germany).

Alternatively, after 6 to 8 days following subculturing, Arabidopsis suspension-cultured cells were collected by centrifugation at 300 *g* and washed once with 10 ml of Solution 1 (5 mM EGTA pH 8.2, 0.4 M mannitol). Cells were then incubated in 10 ml of Solution 1 supplemented with 1% (w/v) cellulase and 0.25% (w/v) macerozyme for 1 h at RT in the dark with gentle agitation. The protoplasts were filtrated through nylon mesh. Cells were washed twice with 10 ml of Solution A (70 mM $CaCl_2$, 5 mM MES pH 5.7, 0.4 M mannitol) and then resuspended in MMM Solution (15 mM $MgCl_2$, 5 mM MES, 0.4 M mannitol). 20 µg of plasmid DNA was added to 100 µl of protoplasts, mixed with 400 µl of DNA Uptake Solution [40% (w/v) PEG6000, 20 mM $Ca(NO_3)_2$, 0.4 M mannitol] and incubated on ice for 30 min. Protoplasts were subsequently washed twice with 2 ml of Dilution Solution (125 mM $CaCl_2$, 5mM KCl, 1.5 mM MES pH 5.7, 5 mM glucose, 0.4 M mannitol) and resuspended in 500 µl of MS+Mannitol [0.46% (w/v) MS-0, 0.4 M mannitol]. Similar to the protocol above, transformed cells were incubated for 16 to 20 h at RT in the dark prior to the analysis.

4.2.2. Molecular biology methods

4.2.2.1. Purification of plasmid DNA from *E. coli*

Plasmid DNA was purified from *E. coli* using the alkaline lysis-based method. For mini-scale purification, cells from a 3-ml overnight culture were harvested by centrifugation and resuspended in 200 µl of Buffer P1 (50 mM Tris-HCl pH 8.0, 10 mM EDTA). Cell membranes were lysed by the addition of 200 µl of Buffer P2 [200 mM NaOH, 1% (w/v) SDS] and the plasmid DNA was renatured by the addition of 200 µl of Buffer P3 (3 M potassium acetate, pH 5.5). 100 µl of phenol:chloroform (1:1, v/v) were added and the samples were centrifuged at 13,000 *g* for 3 min. The water phase was mixed with 500 µl of isopropanol and centrifuged at 13,000 *g* for 20 min at 4°C. The DNA pellet was washed once with 500 µl of 70% (v/v) ethanol. The dry pellet was resolved in distilled water supplemented with Ribonuclease A (Carl Roth, Germany) and incubated for 20 min at 37°C.

For midi- or maxi-scale purifications, JETstar 2.0 Plasmid Purification MIDI- and MAXI Kit (GENOMED, Germany) were used, respectively.

4.2.2.2. Cloning

All primers used for cloning were ordered from Sigma-Aldrich, Germany, and are listed in Appendix Table 7.

4.2.2.2.1. Classical cloning procedure

For PCR-amplification of different DNA-fragments, the Phusion High-Fidelity DNA Polymerase (Thermo Fisher Scientific, Germany) was used. A 50-µl reaction tube contained 1x Phusion HF Buffer, 200 µM dNTP (deoxynucleotide) mix, 0.5 µM forward and reverse primers, 250 ng template and 1 U (enzyme unit) of Phusion polymerase. In some cases 0.5 mM $MgCl_2$ or 3% (v/v) DMSO (dimethyl sulfoxide) were added to the reaction. PCR products were purified using Wizard SV Gel and PCR Clean-Up System (Promega, Germany). 40 µg of purified PCR products and cloning vectors were digested in a 50-µl reaction mix containing 10 U of the appropriate restriction enzyme(s) for 3 h at 37°C. Digested vectors were run on 1% (w/v) ethidium bromide-containing agarose gel and the DNA-bands representing the digested plasmid were purified from the agarose gel using Wizard SV Gel and PCR Clean-Up System. Digested PCR products were purified by ethanol precipitation. 125 µl of 100% (v/v) ethanol and 5 µl of 3 M natrium acetate pH 5.2 were added to 50 µl of digested PCR product. Samples were incubated at RT for 5 min and centrifuged at 13,000 *g* for 15 min. The DNA pellet was

washed once with 200 µl of 70% (v/v) ethanol. The dry pellet was resolved in 20 µl of distilled water.

Concentrations of the vector and insert were controlled after the electrophoresis on 1% (w/v) agarose gel. For the ligation reaction, a ratio of 1:3 to 1:10 of vector to insert was applied. 2.5 U of T4 DNA Ligase (Thermo Fisher Scientific, Germany) was used for ligation together with the supplied buffer. The reaction was incubated for 1- to 3 h at RT or overnight at 16°C. The ligation reaction was terminated by heating at 80°C for 5 min. The whole post-ligation mix was used for *E. coli* (DH5α or TOP10, Appendix Table 10) transformation. Plasmid DNA was isolated from single colonies, analyzed by restriction digest and sequenced using vector- and gene-specific primers.

4.2.2.2.1.1. Constructs obtained by classical cloning

For Y2H assays with ALIX, GBD-ALIX(FL) (pKK41), GBD-ALIX(BRO1) (pKK49), GBD-ALIX(∆BRO1) (pKK50), GBD-ALIX(∆C-terminus) (pKK51), GBD-ALIX(V-fragm.1) (pKK63) and GBD-ALIX(V-fragm.2) (pKK81) were cloned. *ALIX* fragments were amplified from Arabidopsis cDNA using primer pairs KK77-KK78, KK77-KK126, KK125-KK78, KK77-KK127, KK143-KK127 and KK193-KK127, respectively. PCR products were subsequently cloned into pGBKT7 (Clontech Laboratories, France) between the *Nde*I-*Bam*HI sites.

For verification of ALIX interactor candidates found in a Y2H screen, GAD-FIP1 (pKK58), GAD-CaLB-family protein (pKK90) and GAD-XBAT35 (pKK96) were cloned. ORFs were amplified from Arabidopsis cDNA using primer pairs KK150-KK151, KK156-KK157, KK154-KK155, KK152-KK153, respectively. PCR products were cloned into pGADT7 (Clontech Laboratories, France) between the *Nde*I-*Bam*HI sites. GAD-AMSH3(WT) (pAK18), GAD-AMSH3(N154) (pAK83), GAD-AMSH3(∆MIT) (pAK85), GAD-AMSH3(∆MPN) (pAK88) were cloned by A. Katsiarimpa and published previously (Katsiarimpa et al., 2011). GAD-AMSH3(middle) (pFA171) was cloned by F. Anzenberger and published in (Kalinowska et al., 2015).

For *in vitro* pulldown assays, GST-AMSH1(N154) (pKK10) was amplified using primers EI9 and KK10. Obtained PCR product was cloned into pGEX-6P-1 (GE Healthcare Life Sciences, Germany) between the *Bam*HI and *Sal*I sites. To generate MBP-ALIX (pKK20), MBP-AAA ATPase (pKK17), MBP-EML2 (pKK18), MBP-EXO70E2 (pKK21) and MBP-unknown protein no. 1 (pKK24), ORFs were amplified from cDNA using primer pairs: KK40-KK41, KK44-KK45, KK46-KK47, KK23-KK24 and KK42-KK43, respectively. Inserts were cloned into pMAL-p2T (New England Biolabs, Germany) using following restriction sites:

*Bam*HI-*Sal*I for ALIX, AAA ATPase and unknown protein no. 1, and *Bam*HI-*Xho*I for EML2 and EXO70E2. For cloning of MBP-VPS2.1 and MBP-VPS60.1, inserts were cut out from pGEX-6P-1 with *Bam*HI and *Sal*I (Katsiarimpa et al., 2013), and ligated into pMAL-p2p (based on pMAL-p2 from New England Biolabs, Germany; a gift from K. Tanaka lab, Tokyo Metropolitan Institute for Medical Science, Japan).

For DUB assays, GST-AMSH1(MPN) (pKK8) was generated. The *AMSH1* fragment was amplified using primers KK8 and EI10 and cloned into pGEX-6P-1 between the *Bam*HI-*Sal*I sites. GST-AMSH1 (pEI1) and GST-AMSH3 (pEI3) were cloned by E. Isono and published in (Isono et al., 2010; Katsiarimpa et al., 2013). GST-VPS2.1(MIM) (pAK36) was cloned by A. Katsiarimpa and published in (Katsiarimpa et al., 2013).

4.2.2.2.2. Gateway cloning

The PCR conditions for amplification of the insert were identical as described in 4.2.2.2.1. The Gateway cloning was conducted using Gateway BP Clonase II Enzyme Mix and Gateway LR Clonase II Enzyme Mix (Bio-Rad Laboratories, Germany) according to manufacturer's recommendations.

4.2.2.2.2.1. Constructs obtained by Gateway cloning

For the Y2H screen, GBD-AMSH1(WT) (pKK1), GBD-AMSH2(WT) (pKK2), GBD-AMSH3(WT) (pKK3) and GBD-AMSH3(AXA) (pKK4) were generated by LR reaction using constructs *pDONR207-AMSH1(WT)* (pEI7)*, pDONR207-AMSH2(WT)* (pEI8)*, pDONR207-AMSH3(WT)* (pEI9) and *pDONR207-AMSH3(AXA)* (pEI12). pENTR constructs were cloned by E. Isono (Isono et al., 2010; Katsiarimpa et al., 2011; Katsiarimpa et al., 2013; Kalinowska et al., 2015), the destination vector used was pDEST-BD_pPC97 (Dreze et al., 2010). To create GBD- and GAD-ALIX, the *ALIX* ORF was amplified using primers TF1 and TF2 (primers designed by T. Fischer), transformed into pDONR207 (Thermo Fisher Scientific, Germany) (pKK36) and subsequently into pDEST-BD_pPC97 (pKK44) and pDEST-AD-CYH2 (pKK45) (Dreze et al., 2010).

For overexpression in plants, the ORF of *ALIX* was amplified using primers KK169 and TF2, cloned into pDONR207 (pKK69) and subsequently into pFAST-R05 (Shimada et al., 2010) to obtain *35Spro:ALIX* (pKK72). The presence of a stop codon at the end of the sequence caused removal of the C-terminal tag and overexpression of an untagged protein.

35Spro:AMSH3-TagRFP (pKK7) was generated by the LR reaction between the *pDONR207-AMSH3* (pEI54) cloned by E. Isono and a pGWB560 vector [T. Nakagawa, Matsue, Japan (Nakagawa et al., 2007)].

To obtain *UBQ10pro:CFP-ARA7*, the *ARA7* ORF was amplified from cDNA using primers KK101 and KK102 and cloned first into pDONR207 (pKK34) and subsequently into pUBN-CFP-DEST (Grefen et al., 2010) (pKK35).

For generation of *AMSH3pro:AMSH3-YFP* (pFA15) and *AMSH3pro:AMSH3-TagRFP* (pMN73), the stop codon in *AMSH3pro:YFP-AMSH3* construct (pFA14) (Katsiarimpa et al., 2011) was replaced with the *Nco*I site by PCR-based mutagenesis, and the 5' YFP was removed. The coding sequence for YFP or TagRFP were then cloned into the newly created *Nco*I site. Constructs were cloned by F. Anzenberger and M.K. Nagel, respectively, and published in (Kalinowska et al., 2015).

The *ALIXpro:GFP-ALIX* construct was cloned by L. Carrera and published in (Cardona-Lopez et al., 2015). *UBQ10pro:mCherry-VPS2.1* (pAK29) was cloned by A. Katsiarimpa and published in (Katsiarimpa et al., 2011). *35Spro:HA-SKD1(WT)* (pEI151) and *35Spro:HA-SKD1(EQ)* (pEI149) were cloned by E. Isono and published in (Katsiarimpa et al., 2011). Own-promoter-driven mRFP-tagged markers were cloned by T. Uemura, T. Ueda and A. Nakano, and published in (Ueda et al., 2004; Uemura et al., 2004; Ebine et al., 2011).

4.2.2.3. Isolation of genomic DNA from Arabidopsis

Whole seedlings or leaves of adult plants were used for genomic DNA purification. Plant material was ground manually using plastic homogenizers or in TissueLyser II (Quiagen, Germany) in the presence of glass beads. Powdered material was mixed with 200 µl of DNA Extraction Buffer [250 mM NaCl, 200 mM Tris-HCl pH 7.5, 25 mM EDTA pH 8.0, 0.5% (w/v) SDS]. The suspension was incubated for 40 min at 65°C and 200 µl of phenol:chloroform (1:1) was added. The suspension was centrifuged at 13,000 *g* for 5 min at RT. The water phase was transferred to the new tube containing 100 µl of isopropanol and centrifuged at 13,000 *g* for 20 min at 4°C. The DNA pellet was washed once with 200 µl of 70% (v/v) ethanol and dried. After drying, the pellet was resolved in 200 µl of distilled water.

4.2.2.4. PCR conditions for genotyping

For determining the genotype of transgenic plants, a recombinant Taq polymerase was used. 30-µl reaction tubes contained: 20 mM Tris-HCl pH 8.4, 50 mM KCl and 2.5 mM $MgCl_2$, 2.5

mM dNTPs, 0.7 µM primers, 0.2 µl house Taq DNA polymerase and 3 µl of genomic DNA. The PCR program started with an initial denaturation at 94°C for 5 min, followed by 30 to 35 cycles of denaturation at 94°C for 1 min, annealing at 58°C for 1 min and the extension at 72°C for 1 min/kb. The final extension step at 72°C for 7 min was usually included. The PCR products were analyzed on a 1% (w/v) agarose gel or by automated DNA electrophoresis using QUIAxcel Advanced System (Quiagen, Netherlands).

4.2.2.5. Yeast two-hybrid analysis

4.2.2.5.1. Yeast two-hybrid screen

The Y2H screen was conducted as described in (Dreze et al., 2010). The yeast strain Y8930 (*MATα, leu2-3,112 trp1-901 his3-200 ura3-52 gal4Δ gal80Δ GAL2-ADE2 LYS2::GAL1-HIS3 MET2::GAL7-lacZ cyh2^R)* was transformed with one of GBD-AMSH1, -AMSH2, -AMSH3(WT) and -AMSH3(AXA). Autoactivation of reporter genes was tested on SC-LWH (synthetic complete medium lacking leucine, tryptophan and histidine), supplemented with 1-, 3- and 5 mM 3-AT (3-amino-1,2,4-triazole), with or without 3.6 mM CHX (cycloheximide). The baits were screened by yeast mating against a collection of 12,000 GAD-fused Arabidopsis ORFs in the yeast strain Y8800 (*MATa, leu2-3,112 trp1-901 his3-200 ura3-52 gal4Δ gal80Δ GAL2-ADE2 LYS2::GAL1-HIS3 MET2::GAL7-lacZ cyh2^R*). 188 pray clones were collected in one pool for efficient screening. Yeast growth was assayed on SC-LWH+1mM 3-AT, SC-LWH+1mM 3-AT+3.6 mM CHX, SC-LWA (synthetic complete medium lacking leucine, tryptophan and adenine) and SC-LTA+3.6 mM CHX. The screen was carried out twice.

4.2.2.5.2. DNA isolation from yeast and sequencing

For DNA isolation, yeast cells were collected with a pipette tip from a plate and resuspended in 30 µl of Potassium Phosphate Buffer (16 mM KH_2PO_4, 4 mM K_2HPO_4, pH 7.4) containing 1,440 U lyticase (Sigma-Aldrich Germany) to digest the cell walls. After incubation for 1 h at 20°C, the enzyme was inactivated by heating at 95°C for 5 min. 1.8 µl of the post-digest solution were used for PCR in a total volume of 30 µl in conditions described in 4.2.2.4.

Alternatively, DNA was isolated using STES (Sodium chloride-Tris-EDTA-SDS) Buffer. Yeast cells were collected from a plate with a pipette tip and resolved in 50 µl of STES Buffer [200 mM Tris-HCl pH 7.6, 500 mM NaCl, 10 mM EDTA, 0.1% (w/v) SDS]. 30 µl of glass beads were added and samples were vortexed for 5 min at RT. First 200 µl of TE (Tris-EDTA) Buffer (10 mM Tris-HCl pH 8.0, 1 mM EDTA pH 8.0) and then 200 µl of phenol:chloroform (1:1, v/v)

were added to the mixture. After centrifugation at 13,000 *g* for 10 min at RT, 150 µl of the water phase were transferred to a new 1.5-ml tube. 100 µl of chloroform were added and samples were centrifuged again at 13,000 *g* for 10 min. 120 µl of the water phase were transferred to a new tube and DNA was concentrated by ethanol precipitation as described in 4.2.2.2.1. The DNA pellet was resuspended in 50 µl of Ribonuclease A (1,250 U) solution and used for the PCR reaction.

4.2.2.5.3. Targeted yeast two-hybrid assays

For the double transformation of yeast, the strain Y8800 was grown for 4 h in liquid YPD (yeast extract, peptone, dextrose), collected, resuspended in 2 ml of LA (Lithium Acetate) Buffer (100 mM LA, 10 mM Tris pH 8.0, 1 mM EDTA pH 8.0) and incubated at RT for 10 min. 40 to 100 µg plasmid DNA of both pGADT7- and pGBKT7-based constructs were added to 100 µl of yeast cell solution. Samples were thoroughly mixed with 300 µl of 40% (w/v) PEG4000 solution and incubated at RT for 1 h. 35 µl of DMSO were added to the samples and incubated for 10 min at 42°C. Cells were collected by centrifugation at 1,000 *g* for 2 min, washed once with TE Buffer and plated on SC-LW plates. After the incubation for three days at 30°C, the transformants were tested for auxotrophic growth on SC-LWH and SC-LW.

4.2.2.5.4. Total protein extraction from yeast and expression analysis

To verify the expression of Y2H constructs, total proteins were extracted and subjected to immunoblotting. Yeast cells were collected from SC-LW plates, resuspended in 100 µl of 100 mM NaOH and incubated for 5 min at RT. After centrifugation for 1 min at 800 *g*, yeast pellets were washed once with 1 ml of PBS (Phosphate-Buffered Saline) (137 mM NaCl, 2.7 mM KCl, 10 mM Na_2HPO_4, 2 mM KH_2PO_4, pH 7.4) and the supernatant was discarded. Cells were resuspended in 50 µl of 1x Laemmli Buffer [50 mM Tris-HCl pH 6.8, 2% (w/v) SDS, 6% (v/v) glycerol, 1% (v/v) β-mercaptoethanol, 0.01% (w/v) bromophenol blue] and analyzed on immunoblot using anti-GBD (Santa Cruz Biotechnology, Germany), anti-HA-HRP (Roche Diagnostics, Germany) for AD-fused proteins and anti-CDC2 antibodies (Santa Cruz Biotechnology, Germany) for loading control.

4.2.3. Biochemical methods

4.2.3.1. Total protein extraction from plants

Typically 100 mg of fresh plant material was collected and homogenized in the presence of Protein Extraction Buffer [50 mM Tris-HCl pH 7.5, 150 mM NaCl, 0.5% (v/v) Triton X-100, 1x complete EDTA-free protease inhibitor cocktail (Roche Diagnostics, Germany)]. The homogenate was cleared by centrifugation for 15 min at 13,000 *g* at 4°C. Protein concentration of the extracts was quantified by the Bradford assay using Protein Assay Dye Reagent Concentrate (Bio-Rad Laboratories, Germany). 5x Laemmli Buffer was added to plant extracts and the samples were incubated at 98°C for 5 min before being subjected to immunoblot analysis.

4.2.3.2. Immunoprecipitation

2 g 7-day-old seedlings were homogenized using a mortar and pestle, and resuspended in 1.5 ml of Buffer A [50 mM Tris-HCl pH 7.5, 100 mM NaCl, 10% (v/v) glycerol] supplemented with 0.2% (v/v) Triton X-100 and 1x complete EDTA-free protease inhibitor cocktail. The total extract was centrifuged at 13,000 *g* for 15 min at 4°C. Supernatant was diluted with Buffer A without Triton X-100 to the final detergent concentration of 0.06%. 30 µl of GFP-Trap A beads (ChromoTek, Germany) were added to immunoprecipitate GFP-ALIX. After a 2-h incubation at 4°C with rotation, beads were washed extensively with Buffer A without detergent. 50 µl of 5x Laemmli Buffer were added and after heating for 5 min at 98°C, samples were subjected to immunoblot.

4.2.3.3. Recombinant protein purification

For the purification of recombinant proteins, *E.coli* Rosetta (DE3), Rosetta-gami 2 or Rosetta-gami B strains (Merck Millipore, Germany) were transformed (genotypes of bacteria are described in Appendix Table 10). The bacteria were grown in 500-ml cultures and the protein expression was induced by the addition of 0.2 to 1 mM IPTG (isopropyl β-D-1-thiogalactopyranoside). Depending on the protein solubility, *E. coli* cells were incubated at 37°C for 3 h or at 18°C for 18 h. Cells were afterwards collected by centrifugation and the pellet was resuspended in Buffer A supplemented with 0.1 to 0.2% (v/v) Triton X-100 and 1x complete EDTA-free protease inhibitor cocktail. Cells were homogenized using an ultrasonic homogenizer twice for 15 min, 5 cycles at 20% output. After centrifugation for 10 min at 13,000 *g* at 4°C, affinity resins were added to the supernatant. For His-tagged proteins, GST-tagged

proteins and MBP-tagged proteins, TALON Metal Affinity Resin (Clontech Laboratories, France), Protino Glutathione Agarose 4B (Macherey-Nagel, Germany) and Amylose Magnetic Beads (New England Biolabs, Germany) were used, respectively. *E. coli* extracts were incubated with the matrix for 2 h at 4°C with rotation. Afterwards, beads were washed extensively with Buffer A supplemented with Triton X-100 and with Buffer A without detergent. Recombinant proteins were either retained on the matrix, cleaved off from the tag by overnight incubation with 4 U PreScission protease (GE Healthcare Life Sciences, Germany) in 200 µl of Buffer A, or eluted. For elution with the fused tag, 400 mM imidazol, 50 mM glutathione or 10 mM maltose was added to His-tagged-, GST- or MBP-tagged proteins, respectively, and the samples were incubated for 20 min at RT with shaking. The eluate was dialyzed against Buffer A using Mini Bio-Spin Chromatography Columns (Bio-Rad Laboratories, Germany). For quantification of protein concentrations, protein samples were mixed with 5x Laemmli Buffer, loaded on SDS-PAGE and stained with Coomassie Brilliant Blue G (Sigma-Aldrich, Germany) or R-250 (AppliChem, Germany). BenchMark Protein Ladder (Thermo Fisher Scientific, Germany) was used as a concentration standard. Quantification was performed using the LAS-4000 mini system (Fujifilm, Japan).

4.2.3.4. *In vitro* binding assay

For *in vitro* GST-pulldown assay, Protino Glutathione Agarose 4B beads (Macherey-Nagel, Germany) were incubated with 8 µg of GST or GST-fused VPS2.1(MIM) for 2 hours at 4°C with rotation. Beads were washed twice and blocked for 20 min with a saturated skimmed milk solution. The coupled beads were washed once and resuspended in 20 µl of Buffer A. Protein concentrations were determined on after Coomassie Brilliant Blue-staining on a gel as described above. Equal amounts of GST and GST-VPS2.1(MIM) were incubated under agitation with 1 µg AMSH1(N154) in 100 µl Buffer A supplemented with 0.1% (v/v) Triton X-100 for 45 min at 4°C with rotation. Afterwards, the beads were washed twice with Buffer A supplemented with 0.1 % (v/v) Triton X-100 and three times with Buffer A without detergent. The beads were resuspended in 1x Laemmli Buffer and heated at 98°C for 5 min. Beads-bound proteins were analyzed by immunoblotting using anti-GST (GE Healthcare Life Sciences, Germany) and anti-AMSH1 (Katsiarimpa et al., 2013) antibodies.

For *in vitro* MBP-pulldown assays, Amylose Magnetic Beads (New England BioLabs, Germany) containing 1 µg MBP-tagged proteins were incubated for 1 to 4 h (depending on the affinity of interaction) on ice with 1 µg AMSH1 or AMSH3 in either Buffer A supplemented with 0.1% (v/v) Triton X-100 or in Buffer B [50 mM Tris-HCl pH 7.6, 150 mM NaCl, 10 mM $MgCl_2$, 0.05% (v/v) Tween-20]. Afterwards, the beads were washed four times either with

Buffer A or Buffer B. The results were analyzed on immunoblot using anti-MBP (New England BioLabs, Germany), anti-AMSH1 and anti-AMSH3 antibodies (Isono et al., 2010).

4.2.3.5. *In vitro* ubiquitin binding assay

For *in vitro* ubiquitin binding assays, agarose-immobilized monoubiquitin (Enzo Life Sciences, Germany) was used. 20 µl ubiquitin beads were transferred to a mini spin column and washed with PBS. Beads were blocked for 20 min with 0.1% (w/v) bovine serum albumin. Afterwards, 8 µg of His-tagged protein of interest was added. Binding was conducted at 4°C in PBS for 4 h with rotation. Afterwards, the beads were washed four times with PBS, resuspended in 1x NuPAGE SDS Sample Buffer [141 mM Tris hypochloride, 2% (w/v) SDS, 10% (v/v) glycerol, 0.51 mM EDTA, 0.22 mM SERVA Blue G250, 0.175 mM phenol red] and incubated at 80°C for 10 min. Results were analyzed by SDS-PAGE (SDS-Polyacrylamide-Gel Electrophoresis) and NuPAGE SDS-PAGE followed by Coomassie Brilliant Blue G staining or by immunoblot using anti-His-HRP (Sigma-Aldrich, Germany) and anti-ubiquitin (P4D1) (Santa Cruz Biotechnology, Germany) antibodies, respectively.

4.2.3.6. Deubiquitinase assay

For DUB assays, K48- or K63-linked polyubiquitin (Ub2-7) (Enzo Life Sciences, Germany) was used as substrates. Recombinant AMSH1(MPN) was expressed and purified from *E. coli*. 250 ng substrate and 2 pmol enzyme were used for reaction and in DUB Assay Buffer (50 mM Tris-HCl pH 7.2, 25 mM KCl, 5 mM $MgCl_2$, 1 mM DTT). Reactions were initiated by the addition of the substrate and the samples were incubated at 25°C for 0, 5, 15 and 60 min. Reactions were terminated by the addition of 4x NuPAGE SDS Sample Buffer and analyzed on immunoblot using an anti-ubiquitin antibody.

For fluorescence detection-based assay, 0.4 µM diUb (K63-linked) FRET TAMRA Position 3 (R&D Systems, USA) was incubated with 50 nM AMSH3 in TAMRA DUB Assay Buffer [50 mM Tris-HCl pH 7.5, 100 mM NaCl, 0.1% (w/v) Pluronic F-127, 1 mM TCEP]. To examine the effect of ALIX on AMSH3 activity, AMSH3 was pre-incubated with 50 nM His-ALIX(middle) for 30 min at RT prior to addition of the substrate. Fluorescence polarization was measured using Synergy 2 Multi-Mode Microplate Reader (BioTek Instruments, USA). Filters for excitation at 530 nm and emission at 590 nm were used. The fluorescence of the sample was measured every minute.

4.2.3.7. SDS-PAGE

The SDS-PAGE (SDS-Polyacrylamide-Gel Electrophoresis) was conducted as described in (Laemmli, 1970) using Mini-PROTEAN III system (Bio-Rad Laboratories, Germany). For preparation of 5% (v/v) stacking gel and 7.5 to 15% (v/v) resolving (separating) gels, Acrylamide Rotiphorese Gel 30 (37, 5:1) (Carl Roth, Germany) was used. SDS Running Buffer [25 mM Tris, 192 mM glycin and 0.04% (w/v) SDS] was used during electrophoresis. PageRuler Plus Prestained Protein Ladder (Thermo Fisher Scientific, Germany) was applied as a size marker and BenchMark Protein Ladder (Thermo Fisher Scientific, Germany) as a protein quantity marker.

4.2.3.8. Coomassie Brilliant Blue staining

For visualization and quantification of protein amount, SDS-PAGE or NuPAGE gels were stained with Coomassie Brilliant Blue Staining Solution [40% (v/v) ethanol, 7% (V/v) acetic acid, 0.25% (w/v) Coomassie Brilliant Blue G or R-250] for at least 30 min. Gels were destained using Destaining Solution [40% (v/v) ethanol, 7% (V/v) acetic acid].

4.2.3.9. Immunoblot analysis

Proteins from SDS-PAGE were transferred on Immobilon-P (PVDF) Transfer Membrane, pore size 0.45 µm (Merck Millipore, Germany). Before the transfer, the membrane was immersed in 100% (v/v) methanol for 1 min. SD (Semi-Dry) Transfer Buffer [25 mM Tris-HCl pH 8.3, 192 mM glycine, 20% (v/v) methanol, 0.04% (w/v) SDS] and the semi-dry electroblotter (Peqlab Biotechnologie, Germany) were used for the transfer.

Afterwards, the membrane was blocked for 15 min with 10% (w/v) skimmed milk in TBS-T (Tris-Buffered Saline supplemented with Tween-20) [50 mM Tris-HCl pH 7.5, 150 mM NaCl, 1 mM $MgCl_2$, 0.05% (v/v) Tween-20]. The membrane was incubated with the primary antibody in TBS-T containing 5% (w/v) skimmed milk for 1 h at RT or overnight at 4°C. Membrane was washed three times for 15 min with TBS-T. The incubation with the secondary antibody was conducted in TBS-T for 1 h at RT. The washing step was done as described above. The antibodies used for immunoblots are listed in Appendix Table 4.

For colorimetric AP (alkaline phosphatase) detection, 550 µM BCIP and 400 µM NBT in AP-Puffer (100 mM Tris-HCl pH 9.5, 100 mM NaCl, 5 mM $MgCl_2$) were used to visualize protein bands on the membrane.

For HRP (horseradish peroxidase) chemiluminescence detection, Pierce ECL Plus Western Blotting Substrate (Thermo Fisher Scientific, Germany) or SuperSignal Femto Maximum Sensitivity Substrate (Thermo Fisher Scientific, Germany) were used, and the chemiluminescence was detected using the LAS-4000 mini system (Fujifilm, Japan).

4.2.3.10. Gradient gels

For SDS-PAGE using NuPAGE Novex 4-12% Bis-Tris Protein Gels (Thermo Fisher Scientific, Germany), proteins were incubated with NuPAGE SDS Sample Buffer [141 mM Tris hypochloride, 2% (w/v) SDS, 10% (v/v) glycerol, 0.51 mM EDTA, 0.22 mM SERVA Blue G250, 0.175 mM phenol red] before loading. Electrophoresis was conducted in MES SDS Running Buffer [50 mM MES, 50 mM Tris base, 0.1% (w/v) SDS, 1 mM EDTA, pH 7.3] and in the XCell SureLock Mini-Cell Electrophoresis System apparatus (Thermo Fisher Scientific, Germany) at 200 V for 35 min. The SD transfer was conducted using NuPAGE Transfer Buffer [50 mM bicine, 50 mM Bis-Tris (free base), 1mM EDTA, 10% (v/v) methanol] at 25 V for 25 min.

Alternatively, Precise 4-20% Tris-Glycine Gels (Thermo Fisher Scientific, Germany) were used in combination with SDS-PAGE Running Buffer and SD Transfer Buffer.

4.2.3.11. Production of antibodies

For antibody production, His-ALIX(middle) (pKK29) was cloned by amplification of the region containing the V-domain of ALIX using primers KK89 and KK100 and cloning into pET21a (Merck Millipore, Germany) between the *Bam*HI and *Sal*I sites. The polyclonal antibody against the middle domain of ALIX was raised in rabbits (Eurogentec, Belgium). Animals were immunized with 800 µg recombinant His-ALIX(middle) that was overexpressed and purified from *E.coli* Rosetta (DE3) strain. The obtained rabbit serum was used in a 1:1,000 dilution for immunoblot analysis. Specificity of the anti-ALIX antibody was verified on an immunoblot using total extracts from wild type and *alix* null mutants.

4.2.4. Histochemical methods

4.2.4.1. Microscopy

Fluorescently-tagged proteins were imaged using the FV-1000/IX81 confocal laser scanning microscope with UPlanSApo x10 or x60 objective (Olympus Europa, Germany). CFP signals were visualized using the 458-nm laser line, GFP with 488-nm, YFP with 515-nm, RFP-,

mCherry- and mKO with 559-nm. MDC staining and BCECF-AM were visualized with the 405-nm and 488-nm laser lines, respectively. Images were obtained using the Fluoview FV-1000 software (Olympus Europa, Germany) with 0.1 to 18% laser power, 600 to 800 high voltage (HV), 1x gain and 4x Kalman line averaging. The images were processed using Adobe Photoshop CS3 Extended (Version 10.0) and Adobe Illustrator CS3 (Version 13.0.0) (Adobe Systems, USA).

4.2.4.2. Live cell imaging, drug treatment, staining and data analysis

4.2.4.2.1. Image analysis using Imaris 8 and Fiji

For the comparison of the number of vesicles per area, the area of 100 µm^2 in root epidermis tissue was determined using Fluoview FV-1000 software (Olympus Europa, Germany). Vesicles were counted using the software Imaris 8 (Bitplane, Switzerland). For analysis of signal recruitment to Wortmannin-induced structures, WM compartments were determined using Imaris 8 as structures with a minimal diameter of 1.5 µm. For analysis of colocalization rates between the coexpressed fluorescently-tagged proteins, Arabidopsis seedlings were grown for 5 to 8 days on GM in long day. After imaging, colocalization rates were calculated using Cell Counter Plug-in in Fiji 1.49c (Image J, NIH, USA).

4.2.4.2.2. Brefeldin A and Wortmannin treatment

For WM treatment, 7-day-old seedlings were incubated in liquid GM supplemented with 33 µM WM (AppliChem, Germany) for 60 to 120 min. For BFA treatment, seedlings were incubated in liquid GM containing 50 µM BFA (Thermo Fisher Scientific, Germany) for 30 to 60 min. To prevent washout of the drugs, seedlings were immersed in medium containing the inhibitors during observation under the confocal laser scanning microscope.

4.2.4.2.3. BCECF-AM staining and 3D reconstruction

For visualization of vacuoles in root epidermis cells, 2- and 9-day-old seedlings were incubated in liquid GM supplemented with 5 µM BCECF-AM (Thermo Fisher Scientific, Germany) and 0.02% (w/v) Pluronic F-127 (Sigma-Aldrich, Germany) for 60 min at RT in the dark. 70 Z-stacks images with 0.2 µm step size were obtained using confocal laser scanning microscope and a 488 nm laser line. Images were processed using Imaris 8 (Bitplane, Switzerland).

Surface renderings were performed with the surface area detail level set to 0.122 µm and signal intensity threshold to 80 units.

4.2.4.2.4. E-64d treatment and MDC staining

Arabidopsis seedlings were grown on ½ MS medium first for 7 days in long day and then for 2 days in the dark to induce carbon deficiency conditions. To trigger the accumulation of autophagic bodies, seedlings were subsequently incubated in liquid ½ MS supplemented with 100 µM E-64d (Santa Cruz Biotechnology, Germany) for 30 min. For visualization of autophagic bodies, seedlings were stained with 50 µM MDC (Sigma-Aldrich, Germany) in PBS for 10 min at RT. After extensive washing, MDC signals were examined under the confocal laser scanning microscope. The area of MDC-stained structures was analyzed using the Fluoview FV1000 software (Olympus Europa, Germany).

References

Abas, L., Benjamins, R., Malenica, N., Paciorek, T., Wisniewska, J., Moulinier-Anzola, J.C., Sieberer, T., Friml, J., and Luschnig, C. (2006). Intracellular trafficking and proteolysis of the Arabidopsis auxin-efflux facilitator PIN2 are involved in root gravitropism. Nature cell biology **8,** 249-256.

Agromayor, M., and Martin-Serrano, J. (2006). Interaction of AMSH with ESCRT-III and deubiquitination of endosomal cargo. The Journal of biological chemistry **281,** 23083-23091.

Ali, N., Zhang, L., Taylor, S., Mironov, A., Urbe, S., and Woodman, P. (2013). Recruitment of UBPY and ESCRT exchange drive HD-PTP-dependent sorting of EGFR to the MVB. Current biology : CB **23,** 453-461.

Amerik, A.Y., Nowak, J., Swaminathan, S., and Hochstrasser, M. (2000). The Doa4 deubiquitinating enzyme is functionally linked to the vacuolar protein-sorting and endocytic pathways. Molecular biology of the cell **11,** 3365-3380.

Arabidopsis Interactome Mapping, C. (2011). Evidence for network evolution in an Arabidopsis interactome map. Science **333,** 601-607.

Babst, M., Wendland, B., Estepa, E.J., and Emr, S.D. (1998). The Vps4p AAA ATPase regulates membrane association of a Vps protein complex required for normal endosome function. The EMBO journal **17,** 2982-2993.

Bachmair, A., Novatchkova, M., Potuschak, T., and Eisenhaber, F. (2001). Ubiquitylation in plants: a post-genomic look at a post-translational modification. Trends in plant science **6,** 463-470.

Banno, H., and Chua, N.H. (2000). Characterization of the arabidopsis formin-like protein AFH1 and its interacting protein. Plant & cell physiology **41,** 617-626.

Banta, L.M., Robinson, J.S., Klionsky, D.J., and Emr, S.D. (1988). Organelle assembly in yeast: characterization of yeast mutants defective in vacuolar biogenesis and protein sorting. The Journal of cell biology **107,** 1369-1383.

Barberon, M., Dubeaux, G., Kolb, C., Isono, E., Zelazny, E., and Vert, G. (2014). Polarization of IRON-REGULATED TRANSPORTER 1 (IRT1) to the plant-soil interface plays crucial role in metal homeostasis. Proceedings of the National Academy of Sciences of the United States of America **111,** 8293-8298.

Barberon, M., Zelazny, E., Robert, S., Conejero, G., Curie, C., Friml, J., and Vert, G. (2011). Monoubiquitin-dependent endocytosis of the iron-regulated transporter 1 (IRT1) transporter controls iron uptake in plants. Proceedings of the National Academy of Sciences of the United States of America **108,** E450-458.

Barbosa, I.C., Zourelidou, M., Willige, B.C., Weller, B., and Schwechheimer, C. (2014). D6 PROTEIN KINASE activates auxin transport-dependent growth and PIN-FORMED phosphorylation at the plasma membrane. Developmental cell **29,** 674-685.

Bartel, B. (2015). Proteaphagy-Selective Autophagy of Inactive Proteasomes. Molecular cell **58,** 970-971.

Bassham, D.C. (2009). Function and regulation of macroautophagy in plants. Biochim Biophys Acta **1793,** 1397-1403.

Beal, R., Deveraux, Q., Xia, G., Rechsteiner, M., and Pickart, C. (1996). Surface hydrophobic residues of multiubiquitin chains essential for proteolytic targeting. Proceedings of the National Academy of Sciences of the United States of America **93,** 861-866.

Bissig, C., and Gruenberg, J. (2014). ALIX and the multivesicular endosome: ALIX in Wonderland. Trends in cell biology **24,** 19-25.

Blanc, C., Charette, S.J., Mattei, S., Aubry, L., Smith, E.W., Cosson, P., and Letourneur, F. (2009). Dictyostelium Tom1 participates to an ancestral ESCRT-0 complex. Traffic **10,** 161-171.

Book, A.J., Gladman, N.P., Lee, S.S., Scalf, M., Smith, L.M., and Vierstra, R.D. (2010). Affinity purification of the Arabidopsis 26 S proteasome reveals a diverse array of plant proteolytic complexes. The Journal of biological chemistry **285,** 25554-25569.

Book, A.J., Smalle, J., Lee, K.H., Yang, P., Walker, J.M., Casper, S., Holmes, J.H., Russo, L.A., Buzzinotti, Z.W., Jenik, P.D., and Vierstra, R.D. (2009). The RPN5 subunit of the 26s proteasome is essential for gametogenesis, sporophyte development, and complex assembly in Arabidopsis. The Plant cell **21,** 460-478.

Boonyaratanakornkit, J., Schomacker, H., Collins, P., and Schmidt, A. (2013). Alix serves as an adaptor that allows human parainfluenza virus type 1 to interact with the host cell ESCRT system. PloS one **8,** e59462.

Boysen, J.H., and Mitchell, A.P. (2006). Control of Bro1-domain protein Rim20 localization by external pH, ESCRT machinery, and the Saccharomyces cerevisiae Rim101 pathway. Molecular biology of the cell **17,** 1344-1353.

Bozkurt, T.O., Belhaj, K., Dagdas, Y.F., Chaparro-Garcia, A., Wu, C.H., Cano, L.M., and Kamoun, S. (2015). Rerouting of plant late endocytic trafficking toward a pathogen interface. Traffic **16,** 204-226.

Brukhin, V., Gheyselinck, J., Gagliardini, V., Genschik, P., and Grossniklaus, U. (2005). The RPN1 subunit of the 26S proteasome in Arabidopsis is essential for embryogenesis. The Plant cell **17,** 2723-2737.

Buono, R.A., Paez-Valencia, J., Miller, N.D., Goodman, K., Spitzer, C., Spalding, E.P., and Otegui, M.S. (2016). Role of SKD1 Regulators LIP5 and IST1-LIKE1 in Endosomal Sorting and Plant Development. Plant physiology **171,** 251-264.

Cardona-Lopez, X., Cuyas, L., Marin, E., Rajulu, C., Irigoyen, M.L., Gil, E., Puga, M.I., Bligny, R., Nussaume, L., Geldner, N., Paz-Ares, J., and Rubio, V. (2015). ESCRT-III-Associated Protein ALIX Mediates High-Affinity Phosphate Transporter Trafficking to Maintain Phosphate Homeostasis in Arabidopsis. The Plant cell **27,** 2560-2581.

Carlton, J.G., Agromayor, M., and Martin-Serrano, J. (2008). Differential requirements for Alix and ESCRT-III in cytokinesis and HIV-1 release. Proceedings of the National Academy of Sciences of the United States of America **105,** 10541-10546.

Carter, M.T., Mirzaa, G., McDonell, L.M., and Boycott, K.M. (1993). Microcephaly-Capillary Malformation Syndrome. In GeneReviews(R), R.A. Pagon, M.P. Adam, H.H. Ardinger, S.E. Wallace, A. Amemiya, L.J.H. Bean, T.D. Bird, C.T. Fong, H.C. Mefford, R.J.H. Smith, and K. Stephens, eds (Seattle (WA).

Carvalho, S.D., Saraiva, R., Maia, T.M., Abreu, I.A., and Duque, P. (2012). XBAT35, a novel Arabidopsis RING E3 ligase exhibiting dual targeting of its splice isoforms, is involved in ethylene-mediated regulation of apical hook curvature. Mol Plant **5,** 1295-1309.

Castiglioni, S., and Maier, J.A. (2012). The tyrosine phosphatase HD-PTP (PTPN23) is degraded by calpains in a calcium-dependent manner. Biochemical and biophysical research communications **421,** 380-383.

Chakravorty, D., Gookin, T.E., Milner, M.J., Yu, Y., and Assmann, S.M. (2015). Extra-Large G Proteins Expand the Repertoire of Subunits in Arabidopsis Heterotrimeric G Protein Signaling. Plant physiology **169,** 512-529.

Chamovitz, D.A., Wei, N., Osterlund, M.T., von Arnim, A.G., Staub, J.M., Matsui, M., and Deng, X.W. (1996). The COP9 complex, a novel multisubunit nuclear regulator involved in light control of a plant developmental switch. Cell **86,** 115-121.

Chatellard-Causse, C., Blot, B., Cristina, N., Torch, S., Missotten, M., and Sadoul, R. (2002). Alix (ALG-2-interacting protein X), a protein involved in apoptosis, binds to endophilins and induces cytoplasmic vacuolization. The Journal of biological chemistry **277,** 29108-29115.

Chen, B., Borinstein, S.C., Gillis, J., Sykes, V.W., and Bogler, O. (2000). The glioma-associated protein SETA interacts with AIP1/Alix and ALG-2 and modulates apoptosis in astrocytes. The Journal of biological chemistry **275,** 19275-19281.

Chen, Y.A., and Scheller, R.H. (2001). SNARE-mediated membrane fusion. Nature reviews. Molecular cell biology **2,** 98-106.

Ciechanover, A. (1998). The ubiquitin-proteasome pathway: on protein death and cell life. The EMBO journal **17,** 7151-7160.

Clague, M.J., and Urbe, S. (2006). Endocytosis: the DUB version. Trends in cell biology **16,** 551-559.

Clough, S.J., and Bent, A.F. (1998). Floral dip: a simplified method for Agrobacterium-mediated transformation of Arabidopsis thaliana. The Plant journal : for cell and molecular biology **16,** 735-743.

Contento, A.L., Xiong, Y., and Bassham, D.C. (2005). Visualization of autophagy in Arabidopsis using the fluorescent dye monodansylcadaverine and a GFP-AtATG8e fusion protein. The Plant journal : for cell and molecular biology **42,** 598-608.

Cook, W.J., Jeffrey, L.C., Kasperek, E., and Pickart, C.M. (1994). Structure of tetraubiquitin shows how multiubiquitin chains can be formed. J Mol Biol **236,** 601-609.

Cope, G.A., and Deshaies, R.J. (2003). COP9 signalosome: a multifunctional regulator of SCF and other cullin-based ubiquitin ligases. Cell **114,** 663-671.

Cope, G.A., Suh, G.S., Aravind, L., Schwarz, S.E., Zipursky, S.L., Koonin, E.V., and Deshaies, R.J. (2002). Role of predicted metalloprotease motif of Jab1/Csn5 in cleavage of Nedd8 from Cul1. Science **298,** 608-611.

Davies, C.W., Paul, L.N., and Das, C. (2013). Mechanism of recruitment and activation of the endosome-associated deubiquitinase AMSH. Biochemistry **52,** 7818-7829.

Davies, C.W., Paul, L.N., Kim, M.I., and Das, C. (2011). Structural and thermodynamic comparison of the catalytic domain of AMSH and AMSH-LP: nearly identical fold but different stability. J Mol Biol **413,** 416-429.

de Silva, K., Laska, B., Brown, C., Sederoff, H.W., and Khodakovskaya, M. (2011). Arabidopsis thaliana calcium-dependent lipid-binding protein (AtCLB): a novel repressor of abiotic stress response. Journal of experimental botany **62,** 2679-2689.

Dejournett, R.E., Kobayashi, R., Pan, S., Wu, C., Etkin, L.D., Clark, R.B., Bogler, O., and Kuang, J. (2007). Phosphorylation of the proline-rich domain of Xp95 modulates Xp95 interaction with partner proteins. Biochem J **401,** 521-531.

Deng, L., Wang, C., Spencer, E., Yang, L., Braun, A., You, J., Slaughter, C., Pickart, C., and Chen, Z.J. (2000). Activation of the IkappaB kinase complex by TRAF6 requires a dimeric ubiquitin-conjugating enzyme complex and a unique polyubiquitin chain. Cell **103,** 351-361.

Deosaran, E., Larsen, K.B., Hua, R., Sargent, G., Wang, Y., Kim, S., Lamark, T., Jauregui, M., Law, K., Lippincott-Schwartz, J., Brech, A., Johansen, T., and Kim, P.K. (2013). NBR1 acts as an autophagy receptor for peroxisomes. Journal of cell science **126,** 939-952.

Doelling, J.H., Walker, J.M., Friedman, E.M., Thompson, A.R., and Vierstra, R.D. (2002). The APG8/12-activating enzyme APG7 is required for proper nutrient recycling and senescence in Arabidopsis thaliana. The Journal of biological chemistry **277,** 33105-33114.

Dores, M.R., Paing, M.M., Lin, H., Montagne, W.A., Marchese, A., and Trejo, J. (2012a). AP-3 regulates PAR1 ubiquitin-independent MVB/lysosomal sorting via an ALIX-mediated pathway. Molecular biology of the cell **23,** 3612-3623.

Dores, M.R., Chen, B., Lin, H., Soh, U.J., Paing, M.M., Montagne, W.A., Meerloo, T., and Trejo, J. (2012b). ALIX binds a YPX(3)L motif of the GPCR PAR1 and mediates ubiquitin-independent ESCRT-III/MVB sorting. The Journal of cell biology **197,** 407-419.

Dowlatshahi, D.P., Sandrin, V., Vivona, S., Shaler, T.A., Kaiser, S.E., Melandri, F., Sundquist, W.I., and Kopito, R.R. (2012). ALIX is a Lys63-specific polyubiquitin binding protein that functions in retrovirus budding. Developmental cell **23,** 1247-1254.

Doyle, S.M., Haeger, A., Vain, T., Rigal, A., Viotti, C., Langowska, M., Ma, Q., Friml, J., Raikhel, N.V., Hicks, G.R., and Robert, S. (2015). An early secretory pathway mediated by GNOM-LIKE 1 and GNOM is essential for basal polarity establishment in Arabidopsis thaliana. Proceedings of the National Academy of Sciences of the United States of America **112,** E806-815.

Dreze, M., Monachello, D., Lurin, C., Cusick, M.E., Hill, D.E., Vidal, M., and Braun, P. (2010). High-quality binary interactome mapping. Methods in enzymology **470,** 281-315.

Ebine, K., Inoue, T., Ito, J., Ito, E., Uemura, T., Goh, T., Abe, H., Sato, K., Nakano, A., and Ueda, T. (2014). Plant vacuolar trafficking occurs through distinctly regulated pathways. Current biology : CB **24,** 1375-1382.

Ebine, K., Fujimoto, M., Okatani, Y., Nishiyama, T., Goh, T., Ito, E., Dainobu, T., Nishitani, A., Uemura, T., Sato, M.H., Thordal-Christensen, H., Tsutsumi, N., Nakano, A., and Ueda, T. (2011). A membrane trafficking pathway regulated by the plant-specific RAB GTPase ARA6. Nature cell biology **13,** 853-859.

Fabbro, M., Zhou, B.B., Takahashi, M., Sarcevic, B., Lal, P., Graham, M.E., Gabrielli, B.G., Robinson, P.J., Nigg, E.A., Ono, Y., and Khanna, K.K. (2005). Cdk1/Erk2- and Plk1-dependent phosphorylation of a centrosome protein, Cep55, is required for its recruitment to midbody and cytokinesis. Developmental cell **9,** 477-488.

Faqeih, E.A., Bastaki, L., Rosti, R.O., Spencer, E.G., Zada, A.P., Saleh, M.A., Um, K., and Gleeson, J.G. (2015). Novel STAMBP mutation and additional findings in an Arabic family. Am J Med Genet A **167A,** 805-809.

Feraru, E., Paciorek, T., Feraru, M.I., Zwiewka, M., De Groodt, R., De Rycke, R., Kleine-Vehn, J., and Friml, J. (2010). The AP-3 beta adaptin mediates the biogenesis and function of lytic vacuoles in Arabidopsis. The Plant cell **22,** 2812-2824.

Finn, R.D., Bateman, A., Clements, J., Coggill, P., Eberhardt, R.Y., Eddy, S.R., Heger, A., Hetherington, K., Holm, L., Mistry, J., Sonnhammer, E.L., Tate, J., and Punta, M. (2014). Pfam: the protein families database. Nucleic acids research **42,** D222-230.

Frigerio, L., Hinz, G., and Robinson, D.G. (2008). Multiple vacuoles in plant cells: rule or exception? Traffic **9,** 1564-1570.

Fujimoto, M., Arimura, S., Ueda, T., Takanashi, H., Hayashi, Y., Nakano, A., and Tsutsumi, N. (2010). Arabidopsis dynamin-related proteins DRP2B and DRP1A participate together in clathrin-coated vesicle formation during endocytosis. Proceedings of the National Academy of Sciences of the United States of America **107,** 6094-6099.

Galan, J.M., and Haguenauer-Tsapis, R. (1997). Ubiquitin lys63 is involved in ubiquitination of a yeast plasma membrane protein. The EMBO journal **16,** 5847-5854.

Galindo, A., Hervas-Aguilar, A., Rodriguez-Galan, O., Vincent, O., Arst, H.N., Jr., Tilburn, J., and Penalva, M.A. (2007). PalC, one of two Bro1 domain proteins in the fungal pH signalling pathway, localizes to cortical structures and binds Vps32. Traffic **8,** 1346-1364.

Gallois, J.L., Guyon-Debast, A., Lecureuil, A., Vezon, D., Carpentier, V., Bonhomme, S., and Guerche, P. (2009). The Arabidopsis proteasome RPT5 subunits are essential for gametophyte development and show accession-dependent redundancy. The Plant cell **21,** 442-459.

Gao, C., Luo, M., Zhao, Q., Yang, R., Cui, Y., Zeng, Y., Xia, J., and Jiang, L. (2014). A unique plant ESCRT component, FREE1, regulates multivesicular body protein sorting and plant growth. Current biology : CB **24,** 2556-2563.

Geldner, N., Denervaud-Tendon, V., Hyman, D.L., Mayer, U., Stierhof, Y.D., and Chory, J. (2009). Rapid, combinatorial analysis of membrane compartments in intact plants with a multicolor marker set. The Plant journal : for cell and molecular biology **59,** 169-178.

Geldner, N., Anders, N., Wolters, H., Keicher, J., Kornberger, W., Muller, P., Delbarre, A., Ueda, T., Nakano, A., and Jurgens, G. (2003). The Arabidopsis GNOM ARF-GEF mediates endosomal recycling, auxin transport, and auxin-dependent plant growth. Cell **112,** 219-230.

Gingras, M.C., Zhang, Y.L., Kharitidi, D., Barr, A.J., Knapp, S., Tremblay, M.L., and Pause, A. (2009). HD-PTP is a catalytically inactive tyrosine phosphatase due to a conserved divergence in its phosphatase domain. PloS one **4,** e5105.

Glickman, M.H., Rubin, D.M., Coux, O., Wefes, I., Pfeifer, G., Cjeka, Z., Baumeister, W., Fried, V.A., and Finley, D. (1998). A subcomplex of the proteasome regulatory particle required for ubiquitin-conjugate degradation and related to the COP9-signalosome and eIF3. Cell **94,** 615-623.

Gonzalez-Lamothe, R., Tsitsigiannis, D.I., Ludwig, A.A., Panicot, M., Shirasu, K., and Jones, J.D. (2006). The U-box protein CMPG1 is required for efficient activation of defense mechanisms triggered by multiple resistance genes in tobacco and tomato. The Plant cell **18,** 1067-1083.

Gottlinger, H.G. (2007). How HIV-1 hijacks ALIX. Nature structural & molecular biology **14,** 254-256.

Grabbe, C., Husnjak, K., and Dikic, I. (2011). The spatial and temporal organization of ubiquitin networks. Nature reviews. Molecular cell biology **12,** 295-307.

Grefen, C., Donald, N., Hashimoto, K., Kudla, J., Schumacher, K., and Blatt, M.R. (2010). A ubiquitin-10 promoter-based vector set for fluorescent protein tagging facilitates temporal stability and native protein distribution in transient and stable expression studies. The Plant journal : for cell and molecular biology **64,** 355-365.

Gruenberg, J., and Stenmark, H. (2004). The biogenesis of multivesicular endosomes. Nature reviews. Molecular cell biology **5,** 317-323.

Haas, T.J., Sliwinski, M.K., Martinez, D.E., Preuss, M., Ebine, K., Ueda, T., Nielsen, E., Odorizzi, G., and Otegui, M.S. (2007). The Arabidopsis AAA ATPase SKD1 is involved in multivesicular endosome function and interacts with its positive regulator LYST-INTERACTING PROTEIN5. The Plant cell **19,** 1295-1312.

Han, Z., Madara, J.J., Liu, Y., Liu, W., Ruthel, G., Freedman, B.D., and Harty, R.N. (2015). ALIX Rescues Budding of a Double PTAP/PPEY L-Domain Deletion Mutant of Ebola VP40: A Role for ALIX in Ebola Virus Egress. J Infect Dis **212 Suppl 2,** S138-145.

Hanaoka, H., Noda, T., Shirano, Y., Kato, T., Hayashi, H., Shibata, D., Tabata, S., and Ohsumi, Y. (2002). Leaf senescence and starvation-induced chlorosis are accelerated by the disruption of an Arabidopsis autophagy gene. Plant physiology **129,** 1181-1193.

Harding, T.M., Morano, K.A., Scott, S.V., and Klionsky, D.J. (1995). Isolation and characterization of yeast mutants in the cytoplasm to vacuole protein targeting pathway. The Journal of cell biology **131,** 591-602.

Hasdemir, B., Murphy, J.E., Cottrell, G.S., and Bunnett, N.W. (2009). Endosomal deubiquitinating enzymes control ubiquitination and down-regulation of protease-activated receptor 2. The Journal of biological chemistry **284,** 28453-28466.

Hay, J.C. (2007). Calcium: a fundamental regulator of intracellular membrane fusion? EMBO reports **8,** 236-240.

Hayashi, S., and Hirayama, T. (2016). ahg12 is a dominant proteasome mutant that affects multiple regulatory systems for germination of Arabidopsis. Sci Rep **6,** 25351.

Heider, M.R., and Munson, M. (2012). Exorcising the exocyst complex. Traffic **13,** 898-907.

Heise, A., Lippok, B., Kirsch, C., and Hahlbrock, K. (2002). Two immediate-early pathogen-responsive members of the AtCMPG gene family in Arabidopsis thaliana and the W-box-containing elicitor-response element of AtCMPG1. Proceedings of the National Academy of Sciences of the United States of America **99,** 9049-9054.

Herrera-Vigenor, F., Hernandez-Garcia, R., Valadez-Sanchez, M., Vazquez-Prado, J., and Reyes-Cruz, G. (2006). AMSH regulates calcium-sensing receptor signaling through direct interactions. Biochemical and biophysical research communications **347,** 924-930.

Hershko, A., and Ciechanover, A. (1998). The ubiquitin system. Annual review of biochemistry **67,** 425-479.

Hicke, L. (2001). Protein regulation by monoubiquitin. Nature reviews. Molecular cell biology **2,** 195-201.

Hinderliter, A.K., Almeida, P.F., Biltonen, R.L., and Creutz, C.E. (1998). Membrane domain formation by calcium-dependent, lipid-binding proteins: insights from the C2 motif. Biochim Biophys Acta **1448,** 227-235.

Hislop, J.N., Henry, A.G., Marchese, A., and von Zastrow, M. (2009). Ubiquitination regulates proteolytic processing of G protein-coupled receptors after their sorting to lysosomes. The Journal of biological chemistry **284,** 19361-19370.

Hofius, D., Schultz-Larsen, T., Joensen, J., Tsitsigiannis, D.I., Petersen, N.H., Mattsson, O., Jorgensen, L.B., Jones, J.D., Mundy, J., and Petersen, M. (2009). Autophagic components contribute to hypersensitive cell death in Arabidopsis. Cell **137,** 773-783.

Hofmann, R.M., and Pickart, C.M. (1999). Noncanonical MMS2-encoded ubiquitin-conjugating enzyme functions in assembly of novel polyubiquitin chains for DNA repair. Cell **96,** 645-653.

Hoppe, T. (2005). Multiubiquitylation by E4 enzymes: 'one size' doesn't fit all. Trends in biochemical sciences **30,** 183-187.

Huotari, J., and Helenius, A. (2011). Endosome maturation. The EMBO journal **30,** 3481-3500.

Ichioka, F., Kobayashi, R., Katoh, K., Shibata, H., and Maki, M. (2008). Brox, a novel farnesylated Bro1 domain-containing protein that associates with charged multivesicular body protein 4 (CHMP4). FEBS J **275,** 682-692.

Ichioka, F., Takaya, E., Suzuki, H., Kajigaya, S., Buchman, V.L., Shibata, H., and Maki, M. (2007). HD-PTP and Alix share some membrane-traffic related proteins that interact with their Bro1 domains or proline-rich regions. Arch Biochem Biophys **457,** 142-149.

Inada, N., Betsuyaku, S., Shimada, T.L., Ebine, K., Ito, E., Kutsuna, N., Hasezawa, S., Takano, Y., Fukuda, H., Nakano, A., and Ueda, T. (2016). Modulation of Plant RAB GTPase-Mediated Membrane Trafficking Pathway at the Interface Between Plants and Obligate Biotrophic Pathogens. Plant & cell physiology.

Inoue, Y., Suzuki, T., Hattori, M., Yoshimoto, K., Ohsumi, Y., and Moriyasu, Y. (2006). AtATG genes, homologs of yeast autophagy genes, are involved in constitutive autophagy in Arabidopsis root tip cells. Plant & cell physiology **47,** 1641-1652.

Isono, E., and Nagel, M.K. (2014). Deubiquitylating enzymes and their emerging role in plant biology. Frontiers in plant science **5,** 56.

Isono, E., Katsiarimpa, A., Muller, I.K., Anzenberger, F., Stierhof, Y.D., Geldner, N., Chory, J., and Schwechheimer, C. (2010). The deubiquitinating enzyme AMSH3 is required for intracellular trafficking and vacuole biogenesis in Arabidopsis thaliana. The Plant cell **22,** 1826-1837.

Ito, E., Fujimoto, M., Ebine, K., Uemura, T., Ueda, T., and Nakano, A. (2012). Dynamic behavior of clathrin in Arabidopsis thaliana unveiled by live imaging. The Plant journal : for cell and molecular biology **69,** 204-216.

Jacomin, A.C., Bescond, A., Soleilhac, E., Gallet, B., Schoehn, G., Fauvarque, M.O., and Taillebourg, E. (2015). The Deubiquitinating Enzyme UBPY Is Required for Lysosomal Biogenesis and Productive Autophagy in Drosophila. PloS one **10,** e0143078.

Jager, S., Bucci, C., Tanida, I., Ueno, T., Kominami, E., Saftig, P., and Eskelinen, E.L. (2004). Role for Rab7 in maturation of late autophagic vacuoles. Journal of cell science **117,** 4837-4848.

Jaillais, Y., Santambrogio, M., Rozier, F., Fobis-Loisy, I., Miege, C., and Gaude, T. (2007). The retromer protein VPS29 links cell polarity and organ initiation in plants. Cell **130,** 1057-1070.

Jang, K., Lee, H.G., Jung, S.J., Paek, N.C., and Seo, P.J. (2015). The E3 Ubiquitin Ligase COP1 Regulates Thermosensory Flowering by Triggering GI Degradation in Arabidopsis. Sci Rep **5,** 12071.

Jena, B.P. (2009). Membrane fusion: role of SNAREs and calcium. Protein Pept Lett **16,** 712-717.

Joshi, A., Munshi, U., Ablan, S.D., Nagashima, K., and Freed, E.O. (2008). Functional replacement of a retroviral late domain by ubiquitin fusion. Traffic **9,** 1972-1983.

Kalinowska, K., Nagel, M.K., Goodman, K., Cuyas, L., Anzenberger, F., Alkofer, A., Paz-Ares, J., Braun, P., Rubio, V., Otegui, M.S., and Isono, E. (2015). Arabidopsis ALIX is required for the endosomal localization of the deubiquitinating enzyme AMSH3. Proceedings of the National Academy of Sciences of the United States of America **112,** E5543-5551.

Kato, M., Miyazawa, K., and Kitamura, N. (2000). A deubiquitinating enzyme UBPY interacts with the Src homology 3 domain of Hrs-binding protein via a novel binding motif PX(V/I)(D/N)RXXKP. The Journal of biological chemistry **275,** 37481-37487.

Katsiarimpa, A., Munoz, A., Kalinowska, K., Uemura, T., Rojo, E., and Isono, E. (2014). The ESCRT-III-interacting deubiquitinating enzyme AMSH3 is essential for degradation of ubiquitinated membrane proteins in Arabidopsis thaliana. Plant & cell physiology **55,** 727-736.

Katsiarimpa, A., Anzenberger, F., Schlager, N., Neubert, S., Hauser, M.T., Schwechheimer, C., and Isono, E. (2011). The Arabidopsis deubiquitinating enzyme AMSH3 interacts with ESCRT-III subunits and regulates their localization. The Plant cell **23,** 3026-3040.

Katsiarimpa, A., Kalinowska, K., Anzenberger, F., Weis, C., Ostertag, M., Tsutsumi, C., Schwechheimer, C., Brunner, F., Huckelhoven, R., and Isono, E. (2013). The deubiquitinating enzyme AMSH1 and the ESCRT-III subunit VPS2.1 are required for autophagic degradation in Arabidopsis. The Plant cell **25,** 2236-2252.

Kawasaki, T., Nam, J., Boyes, D.C., Holt, B.F., 3rd, Hubert, D.A., Wiig, A., and Dangl, J.L. (2005). A duplicated pair of Arabidopsis RING-finger E3 ligases contribute to the RPM1- and RPS2-mediated hypersensitive response. The Plant journal : for cell and molecular biology **44,** 258-270.

Kee, Y., Lyon, N., and Huibregtse, J.M. (2005). The Rsp5 ubiquitin ligase is coupled to and antagonized by the Ubp2 deubiquitinating enzyme. The EMBO journal **24,** 2414-2424.

Keren-Kaplan, T., Attali, I., Estrin, M., Kuo, L.S., Farkash, E., Jerabek-Willemsen, M., Blutraich, N., Artzi, S., Peri, A., Freed, E.O., Wolfson, H.J., and Prag, G. (2013). Structure-based in silico identification of ubiquitin-binding domains provides insights into the ALIX-V:ubiquitin complex and retrovirus budding. The EMBO journal **32,** 538-551.

Kerscher, O., Felberbaum, R., and Hochstrasser, M. (2006). Modification of proteins by ubiquitin and ubiquitin-like proteins. Annu Rev Cell Dev Biol **22,** 159-180.

Kikuchi, K., Ishii, N., Asao, H., and Sugamura, K. (2003). Identification of AMSH-LP containing a Jab1/MPN domain metalloenzyme motif. Biochemical and biophysical research communications **306,** 637-643.

Kim, J., Sitaraman, S., Hierro, A., Beach, B.M., Odorizzi, G., and Hurley, J.H. (2005). Structural basis for endosomal targeting by the Bro1 domain. Developmental cell **8,** 937-947.

Kim, J., Lee, H., Lee, H.N., Kim, S.H., Shin, K.D., and Chung, T. (2013a). Autophagy-related proteins are required for degradation of peroxisomes in Arabidopsis hypocotyls during seedling growth. The Plant cell **25,** 4956-4966.

Kim, M.S., Kim, J.A., Song, H.K., and Jeon, H. (2006). STAM-AMSH interaction facilitates the deubiquitination activity in the C-terminal AMSH. Biochemical and biophysical research communications **351,** 612-618.

Kim, S.Y., Xu, Z.Y., Song, K., Kim, D.H., Kang, H., Reichardt, I., Sohn, E.J., Friml, J., Juergens, G., and Hwang, I. (2013b). Adaptor protein complex 2-mediated endocytosis is crucial for male reproductive organ development in Arabidopsis. The Plant cell **25,** 2970-2985.

Kirik, A., Ehrhardt, D.W., and Kirik, V. (2012). TONNEAU2/FASS regulates the geometry of microtubule nucleation and cortical array organization in interphase Arabidopsis cells. The Plant cell **24,** 1158-1170.

Kirsch, C., Logemann, E., Lippok, B., Schmelzer, E., and Hahlbrock, K. (2001). A highly specific pathogen-responsive promoter element from the immediate-early activated CMPG1 gene in Petroselinum crispum. The Plant journal : for cell and molecular biology **26,** 217-227.

Kobayashi, S., Tsugama, D., Liu, S., and Takano, T. (2012). A U-Box E3 ubiquitin ligase, PUB20, interacts with the Arabidopsis G-protein beta subunit, AGB1. PloS one **7,** e49207.

Koegl, M., Hoppe, T., Schlenker, S., Ulrich, H.D., Mayer, T.U., and Jentsch, S. (1999). A novel ubiquitination factor, E4, is involved in multiubiquitin chain assembly. Cell **96,** 635-644.

Kojima, R., Obita, T., Onoue, K., and Mizuguchi, M. (2016). Structural Fine-Tuning of MIT-Interacting Motif 2 (MIM2) and Allosteric Regulation of ESCRT-III by Vps4 in Yeast. J Mol Biol **428,** 2392-2404.

Kolb, C., Nagel, M.K., Kalinowska, K., Hagmann, J., Ichikawa, M., Anzenberger, F., Alkofer, A., Sato, M.H., Braun, P., and Isono, E. (2015). FYVE1 is essential for vacuole biogenesis and intracellular trafficking in Arabidopsis. Plant physiology **167,** 1361-1373.

Komander, D. (2009). The emerging complexity of protein ubiquitination. Biochemical Society transactions **37,** 937-953.

Komander, D., Clague, M.J., and Urbe, S. (2009). Breaking the chains: structure and function of the deubiquitinases. Nature reviews. Molecular cell biology **10,** 550-563.

Korbei, B., Moulinier-Anzola, J., De-Araujo, L., Lucyshyn, D., Retzer, K., Khan, M.A., and Luschnig, C. (2013). Arabidopsis TOL proteins act as gatekeepers for vacuolar sorting of PIN2 plasma membrane protein. Current biology : CB **23,** 2500-2505.

Kraft, C., Peter, M., and Hofmann, K. (2010). Selective autophagy: ubiquitin-mediated recognition and beyond. Nature cell biology **12,** 836-841.

Kraft, C., Deplazes, A., Sohrmann, M., and Peter, M. (2008). Mature ribosomes are selectively degraded upon starvation by an autophagy pathway requiring the Ubp3p/Bre5p ubiquitin protease. Nature cell biology **10,** 602-610.

Kraft, E., Stone, S.L., Ma, L., Su, N., Gao, Y., Lau, O.S., Deng, X.W., and Callis, J. (2005). Genome analysis and functional characterization of the E2 and RING-type E3 ligase ubiquitination enzymes of Arabidopsis. Plant physiology **139,** 1597-1611.

Kulich, I., Pecenkova, T., Sekeres, J., Smetana, O., Fendrych, M., Foissner, I., Hoftberger, M., and Zarsky, V. (2013). Arabidopsis exocyst subcomplex containing subunit EXO70B1 is involved in autophagy-related transport to the vacuole. Traffic **14,** 1155-1165.

Kwon, S.I., Cho, H.J., Jung, J.H., Yoshimoto, K., Shirasu, K., and Park, O.K. (2010). The Rab GTPase RabG3b functions in autophagy and contributes to tracheary element differentiation in Arabidopsis. The Plant journal : for cell and molecular biology **64,** 151-164.

Laemmli, U.K. (1970). Cleavage of structural proteins during the assembly of the head of bacteriophage T4. Nature **227,** 680-685.

Le Bars, R., Marion, J., Satiat-Jeunemaitre, B., and Bianchi, M.W. (2014a). Folding into an autophagosome: ATG5 sheds light on how plants do it. Autophagy **10,** 1861-1863.

Le Bars, R., Marion, J., Le Borgne, R., Satiat-Jeunemaitre, B., and Bianchi, M.W. (2014b). ATG5 defines a phagophore domain connected to the endoplasmic reticulum during autophagosome formation in plants. Nat Commun **5,** 4121.

Lee, H.K., Cho, S.K., Son, O., Xu, Z., Hwang, I., and Kim, W.T. (2009). Drought stress-induced Rma1H1, a RING membrane-anchor E3 ubiquitin ligase homolog, regulates aquaporin levels via ubiquitination in transgenic Arabidopsis plants. The Plant cell **21,** 622-641.

Lee, J., Oh, K.J., Lee, D., Kim, B.Y., Choi, J.S., Ku, B., and Kim, S.J. (2016). Structural Study of the HD-PTP Bro1 Domain in a Complex with the Core Region of STAM2, a Subunit of ESCRT-0. PloS one **11,** e0149113.

Li, F., Chung, T., and Vierstra, R.D. (2014). AUTOPHAGY-RELATED11 plays a critical role in general autophagy- and senescence-induced mitophagy in Arabidopsis. The Plant cell **26,** 788-807.

Li, F., Chung, T., Pennington, J.G., Federico, M.L., Kaeppler, H.F., Kaeppler, S.M., Otegui, M.S., and Vierstra, R.D. (2015). Autophagic recycling plays a central role in maize nitrogen remobilization. The Plant cell **27,** 1389-1408.

Li, H., and Seth, A. (2004). An RNF11: Smurf2 complex mediates ubiquitination of the AMSH protein. Oncogene **23,** 1801-1808.

Lin, G., Aranda, V., Muthuswamy, S.K., and Tonks, N.K. (2011). Identification of PTPN23 as a novel regulator of cell invasion in mammary epithelial cells from a loss-of-function screen of the 'PTP-ome'. Genes & development **25,** 1412-1425.

Liu, H., Urbe, S., and Clague, M.J. (2012a). Selective protein degradation in cell signalling. Semin Cell Dev Biol **23,** 509-514.

Liu, Y., Burgos, J.S., Deng, Y., Srivastava, R., Howell, S.H., and Bassham, D.C. (2012b). Degradation of the endoplasmic reticulum by autophagy during endoplasmic reticulum stress in Arabidopsis. The Plant cell **24,** 4635-4651.

Lu, D., Lin, W., Gao, X., Wu, S., Cheng, C., Avila, J., Heese, A., Devarenne, T.P., He, P., and Shan, L. (2011). Direct ubiquitination of pattern recognition receptor FLS2 attenuates plant innate immunity. Science **332,** 1439-1442.

Lucena-Agell, D., Galindo, A., Arst, H.N., Jr., and Penalva, M.A. (2015). Aspergillus nidulans Ambient pH Signaling Does Not Require Endocytosis. Eukaryot Cell **14,** 545-553.

Luhtala, N., and Odorizzi, G. (2004). Bro1 coordinates deubiquitination in the multivesicular body pathway by recruiting Doa4 to endosomes. The Journal of cell biology **166,** 717-729.

Ma, Y.M., Boucrot, E., Villen, J., Affar el, B., Gygi, S.P., Gottlinger, H.G., and Kirchhausen, T. (2007). Targeting of AMSH to endosomes is required for epidermal growth factor receptor degradation. The Journal of biological chemistry **282,** 9805-9812.

Magori, S., and Citovsky, V. (2011a). Hijacking of the Host SCF Ubiquitin Ligase Machinery by Plant Pathogens. Frontiers in plant science **2,** 87.

Magori, S., and Citovsky, V. (2011b). Agrobacterium counteracts host-induced degradation of its effector F-box protein. Sci Signal **4,** ra69.

Malolepszy, A., Urbanski, D.F., James, E.K., Sandal, N., Isono, E., Stougaard, J., and Andersen, S.U. (2015). The deubiquitinating enzyme AMSH1 is required for rhizobial infection and nodule organogenesis in Lotus japonicus. The Plant journal : for cell and molecular biology **83,** 719-731.

Mariotti, M., Castiglioni, S., Garcia-Manteiga, J.M., Beguinot, L., and Maier, J.A. (2009). HD-PTP inhibits endothelial migration through its interaction with Src. Int J Biochem Cell Biol **41,** 687-693.

Marmor, M.D., and Yarden, Y. (2004). Role of protein ubiquitylation in regulating endocytosis of receptor tyrosine kinases. Oncogene **23,** 2057-2070.

Marshall, R.S., and Vierstra, R.D. (2015). Eat or be eaten: The autophagic plight of inactive 26S proteasomes. Autophagy **11,** 1927-1928.

Martens, S., and McMahon, H.T. (2008). Mechanisms of membrane fusion: disparate players and common principles. Nature reviews. Molecular cell biology **9,** 543-556.

Martin-Serrano, J., Yarovoy, A., Perez-Caballero, D., and Bieniasz, P.D. (2003). Divergent retroviral late-budding domains recruit vacuolar protein sorting factors by using alternative adaptor proteins. Proceedings of the National Academy of Sciences of the United States of America **100,** 12414-12419.

Martinez-Garay, I., Rustom, A., Gerdes, H.H., and Kutsche, K. (2006). The novel centrosomal associated protein CEP55 is present in the spindle midzone and the midbody. Genomics **87,** 243-253.

Martiniere, A., Gayral, P., Hawes, C., and Runions, J. (2011). Building bridges: formin1 of Arabidopsis forms a connection between the cell wall and the actin cytoskeleton. The Plant journal : for cell and molecular biology **66,** 354-365.

Maruta, N., Trusov, Y., Brenya, E., Parekh, U., and Botella, J.R. (2015). Membrane-localized extra-large G proteins and Gbg of the heterotrimeric G proteins form functional complexes engaged in plant immunity in Arabidopsis. Plant physiology **167,** 1004-1016.

Matsuo, H., Chevallier, J., Mayran, N., Le Blanc, I., Ferguson, C., Faure, J., Blanc, N.S., Matile, S., Dubochet, J., Sadoul, R., Parton, R.G., Vilbois, F., and Gruenberg, J. (2004). Role of LBPA and Alix in multivesicular liposome formation and endosome organization. Science **303,** 531-534.

Mazzucotelli, E., Belloni, S., Marone, D., De Leonardis, A., Guerra, D., Di Fonzo, N., Cattivelli, L., and Mastrangelo, A. (2006). The e3 ubiquitin ligase gene family in plants: regulation by degradation. Curr Genomics **7,** 509-522.

McCullough, J., Clague, M.J., and Urbe, S. (2004). AMSH is an endosome-associated ubiquitin isopeptidase. The Journal of cell biology **166,** 487-492.

McCullough, J., Fisher, R.D., Whitby, F.G., Sundquist, W.I., and Hill, C.P. (2008). ALIX-CHMP4 interactions in the human ESCRT pathway. Proceedings of the National Academy of Sciences of the United States of America **105,** 7687-7691.

McCullough, J., Row, P.E., Lorenzo, O., Doherty, M., Beynon, R., Clague, M.J., and Urbe, S. (2006). Activation of the endosome-associated ubiquitin isopeptidase AMSH by STAM, a component of the multivesicular body-sorting machinery. Current biology : CB **16,** 160-165.

McDonell, L.M., Mirzaa, G.M., Alcantara, D., Schwartzentruber, J., Carter, M.T., Lee, L.J., Clericuzio, C.L., Graham, J.M., Jr., Morris-Rosendahl, D.J., Polster, T., Acsadi, G., Townshend, S., Williams, S., Halbert, A., Isidor, B., David, A., Smyser, C.D., Paciorkowski, A.R., Willing, M., Woulfe, J., Das, S., Beaulieu, C.L., Marcadier, J., Consortium, F.C., Geraghty, M.T., Frey, B.J., Majewski, J., Bulman, D.E., Dobyns, W.B., O'Driscoll, M., and Boycott, K.M. (2013). Mutations in STAMBP, encoding a deubiquitinating enzyme, cause microcephaly-capillary malformation syndrome. Nat Genet **45,** 556-562.

McDowell, G.S., and Philpott, A. (2016). New Insights Into the Role of Ubiquitylation of Proteins. Int Rev Cell Mol Biol **325,** 35-88.

Meijer, I.M., van Rotterdam, W., van Zoelen, E.J., and van Leeuwen, J.E. (2012). Recycling of EGFR and ErbB2 is associated with impaired Hrs tyrosine phosphorylation and decreased deubiquitination by AMSH. Cell Signal **24,** 1981-1988.

Meusser, B., Hirsch, C., Jarosch, E., and Sommer, T. (2005). ERAD: the long road to destruction. Nature cell biology **7,** 766-772.

Michaeli, S., Galili, G., Genschik, P., Fernie, A.R., and Avin-Wittenberg, T. (2016). Autophagy in Plants--What's New on the Menu? Trends in plant science **21,** 134-144.

Miura, G.I., Roignant, J.Y., Wassef, M., and Treisman, J.E. (2008). Myopic acts in the endocytic pathway to enhance signaling by the Drosophila EGF receptor. Development **135,** 1913-1922.

Mizuno, E., Kobayashi, K., Yamamoto, A., Kitamura, N., and Komada, M. (2006). A deubiquitinating enzyme UBPY regulates the level of protein ubiquitination on endosomes. Traffic **7,** 1017-1031.

Morita, E., Sandrin, V., Chung, H.Y., Morham, S.G., Gygi, S.P., Rodesch, C.K., and Sundquist, W.I. (2007). Human ESCRT and ALIX proteins interact with proteins of the midbody and function in cytokinesis. The EMBO journal **26,** 4215-4227.

Muziol, T., Pineda-Molina, E., Ravelli, R.B., Zamborlini, A., Usami, Y., Gottlinger, H., and Weissenhorn, W. (2006). Structural basis for budding by the ESCRT-III factor CHMP3. Developmental cell **10,** 821-830.

Nakagawa, T., Kurose, T., Hino, T., Tanaka, K., Kawamukai, M., Niwa, Y., Toyooka, K., Matsuoka, K., Jinbo, T., and Kimura, T. (2007). Development of series of gateway binary vectors, pGWBs, for realizing efficient construction of fusion genes for plant transformation. J Biosci Bioeng **104,** 34-41.

Nakamura, M., Tanaka, N., Kitamura, N., and Komada, M. (2006). Clathrin anchors deubiquitinating enzymes, AMSH and AMSH-like protein, on early endosomes. Genes Cells **11,** 593-606.

Naramoto, S., Otegui, M.S., Kutsuna, N., de Rycke, R., Dainobu, T., Karampelias, M., Fujimoto, M., Feraru, E., Miki, D., Fukuda, H., Nakano, A., and Friml, J. (2014). Insights into the localization and function of the membrane trafficking regulator GNOM ARF-GEF at the Golgi apparatus in Arabidopsis. The Plant cell **26,** 3062-3076.

Negrete-Urtasun, S., Denison, S.H., and Arst, H.N., Jr. (1997). Characterization of the pH signal transduction pathway gene palA of Aspergillus nidulans and identification of possible homologs. J Bacteriol **179,** 1832-1835.

Nickas, M.E., and Yaffe, M.P. (1996). BRO1, a novel gene that interacts with components of the Pkc1p-mitogen-activated protein kinase pathway in Saccharomyces cerevisiae. Mol Cell Biol **16,** 2585-2593.

Niendorf, S., Oksche, A., Kisser, A., Lohler, J., Prinz, M., Schorle, H., Feller, S., Lewitzky, M., Horak, I., and Knobeloch, K.P. (2007). Essential role of ubiquitin-specific protease 8 for receptor tyrosine kinase stability and endocytic trafficking in vivo. Mol Cell Biol **27,** 5029-5039.

Nikko, E., and Andre, B. (2007). Split-ubiquitin two-hybrid assay to analyze protein-protein interactions at the endosome: application to Saccharomyces cerevisiae Bro1 interacting with ESCRT complexes, the Doa4 ubiquitin hydrolase, and the Rsp5 ubiquitin ligase. Eukaryot Cell **6,** 1266-1277.

Odorizzi, G. (2006). The multiple personalities of Alix. Journal of cell science **119,** 3025-3032.

Odorizzi, G., Katzmann, D.J., Babst, M., Audhya, A., and Emr, S.D. (2003). Bro1 is an endosome-associated protein that functions in the MVB pathway in Saccharomyces cerevisiae. Journal of cell science **116,** 1893-1903.

Otegui, M.S., and Spitzer, C. (2008). Endosomal functions in plants. Traffic **9,** 1589-1598.

Otegui, M.S., Herder, R., Schulze, J., Jung, R., and Staehelin, L.A. (2006). The proteolytic processing of seed storage proteins in Arabidopsis embryo cells starts in the multivesicular bodies. The Plant cell **18,** 2567-2581.

Paez Valencia, J., Goodman, K., and Otegui, M.S. (2016). Endocytosis and Endosomal Trafficking in Plants. Annual review of plant biology **67,** 309-335.

Pashkova, N., Gakhar, L., Winistorfer, S.C., Sunshine, A.B., Rich, M., Dunham, M.J., Yu, L., and Piper, R.C. (2013). The yeast Alix homolog Bro1 functions as a ubiquitin receptor for protein sorting into multivesicular endosomes. Developmental cell **25,** 520-533.

Pavlovic, M., Neubauer, D., Al Tawari, A., and Heberle, L.C. (2014). The microcephaly-capillary malformation syndrome in two brothers with novel clinical features. Pediatr Neurol **51,** 560-565.

Peck, J.W., Oberst, M., Bouker, K.B., Bowden, E., and Burbelo, P.D. (2002). The RhoA-binding protein, rhophilin-2, regulates actin cytoskeleton organization. The Journal of biological chemistry **277,** 43924-43932.

Peth, A., Kukushkin, N., Bosse, M., and Goldberg, A.L. (2013). Ubiquitinated proteins activate the proteasomal ATPases by binding to Usp14 or Uch37 homologs. The Journal of biological chemistry **288,** 7781-7790.

Petiot, A., and Sadoul, R. (2009). Autophagy discriminates between Alix and ESCRTs. Autophagy **5,** 106-107.

Petiot, A., Strappazzon, F., Chatellard-Causse, C., Blot, B., Torch, S., Verna, J.M., and Sadoul, R. (2008). Alix differs from ESCRT proteins in the control of autophagy. Biochemical and biophysical research communications **375,** 63-68.

Pickart, C.M. (2001). Mechanisms underlying ubiquitination. Annual review of biochemistry **70,** 503-533.

Piper, R.C., and Katzmann, D.J. (2007). Biogenesis and function of multivesicular bodies. Annu Rev Cell Dev Biol **23,** 519-547.

Pires, R., Hartlieb, B., Signor, L., Schoehn, G., Lata, S., Roessle, M., Moriscot, C., Popov, S., Hinz, A., Jamin, M., Boyer, V., Sadoul, R., Forest, E., Svergun, D.I., Gottlinger, H.G., and Weissenhorn, W. (2009). A crescent-shaped ALIX dimer targets ESCRT-III CHMP4 filaments. Structure (London, England : 1993) **17,** 843-856.

Pogany, M., Danko, T., Kaman-Toth, E., Schwarczinger, I., and Bozso, Z. (2015). Regulatory Proteolysis in Arabidopsis-Pathogen Interactions. International journal of molecular sciences **16,** 23177-23194.

Pradhan-Sundd, T., and Verheyen, E.M. (2014). The role of Bro1- domain-containing protein Myopic in endosomal trafficking of Wnt/Wingless. Dev Biol **392,** 93-107.

Pradhan-Sundd, T., and Verheyen, E.M. (2015). The Myopic-Ubpy-Hrs nexus enables endosomal recycling of Frizzled. Molecular biology of the cell **26,** 3329-3342.

Puertollano, R. (2005). Interactions of TOM1L1 with the multivesicular body sorting machinery. The Journal of biological chemistry **280,** 9258-9264.

Puertollano, R., and Bonifacino, J.S. (2004). Interactions of GGA3 with the ubiquitin sorting machinery. Nature cell biology **6,** 244-251.

Raymond, C.K., Howald-Stevenson, I., Vater, C.A., and Stevens, T.H. (1992). Morphological classification of the yeast vacuolar protein sorting mutants: evidence for a prevacuolar compartment in class E vps mutants. Molecular biology of the cell **3,** 1389-1402.

Ren, J., Kee, Y., Huibregtse, J.M., and Piper, R.C. (2007). Hse1, a component of the yeast Hrs-STAM ubiquitin-sorting complex, associates with ubiquitin peptidases and a ligase to control sorting efficiency into multivesicular bodies. Molecular biology of the cell **18,** 324-335.

Reyes-Ibarra, A.P., Garcia-Regalado, A., Ramirez-Rangel, I., Esparza-Silva, A.L., Valadez-Sanchez, M., Vazquez-Prado, J., and Reyes-Cruz, G. (2007). Calcium-sensing receptor endocytosis links extracellular calcium signaling to parathyroid hormone-related peptide secretion via a Rab11a-dependent and AMSH-sensitive mechanism. Mol Endocrinol **21,** 1394-1407.

Reyes, F.C., Buono, R., and Otegui, M.S. (2011). Plant endosomal trafficking pathways. Current opinion in plant biology **14,** 666-673.

Richardson, L.G., and Mullen, R.T. (2011). Meta-analysis of the expression profiles of the Arabidopsis ESCRT machinery. Plant signaling & behavior **6,** 1897-1903.

Richardson, L.G., Howard, A.S., Khuu, N., Gidda, S.K., McCartney, A., Morphy, B.J., and Mullen, R.T. (2011). Protein-Protein Interaction Network and Subcellular Localization of the Arabidopsis Thaliana ESCRT Machinery. Frontiers in plant science **2,** 20.

Richter, C., West, M., and Odorizzi, G. (2007). Dual mechanisms specify Doa4-mediated deubiquitination at multivesicular bodies. The EMBO journal **26,** 2454-2464.

Richter, C.M., West, M., and Odorizzi, G. (2013). Doa4 function in ILV budding is restricted through its interaction with the Vps20 subunit of ESCRT-III. Journal of cell science **126,** 1881-1890.

Robatzek, S., and Wirthmueller, L. (2013). Mapping FLS2 function to structure: LRRs, kinase and its working bits. Protoplasma **250,** 671-681.

Robatzek, S., Chinchilla, D., and Boller, T. (2006). Ligand-induced endocytosis of the pattern recognition receptor FLS2 in Arabidopsis. Genes & development **20,** 537-542.

Rojo, E., Gillmor, C.S., Kovaleva, V., Somerville, C.R., and Raikhel, N.V. (2001). VACUOLELESS1 is an essential gene required for vacuole formation and morphogenesis in Arabidopsis. Developmental cell **1,** 303-310.

Rosero, A., Zarsky, V., and Cvrckova, F. (2013). AtFH1 formin mutation affects actin filament and microtubule dynamics in Arabidopsis thaliana. Journal of experimental botany **64,** 585-597.

Rosero, A., Oulehlova, D., Stillerova, L., Schiebertova, P., Grunt, M., Zarsky, V., and Cvrckova, F. (2016). Arabidopsis FH1 Formin Affects Cotyledon Pavement Cell Shape by Modulating Cytoskeleton Dynamics. Plant & cell physiology **57,** 488-504.

Row, P.E., Prior, I.A., McCullough, J., Clague, M.J., and Urbe, S. (2006). The ubiquitin isopeptidase UBPY regulates endosomal ubiquitin dynamics and is essential for receptor down-regulation. The Journal of biological chemistry **281,** 12618-12624.

Row, P.E., Liu, H., Hayes, S., Welchman, R., Charalabous, P., Hofmann, K., Clague, M.J., Sanderson, C.M., and Urbe, S. (2007). The MIT domain of UBPY constitutes a CHMP binding and endosomal localization signal required for efficient epidermal growth factor receptor degradation. The Journal of biological chemistry **282,** 30929-30937.

Rowe, T., and Balch, W.E. (1997). Membrane fusion. Bridging the gap by AAA ATPases. Nature **388,** 20-21.

Royle, S.J. (2006). The cellular functions of clathrin. Cell Mol Life Sci **63,** 1823-1832.

Rusten, T.E., and Stenmark, H. (2009). How do ESCRT proteins control autophagy? Journal of cell science **122,** 2179-2183.

Rusten, T.E., Vaccari, T., Lindmo, K., Rodahl, L.M., Nezis, I.P., Sem-Jacobsen, C., Wendler, F., Vincent, J.P., Brech, A., Bilder, D., and Stenmark, H. (2007). ESCRTs and Fab1 regulate distinct steps of autophagy. Current biology : CB **17,** 1817-1825.

Sakai, M., Shimokawa, T., Kobayashi, T., Matsushima, S., Yamada, Y., Nakamura, Y., and Furukawa, Y. (2006). Elevated expression of C10orf3 (chromosome 10 open reading frame 3) is involved in the growth of human colon tumor. Oncogene **25,** 480-486.

Sanmartin, M., Ordonez, A., Sohn, E.J., Robert, S., Sanchez-Serrano, J.J., Surpin, M.A., Raikhel, N.V., and Rojo, E. (2007). Divergent functions of VTI12 and VTI11 in trafficking to storage and lytic vacuoles in Arabidopsis. Proceedings of the National Academy of Sciences of the United States of America **104,** 3645-3650.

Sato, Y., Yoshikawa, A., Yamagata, A., Mimura, H., Yamashita, M., Ookata, K., Nureki, O., Iwai, K., Komada, M., and Fukai, S. (2008). Structural basis for specific cleavage of Lys 63-linked polyubiquitin chains. Nature **455,** 358-362.

Scheuring, D., Lofke, C., Kruger, F., Kittelmann, M., Eisa, A., Hughes, L., Smith, R.S., Hawes, C., Schumacher, K., and Kleine-Vehn, J. (2016). Actin-dependent vacuolar occupancy of the cell determines auxin-induced growth repression. Proceedings of the National Academy of Sciences of the United States of America **113,** 452-457.

Schmidt, M.H., Dikic, I., and Bogler, O. (2005). Src phosphorylation of Alix/AIP1 modulates its interaction with binding partners and antagonizes its activities. The Journal of biological chemistry **280,** 3414-3425.

Schmidt, O., and Teis, D. (2012). The ESCRT machinery. Current biology : CB **22,** R116-120.

Scott, C.C., Vacca, F., and Gruenberg, J. (2014). Endosome maturation, transport and functions. Semin Cell Dev Biol **31,** 2-10.

Segura-Morales, C., Pescia, C., Chatellard-Causse, C., Sadoul, R., Bertrand, E., and Basyuk, E. (2005). Tsg101 and Alix interact with murine leukemia virus Gag and cooperate with Nedd4 ubiquitin ligases during budding. The Journal of biological chemistry **280,** 27004-27012.

Shahriari, M., Richter, K., Keshavaiah, C., Sabovljevic, A., Huelskamp, M., and Schellmann, S. (2011). The Arabidopsis ESCRT protein-protein interaction network. Plant molecular biology **76,** 85-96.

Shahriari, M., Keshavaiah, C., Scheuring, D., Sabovljevic, A., Pimpl, P., Hausler, R.E., Hulskamp, M., and Schellmann, S. (2010). The AAA-type ATPase AtSKD1 contributes to vacuolar maintenance of Arabidopsis thaliana. The Plant journal : for cell and molecular biology **64,** 71-85.

Shen, B., Li, C., Min, Z., Meeley, R.B., Tarczynski, M.C., and Olsen, O.A. (2003). sal1 determines the number of aleurone cell layers in maize endosperm and encodes a class E vacuolar sorting protein. Proceedings of the National Academy of Sciences of the United States of America **100,** 6552-6557.

Shi, A., Pant, S., Balklava, Z., Chen, C.C., Figueroa, V., and Grant, B.D. (2007). A novel requirement for C. elegans Alix/ALX-1 in RME-1-mediated membrane transport. Current biology : CB **17,** 1913-1924.

Shi, X., Opi, S., Lugari, A., Restouin, A., Coursindel, T., Parrot, I., Perez, J., Madore, E., Zimmermann, P., Corbeil, J., Huang, M., Arold, S.T., Collette, Y., and Morelli, X. (2010). Identification and biophysical assessment of the molecular recognition mechanisms between the human haemopoietic cell kinase Src homology domain 3 and ALG-2-interacting protein X. Biochem J **431,** 93-102.

Shimada, T., Koumoto, Y., Li, L., Yamazaki, M., Kondo, M., Nishimura, M., and Hara-Nishimura, I. (2006). AtVPS29, a putative component of a retromer complex, is required for the efficient sorting of seed storage proteins. Plant & cell physiology **47,** 1187-1194.

Shimada, T.L., Shimada, T., and Hara-Nishimura, I. (2010). A rapid and non-destructive screenable marker, FAST, for identifying transformed seeds of Arabidopsis thaliana. The Plant journal : for cell and molecular biology **61,** 519-528.

Shin, L.J., Lo, J.C., Chen, G.H., Callis, J., Fu, H., and Yeh, K.C. (2013). IRT1 degradation factor1, a ring E3 ubiquitin ligase, regulates the degradation of iron-regulated transporter1 in Arabidopsis. The Plant cell **25,** 3039-3051.

Shirahama, K., Noda, T., and Ohsumi, Y. (1997). Mutational analysis of Csc1/Vps4p: involvement of endosome in regulation of autophagy in yeast. Cell Struct Funct **22,** 501-509.

Shope, J.C., DeWald, D.B., and Mott, K.A. (2003). Changes in surface area of intact guard cells are correlated with membrane internalization. Plant physiology **133,** 1314-1321.

Sierra, M.I., Wright, M.H., and Nash, P.D. (2010). AMSH interacts with ESCRT-0 to regulate the stability and trafficking of CXCR4. The Journal of biological chemistry **285,** 13990-14004.

Silady, R.A., Kato, T., Lukowitz, W., Sieber, P., Tasaka, M., and Somerville, C.R. (2004). The gravitropism defective 2 mutants of Arabidopsis are deficient in a protein implicated in endocytosis in Caenorhabditis elegans. Plant physiology **136,** 3095-3103; discussion 3002.

Simon, M.L., Platre, M.P., Assil, S., van Wijk, R., Chen, W.Y., Chory, J., Dreux, M., Munnik, T., and Jaillais, Y. (2014). A multi-colour/multi-affinity marker set to visualize phosphoinositide dynamics in Arabidopsis. The Plant journal : for cell and molecular biology **77,** 322-337.

Smalle, J., and Vierstra, R.D. (2004). The ubiquitin 26S proteasome proteolytic pathway. Annual review of plant biology **55,** 555-590.

Snider, J., Thibault, G., and Houry, W.A. (2008). The AAA+ superfamily of functionally diverse proteins. Genome Biol **9,** 216.

Solomons, J., Sabin, C., Poudevigne, E., Usami, Y., Hulsik, D.L., Macheboeuf, P., Hartlieb, B., Gottlinger, H., and Weissenhorn, W. (2011). Structural basis for ESCRT-III CHMP3 recruitment of AMSH. Structure (London, England : 1993) **19,** 1149-1159.

Spence, J., Gali, R.R., Dittmar, G., Sherman, F., Karin, M., and Finley, D. (2000). Cell cycle-regulated modification of the ribosome by a variant multiubiquitin chain. Cell **102,** 67-76.

Spitzer, C., Li, F., Buono, R., Roschzttardtz, H., Chung, T., Zhang, M., Osteryoung, K.W., Vierstra, R.D., and Otegui, M.S. (2015). The endosomal protein CHARGED MULTIVESICULAR BODY PROTEIN1 regulates the autophagic turnover of plastids in Arabidopsis. The Plant cell **27,** 391-402.

Spitzer, C., Schellmann, S., Sabovljevic, A., Shahriari, M., Keshavaiah, C., Bechtold, N., Herzog, M., Muller, S., Hanisch, F.G., and Hulskamp, M. (2006). The Arabidopsis elch mutant reveals functions of an ESCRT component in cytokinesis. Development **133,** 4679-4689.

Steuve, S., Devosse, T., Lauwers, E., Vanderwinden, J.M., Andre, B., Courtoy, P.J., and Pirson, I. (2006). Rhophilin-2 is targeted to late-endosomal structures of the vesicular machinery in the presence of activated RhoB. Exp Cell Res **312,** 3981-3989.

Stone, S.L., Hauksdottir, H., Troy, A., Herschleb, J., Kraft, E., and Callis, J. (2005). Functional analysis of the RING-type ubiquitin ligase family of Arabidopsis. Plant physiology **137,** 13-30.

Strack, B., Calistri, A., Craig, S., Popova, E., and Gottlinger, H.G. (2003). AIP1/ALIX is a binding partner for HIV-1 p6 and EIAV p9 functioning in virus budding. Cell **114,** 689-699.

Sutter, J.U., Sieben, C., Hartel, A., Eisenach, C., Thiel, G., and Blatt, M.R. (2007). Abscisic acid triggers the endocytosis of the arabidopsis KAT1 K+ channel and its recycling to the plasma membrane. Current biology : CB **17,** 1396-1402.

Svenning, S., Lamark, T., Krause, K., and Johansen, T. (2011). Plant NBR1 is a selective autophagy substrate and a functional hybrid of the mammalian autophagic adapters NBR1 and p62/SQSTM1. Autophagy **7,** 993-1010.

Swatek, K.N., and Komander, D. (2016). Ubiquitin modifications. Cell Res **26,** 399-422.

Takac, T., Pechan, T., Samajova, O., Ovecka, M., Richter, H., Eck, C., Niehaus, K., and Samaj, J. (2012). Wortmannin treatment induces changes in Arabidopsis root proteome and post-Golgi compartments. J Proteome Res **11,** 3127-3142.

Tamai, K., Tanaka, N., Nara, A., Yamamoto, A., Nakagawa, I., Yoshimori, T., Ueno, Y., Shimosegawa, T., and Sugamura, K. (2007). Role of Hrs in maturation of autophagosomes in mammalian cells. Biochemical and biophysical research communications **360,** 721-727.

Tamura, K., Takahashi, H., Kunieda, T., Fuji, K., Shimada, T., and Hara-Nishimura, I. (2007). Arabidopsis KAM2/GRV2 is required for proper endosome formation and functions in vacuolar sorting and determination of the embryo growth axis. The Plant cell **19,** 320-332.

Tanaka, N., Kaneko, K., Asao, H., Kasai, H., Endo, Y., Fujita, T., Takeshita, T., and Sugamura, K. (1999). Possible involvement of a novel STAM-associated molecule "AMSH" in intracellular

signal transduction mediated by cytokines. The Journal of biological chemistry **274,** 19129-19135.

Tasdemir, E., Galluzzi, L., Maiuri, M.C., Criollo, A., Vitale, I., Hangen, E., Modjtahedi, N., and Kroemer, G. (2008). Methods for assessing autophagy and autophagic cell death. Methods Mol Biol **445,** 29-76.

Teh, O.K., Hatsugai, N., Tamura, K., Fuji, K., Tabata, R., Yamaguchi, K., Shingenobu, S., Yamada, M., Hasebe, M., Sawa, S., Shimada, T., and Hara-Nishimura, I. (2015). BEACH-domain proteins act together in a cascade to mediate vacuolar protein trafficking and disease resistance in Arabidopsis. Mol Plant **8,** 389-398.

Teis, D., Saksena, S., Judson, B.L., and Emr, S.D. (2010). ESCRT-II coordinates the assembly of ESCRT-III filaments for cargo sorting and multivesicular body vesicle formation. The EMBO journal **29,** 871-883.

Terrell, J., Shih, S., Dunn, R., and Hicke, L. (1998). A function for monoubiquitination in the internalization of a G protein-coupled receptor. Molecular cell **1,** 193-202.

Thumm, M., Egner, R., Koch, B., Schlumpberger, M., Straub, M., Veenhuis, M., and Wolf, D.H. (1994). Isolation of autophagocytosis mutants of Saccharomyces cerevisiae. FEBS Lett **349,** 275-280.

Thurston, T.L., Ryzhakov, G., Bloor, S., von Muhlinen, N., and Randow, F. (2009). The TBK1 adaptor and autophagy receptor NDP52 restricts the proliferation of ubiquitin-coated bacteria. Nat Immunol **10,** 1215-1221.

Tian, Q., Olsen, L., Sun, B., Lid, S.E., Brown, R.C., Lemmon, B.E., Fosnes, K., Gruis, D.F., Opsahl-Sorteberg, H.G., Otegui, M.S., and Olsen, O.A. (2007). Subcellular localization and functional domain studies of DEFECTIVE KERNEL1 in maize and Arabidopsis suggest a model for aleurone cell fate specification involving CRINKLY4 and SUPERNUMERARY ALEURONE LAYER1. The Plant cell **19,** 3127-3145.

Tsuchiya, T., and Eulgem, T. (2011). EMSY-like genes are required for full RPP7-mediated race-specific immunity and basal defense in Arabidopsis. Mol Plant Microbe Interact **24,** 1573-1581.

Tsukada, M., and Ohsumi, Y. (1993). Isolation and characterization of autophagy-defective mutants of Saccharomyces cerevisiae. FEBS Lett **333,** 169-174.

Ueda, T., Yamaguchi, M., Uchimiya, H., and Nakano, A. (2001). Ara6, a plant-unique novel type Rab GTPase, functions in the endocytic pathway of Arabidopsis thaliana. The EMBO journal **20,** 4730-4741.

Ueda, T., Uemura, T., Sato, M.H., and Nakano, A. (2004). Functional differentiation of endosomes in Arabidopsis cells. The Plant journal : for cell and molecular biology **40,** 783-789.

Uemura, T., Suda, Y., Ueda, T., and Nakano, A. (2014). Dynamic behavior of the trans-golgi network in root tissues of Arabidopsis revealed by super-resolution live imaging. Plant & cell physiology **55,** 694-703.

Uemura, T., Ueda, T., Ohniwa, R.L., Nakano, A., Takeyasu, K., and Sato, M.H. (2004). Systematic analysis of SNARE molecules in Arabidopsis: dissection of the post-Golgi network in plant cells. Cell Struct Funct **29,** 49-65.

Uemura, T., Kim, H., Saito, C., Ebine, K., Ueda, T., Schulze-Lefert, P., and Nakano, A. (2012). Qa-SNAREs localized to the trans-Golgi network regulate multiple transport pathways and extracellular disease resistance in plants. Proceedings of the National Academy of Sciences of the United States of America **109,** 1784-1789.

Urbe, S. (2005). Ubiquitin and endocytic protein sorting. Essays Biochem **41,** 81-98.

Usami, Y., Popov, S., and Gottlinger, H.G. (2007). Potent rescue of human immunodeficiency virus type 1 late domain mutants by ALIX/AIP1 depends on its CHMP4 binding site. Journal of virology **81,** 6614-6622.

Verma, R., Aravind, L., Oania, R., McDonald, W.H., Yates, J.R., 3rd, Koonin, E.V., and Deshaies, R.J. (2002). Role of Rpn11 metalloprotease in deubiquitination and degradation by the 26S proteasome. Science **298,** 611-615.

Vernoud, V., Horton, A.C., Yang, Z., and Nielsen, E. (2003). Analysis of the small GTPase gene superfamily of Arabidopsis. Plant physiology **131,** 1191-1208.

Vierstra, R.D. (2003). The ubiquitin/26S proteasome pathway, the complex last chapter in the life of many plant proteins. Trends in plant science **8,** 135-142.

Vierstra, R.D. (2009). The ubiquitin-26S proteasome system at the nexus of plant biology. Nature reviews. Molecular cell biology **10,** 385-397.

Vierstra, R.D. (2012). The expanding universe of ubiquitin and ubiquitin-like modifiers. Plant physiology **160,** 2-14.

Viotti, C., Kruger, F., Krebs, M., Neubert, C., Fink, F., Lupanga, U., Scheuring, D., Boutte, Y., Frescatada-Rosa, M., Wolfenstetter, S., Sauer, N., Hillmer, S., Grebe, M., and Schumacher, K. (2013). The endoplasmic reticulum is the main membrane source for biogenesis of the lytic vacuole in Arabidopsis. The Plant cell **25,** 3434-3449.

Vogelmann, K., Drechsel, G., Bergler, J., Subert, C., Philippar, K., Soll, J., Engelmann, J.C., Engelsdorf, T., Voll, L.M., and Hoth, S. (2012). Early senescence and cell death in Arabidopsis saul1 mutants involves the PAD4-dependent salicylic acid pathway. Plant physiology **159,** 1477-1487.

von Schwedler, U.K., Stuchell, M., Muller, B., Ward, D.M., Chung, H.Y., Morita, E., Wang, H.E., Davis, T., He, G.P., Cimbora, D.M., Scott, A., Krausslich, H.G., Kaplan, J., Morham, S.G., and Sundquist, W.I. (2003). The protein network of HIV budding. Cell **114,** 701-713.

Walker, K.L., and Smith, L.G. (2002). Investigation of the role of cell-cell interactions in division plane determination during maize leaf development through mosaic analysis of the tangled mutation. Development **129,** 3219-3226.

Wang, J., Cai, Y., Miao, Y., Lam, S.K., and Jiang, L. (2009a). Wortmannin induces homotypic fusion of plant prevacuolar compartments. Journal of experimental botany **60,** 3075-3083.

Wang, S., Kurepa, J., and Smalle, J.A. (2009b). The Arabidopsis 26S proteasome subunit RPN1a is required for optimal plant growth and stress responses. Plant & cell physiology **50,** 1721-1725.

Wang, Y., and Liu, Y. (2013). Autophagic degradation of leaf starch in plants. Autophagy **9,** 1247-1248.

Wang, Y., Yu, B., Zhao, J., Guo, J., Li, Y., Han, S., Huang, L., Du, Y., Hong, Y., Tang, D., and Liu, Y. (2013). Autophagy contributes to leaf starch degradation. The Plant cell **25,** 1383-1399.

Wang, Y.S., Pi, L.Y., Chen, X., Chakrabarty, P.K., Jiang, J., De Leon, A.L., Liu, G.Z., Li, L., Benny, U., Oard, J., Ronald, P.C., and Song, W.Y. (2006). Rice XA21 binding protein 3 is a ubiquitin ligase required for full Xa21-mediated disease resistance. The Plant cell **18,** 3635-3646.

Wauer, T., and Komander, D. (2014). The JAMM in the proteasome. Nature structural & molecular biology **21,** 346-348.

Wemmer, M., Azmi, I., West, M., Davies, B., Katzmann, D., and Odorizzi, G. (2011). Bro1 binding to Snf7 regulates ESCRT-III membrane scission activity in yeast. The Journal of cell biology **192,** 295-306.

Wessling, R., Epple, P., Altmann, S., He, Y., Yang, L., Henz, S.R., McDonald, N., Wiley, K., Bader, K.C., Glasser, C., Mukhtar, M.S., Haigis, S., Ghamsari, L., Stephens, A.E., Ecker, J.R., Vidal, M., Jones, J.D., Mayer, K.F., Ver Loren van Themaat, E., Weigel, D., Schulze-Lefert, P., Dangl, J.L., Panstruga, R., and Braun, P. (2014). Convergent targeting of a common host protein-network by pathogen effectors from three kingdoms of life. Cell host & microbe **16,** 364-375.

Winter, V., and Hauser, M.T. (2006). Exploring the ESCRTing machinery in eukaryotes. Trends in plant science **11,** 115-123.

Wormit, A., Traub, M., Florchinger, M., Neuhaus, H.E., and Mohlmann, T. (2004). Characterization of three novel members of the Arabidopsis thaliana equilibrative nucleoside transporter (ENT) family. Biochem J **383,** 19-26.

Wright, M.H., Berlin, I., and Nash, P.D. (2011). Regulation of endocytic sorting by ESCRT-DUB-mediated deubiquitination. Cell Biochem Biophys **60,** 39-46.

Wu, X., Ebine, K., Ueda, T., and Qiu, Q.S. (2016). AtNHX5 and AtNHX6 Are Required for the Subcellular Localization of the SNARE Complex That Mediates the Trafficking of Seed Storage Proteins in Arabidopsis. PloS one **11,** e0151658.

Xie, Q., Michaeli, S., Peled-Zehavi, H., and Galili, G. (2015). Chloroplast degradation: one organelle, multiple degradation pathways. Trends in plant science **20,** 264-265.

Xing, S., Wallmeroth, N., Berendzen, K.W., and Grefen, C. (2016). Techniques for the Analysis of Protein-Protein Interactions in Vivo. Plant physiology **171,** 727-758.

Xu, P., Duong, D.M., Seyfried, N.T., Cheng, D., Xie, Y., Robert, J., Rush, J., Hochstrasser, M., Finley, D., and Peng, J. (2009). Quantitative proteomics reveals the function of unconventional ubiquitin chains in proteasomal degradation. Cell **137,** 133-145.

Xu, W., and Mitchell, A.P. (2001). Yeast PalA/AIP1/Alix homolog Rim20p associates with a PEST-like region and is required for its proteolytic cleavage. J Bacteriol **183,** 6917-6923.

Xu, X.M., Zhao, Q., Rodrigo-Peiris, T., Brkljacic, J., He, C.S., Muller, S., and Meier, I. (2008). RanGAP1 is a continuous marker of the Arabidopsis cell division plane. Proceedings of the National Academy of Sciences of the United States of America **105,** 18637-18642.

Yamazaki, M., Shimada, T., Takahashi, H., Tamura, K., Kondo, M., Nishimura, M., and Hara-Nishimura, I. (2008). Arabidopsis VPS35, a retromer component, is required for vacuolar protein sorting and involved in plant growth and leaf senescence. Plant & cell physiology **49,** 142-156.

Yau, R., and Rape, M. (2016). The increasing complexity of the ubiquitin code. Nature cell biology **18,** 579-586.

Yoshimoto, K. (2010). Plant autophagy puts the brakes on cell death by controlling salicylic acid signaling. Autophagy **6,** 192-193.

Yu, D., Yu, F., Du, C., Li, X., Zhao, X., and Liu, X. (2015). RPN1a, a subunit of the 26S proteasome, controls trichome development in Arabidopsis. Plant Physiol Biochem **88,** 82-88.

Zhai, Q., Fisher, R.D., Chung, H.Y., Myszka, D.G., Sundquist, W.I., and Hill, C.P. (2008). Structural and functional studies of ALIX interactions with YPX(n)L late domains of HIV-1 and EIAV. Nature structural & molecular biology **15,** 43-49.

Zhao, W.M., Seki, A., and Fang, G. (2006). Cep55, a microtubule-bundling protein, associates with centralspindlin to control the midbody integrity and cell abscission during cytokinesis. Molecular biology of the cell **17,** 3881-3896.

Zhou, J., Wang, J., Cheng, Y., Chi, Y.J., Fan, B., Yu, J.Q., and Chen, Z. (2013). NBR1-mediated selective autophagy targets insoluble ubiquitinated protein aggregates in plant stress responses. PLoS genetics **9,** e1003196.

Zhou, X., Pan, S., Sun, L., Corvera, J., Lee, Y.C., Lin, S.H., and Kuang, J. (2009). The CHMP4b- and Src-docking sites in the Bro1 domain are autoinhibited in the native state of Alix. Biochem J **418,** 277-284.

Zhu, H., Li, G.J., Ding, L., Cui, X., Berg, H., Assmann, S.M., and Xia, Y. (2009). Arabidopsis extra large G-protein 2 (XLG2) interacts with the Gbeta subunit of heterotrimeric G protein and functions in disease resistance. Mol Plant **2,** 513-525.

Zouhar, J., and Rojo, E. (2009). Plant vacuoles: where did they come from and where are they heading? Current opinion in plant biology **12,** 677-684.

Zouhar, J., Rojo, E., and Bassham, D.C. (2009). AtVPS45 is a positive regulator of the SYP41/SYP61/VTI12 SNARE complex involved in trafficking of vacuolar cargo. Plant physiology **149,** 1668-1678.

Appendix

Appendix Table 1. Accession numbers.

Name	Gene ID
AAA ATPase (interaction candidate isolated in the Y2H screen)	AT4G24710
ALIX (ALG-2-INTERACTING PROTEIN X)	AT1G15130
AMSH1 (ASSOCIATED MOLECULE WITH THE SH3 DOMAIN OF STAM 1)	AT1G48790
AMSH2	AT1G10600
AMSH3	AT4G16144
ARA6 (ARABIDOPSIS RAB GTPase 6)	AT3G54840
ARA7	AT4G19640
CaLB-family protein (interaction candidate isolated in the Y2H screen)	AT4G34150
CLC (CLATHRIN LIGHT CHAIN), homolog 2	AT2G40060
CDC2 (CYCLIN-DEPENDENT KINASE 1)	AT3G48750
FIP1 (VirF-INTERACTING PROTEIN 1 or FH1-INTERACTING PROTEIN 1)	AT1G28200
FYVE1 (FYVE-DOMAIN PROTEIN 1)	AT1G20110
RABG3c (RAB GTPase HOMOLOG G3c)	AT3G16100
SKD1 (SUPPRESSOR OF K+ TRANSPORT GROWTH DEFECT 1)	AT2G27600
SNF7.1 (SUGAR NON-FERMENTING 7.1)	AT4G29160
SNF7.2	AT2G19830
SYP43 (SYNTAXIN OF PLANTS 43)	AT3G05710
VPS2.1 (VACUOLAR PROTEIN SORTING 2.1)	AT2G06530
VPS60.1	AT3G10640
XBAT35 (XB3 ORTHOLOG 5 IN ARABIDOPSIS THALIANA)	AT3G23280

Appendix Table 2. Results of the Y2H screen and pairwise Y2H assays.

No.	Gene ID	Name or description	Confirmed interaction
Y2H screen using GBD-AMSH1 and GBD-AMSH2 as bait			
1	AT1G15130	ALIX (ALG-2-INTERACTING PROTEIN X)	AMSH1
2	AT1G15710	prephenate dehydrogenase	AMSH1
3	AT1G71230	CSN5B (COP9 SIGNALOSOME 5B)	AMSH1
4	AT1G24590	DRNL (DORNROSCHEN-LIKE)	Negative
5	AT1G54220	dihydrolipoamide S-acetyltransferase	Negative
6	AT1G65410	ATNAP11 (ARABIDOPSIS THALIANA NON-INTRINSIC ABC PROTEIN 11)	(Not tested)
7	AT1G66350	RGL1 (RGA-LIKE 1)	Negative
8	AT1G68670	myb family transcription factor	Negative
9	AT1G22920	CSN5A	(Not tested)
10	AT1G76370	putative protein kinase	(Not tested)
11	AT2G23760	BLH4 (BEL1-LIKE HOMEODOMAIN 4)	(Not tested)
12	AT2G30340	LBD13 (LOB DOMAIN-CONTAINING PROTEIN 13)	AMSH1
13	AT2G45680	TCP9 (TEOSINTE BRANCHED, CYCLOIDEA AND PCF 9)	(Not tested)
14	AT2G45890	GEF4 (GUANINE EXCHANGE FACTOR 4)	(Not tested)
15	AT3G01090	AKIN10 (ARABIDOPSIS SNF1 KINASE HOMOLOG 10)	(Not tested)
16	AT3G01670	unknown protein	(Not tested)
17	AT3G07630	ADT2 (AROGENATE DEHYDRATASE 2)	AMSH1 and AMSH2
18	AT3G09250	NTF2-LIKE (NUCLEAR TRANSPORT FACTOR 2-LIKE)	(Not tested)
19	AT3G11410	PP2CA (PROTEIN PHOSPHATASE 2CA)	(Not tested)
20	AT3G15030	TCP4	(Not tested)
21	AT3G19895	unknown protein 1	AMSH1
22	AT3G23240	ERF1B (ETHYLENE RESPONSE FACTOR 1)	(Not tested)
23	AT3G25800	PP2AA2 (PROTEIN PHOSPHATASE 2A SUBUNIT A2)	(Not tested)
24	AT3G44940	unknown protein 2	AMSH1
25	AT3G47620	TCP14	(Not tested)
26	AT3G50820	PSBO2 (PHOTOSYSTEM II SUBUNIT O-2)	(Not tested)
27	AT3G54000	unknown protein 4	Negative
28	AT4G01090	extra-large G-protein-related	AMSH1
29	AT4G03415	PP2C52 (2C-TYPE PROTEIN PHOSPHATASE 52)	Negative
30	AT4G16447	unknown protein 3	AMSH2
31	AT4G18370	DEG5 (DEGP PROTEASE 5)	Negative
32	AT4G21800	QQT2 (QUATRE-QUART2)	Negative
33	AT4G24710	AAA ATPase	AMSH1
34	AT4G27240	C2H2-type zinc finger family protein	AMSH2
35	AT5G06780	EML2 (EMSY-LIKE 2)	AMSH1
36	AT5G08440	hypothetical protein	(Not tested)
37	AT5G16450	dimethylmenaquinone methyltransferase	AMSH1
38	AT5G17840	chaperone protein dnaJ-related	(Not tested)
39	AT5G24660	LSU2 (RESPONSE TO LOW SULFUR 2)	(Not tested)
40	AT5G51440	mitochondrial small heat shock protein	(Not tested)
41	AT5G51910	TCP19	(Not tested)
42	AT5G52640	HSP90.1 (HEAT SHOCK PROTEIN 90.1)	(Not tested)

43	AT5G61010	EXO70E2 (EXOCYST SUBUNIT EXO70 PROTEIN E2)	AMSH1

Y2H screen using GBD-ALIX as bait

1	AT1G01010	NAC001 (NAC DOMAIN-CONTAINING PROTEIN 001)	(Not tested)
2	AT1G06510	unknown chloroplast protein	(Not tested)
3	AT1G28200	FIP1 (VirF-INTERACTING PROTEIN 1 or FH1-INTERACTING PROTEIN 1)	ALIX
4	AT1G67170	unknown protein	(Not tested)
5	AT2G19830	SNF7.2 (SUGAR NON-FERMENTING 7.2)	(Verified elsewhere)
6	AT2G43410	FPA (FLOWERING TIME CONTROL PROTEIN A)	(Not tested)
7	AT3G23280	XBAT35 (XB3 ORTHOLOG 5 IN ARABIDOPSIS THALIANA)	Negative
8	AT4G29160	SNF7.1	(Verified elsewhere)
9	AT4G34150	CaLB (Calcium-dependent lipid-binding)-domain family protein	ALIX

Appendix Table 3. Chemicals used in this study.

Name	Supplier
2-Mercaptoethanol	Carl Roth, Germany
2-(N-morpholino)ethanesulfonic acid (MES monohydrate)	Carl Roth, Germany
2-(N-morpholino)ethanesulfonic acid (MES hydrate)	Sigma-Aldrich, Germany
2S,3S-trans-(ethoxycarbonyloxirane-2-carbonyl)-L-leucine-(3-methylbutyl) amide (E-64d)	Santa Cruz Biotechnology, Germany
2',7'-Bis-(2-carboxyethyl)-5-(and-6)-carboxyfluorescein, acetoxymethyl ester (BCECF-AM)	Thermo Fisher Scientific, Germany
3-Amino-1,2,4-triazole (3-AT)	Sigma-Aldrich, Germany
5-Bromo-4-chloro-3-indolyl phosphate (BCIP)	Sigma-Aldrich, Germany
6-Benzylaminopurine (6-BA)	Sigma-Aldrich, Germany
Acetic acid	Carl Roth, Germany
Acrylamide Rotiphorese Gel 30 (37, 5:1)	Carl Roth, Germany
Agar, bacteriological grade	AppliChem, Germany
Agarose, peqGOLD Universal	Peqlab, Germany
Ammonium peroxydisulphate (APS)	Carl Roth, Germany
Ampicillin	Carl Roth, Germany
Basta	Bayer CropScience, Germany
Bicine	Carl Roth, Germany
Bis-(2-hydroxyethyl)-imino-tris-(hydroxymethyl)-methan (Bis-Tris)	Carl Roth, Germany
Bovine serum albumin (albumin fraction V, BSA)	AppliChem, Germany
Brefeldin A (BFA)	Thermo Fisher Scientific, Germany
Bromophenol blue	Carl Roth, Germany
Calcium chloride	Sigma-Aldrich, Germany
Calcium hypochloride	Carl Roth, Germany
Cellulase “Onozuka R-10”	Yakult Pharmaceutical Industry, Japan
Chloroform	Carl Roth, Germany
Coomassie Brilliant Blue G	Sigma-Aldrich, Germany
Coomassie Brilliant Blue R-250	AppliChem, Germany
D-Glucose	AppliChem, Germany
D-Mannitol	AppliChem, Germany
Deoxyribonucleoside triphosphates (dNTPs)-Set	Carl Roth, Germany
Dimethyl sulfoxide (DMSO)	Carl Roth, Germany
Dithiothreitol (DTT)	Sigma-Aldrich, Germany
Ethanol	Carl Roth, Germany
Ethidium bromide	Carl Roth, Germany
Gentamicin sulfate	Duchefa Biochemie, Netherlands
Glycerol	AppliChem, Germany
Hydrochloric acid	Carl Roth, Germany
Hygromycin B	Sigma-Aldrich, Germany
Imidazole	Carl Roth, Germany
Isopropanol (2-Propanol)	Carl Roth, Germany
Isopropyl β-D-1-thiogalactopyranoside (IPTG)	AppliChem, Germany
Kanamycin	AppliChem, Germany
L-Glutathione	Sigma-Aldrich, Germany

L-Histidine	Sigma-Aldrich, Germany
L-Leucine	Sigma-Aldrich, Germany
L-Tryptophan	Sigma-Aldrich, Germany
Lithium acetate	Carl Roth, Germany
Macerozyme R-10	Yakult Pharmaceutical Industry, Japan
Magnesium chloride hexahydrate	Sigma-Aldrich, Germany
Magnesium sulfate heptahydrate	AppliChem, Germany
Methanol	Carl Roth, Germany
Monodansylcadaverine (MDC)	Sigma-Aldrich, Germany
Murashige & Skoog (MS-0)	Duchefa Biochemie, Netherlands
N-(3-triethylammoniumpropyl)-4-(6-(4-(diethylamino) phenyl) hexatrienyl) pyridinium dibromide (FM4-64)	Thermo Fisher Scientific, Germany
N,N-Dimethylformamid (DMF)	Carl Roth, Germany
Nitro blue tetrazolium chloride (NBT)	Sigma-Aldrich, Germany
Phenol	Carl Roth, Germany
Plant agar	Duchefa Biochemie, Netherlands
Pluronic F-127	Sigma-Aldrich, Germany
Poly(ethylene glycol) 4000 (PEG4000)	Carl Roth, Germany
Poly(ethylene glycol) 4000 (PEG4000)	Sigma-Aldrich, Germany
Poly(ethylene glycol) 6000 (PEG6000)	Sigma-Aldrich, Germany
Potassium acetate	Carl Roth, Germany
Potassium chloride	AppliChem, Germany
Potassium hydroxide	AppliChem, Germany
Silwet L-77	Lehle Seeds, USA
Sodium hydroxide	Carl Roth, Germany
Rifampicin	Duchefa Biochemie, Netherlands
Skimmed milk powder	Carl Roth, Germany
Tris(2-carboxyethyl)phosphine (TCEP)	Sigma-Aldrich, Germany
Wortmannin (WM)	AppliChem, Germany

Appendix Table 4. Antibodies used in this study.

Antibody	Reference or supplier
Primary antibodies	
Anti-ALIX, rabbit	(Kalinowska et al., 2015)
Anti-AMSH1, rabbit	(Katsiarimpa et al., 2013)
Anti-AMSH3, rabbit	(Isono et al., 2010)
Anti-BiP (HSC70), mouse	Enzo Life Sciences, Germany
Anti-CDC2, rabbit	Santa Cruz Biotechnology, Germany
Anti-CHC, rabbit	Agrisera, Sweden
Anti-GBD, mouse	Santa Cruz Biotechnology, Germany
Anti-GFP, rabbit	Thermo Fisher Scientific, Germany
anti-GST, goat	GE Healthcare Life Sciences, Germany
Anti-H^+-ATPase, rabbit	Agrisera, Sweden
anti-HA-HRP	Roche Diagnostics, Germany
Anti-His-HRP	Sigma-Aldrich, Germany
Anti-MBP, mouse	New England BioLabs, Germany
Anti-Sec21, rabbit	Agrisera, Sweden
Anti-ubiquitin (P4D1), mouse	Santa Cruz Biotechnology, Germany
Anti-ubiquitin (P4D1)-HRP	Santa Cruz Biotechnology, Germany
Anti-UGPase, rabbit	Agrisera, Sweden
Anti-V-ATPase, rabbit	Agrisera, Sweden
Secondary antibodies	
Anti-goat-HRP	Sigma-Aldrich, Germany
Anti-mouse-HRP	Sigma-Aldrich, Germany
Anti-rabbit-AP	Sigma-Aldrich, Germany
Anti-rabbit-HRP	Sigma-Aldrich, Germany

Appendix Table 5. Vectors used for cloning in this study.

Name	Description	Reference
Entry vectors		
pDONR207	Gateway donor vector, *E. coli* selection: Gen^R	Thermo Fisher Scientific, Germany
Yeast expression vectors		
pDEST-AD-CYH2	GAL4 AD fusion vector, *ADH1* promoter, ADH1 terminator, *CYH2*, *E. coli* selection: Amp^R, yeast selection: *TRP1*	(Dreze et al., 2010)
pDEST-BD_pPC97	GAL4 BD fusion vector, ADH1 promoter, ADH1 terminator, *E. coli* selection: Amp^R, yeast selection: *LEU2*	(Dreze et al., 2010)
pGADT7	GAL4 AD fusion vector, ADH1 promoter, ADH1 terminator, *E. coli* selection: Amp^R, yeast selection: *LEU2*	Takara Bio, Japan
pGBKT7	GAL4 BD fusion vector, ADH1 promoter, ADH1 terminator, *E. coli* selection: Kan^R, yeast selection: *TRP1*	Takara Bio, Japan
Recombinant protein expression vectors		
pET21a	T7 and His fusion vector, T7 promoter, T7 terminator, *E. coli* selection: Amp^R	Merck Millipore, Germany
pGEX-6P-1	GST fusion vector, tac promoter, PreScission cleavage site, *E. coli* selection: Amp^R	GE Healthcare Life Sciences, Germany
pMAL-p2p	MBP fusion vector, tac promoter, T1 and T2 terminators, PreScission cleavage site, *E. coli* selection: Amp^R	gift from K. Tanaka lab, based on pMAL-p2 (New England BioLabs, Germany)
pMAL-p2T	GST fusion vector, tac promoter, T1 and T2 terminators, Thrombin cleavage site, *E. coli* selection: Amp^R	gift from K. Tanaka lab, based on pMAL-p2 (New England BioLabs, Germany)
Plant expression vectors		
pFAST-R05	sGFP fusion vector, Gateway, 35S promoter, NOS terminator, *E. coli* selection: Spc^R, plant selection: Kan^R, fluorescent reporter	(Shimada et al., 2010)

pGWB560	TagRFP fusion vector, Gateway, 35S promoter, NOS terminator, *E. coli* selection: Spc^R, plant selection: Hyg^R	T. Nakagawa, Matsue, Japan
pJawohl2B-3xHA	3xHA fusion vector, Gateway, 35S promoter, *E. coli* selection: Amp^R, plant selection: Bar^R	J. Parker, Cologne, Germany
pUBN-CFP-DEST	CFP fusion vector, Gateway, UBQ10 promoter, 35S terminator, *E. coli* selection: Sm^R, plant selection: Bar^R	(Grefen et al., 2010)

Appendix Table 6. All DNA constructs generated during this study.

No.	Construct	Vector backbone	Comment/reference
pKK1	*ADH1pro:GBD-AMSH1(WT)*	pDEST-BD_pPC97	pENTR: pEI7; (Kalinowska et al., 2015)
pKK2	*ADH1pro:GBD-AMSH2(WT)*	pDEST-BD_pPC97	pENTR: pEI8; (Kalinowska et al., 2015)
pKK3	*ADH1pro:GBD-AMSH3(WT)*	pDEST-BD_pPC97	pENTR: pEI9; autoactivates in yeast; (Kalinowska et al., 2015)
pKK4	*ADH1pro:GBD-AMSH3(AXA)*	pDEST-BD_pPC97	pENTR: pEI12; (Kalinowska et al., 2015)
pKK5	*35Spro:AMSH1-GFP*	p35S-GFP	pENTR: pEI52
pKK6	*35Spro:AMSH1-TagRFP*	pGWB460	pENTR: pEI52
pKK7	*35Spro:AMSH3-TagRFP*	pGWB560	pENTR: pEI54; expressed in protoplasts, no expression in plants under the confocal microscope; (Kalinowska et al., 2015)
pKK8	*Tac-pro:GST-AMSH1(MPN, longer)*	pGEX-6P-1	PreScission cutting site; Active against K63-, not K48-linked polyUb; (Katsiarimpa et al., 2013)
pKK9	*Tac-pro:GST-AMSH1(MPN, shorter)*	pGEX-6P-1	PreScission cutting site
pKK10	*Tac-pro:GST-AMSH1(N154)*	pGEX-6P-1	PreScission cutting site; (Katsiarimpa et al., 2013)
pKK11	*Tac-pro:GST-AMSH1(∆MPN)*	pGEX-6P-1	PreScission cutting site
pKK12	*Tac-pro:GST-AMSH1(∆MIT)*	pGEX-6P-1	PreScission cutting site
pKK13	*Tac-pro:MBP-dehydrogenase* (AT1G15710)	pMAL-p2T	thrombin cutting site
pKK14	*Tac-pro:MBP-CSN5A* (AT1G22920)	pMAL-p2T	thrombin cutting site
pKK15	*Tac-pro:MBP-LBD13* (AT2G30340)	pMAL-p2T	thrombin cutting site
pKK16	*Tac-pro:MBP-extra-large G-protein-related* (AT4G01090)	pMAL-p2T	thrombin cutting site
pKK17	*Tac-pro:MBP-AAA ATPase* (AT4G24710)	pMAL-p2T	thrombin cutting site
pKK18	*Tac-pro:MBP-EML2* (AT5G06780)	pMAL-p2T	thrombin cutting site
pKK19	*Tac-pro:MBP-methyltransferase* (AT5G16450)	pMAL-p2T	thrombin cutting site
pKK20	*Tac-pro:MBP-ALIX*	pMAL-p2T	thrombin cutting site (Kalinowska et al., 2015)
pKK21	*Tac-pro:MBP-Exo70E2* (AT5G61010)	pMAL-p2T	thrombin cutting site
pKK22	*Tac-pro:MBP-unknown 1* (AT3G01670)	pMAL-p2T	thrombin cutting site

pKK23	*Tac-pro:MBP-ADT2* (AT3G07630)	pMAL-p2T	thrombin cutting site
pKK24	*Tac-pro:MBP-unknown 2* (AT3G44940)	pMAL-p2T	thrombin cutting site
pKK25	*Tac-pro:MBP-unknown 3* (AT4G16447)	pMAL-p2T	thrombin cutting site
pKK26	*Tac-pro:MBP-VPS2.1*	pMAL-p2T	Insert from pAK7; thrombin cutting site
pKK27	*Tac-pro:MBP-VPS24.1*	pMAL-p2T	Insert from pAK55; contains point mutations; thrombin cutting site
pKK28	*Tac-pro:MBP-VPS60.1*	pMAL-p2T	Insert from pAK56; thrombin cutting site; (Kalinowska et al., 2015)
pKK29	*T7pro:His-ALIX(middle)*	pET21a	Used for anti-ALIX antibody production; (Kalinowska et al., 2015)
pKK30	*Tac-pro:MBP-ALIX(middle)*	pMAL-p2p	PreScission cutting site
pKK31	*Tac-pro:MBP-ALIX(BRO1)*	pMAL-p2p	PreScission cutting site
pKK32	*Tac-pro:MBP-ALIX(∆C-term)*	pMAL-p2p	PreScission cutting site
pKK33	*Tac-pro:MBP-ALIX(∆BRO1)*	pMAL-p2p	PreScission cutting site
pKK34	*ARA7* entry clone, N-term	pDONR207	
pKK35	*UBQ10pro:CFP-ARA7*	pUBN-CFP-DEST	
pKK36	*ALIX* entry clone, CDS	pDONR207	
pKK37	*ALIX amiR2-2* entry clone	pDONR207	
pKK38	*35Spro:amiR2(ALIX)*	pGWB560	pENTR: pKK37
pKK39	*UBQ10pro:amiR2(ALIX)*	pUBC-DEST-CFP	pENTR: pKK37; no downregulation of *ALIX* observed in plants
pKK40	*XVE-35Spro:amiR2(ALIX)*	pABindGFP	pENTR: pKK37
pKK41	*ADH1pro:GBD-ALIX*	pGBKT7	(Kalinowska et al., 2015)
pKK42	*35Spro:3xHA-ALIX*	pJawohl2B-3xHA-GW	pENTR: pKK36
pKK43	*ADH1pro:GAD-HA-ALIX*	pGADT7	
pKK44	*ADH1pro:GDB-Myc-ALIX*	pDEST-BD_pPC97	
pKK45	*ADH1pro:GAD-HA-ALIX*	pDEST-AD-CYH2	
pKK46	*35Spro:FLAG-ALIX*	pGWB412	pENTR: pKK36
pKK47	*35Spro:TagRFP-ALIX(genomic)*	pGWB461	pENTR from Laura Cuyas: (Cardona-Lopez et al., 2015)
pKK48	*Tac-pro:GST-ALIX*	pGEX-6P-1	PreScission cutting site
pKK49	*ADH1pro:GBD-Myc-ALIX (BRO1)*	pGBKT7	(Kalinowska et al., 2015)
pKK50	*ADH1pro:GBD-Myc-ALIX (∆BRO1)*	pGBKT7	(Kalinowska et al., 2015)
pKK51	*ADH1pro:GBD-Myc-ALIX (∆C-term)*	pGBKT7	(Kalinowska et al., 2015)
pKK52	*ADH1pro:GBD-Myc-ALIX (∆PRD)*	pGBKT7	Autoactivates in yeast
pKK53	*ADH1pro:GAD-HA-AMSH3 (fragm.A, 322-981 bp)*	pGADT7	

pKK54	*ADH1pro:GAD-HA-AMSH3 (fragm.C, 523-981 bp)*	pGADT7	
pKK55	*ADH1pro:GAD-HA-AMSH3 (fragm.D, 322-777 bp)*	pGADT7	
pKK56	*ADH1pro:GAD-HA-AMSH3 (fragm.E, 766-981 bp)*	pGADT7	
pKK57	*ADH1pro:GAD-HA-AMSH3 (fragm.F, 523-777 bp)*	pGADT7	
pKK58	*ADH1pro:GAD-HA-FIP1 (AT1G28200)*	pGADT7	
pKK59	*ADH1pro:GBD-Myc-ALIX (fragm.A, 1180-1893 bp)*	pGBKT7	
pKK60	*ADH1pro:GBD-Myc-ALIX (fragm.B, 1180-1461 bp)*	pGBKT7	
pKK61	*ADH1pro:GBD-Myc-ALIX (fragm.C, 1461-1893 bp)*	pGBKT7	
pKK62	*ADH1pro:GBD-Myc-ALIX (fragm.D, 1180-1581 bp)*	pGBKT7	
pKK63	*ADH1pro:GBD-Myc-ALIX (fragm.E, „V-fragm.1"; 1581-1893 bp)*	pGBKT7	(Kalinowska et al., 2015)
pKK64	*ADH1pro:GBD-Myc-ALIX (fragm.F, 1461-1581 bp)*	pGBKT7	
pKK65	*ADH1pro:GBD-Myc-FIP1* (AT1G28200)	pGBKT7	
pKK66	*ADH1pro:GBD-Myc-XBAT35, splice form 2* (AT3G23280.2)	pGBKT7	
pKK67	*ADH1pro:GBD-Myc-XBAT34* (AT4G14365)	pGBKT7	
pKK68	*ADH1pro:GAD-HA-AMSH3 (fragm.B, 322-523 bp)*	pGADT7	
pKK69	*ALIX(FL)* entry clone, with ATG	pDONR207	(Kalinowska et al., 2015)
pKK70	*ALIX(BRO1)* entry clone, with ATG	pDONR207	
pKK71	*ALIX(∆BRO1)* entry clone, with ATG	pDONR207	
pKK72	*35Spro:ALIX(FL)-STOP*	pFAST-R05	pENTR: pKK69; dominant-negative effect in plants (downregulation of ALIX) (Kalinowska et al., 2015)
pKK73	*35Spro:ALIX(BRO1)-STOP*	pFAST-R05	pENTR: pKK70; dominant-negative effect in plants (downregulation of ALIX)
pKK74	*35Spro:ALIX(deltaBRO1)-STOP*	pFAST-R05	pENTR: pKK71; dominant-negative effect in plants (downregulation of ALIX)
pKK75	*ADH1pro:GBD-Myc-ALIX(∆E1)*	pGBKT7	
pKK76	*ADH1pro:GBD-Myc-ALIX(∆E3)*	pGBKT7	Autoactivates in yeast
pKK77	*ADH1pro:GBD-Myc-ALIX(∆E4)*	pGBKT7	
pKK78	*35Spro:3xHA-ALIX(∆BRO1)*	pJawohl2B-3xHA-GW	pENTR: pKK71
pKK79	*ADH1pro:GBD-Myc-ALIX(∆E2)*	pGBKT7	

pKK80	*35Spro:3xHA-ALIX(BRO1)*	pJawohl2B-3xHA-GW	pENTR: pKK70
pKK81	*ADH1pro:GBD-Myc-ALIX(E3+4; „V-fragm.2“)*	pGBKT7	(Kalinowska et al., 2015)
pKK82	*ADH1pro:GBD-Myc-ALIX (E4;WT)*	pGBKT7	Autoactivates in yeast
pKK83	*ADH1pro:GBD-Myc-ALIX (E4;L596P)*	pGBKT7	
pKK84	*T7pro:HsALIX(V)-His* (PDCD6IP)	pET21a	
pKK85	*35Spro:AMSH3(Y213A)-sGFP*	pFAST-R05	pENTR: pFA186
pKK86	*35Spro:AMSH3(H190A)-sGFP*	pFAST-R05	pENTR: pFA190
pKK87	*ADH1pro:GAD-HA-Bem1-homolog 1 (AT5G64430)*	pGADT7	
pKK88	*ADH1pro:GAD-HA-Bem1-homolog 2 (AT5G09620)*	pGADT7	
pKK89	*ADH1pro:GAD-HA-UBQ10 (fragm.) (AT4G05320)*	pGADT7	
pKK90	*ADH1pro:GAD-HA-CaLB family protein (AT4G34150)*	pGADT7	
pKK91	*ALIX(E3+4; „V-fragm.2“)* entry clone	pDONR207	
pKK92	*T7pro:His-ALIX(E3+4; „V-fragm.2“)*	pET21a	No expression in Rosetta
pKK93	*Tac-pro:MBP-ALIX(E3+4; „V-fragm.2“)*	pMAL-p2p	PreScission cutting site
pKK94	*35Spro:AMSH3(Y213A,L193D,H190A)-sGFP*	pFAST-R05	pENTR: pFA198; does not complement *amsh3-1*
pKK95	*ADH1pro:GAD-HA-XBAT34 (AT4G14365)*	pGADT7	
pKK96	*ADH1pro:GAD-HA-XBAT35, splice form 2 (AT3G23280.2)*	pGADT7	
pKK97	*Tac-pro:GST-AMSH3(∆D1)*	pGEX-6P-1	PreScission cutting site
pKK98	*Tac-pro:GST-AMSH3(∆C)*	pGEX-6P-1	PreScission cutting site
pKK99	*OTU11* entry clone, C-term.	pDONR207	
pKK100	*OTU12* entry clone, C-term.	pDONR207	
pKK101	*35Spro:OTU12-GFP*	p35S-GFP	pENTR: pKK100; OTU11-GFP was cloned by A. Schöllkopf

Appendix Table 7. All primers generated in this study.

Prime name	Sequence 5' - 3'	Tm [°C]	Comment or reference
KK1 pDEST CAN1 F seq	GAAGAGTGGTTGCGAAC	57.0	pDEST-BD sequencing primer
KK2 AMSH1(MPN-long) +979 *Bam*HI F	AAGGGGATCCATGTCGGAGTCTCCTCTTGAACTTCATATT	69.3	classical cloning
KK3 AMSH1(MPN-short) +1063 *Bam*HI F	AAGGGGATCCATGTTAGAGACGTGTGGTATTCTTGCCGGT	73.4	classical cloning
(KK4 pDEST-BD_pC97 F)	CGCGTTTGGAATCACTACAGGG	60.2	sequencing primer
(KK5 pDEST-AD-CYH2 F)	GGCTTCAGTGGAGACTGATATGCCTC	63.2	sequencing primer
(KK6 pDEST Term R)	GGAGACTTGACCAAACCTCTGGCG	64.3	sequencing primer
KK7 AMSH1(MIT) +352 *Sal*I R	AAGGGTCGACTCACAGTTCATCAATCCTTTG	60.7	classical cloning
KK8 AMSH1(N154) SalI R	AAGGGTCGACTCAGCCAGAATTATGTCCAG	60.8	classical cloning
KK9 AMSH1(ΔMPN) +978 *Sal*I R	AAGGGTCGACTCACCGTAGAGACTCATCCG	63.4	classical cloning
KK10 AMSH1(MIT) +325 *Bam*HI F	AAGGGGATCCTATCCCAAGCTCAAACCTCGATATAAC	66.8	classical cloning
KK11 dehydr *Bam*HI F	AAGGGGATCCTTGCTACTCCATTTCTCTCCG	62.4	classical cloning
KK12 dehydr *Sal*I R	AAGGGTCGACTTAAGATGATGATGATGATGATGATGAT	65.4	classical cloning
KK13 CSN5B *Bam*HI F	AAGGGGATCCTTGGAGGGTTCGTCGTCG	67.8	classical cloning
KK14 CSN5B *Sal*I R	AAGGGTCGACTCAATATGTAATCATAGGGTCTGGATC	64.0	classical cloning
KK15 CSN5A *Bam*HI F	AAGGGGATCCTTGGAAGGTTCCTCGTCAGC	66.9	classical cloning
KK16 CSN5A *Sal*I R	AAGGGTCGACTCACGATGTAATCATGGGCTCTG	68.3	classical cloning
KK17 LBD13 *Bam*HI F	AAGGGGATCCTTGTCCCGAGAAAGGGAAGG	67.7	classical cloning
KK18 LBD13 *Sal*I R	AAGGGTCGACTTAATCAAAGTAATGAACATTATTATCACT	59.6	classical cloning
KK19 extra-large G-prot *Bam*HI F	AAGGGGATCCTTGAGGTCGCGAGGCG	68.3	classical cloning
KK20 extra-large G-prot *Sal*I R	AAGGGTCGACTCATGAAGCTAATGATCTTGGAACTCTCAT	69.2	classical cloning
KK21 methyltrans *Bam*HI F	AAGGGGATCCTTGGCGTTTGTGACAACTGC	67.6	classical cloning
KK22 methyltrans *Sal*I R	AAGGGTCGACTTAAACGGATAACTCAATTTGGGAGAC	66.7	classical cloning
KK23 EXO70E2 *Bam*HI F	AAGGGGATCCTTGGCAGAGTTTGATTCCAAG	64.4	classical cloning
KK24 EXO70E2 *Sal*I R	AAGGGTCGACTCATCTCTTACGAGAGCTGCG	65.0	classical cloning
KK25 CSN5A,B +733 F seq	TGGAACAAGTACTGGGTGAACACTC	67.4	sequencing primer

KK26 pMAL-p2 seq MBP F	GTCGTCAGACTGTCGATG	58.3	pMAL sequencing primer
KK27 pMAL-p2 seq lacZ R	TGTGCTGCAAGGCGATTA	64.7	pMAL sequencing primer
KK28 unkn attB1	AAAAAGCAGGCTTGGACC	62.0	Gateway
KK29 unkn attB2	AGAAAGCTGGGTTTAATGGAG	61.5	Gateway
KK30 extra attB1	AAAAAGCAGGCTTGAGGTC	61.5	Gateway
KK31 extra attB2	AGAAAGCTGGGTTCATGAAG	61.3	Gateway
KK32 extra seq +686	TCGCTACACAGTACAGTGATATG	59.9	sequencing primer
KK33 extra seq +1413	TCCTGATAATGCCAGTCTCCT	63.0	sequencing primer
KK34 32-methyltr attB1	AAAAAGCAGGCTTGGC	59.6	Gateway
KK35 methyltrans attB2	AGAAAGCTGGGTTTAAACG	59.0	Gateway
KK36 EXO70E2 attB1	AAAAAGCAGGCTATGGCA	61.2	Gateway
KK37 EXO70E2 attB2	AGAAAGCTGGGTTCATCTCTTA	61.2	Gateway
KK38 methyltrans *Xho*I R	AAGGCTCGAGTTAAACGGATAACTCAATTTGGGAGAC	66.7	classical cloning
KK39 EXO70E2 *Xho*I R	AAGGCTCGAGTCATCTCTTACGAGAGCTGCG	65.0	classical cloning
KK40 ALIX *Bam*HI F	AAGGGGATCCTTGGCTTCTTCTTCGCTCT	61.0	classical cloning
KK41 ALIX *Sal*I R	AAGGGTCGACTCATTGCCTGTAGTATCCTCC	61.0	classical cloning
KK42 unkn2 *Bam*HI F	AAGGGGATCCTTGGACCAAAGCAATTCTCT	60.4	classical cloning
KK43 unkn2 *Sal*I R	AAGGGTCGACTTAATGGAGAAGAACTTTCTGATACTTA	60.8	classical cloning
KK44 ATPase *Bam*HI F	AAGGGGATCCTTGGAGATTGCCGAGC	61.7	classical cloning
KK45 ATPase *Sal*I R	AAGGGTCGACTCATTCAGGTTGTTCAGACTTC	61.2	classical cloning
KK46 EML2 *Bam*HI F	AAGGGGATCCTTGGTAGGTCTACACATTAATATGGAA	61.6	classical cloning
KK47 EML2 *Xho*I R	AAGGCTCGAGTCACCCCAGCAGCAT	60.5	classical cloning
KK48 ALIX +768 F seq	ACTCTTCTATGGTGAAGCT	53.5	sequencing primer
KK49 ALIX +1416 F seq	AGAAGCAACTGAAGATTCTCA	58.8	sequencing primer
KK50 ALIX +2000 F seq	CTGCAATAATGAAGTATCGAGA	59.0	sequencing primer
KK51 EXO70E2 +746 F seq	CTCTCGAAATGGAAAGATTC	58.4	sequencing primer
KK52 unkn1 *Bam*HI F	AAGGGGATCCTTGGCCCAACGCTTT	60.5	classical cloning
KK53 unkn1 *Xho*I R	AAGGCTCGAGTTACTCAAGGCAGCATTG	58.0	classical cloning
KK54 ADT2 *Bam*HI F	AAGGGGATCCTTGGCAATGCACACTGTT	60.5	classical cloning
KK55 ADT2 *Sal*I R	AAGGGTCGACTTAGAGCATTGTAGTGTCCACT	58.5	classical cloning
KK56 unkn3 *Bam*HI F	AAGGGGATCCTTGAGTTCAATAGCAAGAGACC	59.1	classical cloning
KK57 unkn3 *Sal*I R	AAGGGTCGACTTAGAGATGCAGAGACGTGT	58.1	classical cloning
KK58 unkn1 +746 F seq	GTTGGGATGCTAAGCTAGT	56.6	sequencing primer
KK59 unkn1 +1400 F seq	CAGACCTAGAAAACATCGAA	57.8	sequencing primer

KK60 unkn1 +2000 F seq	ATCTCAGCCATACTTTGC	55.8	sequencing primer
KK61 VPS2.1 *Sal*I F	AAGGGTCGACTGATGAATTCAATCTTCGG	59.1	classical cloning
KK62 VPS2.1 *Not*I R	AAGGGCGGCCGCTCACATTTTTCTAAGGTTATCCA	59.5	classical cloning
KK63 SAIL 54 E10 F unkn2	ACCTCCAAACCATAGACCTCT	60.9	genotyping
KK64 SAIL 54 E10 R unkn2	GTTTGTTCTAACTCCATTGTTGT	59.1	genotyping
KK65 GABI 072F12 F Exo70E2	TAGCTGATCATACAACCACAAC	59.6	genotyping
KK66 GABI 072F12 R Exo70E2	TGAATTTGTATTAAGCATGTCAA	59.2	genotyping
KK67 SALK 005395 F methyltrans	GGATTTTTGTTGCAGTTGA	59.2	genotyping
KK68 SALK 005395 R methyltrans	TGATGATTACATACACTAAGCCACTA	60.8	genotyping
KK69 SAIL 54 E10 F unkn2	ATATACAGTCAAGAATCTCTAATTCATGAT	60.8	genotyping
KK70 SALK and GABI EML2 F	TATCATAAAATAGGCCCAAAATG	60.8	genotyping
KK71 SALK and GABI EML2 R	AATCGACGGATAGGATTGG	61.8	genotyping
KK72 SALK 063124 ALIX F	TGCTGTGCGGACAGA	60.4	genotyping
KK73 SALK 063124 ALIX R	TGAATAGAACAGCTGCTTTCTC	60.7	genotyping
KK74 SALK 116222 R EML2	CGTAGGTTTGTCATCACGG	62.1	genotyping
KK75 GABI 072F12 F EXO70E2	CGGTACGTTTACTCTGTTCG	60.3	genotyping
KK76 GABI 072F12 R EXO70E2	GATATCTGTTCATCATCTTCATGTG	61.6	genotyping
KK77 ALIX *Nde*I F	AAGGCATATGTTGGCTTCTTCTTCGCTC	61.4	classical cloning
KK78 ALIX *Bam*HI R	AAGGGGATCCTCATTGCCTGTAGTATCCTCC	61.0	classical cloning
KK79 EML2 *Nde*I F	AAGGCATATGTTGGTAGGTCTACACATTAATATGG	60.1	classical cloning
KK80 EML2 *Bam*HI R	AAGGGGATCCTCACCCCAGCAGCAT	60.5	classical cloning
KK81 GEF4 *Nde*I F	AAGGCATATGTTGGAGAGTTCTTCGAATTC	59.0	classical cloning
KK82 GEF4 *Bam*HI R	AAGGGGATCCCTAATCATCTCTGTTTCTCACTGT	58.6	classical cloning
KK83 hypoth *Eco*RI F	AAGGGAATTCTTGGACAACGGCCAT	60.2	classical cloning
KK84 hypoth *Bam*HI R	AAGGGGATCCTCATTTGTTAAACAAAAATCCTTTT	60.9	classical cloning
KK85 hypoth seq +653F	AACTCATTCACAAGGTCCAAG	61.1	sequencing primer
KK86 hypoth seq +1298F	CAACAGATTCAGAACACCATC	60.1	sequencing primer
KK87 BRO1-domain *Sal*I R	AAGGGTCGACTCACGCCTGAGTTCTAATTACATCA	61.1	classical cloning
KK88 BRO1 ΔPRD *Sal*I R	AAGGGTCGACTCAGCCGGAGCTTCTATGATC	60.5	classical cloning
KK89 ΔBRO1 *Bam*HI F	AAGGGGATCCGAGAGATTACAGCAAGCTAGC	58.1	classical cloning
KK90 BRO1 C-term *Bam*HI F	AAGGGGATCCCAAGAACAATTATTGATGCAAATT	61.0	classical cloning

KK91 BRO1 PRD *Bam*HI F	AAGGGGATCCCCATACCCATCTGTGCAT	59.9	classical cloning
KK92 BRO1 V-domain *Sal*I R	AAGGGTCGACTCAAACTTCAATGTTTTGG GAAATATC	61.2	classical cloning
KK93 BRO1 V-domain *Bam*HI F	AAGGGGATCCGACAGCAGTGCAAAGGC	61.4	classical cloning
KK94 ALIX GABI 837H11 F	GCTGGCGAAAGTGATGT	60.6	genotyping
KK95 ALIX GABI 837H11 R	ACCATCGTATAGAATGCAATACA	60.3	genotyping
KK96 ALIX GABI 780B02 F	GTTTTCATATTTTATCATGGTTTTTATC	60.1	genotyping
KK97 ALIX GABI 780B02 R	AGTAACTCATTGCCTGTAGTATCCT	60.4	genotyping
KK98 eGFP F	ATGGTGAGCAAGGGC	58.0	genotyping
KK99 eGFP R	TTACTTGTACAGCTCGTCCA	59.0	genotyping
KK100 BRO1 ΔPRD pET21 *Sal*I R	AAGGGTCGACGCCGGAGCTTCTATGATC	60.5	classical cloning
KK101 ARA7 attB1-N	AAAAAGCAGGCTTGGCTGCAGCTGGA	60.6	Gateway
KK102 ARA7 attB2-N	AGAAAGCTGGGTCTAAGCACAACAAGAT GAGCTC	61.1	Gateway
KK103 ARA7 attB1-C	AAAAAGCAGGCTAAATGGCTGCAGCTGG A	60.9	Gateway
KK104 ARA7 attB2-C	AGAAAGCTGGGTAGCACAACAAGATGAG CTCA	61.8	Gateway
KK105 ALIX +481 seq F	TTCGCTCACTTGAGGGATA	61.5	sequencing primer
KK106 amiR1 ALIX I	GATGAATAACGTGCTTTAGACAATCTCTC TTTTGTATTCC	72.7	overlap PCR
KK107 amiR1 ALIX II	GATTGTCTAAAGCACGTTATTCATCAAAG AGAATCAATGA	74.3	overlap PCR
KK108 amiR1 ALIX III	GATTATCTAAAGCACCTTATTCTTCACAG GTCGTGATATG	73.2	overlap PCR
KK109 amiR1 ALIX IV	GAAGAATAAGGTGCTTTAGATAATCTACA TATATATTCCT	65.6	overlap PCR
KK110 amiR2 ALIX I	GATGATATTCAATTTCACGACAGTCTCTC TTTTGTATTCC	73.5	overlap PCR
KK111 amiR2 ALIX II	GACTGTCGTGAAATTGAATATCATCAAAG AGAATCAATGA	75.2	overlap PCR
KK112 amiR2 ALIX III	GACTATCGTGAAATTCAATATCTTCACAG GTCGTGATATG	74.6	overlap PCR
KK113 amiR2 ALIX IV	GAAGATATTGAATTTCACGATAGTCTACA TATATATTCCT	66.7	overlap PCR
KK114 amiR3 ALIX I	GATTAACGTGCTTTACCCAACTTTCTCTCT TTTGTATTCC	74.1	overlap PCR
KK115 amiR3 ALIX II	GAAAGTTGGGTAAAGCACGTTAATCAAAG AGAATCAATGA	75.6	overlap PCR
KK116 amiR3 ALIX III	GAAAATTGGGTAAAGGACGTTATTCACAG GTCGTGATATG	76.8	overlap PCR
KK117 amiR3 ALIX IV	GAATAACGTCCTTTACCCAATTTTCTACAT ATATATTCCT	69,2	overlap PCR
KK118 p35S attB1	GGGGACAAGTTTGTACAAAAAAGCAGGC TTAATGCCTGCAGGTCCCC	65.6	multiside Gateway
KK119 p35S attB5r	GGGGACAACTTTTGTATACAAAGTTGTAC TTGTTGATAACTCTAGAGTCCCC	62.0	multiside Gateway
KK120 pUBQ10 attB1	GGGGACAAGTTTGTACAAAAAAGCAGGC TTATACGAATTCGAGCTCGG	60.6	multiside Gateway
KK121 pUBQ10 attB5r	GGGGACAACTTTTGTATACAAAGTTGTAG GATCCCGCACTCG	61.6	multiside Gateway

KK122 ALIX amiR attB5	GGGGACAACTTTGTATACAAAAGTTGTAG AATTCCTGCAGCCCC	62.4	multiside Gateway
KK123 ALIX amiR attB2	GGGGACCACTTTGTACAAGAAAGCTGGG TTGGATCCCCCCATGG	61.3	multiside Gateway
KK124 ALIX amiR attB1	GGGGACAAGTTTGTACAAAAAAGCAGGC TCAGAATTCCTGCAGCCCC	86.1	multiside Gateway
KK125 ΔBRO1 *Nde*I F	AAGGCATATGGAGAGATTACAGCAAGCTA GC	58.1	classical cloning
KK126 BRO1 *Bam*HI R	AAGGGGATCCTCACGCCTGAGTTCTAATT ACATC	63.5	classical cloning
KK127 ΔC-term *Bam*HI R	AAGGGGATCCTCAAACTTCAATGTTTTGG GAAATATC	65.7	classical cloning
KK128 ΔPRD *Bam*HI R	AAGGGGATCCTCAGCCGGAGCTTCTATG ATC	65.9	classical cloning
KK129 ΔBRO1 attB1	GGGGACAAGTTTGTACAAAAAAGCAGGC TCGGAGAGATTACAGCAAGCTAGC	58.1	Gateway
KK130 BRO1 attB2	GGGGACCACTTTGTACAAGAAAGCTGGG TGTCACGCCTGAGTTCTAATTACATC	63.5	Gateway
KK131 ΔC-term attB2	GGGGACCACTTTGTACAAGAAAGCTGGG TGTCAAACTTCAATGTTTTGGGAAATATC	65.7	Gateway
KK132 ΔPRD attB2	GGGGACCACTTTGTACAAGAAAGCTGGG TGTCAGCCGGAGCTTCTATGATC	65.9	Gateway
KK133 Bem1-1 *Bam*HI F	AAGGGGATCCATGAGAAATTCTCGTACAA CTCTTATC	61.1	classical cloning
KK134 Bem1-1 (GAD) XhoI R	AAGGCTCGAGTCAAACAGCCGAATCTGA	61.1	classical cloning
KK135 Bem1-1 (GBD) SalI R	AAGGGTCGACTCAAACAGCCGAATCTGA	61.1	classical cloning
KK136 Bem1-2 *Bam*HI F	AAGGGGATCCATGACAAGTTCTCGTACAA TTCG	62.3	classical cloning
KK137 Bem1-2 (GAD) *Xho*I R	AAGGCTCGAGTCACACCGAATCTGAAACT T	60.3	classical cloning
KK138 Bem1-2 (GBD) *Sal*I R	AAGGGTCGACTCACACCGAATCTGAAACT T	60.3	classical cloning
KK139 ALIX qRT 1674 L	ATCGACGGCCGATAGAGTC	64.6	qRT-PCR
KK140 ALIX qRT 1793 R	CAAGATTTTCCAGTTGCCTCA	64.4	qRT-PCR
KK141 ALIX +1444 *Nde*I F	AAGGCATATGAGTCAATTTGGGACTCGG	60.6	classical cloning
KK142 ALIX +1461 *Bam*HI R	AAGGGGATCCTCACCGAGTCCCAAATTG ACT	60.6	classical cloning
KK143 ALIX +1564 *Nde*I F	AAGGCATATGGAGCGATCAGTGAGAGAT	55.7	classical cloning
KK144 ALIX +1581 *Bam*HI R	AAGGGGATCCTCAATCTCTCACTGATCGC TC	55.7	classical cloning
KK145 AMSH3 +981 *Bam*HI R	AAGGGGATCCTCAGCTGCCCTCTTTTCCT TC	62.0	classical cloning
KK146 AMSH3 +523 *Nde*I F	AAGGCATATGCTATCTTTTGATTTCCTGC CT	59.3	classical cloning
KK147 AMSH3 +537 *Bam*HI R	AAGGGGATCCTCAGAAATCAAAAGATAGC TTCTGGAA	61.8	classical cloning
KK148 AMSH3 +766 *Nde*I F	AAGGCATATGGATGATGGTCGATGGCAG	63.4	classical cloning
KK149 AMSH3 +777 *Bam*HI R	AAGGGGATCCTCATCGACCATCATCTAAG GAGAG	61.3	classical cloning
KK150 FIP1 *Nde*I F	AAGGCATATGTTGAGTGGGCAAGAGAAT C	60.9	classical cloning
KK151 FIP1 *Bam*HI R	AAGGGGATCCTCACGGACCATGTGACTG	62.6	classical cloning

KK152 XBAT35 *Nde*I F	AAGGCATATGTTGGGACAACAGCAATCA	61.9	classical cloning
KK153 XBAT35 *Bam*HI R	AAGGGGATCCTCAGACACGGTACAGCTTAATAAC	61.4	classical cloning
KK154 XBAT34 *Nde*I F	AAGGCATATGTTGGGGCAACAACAATC	61.1	classical cloning
KK155 XBAT34 *Bam*HI R	AAGGGGATCCTCAAACATGATATAGCTTAATGACCT	61.0	classical cloning
KK156 CaLB *Nde*I F	AAGGCATATGTTGTCGATGATGGCG	59.3	classical cloning
KK157 CaLB *Bam*HI R	AAGGGGATCCCTAGTATGGAGGAGGTGGGTAT	60.2	classical cloning
KK158 AMSH3 +322 *Nde*I F	AAGGCATATGGATGAATCCCGTCAGGAT	60.4	classical cloning
KK159 Ub *Nde*I F	AAGGCATATGATGCAGATCTTTGTTAAGACTCTC	59.9	classical cloning
KK160 Ub *Bam*HI R	AAGGGGATCCTCAACCACCACGGAGCCT	60.9	classical cloning
KK161 ALIX-ΔE1 *Nde*I F	AAGGCATATGGATAGAGTCTGCTGTCCCAAC	60.8	classical cloning
KK162 Y2H ALIX-dE4 *Bam*HI R	AAGGGGATCCTCATTCTCTTCATCTCTTTGAGCAT	60.1	classical cloning
KK163 ALIX-E attB1	GGGGACAAGTTTGTACAAAAAAGCAGGCTTCGAGCGATCAGTGAGAGAT	63.3	Gateway
KK164 ALIX-E attB2	GGGGACCACTTTGTACAAGAAAGCTGGGTCTCAGATATTTCCCAAAACATTGAAGTT	66.0	incorrect
KK165 ALIX-ΔE2 overlap F	GACGGCCGAGGCAA	64.2	overlap PCR
KK166 ALIX-ΔE2 overlap R	TTGCCTCGGCCGTC	64.2	overlap PCR
KK167 ALIX-ΔE3 overlap F	TGAAGCAGAGTCTAGGATGACATACT	63.5	overlap PCR
KK168 ALIX-ΔE3 overlap R	AGTATGTCATCCTAGACTCTGCTTCA	63.5	overlap PCR
KK169 ALIX attB1	GGGGACAAGTTTGTACAAAAAAGCAGGCTTGATGGCTTCTTCTTCGCTCT	61.2	Gateway
KK170 ALIX-ΔE1 overlap F	TGATGTTAAGATTGATAGAGTCTGCT	61.4	overlap PCR
KK171 ALIX-ΔE1 overlap R	AGCAGACTCTATCAATCTTAACATCA	61.4	overlap PCR
KK172 ALIX-ΔE4 overlap F	AGAGATGAAGAGAACAAGAACAATTATT	61.8	overlap PCR
KK173 ALIX-ΔE4 overlap R	AATAATTGTTCTTGTTCTCTTCATCTCT	61.8	overlap PCR
KK174 ALIX-ΔE1 overlap F	TGATGTTAAGATTATAGAGTCTGCTGT	60.6	overlap PCR
KK175 ALIX-ΔE1 overlap R	ACAGCAGACTCTATAATCTTAACATCA	60.6	overlap PCR
KK176 ALIX-ΔE2 overlap F	ACGGCCGCTGAGGCA	69.1	overlap PCR
KK177 ALIX-ΔE2 overlap R	TGCCTCAGCGGCCGT	69.1	overlap PCR
KK178 ALIX-ΔE3 overlap F	TTGAAGCAGAGTGATGACATACTG	63.5	overlap PCR
KK179 ALIX-ΔE3 overlap R	CAGTATGTCATCACTCTGCTTCAA	63.5	overlap PCR
KK180 ALIX-ΔE4 overlap F	AGATGAAGAGAAAGCAAGAACAATTATT	63.5	overlap PCR
KK181 ALIX-ΔE4 overlap R	AATAATTGTTCTTGCTTTCTCTTCATCT	63.5	overlap PCR

KK182 ALIX-ΔE1 F	AAGGCATATGATAGAGTCTGCTGTCCCAACTCTT	63.6	overlap PCR
KK183 ALIX-ΔE4 R	AAGGGGATCCTCAATGCTCAAAGAGATGAAGAGAAAG	62.2	incorrect
KK184 ΔBRO1 ATG attB1	GGGGACAAGTTTGTACAAAAAAGCAGGCTGGATGGCGGAGAGATTACAGCAAGCTAGC	64.5	Gateway
KK185 ALIX-ΔE4 R	AAGGGGATCCTCACTTTCTCTTCATCTCTTTGAGCAT	62.2	overlap PCR
KK186 ALIXpro genot F	GAAGAAAATTAGAAAAATCGGAAG	60.4	genotyping
KK187 ALIX genot +689 R	CAATGGTATTTTCAAAGACACAT	59.8	genotyping
KK188 ALIX-ΔE2 middle F	CGACGGCCGCTGAGGCAA	66.6	overlap PCR
KK189 ALIX-ΔE2 middle R	TTGCCTCAGCGGCCGTCG	66.6	overlap PCR
KK190 ALIX-ΔE2 long F	CTTGATCGACGGCCGCTGAGGCAACTGGAA	71.6	overlap PCR
KK191 ALIX-ΔE2 long R	TTCCAGTTGCCTCAGCGGCCGTCGATCAAG	71.6	overlap PCR
KK192 ALIX-E4 *Nde*I F	AAGGCATATGGATGACATACTGCCAAAGCTG	63.7	classical cloning
KK193 ALIX-E3+4 *Nde*I F	AAGGCATATGCTGAGGCAACTGGAAAATC	62.9	classical cloning
KK194 ALIX-E4 attB1	GGGGACAAGTTTGTACAAAAAAGCAGGCTTGGATGACATACTGCCAAAGCTG	67.7	Gateway
KK195 ALIX-E3+4 attB1	GGGGACAAGTTTGTACAAAAAAGCAGGCTTGCTGAGGCAACTGGAAAATC	66.1	Gateway
KK196 pMAL ALIX-E4 *Bam*HI F	AAGGGGATCCGATGACATACTGCCAAAGCTG	65.2	classical cloning
KK197 pMAL ALIX-E3+4 *Bam*HI F	AAGGGGATCCCTGAGGCAACTGGAAAATC	62.5	classical cloning
KK198 pET21 ALIX-E4 *Sal*I R	AAGGGTCGACAACTTCAATGTTTTGGGAAATATC	60.4	classical cloning
KK199 pGEX AMSH3-ΔMIT *Bam*HI F	AAGGGGATCCCGTCAGGATGGAAGTGATCT	65.3	classical cloning
KK200 pGEX AMSH3-ΔMPN *Sal*I R	AAGGGTCGACTCAGCTGCCCTCTTTTCCTTC	69.4	classical cloning
KK201 pGEX AMSH3 +517 *Bam*HI F	AAGGGGATCCCAGAAGCTATCTTTTGATTTCCTG	62.8	classical cloning
KK202 pGEX AMSH3 +517 *Sal*I R	AAGGGTCGACTCACAGGAAATCAAAAGATAGCTTCTG	66.3	classical cloning
KK203 pGEX AMSH3 +754 *Bam*HI F	AAGGGGATCCGTGCTCTCCTTAGATGATGGT	60.3	classical cloning
KK204 pGEX AMSH3 +754 *Sal*I R	AAGGGTCGACTCAACCATCATCTAAGGAGAGCAC	65.7	classical cloning
KK205 pET21 ALIX-E4 *Bam*HI F	AAGGGGATCCATGGATGACATACTGCCAAAGCTG	62.7	classical cloning
KK206 pET21 ALIX-E3+4 *Bam*HI F	AAGGGGATCCATGCTGAGGCAACTGGAAAATC	60.4	classical cloning
KK207 pMAL ALIX-E4 *Sal*I R	AAGGGTCGACTCAAACTTCAATGTTTTGGGAAATATC	65.7	classical cloning
KK208 ALIX-E3+4 attB2	GGGGACCACTTTGTACAAGAAAGCTGGGTTCAAACTTCAATGTTTTGGGAAATATC	65.7	Gateway
KK209 ALIX-E3+4 *Sal*I R	AAGGGTCGACCAACTTCAATGTTTTGGGAAATATC	63.5	classical cloning

KK210 *Hs*ALIX pET21 *Bam*HI F	AAGGGGATCCGCTCAGATGAGAGAAGCCAC	62.3	classical cloning
KK211 *Hs*ALIX pET21 *Sal*I R	AAGGGTCGACAGGTGTAGGAATTGAAGGAGC	61.5	classical cloning
KK212 *ALIX* qRT 5'UTR F	TAGAAAAATCGGAAGAGCGATC	63.6	qRT-PCR
KK213 *ALIX* qRT R for 5'UTR	AGCTGGAGAAGGATCGGA	63.1	qRT-PCR
KK214 *ALIX* qRT F for 3'UTR	ATACCATACTCCTCATGGCCA	63.5	qRT-PCR
KK215 *ALIX* qRT 3'UTR R	GGAAACACAACAATAGATATATAACACC	60.9	qRT-PCR
KK216 *35Spro* qRT F	GGAAGTTCATTTCATTTGGAGAGA	64.5	qRT-PCR
KK217 sGFP qRT R	CAAGGGCGAGGAGCTGTT	66.0	qRT-PCR
KK218 AMSH3 attB1	GGGGACAAGTTTGTACAAAAAAGCAGGCTTGAAGATTGATCTGAACAAGG	59.8	Gateway
KK219 AMSH3 attB2	GGGGACCACTTTGTACAAGAAAGCTGGGTCGCGGAGATCGAGGA	63.1	Gateway
KK220 AMSH3-ΔA1 TaKaRa F	GTCCTCCAAACCAAGCAAGACATTCATTTCTAGG	75.3	TaKaRa mutagenesis
KK221 AMSH3-ΔA1 TaKaRa R	CCTAGAAATGAATGTCTTGCTTGGTTTGGAGGAC	75.3	TaKaRa mutagenesis
KK222 AMSH3-ΔA2 TaKaRa F	CCTCCAAACCAAGCATCATTTCTAGGTCCG	76.1	TaKaRa mutagenesis
KK223 AMSH3-ΔA2 TaKaRa R	CGGACCTAGAAATGATGCTTGGTTTGGAGG	76.1	TaKaRa mutagenesis
KK224 AMSH3-ΔB TaKaRa F	TCAAGACATTCATTTAATGGTCTTAAAAGG	66.5	TaKaRa mutagenesis
KK225 AMSH3-ΔB TaKaRa R	CCTTTTAAGACCATTAAATGAATGTCTTGA	66.5	TaKaRa mutagenesis
KK226 AMSH3-ΔC TaKaRa F	TTGCACCCAAGTCAGAGCCGAGTAATACAGATTG	77.2	TaKaRa mutagenesis
KK227 AMSH3-ΔC TaKaRa R	CAATCTGTATTACTCGGCTCTGACTTGGGTGCAA	77.2	TaKaRa mutagenesis
KK228 AMSH3-ΔD1 TaKaRa F	ATAAAGGTTCAATATACAGATTGGGGTTCT	66.1	TaKaRa mutagenesis
KK229 AMSH3-ΔD1 TaKaRa R	AGAACCCCAATCTGTATATTGAACCTTTAT	66.1	TaKaRa mutagenesis
KK230 AMSH3-ΔD2 TaKaRa F	GAGATAAAGGTTCAATATGGTTCTGCGGACAATTCA	75.5	TaKaRa mutagenesis
KK231 AMSH3-ΔD2 TaKaRa R	ATTGTCCGCAGAACCATATTGAACCTTTAT	75.5	TaKaRa mutagenesis
KK232 AMSH3-ΔA2 overlap F	CAAACCAAGCATCATTTCTAGG	62.7	overlap PCR
KK233 AMSH3-ΔA2 overlap R	CCTAGAAATGATGCTTGGTTTG	62.7	overlap PCR
KK234 AMSH3-ΔC overlap F	CCAAGTCAGAGCCGAGTAATACA	64.5	overlap PCR
KK235 AMSH3-ΔC overlap R	TGTATTACTCGGCTCTGACTTGG	64.5	overlap PCR
KK236 AMSH3-ΔD2 overlap F	AGGTTCAATATGGTTCTGCGGA	66.8	overlap PCR
KK237 AMSH3-ΔD2 overlap R	TCCGCAGAACCATATTGAACCT	66.8	overlap PCR

Appendix Table 8. Other primers used for cloning and sequencing.

Primer	Sequence 5’ – 3’	Reference
EI9, AMSH1 BamHI F	AAGGGGATCCATGGGGTCGTCTTTTGAGAC	E. Isono; (Katsiarimpa et al., 2013)
EI10, AMSH1 SalI R	AAGGGTCGACCTATCTGAGATCAATGACAT	E. Isono; (Katsiarimpa et al., 2013)
TF1, ALIX(FL) attB1	GGGGACAAGTTTGTACAAAAAAGCAGGCTTG GCTTCTTCTTCGC	T. Fischer; (Kalinowska et al., 2015)
TF2, ALIX(FL) attB2	GGGGACCACTTTGTACAAGAAAGCTGGGTTC ATTGCCTGTAGTA	T. Fischer; (Kalinowska et al., 2015)
pDEST-BD_pC97 F	CGCGTTTGGAATCACTACAGGG	(Dreze et al., 2010)
pDEST-AD-CYH2 F	GGCTTCAGTGGAGACTGATATGCCTC	(Dreze et al., 2010)
pDEST Term R	GGAGACTTGACCAAACCTCTGGCG	(Dreze et al., 2010)

Appendix Table 9. Primers used for genotyping.

Genotyping	Name	Sequence 5' – 3'
ALIX WT (first exon)	KK72	TGCTGTGCGGACAGA
	KK73	TGAATAGAACAGCTGCTTTCTC
alix-4 (SALK 063124)	KK72	TGCTGTGCGGACAGA
	LBb1.3	ATTTTGCCGATTTCGGAAC
ALIX WT (fifth exon)	KK94	GCTGGCGAAAGTGATGT
	KK95	ACCATCGTATAGAATGCAATACA
alix-2 (GABI-Kat 83711)	KK94	GCTGGCGAAAGTGATGT
	o8409	ATATTGACCATCATACTCATTGC
ALIX WT (seventh exon)	KK96	GTTTTCATATTTTATCATGGTTTTTATC
	KK97	AGTAACTCATTGCCTGTAGTATCCT
alix-3 (GABI-Kat 780B02)	KK96	GTTTTCATATTTTATCATGGTTTTTATC
	o8409	ATATTGACCATCATACTCATTGC
AMSH1 WT (promoter)	a1 F	AACATTGAGGATTGGATGGGATTTTC
	a1 R	CACGGCAGAAGACCA
amsh1-1 (CSHL_ET8678)	DS3.1	ACCCGACCGGATCGTATCGGT
	a1 R	CACGGCAGAAGACCA
AMSH3 WT (sixth exon)	EI40	AAGGCAATGGGTTGCACCCAAGTCAGAGAT
	EI41	CTGCTTTGGGATTATGAGAGTAGTGATATG
amsh3-1 (WiscDsLox412D09)	p745	AACGTCCGGAATGTGTTATTAAGTTGTC
	EI41	CTGCTTTGGGATTATGAGAGTAGTGATATG
FYVE1 WT (first exon)	EI511	GCGACATCACTAAACCC
	EI512	AACCCACCAACATAAGAAC
fyve1-1 (RIKEN pst18264)	Ds5a	TCGTTCCGTTTTCGTTTTTTAC
	EI512	AACCCACCAACATAAGAAC

Appendix Table 10. Genotypes of bacteria, yeast and plants used in this study.

Strain	Genotype
Escherichia coli	
DH5α	F⁻ Φ80*lac*ZΔM15 Δ(*lac*ZYA-*arg*F) U169 *rec*A1 *end*A1 *hsd*R17 (rK⁻, mK⁺) *pho*A *sup*E44 λ⁻ *thi*-1*gyr*A96 *rel*A1
TOP10	F⁻ *mcr*A Δ(*mrr-hsd*RMS-*mcr*BC) Φ80*lac*ZΔM15 Δ*lac*X74 *rec*A1 *ara*D139 Δ(*ara leu*) 7697 *gal*U *gal*K*rps*L (Str^R) *end*A1 *nup*G
Rosetta	F⁻ *ompT hsdS$_B$*(r$_B$⁻ m$_B$⁻) *gal dcm* pRARE^2 (Cam^R)
Rosetta-gami 2	*Δ(ara–leu)7697 ΔlacX74 ΔphoA PvuII phoR araD139 ahpC galE galK rpsL* F'[*lac*$^+$ *lacI^q pro*] *gor522::*Tn*10 trxB* pRARE2^3 (Cam^R, Str^R, Tet^R)^4
Resetta-gami B	F⁻ *ompT hsdS$_B$*(r$_B$⁻ m$_B$⁻) *gal dcm lacY1 aphC gor522::*Tn*10 trxB* pRARE^2 (Cam^R, Kan^R, Tet^R)
Agrobacterium tumefaciens	
GV3101::pMP90	chromosomal background: C58 (Rif^R), plasmid: pMP90(pTiC58ΔT-DNA) (Gent^R)
GV3101::pMP90RK	chromosomal background: C58 (Rif^R), plasmid: pMP90RK(pTiC58ΔT-DNA) (Gent^R, Kan^R)
GV3101::pMP90 pSOUP	chromosomal background: C58 (Rif^R), plasmids: pMP90(pTiC58ΔT-DNA) (Gent^R), pSOUP (Tet^R)
Arabidopsis thaliana	
Col-0 (Colombia-0)	
L*er* (Landsberg *erecta*)	
No-0 (Nossen)	

Appendix Table 11. Plant lines generated and established during this study.

Line	Crossed/ transformed with	Generation	Comment/ reference
Transgenic lines			
AMSH3pro:AMSH3-YFP (pFA15)	*UBQ10pro:mCherry-ARA7* (Wave 2R)	F2, F3	Wave markers: (Geldner et al., 2009)
	UBQ10pro:mCherry-RabC1 (Wave 3R)	F2	
	UBQ10pro:mCherry-RabG3c (Wave 11R)	F2, F3	
	UBQ10pro:mCherry-VTI12 (Wave 13R)	F2, F3	
	UBQ10pro:mCherry-GOT1 (Wave 18R)	F2	
	UBQ10pro:mCherry-RabD1 (Wave 25R)	F2	
	UBQ10pro:mCherry-RabE1d (Wave 27R)	F2	
	UBQ10pro:mCherry-RabA1e (Wave 34R)	F2	
	35Spro:CLC-mKO	F2, F3	
	CLCpro:CLC-mKO	F2, F3	
	SYP43pro:mRFP-SYP43	F2, F3	
	SYP61pro:mRFP-SYP61	F2	
	ARA6pro:ARA6-mRFP	F2	
	ARA7pro:mRFP-ARA7	F2, F3	
	UBQ10pro:2xCherry-1xPH(FAPP1) (P5R)	F2	PIP markers: (Simon et al., 2014)
	UBQ10pro:2xCherry-2xFYVE(HRS) (P18R)	F1	P18R does not express
	35Spro:AMSH1-TagRFP (pKK6)	T0	
35Spro:AMSH3-TagRFP (pKK7)	(Col-0)	T1	expression detectable on immunoblot, not under the confocal microscope
35Spro:AMSH3-GFP (pEI74)	*35Spro:CLC-mKO*	F2	
35Spro:AMSH3(Y213A)-sGFP (pKK85)	*amsh3-1*	T0	
	ARA7pro:mRFP-ARA7	T0	
	CLCpro:CLC-mKO	T0	
	SYP43pro:mRFP-SYP43	T0	
35Spro:AMSH3(H190A)-sGFP (pKK86)	*amsh3-1*	T0	
	ARA7pro:mRFP-ARA7	T0	
	CLCpro:CLC-mKO	T0	
	SYP43pro:mRFP-SYP43	T0	
35Spro:AMSH3(Y213A,L193D,H190A)-sGFP (pKK94)	*amsh3-1*	T2	does not complement *amsh3-1* lethal phenotype
	ARA7pro:mRFP-ARA7	T0	
	CLCpro:CLC-mKO	T0	
	SYP43pro:mRFP-SYP43	T0	
ALIXpro:GFP-ALIX	*35Spro:CLC-mKO*	F2, F3	

(gift from L. Cuyas and V. Rubio)	*CLCpro:CLC-mKO*	F2, F3	
	SYP43pro:mRFP-SYP43	F2, F3	
	ARA6pro:ARA6-mRFP	F2	
	ARA7pro:mRFP-ARA7	F2, F3	
	UBQ10pro:2xCherry-1xPH(FAPP1) (P5R)	F2	
	UBQ10pro:2xCherry-2xFYVE(HRS) (P18R)	F2	
	AMSH3pro:AMSH3-TagRFP (pMN73)	T2	both constructs are genetically linked
35Spro:TagRFP-Gly-ALIX (pKK47)	(Col-0)	T0	
35Spro:3xHA-ALIX(FL) (pKK42)	(Col-0)	T0	
35Spro:FLAG-ALIX(FL) (pKK46)	(Col-0)	T0	
35Spro:ALIX(FL)-STOP (pKK72)	(Col-0)	T2	causes downregulation of ALIX protein levels; (Kalinowska et al., 2015)
35Spro:ALIX(BRO1)-STOP (pKK73)	(Col-0)	T1	causes downregulation of ALIX
35Spro:amiR-ALIX	(Col-0)	T0	
UBQ10pro:amiR-ALIX	(Col-0)	T1	no downregulation of *ALIX* observed in T1 lines
XVE-35Spro:amiR-ALIX	(Col-0)	T2	the effect on *ALIX* levels is unclear
UBQ10pro:YFP-ARA7 (Wave 2Y)	*35Spro:CLC-mKO*	F2	
UBQ10pro:CFP-ARA7 (pKK35)	(Col-0)	T2	
	CLCpro:CLC-mKO	F2	
	AMSH3pro:AMSH3-YFP (pFA15), *CLCpro:CLC-mKO*	F2, F3	
UBQ10pro:2xCyPET-2xFYVE(HRS) (P18C)	*AMSH3pro:AMSH3-YFP* (pFA15), *CLCpro:CLC-mKO*	F1	P18C does not express
35Spro:GFP-ATG8e (gift from D. Bassham)	*35Spro:AMSH3-TagRFP* (pKK7)	F1	AMSH3-TagRFP does not express
	AMSH3pro:AMSH3-CFP (pAK80) (A. Katsiarimpa)	F1	AMSH3-CFP does not express
	UBQ10pro:mCherry-ARA7 (Wave 2R)	F1	

T-DNA insertion lines

amsh3-1 (Col-0) (WiscDsLox412D09), Collection from University of Wisconsin-Madison, obtained through ABRC	*alix-2*	F2, F3	
	alix-4	F2, F3	
	fyve1-1	F2	
	mRFP-VAM3	F2	
	ALIXpro:GFP-ALIX, ARA6pro:ARA6-mRFP	F2	
	UBQ10pro:GFP-ATG8	F2	gift from M. Otegui
alix-2 (Col-0) (GABI-Kat 83711), Collection from Bielefeld University, obtained through NASC	*alix-4*	F1	transheterozygous
	fyve1-1	F2	
	ALIXpro:GFP-ALIX	F2, F3	fully complements the mutant phenotype

	AMSH3pro:AMSH3-YFP (pFA15), *ARA7pro:mRFP-ARA7*	F3	*ALIX(WT)* and *mRFP-ARA7* are genetically linked
	AMSH3pro:AMSH3-YFP (pFA15), *UBQ10pro:mRFP-ARA7* (Wave 2R)	F1	
	UBQ10pro:YFP-VPS2.1 (pAK28), *35Spro:TagRFP-AMSH3* (pEI135)	F2	
	UBQ10pro:GFP-ATG8	F2	gift from M. Otegui
	mRFP-VAMP727	F2	
	mRFP-VAMP713	F2	
	UBQ10pro:PIN1-GFP	F2	
	UBQ10pro:PIN2-GFP	F2	
alix-4 (Col-0) (SALK 063124), Collection from Salk Institute, obtained through NASC	*fyve1-1*	F2	
	UBQ10pro:PIN1-GFP	F2	
fyve1-1(No-0) (RIKEN pst18264), Collection from RIKEN Institute	*AMSH3pro:AMSH3-YFP* (pFA15)	F2	
amsh1-1 (L*er*) (CSHL_ET8678), Collection from Cold Spring Harbor Laboratory	4x *alix-1* (gift from V. Rubio)	F4	(Cardona-Lopez et al., 2015)
	5x Col-0	F5	

Appendix Table 12. K3 Medium used for overnight protoplast culture.

Group of elements	Concentration
Sugars and alcohols	0.4 M sucrose 1.7 mM D-xylose 555.1 µM myo-inositol
EDTA-Fe(II)	127.6 µM EDTA 52.3 µM Fe(II)SO_4
Ca-Phosphate	217.1 µM $CaHPO_4*2H_2O$
Macroelements	10.8 mM $NaH_2PO_4*H_2O$ 6.1 mM $CaCl_2*2H_2O$ 24.7 mM KNO_3 3.1 mM NH_4NO_3 1 mM $(NH_4)_2SO_4$ 2.1 mM $MgSO_4*7H_2O$
Microelements	4.5 µM KI 48.5 µM H_3BO_3 35.5 µM $MnSO_4*7H_2O$ 1.7 µM $ZnSO_4*7H_2O$ 1.2 µM $Na_2MoO_4*2H_2O$ 0.1 µM $CuSO_4*5H_2O$ 0.11 µM $CoCl_2*6H_2O$
Vitamins	8.1 µM nicotinic acid 4.9 µM pyridoxine-HCl 29.7 µM thiamine-HCl

Curriculum vitae

Kamila Kalinowska-Brandt

Date and place of birth: 1987, Bialystok (Poland)
Citizenship: Polish
Marital status: Married, no children

Education

09/2012 –
PhD Studies in Plant Molecular Biology
Technische Universität München, Freising
Chair of Plant Systems Biology

10/2009 – 06/2011
Training in Modern Methods in Biology and Biotechnology
Nicolaus Copernicus University in Torun (Poland)
EU Human Capital Operational Programme

10/2009 – 07/2011
Master of Science ("magister") in Biotechnology
Nicolaus Copernicus University in Torun (Poland)
Chair of Plant Physiology and Biotechnology
Thesis: Identification of *FLOWERING LOCUS C (FLC)* homolog in *Ipomoea nil*

10/2006 – 07/2009
Bachelor of Science ("licencjat") in Biotechnology
Nicolaus Copernicus University in Torun (Poland)
Chair of Plant Physiology and Biotechnology
Thesis: Molecular mechanisms of vernalization

Professional Experience

10/2011 – 06/2012
Ludwig-Maximilians-Universität, Munich (Germany)
Chair of Plant Biochemistry and Physiology
Research Assistant
Project: Regulation of import of proteins into chloroplasts in *Pisum sativum*

06/2010 – 08/2010
Max Planck Institute for Plant Breeding Research, Cologne (Germany)
Chair of Plant Developmental Biology
ERASMUS-Internship
Project: Identification of interaction partners of LIKE HETEROCHROMATIN PROTEIN 1 (LHP1)

07/2009 – 09/2009
Plant Breeding and Acclimatization Institute (IHAR), Radzikow (Poland)
Department of Genetic Engineering
Voluntary Internship
Project: Optimization of transformation and *in vitro* regeneration of wheat and triticale

10/2008
Sanitary-Epidemiological Station, Torun (Poland)
Departments of Food Safety Control, Drinking-Water Quality Control and Laboratory Diagnostics
Voluntary Internship
Project: Identification of bacterial contamination in food, water and stool samples

Other Activities

03/2013 – 06/2016	Co-supervision of three students during internships
04/2015 –	Laboratory first aider
01/2014 – 07/2015	Treasurer of „SFB924 Student Initiative“
10/2009 – 09/2010	Leader of the Science Club of Biotechnology Students at the Nicolaus Copernicus University, Torun (Poland)

Personal Training

Laboratory Methods

2014 EMBO Practical Course in methods for the analysis of protein interactions**:** MST, SPR, ITC, FRET-FLIM, FCS

Software

2015 Imaris 8
2014 Fiji (Image J)
2013 Adobe Illustrator

Soft Skills

2015 Scientific Writing in English
2015 Project Planning
2013 Good Scientific Practice
2012 Presenting Professionally

Laboratory Methods

Laser scanning confocal microscopy
Protein biochemistry
Microbiology, cell culture
Molecular biology, genetics
Plant breeding and biotechnology

Languages

Polish:	mother tongue
English:	advanced (C1)
German:	advanced (B2/C1)
French:	basic (A1)

Personal Interests

Drawing, painting, longsword fighting

Publications

- **Kamila Kalinowska**, Marie-Kristin Nagel and Erika Isono (2016) Measuring the enzyme activity of Arabidopsis deubiquitylating enzymes. ***Methods Mol Biol*** 1450:35-44

- **Kamila Kalinowska**, Marie-Kristin Nagel, Kaija Goodman, Laura Cuyas, Franziska Anzenberger, Angela Alkofer, Javier Paz-Ares, Pascal Braun, Vicente Rubio, Marisa S. Otegui and Erika Isono (2015) Arabidopsis ALIX is required for the endosomal localization of the deubiquitinating enzyme AMSH3. ***Proc Natl Acad Sci U S A***, 112(40):E5543-51

- Cornelia Kolb, Marie-Kristin Nagel, **Kamila Kalinowska**, Jörg Hagmann, Mie Ichikawa, Franziska Anzenberger, Angela Alkofer, Masa H. Sato, Pascal Braun and Erika Isono (2015) FYVE1 is essential for vacuole biogenesis and intracellular trafficking in Arabidopsis. ***Plant Physiol*** 167(4):1361-73

- **Kamila Kalinowska** and Erika Isono (2014) Analysis of global ubiquitylation and ubiquitin-binding domains involved in endosomal trafficking. ***Methods Mol Biol*** 1209:189-202

- Anthi Katsiarimpa*, Alfonso Muñoz, **Kamila Kalinowska**, Tomohiro Uemura, Enrique Rojo and Erika Isono* (2014) The ESCRT-III interacting deubiquitinating enzyme AMSH3 is essential for degradation of ubiquitinated membrane proteins in *Arabidopsis thaliana.* (*equal contribution) ***Plant Cell Physiol*** 55(4):727-36

- Anthi Katsiarimpa*, **Kamila Kalinowska***, Franziska Anzenberger, Corina Weis, Maya Ostertag, Claus Schwechheimer, Frédéric Brunner, Ralph Hückelhoven and Erika Isono (2013) AMSH1 and the ESCRT-III subunit VPS2.1 are required for autophagic degradation in *Arabidopsis thaliana.* (*equal contribution) ***Plant Cell****,* 25(6):2236-52

Conference Presentations and Posters

08/2016	**Poster,** European Endomembrane Meeting (ENPER), Bordeaux (France)
03/2016	**Poster**, German Society for Cell Biology (DGZ)-Annual Meeting, Munich
05/2015	**Talk**, SPP1365-Ubiquitin Family Network- Annual Meeting, Berlin
11/2014	**Poster**, EMBO Practical Course, Porto (Portugal)
11/2014	**Talk**, ZOMES VIII: Ubiquitin Society Meeting, Xiamen (China)
09/2014	**Talk**, European Endomembrane Meeting (ENPER), Lecce (Italy)
03/2014	**Poster**, German Society for Cell Biology (DGZ)-Annual Meeting, Regensburg
08/2013	**Poster**, European Endomembrane Meeting (ENPER), Ghent (Belgium)
05/2013	**Talk**, SPP1365-Ubiquitin Family Network- Annual Meeting, Berlin
05/2011	**Poster**, Symposium of Student Science Clubs, Torun (Poland)
05/2010	**Talk**, Symposium of Student Science Clubs, Torun (Poland)
10/2009	**Poster**, Society of Biotechnology Students-Annual Meeting, Poznan (Poland)

Arabidopsis ALIX is required for the endosomal localization of the deubiquitinating enzyme AMSH3

Kamila Kalinowska[a], Marie-Kristin Nagel[a], Kaija Goodman[b], Laura Cuyas[c], Franziska Anzenberger[a], Angela Alkofer[a], Javier Paz-Ares[c], Pascal Braun[a], Vicente Rubio[c], Marisa S. Otegui[b], and Erika Isono[a,1]

[a]Plant Systems Biology, Technische Universität München, 85354 Freising, Germany; [b]Departments of Botany and Genetics, Laboratory of Cell and Molecular Biology, University of Wisconsin-Madison, Madison, WI 53706; and [c]Centro Nacional de Biotecnología-CSIC, 28049 Madrid, Spain

Edited by Natasha V. Raikhel, Center for Plant Cell Biology, Riverside, CA, and approved August 11, 2015 (received for review June 19, 2015)

Ubiquitination is a signal for various cellular processes, including for endocytic degradation of plasma membrane cargos. Ubiquitinating as well as deubiquitinating enzymes (DUBs) can regulate these processes by modifying the ubiquitination status of target protein. Although accumulating evidence points to the important regulatory role of DUBs, the molecular basis of their regulation is still not well understood. Associated molecule with the SH3 domain of signal transduction adaptor molecule (STAM) (AMSH) is a conserved metalloprotease DUB in eukaryotes. AMSH proteins interact with components of the endosomal sorting complex required for transport (ESCRT) and are implicated in intracellular trafficking. To investigate how the function of AMSH is regulated at the cellular level, we carried out an interaction screen for the *Arabidopsis* AMSH proteins and identified the *Arabidopsis* homolog of apoptosis-linked gene-2 interacting protein X (ALIX) as a protein interacting with AMSH3 in vitro and in vivo. Analysis of *alix* knockout mutants in *Arabidopsis* showed that ALIX is essential for plant growth and development and that ALIX is important for the biogenesis of the vacuole and multivesicular bodies (MVBs). Cell biological analysis revealed that ALIX and AMSH3 colocalize on late endosomes. Although ALIX did not stimulate AMSH3 activity in vitro, in the absence of ALIX, AMSH3 localization on endosomes was abolished. Taken together, our data indicate that ALIX could function as an important regulator for AMSH3 function at the late endosomes.

Arabidopsis | intracellular trafficking | ubiquitin | ESCRT-III

Ubiquitin-dependent protein degradation plays a pivotal role in almost all biological processes, as the timely and selective removal of regulatory proteins is essential in many signaling pathways (1, 2). Ubiquitin molecules can form topologically distinct ubiquitin chains that can serve as signals for different pathways (3). Among them, ubiquitin chains linked through lysine 63 (K63) have been associated with endocytosis and were shown to be required for the efficient endocytic degradation of plasma membrane cargos (4, 5). In eukaryotes, ubiquitinated membrane proteins are transported into the vacuole/lysosome for degradation by resident proteases, depending on the function of the endosomal sorting complex required for transport (ESCRT) machinery. Ubiquitinated cargos are recognized and transported to late endosomes through the function of ESCRT-0, ESCRT-I, and ESCRT-II, and are subsequently sequestered to the intraluminal vesicles (ILVs) of the multivesicular body (MVB) by ESCRT-III (6, 7). Plants lack homologs of ESCRT-0 (8, 9), and it is suggested that ubiquitin binding proteins such as the target of Myb (TOM)-LIKEs (TOLs) take over its function (10).

Ubiquitination of plasma membrane proteins depends on the activity of the ubiquitin conjugating machinery that creates an isopeptide bond between the C-terminal glycine of ubiquitin and a lysine of the substrate proteins or another ubiquitin molecule (11). Deubiquitinating enzymes (DUBs) can counteract the E3 ligase activity, in that they hydrolyze ubiquitin chains. In contrast to earlier assumptions that DUBs play merely a housekeeping role, it has been shown that DUBs can also be actively involved in the regulation of their target proteins (12, 13). The *Arabidopsis* genome encodes for at least 48 DUBs, although most of their molecular and biological functions are yet poorly understood (14). Whereas ubiquitinating enzymes interact specifically with their substrates (11), DUBs also can hydrolyze free ubiquitin chains unattached to target proteins (12, 15), and in most cases, do not require specific interactions with the substrate proteins. The elucidation of the spatiotemporal regulation of DUBs is therefore essential for a better understanding of the molecular mechanisms of DUB function.

Associated molecule with the SH3 domain of STAM (AMSH) is a metalloprotease DUB that was first identified as an interactor of the signaling molecule and ESCRT-0 component signal transduction adaptor molecule (STAM) in mammals (16). *AMSH* genes are conserved in higher eukaryotes and are essential for growth and development. Knockout of *AMSH* in mice causes postnatal lethality and neurodegenerative aberrations (17), and mutations in human *AMSH* were associated with an infant neurodegenerative disease (18), indicating its essential function in mammals. In our previous work, we conducted a genetic analysis of *AMSH* genes in *Arabidopsis*, named *AMSH1*, *AMSH2*, and *AMSH3*. We have shown that knockdown of *AMSH1* causes altered pathogen response, and that the knockout of *AMSH3* is lethal in plants, leading to growth arrest in the early stages of development (19–21).

AMSH proteins were shown to interact with ESCRT-III subunits and were implicated in endocytic protein degradation (21–26). Human AMSH and the Mpr1/Pad1 N-terminal (MPN)+ domain of

Significance

The regulation of protein abundance of receptors and transporters at the plasma membrane is important for proper signaling in many biological pathways. The removal of plasma membrane proteins can occur via the endocytic protein degradation pathway, in which posttranslational modification by ubiquitin plays a key role. The activity of ubiquitinating and deubiquitinating enzymes can determine the ubiquitination status of a given target protein, and it has been shown that both classes of enzymes have important physiological roles. However, how these enzymes themselves are regulated at the molecular level has not yet been completely understood. In this study, we report a possible mechanism by which the deubiquitinating enzyme AMSH3 is regulated by its interacting protein, apoptosis-linked gene-2 interacting protein X (ALIX), in *Arabidopsis*.

Author contributions: K.K. and E.I. designed research; K.K., M.-K.N., K.G., F.A., A.A., M.S.O., and E.I. performed research; K.G. and M.S.O. performed transmission electron microscopy; P.B. supervised the yeast two-hybrid open reading frame screen; L.C., J.P.-A., and V.R. contributed new reagents/analytic tools; K.K., M.-K.N., K.G., F.A., A.A., P.B., M.S.O., and E.I. analyzed data; and E.I. wrote the paper.

The authors declare no conflict of interest.

This article is a PNAS Direct Submission.

[1]To whom correspondence should be addressed. Email: erika.isono@wzw.tum.de.

This article contains supporting information online at www.pnas.org/lookup/suppl/doi:10.1073/pnas.1510516112/-/DCSupplemental.

Arabidopsis AMSH show specificity toward K63-linked ubiquitin chains (20–22), further supporting their function in endocytosis. Defects in AMSH function impair a number of intracellular trafficking events, including degradation of endocytosis cargos (22, 25, 27), vacuolar transport, and vacuole biogenesis (20), as well as defects in autophagic degradation (18, 20, 21). Although AMSH function in intracellular trafficking and protein degradation is well established, the molecular framework surrounding its function is not yet completely understood.

With the aim of elucidating the molecular basis of AMSH regulation, we screened for interactors of *Arabidopsis* AMSH proteins and found a homolog of human apoptosis-linked gene-2 interacting protein X (ALIX) and budding yeast bypass of C kinase 1 (BCK1)-like resistance to osmotic shock 1p (Bro1p) as a direct interactor of AMSH3. ALIX is a conserved protein in eukaryotes that was implicated in cytokinesis, ILV, and exosome biogenesis and endosomal sorting (28). Human ALIX was also suggested to play a role during viral infection and budding (29–31). Mammalian ALIX, yeast Bro1p, and their *Arabidopsis* homolog were all shown to interact with ESCRT-III via the charged multivesicular body protein 4/sucrose nonfermenting 7p (CHMP4/Snf7p) subunit (32–35). Bro1p was shown to interact also with the endosome-associated DUB degradation of alpha 4p (Doa4p) and to be essential for recruiting Doa4p to late endosomes (36). Doa4p belongs to the ubiquitin-specific protease (UBP) family of DUBs and is structurally unrelated to AMSH. The involvement of ALIX/Bro1p in the regulation of other DUBs during endosomal sorting has not yet been reported. Our data show that *ALIX* is essential in *Arabidopsis* and that it is important for the degradation of ubiquitinated proteins, vacuole, and MVB biogenesis, as well as for the localization of AMSH3 to endosomes.

Results

ALIX Can Directly Interact with AMSH3. To identify interacting proteins or potential regulators of AMSH proteins, we carried out a yeast two-hybrid (YTH)-screen against 12,000 *Arabidopsis* ORFs, using AMSH1, AMSH2, and AMSH3 as bait. In this screen, we identified a Bro1 domain containing protein (AT1G15130) as a YTH interactor of AMSH1 and AMSH3, but not AMSH2 (Fig. 1*A* and Fig. S1 *A*–*C*). The identified protein showed highest homology to the yeast Bro1 domain containing proteins Bro1p (15.8% amino acid identities) and regulator of IME2 20 (Rim20p, 18%), as well as human ALIX (25.1%). We thus designated this protein *Arabidopsis* ALIX.

We first wanted to establish whether ALIX directly binds to AMSH proteins. Because we could not obtain enough recombinant AMSH1, we decided to focus our further studies on AMSH3. To analyze the interaction between ALIX and AMSH3, we purified recombinant maltose binding protein (MBP)-fused ALIX, an ESCRT-III subunit MBP-vacuolar protein sorting (VPS)60.1 that was shown not to interact with AMSH3 (26), and untagged AMSH3. In an in vitro binding assay, MBP-ALIX, but not MBP-VPS60.1,

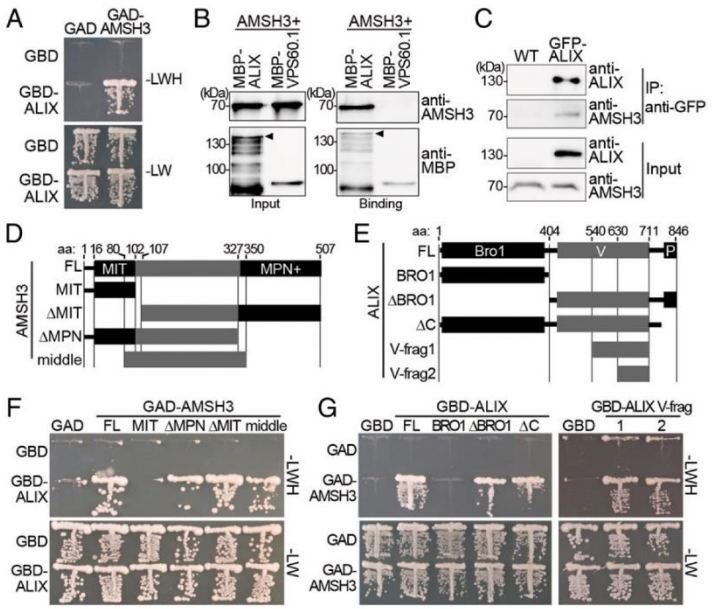

Fig. 1. (*A*) ALIX interacts with AMSH3 in YTH. *GBD* and *GBD-ALIX* were transformed in yeast with either *GAD-* or *GAD-AMSH3*. Transformants were tested for their auxotrophic growth on synthetic complete medium lacking leucine and tryptophan (SC-LW) (-LW: SC-Leu-Trp) or synthetic complete medium lacking leucine, tryptophan, and histidine (SC-LWH) (-LWH: SC-Leu-Trp-His) media. (*B*) ALIX interacts directly with AMSH3 in vitro. Recombinant AMSH3 was incubated with either MBP-ALIX or MBP-VPS60.1 for 1 h at 4 °C and subjected to immunoblot analysis after extensive washing. Anti-AMSH3 and anti-MBP antibodies were used to detect beads-retained material. Arrowheads indicate MBP-ALIX. (*C*) ALIX and AMSH3 interact *in planta*. Immunoprecipitation (IP) was performed from total extracts of wild-type or *GFP-ALIX*-expressing seedlings using anti-GFP immobilized matrix. Immunoprecipitated material was subjected to immunoblot analysis. GFP-ALIX and endogenous AMSH3 were detected with anti-ALIX and anti-AMSH3 antibodies, respectively. (*D* and *E*) AMSH3- (*D*) and ALIX- (*E*) constructs used for YTH interaction studies in *F* and *G*. Bro1, Bro1-domain; FL, full-length; MIT, MIT domain; MPN+, MPN+ domain; P, Proline-rich domain; V, V-domain; V-frag1/2, V-domain fragment 1/2. (*F*) YTH analysis of AMSH3 domains responsible for the interaction with ALIX. GAD-fused AMSH3 constructs shown in *D* were cotransformed with either *GBD* or *GBD-ALIX*. Transformants were tested for their auxotrophic growth on SC-LW and SC-LWH media. (*G*) YTH analysis of ALIX domains responsible for the interaction with AMSH3. GBD-fused ALIX constructs shown in *E* were cotransformed with either *GAD* or *GAD-AMSH3*. Transformants were tested for their auxotrophic growth on SC-LW and SC-LWH media.

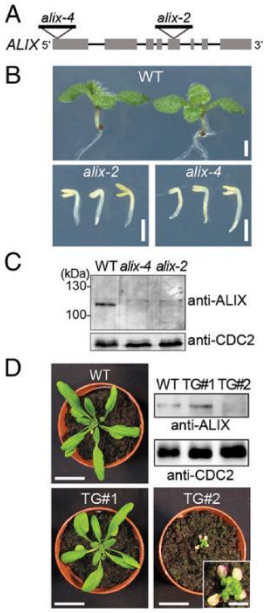

Fig. 2. *alix* null mutants show seedling lethality. (*A*) Schematic presentation of the T-DNA insertion sites of *alix-2* and *alix-4*. Lines indicate introns and gray boxes indicate exons. (*B*) Phenotypes of 9-d-old wild-type (WT), *alix-2*, and *alix-4* seedlings. (Scale bars, 1 mm.) (*C*) *alix-2* and *alix-4* are null mutants. Total extracts from seedlings shown in *B* were subjected to immunoblot analysis, using an anti-ALIX antibody. CDC2 was used as loading control. (*D*) Photographs of 3-wk-old wild-type (WT) and two transgenic plants (TG#1 and TG#2) harboring *35Spro:ALIX*. Total extracts from rosetta leaves were subjected to immunoblot analysis with an anti-ALIX antibody. CDC2 was used as loading control. Note that TG#2 with strongly reduced levels of ALIX (magnification in inset) shows severe growth defects and leaf chlorosis. (Scale bars, 2 cm; scale bar in inset, 0.5 cm.)

bound AMSH3 (Fig. 1*B*), indicating that ALIX and AMSH3 can directly interact with each other. Next, to test whether ALIX and AMSH3 interact *in planta*, we generated plants expressing a functional fusion protein GFP-ALIX driven by a native ALIX promoter fragment (Fig. S2 *A* and *B*). Immunoprecipitation of GFP-ALIX from total protein extracts prepared from wild-type or GFP-ALIX-expressing seedlings and subsequent immunoblotting revealed coimmunoprecipitation of endogenous AMSH3 with GFP-ALIX (Fig. 1*C*). This result indicates that AMSH3 and ALIX can interact *in planta*.

To identify the binding domain of AMSH3 and ALIX, we conducted a directed YTH analysis. AMSH3 has an N-terminal microtubule interacting and trafficking (MIT) domain that interacts with two ESCRT-III subunits, 2.1 and VPS24.1 (26), and an MPN+ domain that comprises the catalytic center (20). Neither the MIT nor the MPN+ domain of AMSH3 was required for the interaction with ALIX, whereas the middle region was necessary and sufficient for the interaction (Fig. 1 *D* and *F* and Fig. S3*A*). A Pfam database search (37) showed that ALIX has an N-terminal Bro1 domain followed by a V-shaped domain (V-domain) and a C-terminal proline-rich domain (Fig. 1*E*). To identify the region in ALIX that is responsible for the binding to AMSH3, YTH interactions between different ALIX fragments and the full-length AMSH3 were tested. Both the Bro1- and the C-terminal region were dispensable for the interaction with AMSH3, whereas an 82-amino acid fragment of the ALIX V-domain was sufficient for the interaction (Fig. 1 *E* and *G* and Fig. S3 *B* and *C*).

***alix* Null Mutants Show Similar Phenotypes to *amsh3*.** AMSH proteins were previously shown to be essential for plant growth and development (20, 27). To investigate whether ALIX functions in the same biological pathway as AMSH3, we analyzed available T-DNA insertion lines of *ALIX*. Two lines, GABI 837H11 and SALK 063124, which we named *alix-2* and *alix-4*, respectively, carried T-DNA insertions in exons (Fig. 2*A*). Homozygous *alix-2* and *alix-4* mutants showed reduced germination compared with the wild-type (Table 1), and even if germinated, did not develop beyond the seedling stage (Table 1 and Fig. 2*B*). This seedling lethal phenotype was very similar to the previously analyzed *amsh3* mutant (Fig. S4*A*) (20), suggesting AMSH3 and ALIX could function in the same biological process. Immunoblotting with an anti-ALIX antibody showed that homozygous *alix-2* and *alix-4* mutants were null mutants (Fig. 2*C*).

To verify that the phenotype is caused by the loss of *ALIX* function, we crossed heterozygous *alix-2* and *alix-4* plants with each other and analyzed the F1 progeny. Transheterozygous (*alix-2*/*alix-4*) F1 progenies showed the same seedling phenotype as homozygous *alix-2* or *alix-4* mutants (Fig. S4*B*), indicating that *alix-2* is allelic to *alix-4*. Moreover, seedling lethality of *alix-2* could be complemented by *ALIXpro:GFP-ALIX* (Fig. S2 *A* and *B*), confirming that *ALIX* is indeed the causative gene for the *alix* mutant phenotype.

To investigate whether *ALIX* is also essential during plant growth, we tried to generate artificial microRNA lines, but were not able to identify lines with significantly reduced *ALIX* transcripts. We realized, however, that the introduction of the *35Spro:ALIX* construct in a wild-type background leads to reduced protein levels of ALIX, probably because of cosuppression. Plants harboring the *35Spro:ALIX* construct showed a range of phenotypes, but the severely growth-defective plants with chlorotic leaves had always reduced amount of ALIX in total protein extracts, whereas larger plants had at least wild-type levels of ALIX (Fig. 2*D*). These results suggest ALIX is indispensable during vegetative plant growth.

ALIX Is Required for Vacuole Biogenesis. *amsh3* mutants showed severe vacuole biogenesis defects and lacked large central vacuoles (20). Confocal microscope analysis of 2′,7′-bis-(2-carboxyethyl)-5-(and-6)- carboxyfluorescein (BCECF)-acetoxymethyl ester (AM)-stained wild-type, *alix-4*, and *amsh3-1* vacuoles revealed that *alix* mutants also have abnormal vacuole morphology similar to *amsh3-1,* indicating that ALIX is necessary for proper vacuole biogenesis (Fig. 3 *A* and *B* and Fig. S5*A*). To analyze the vacuolar structure in more detail, we performed 3D reconstruction analysis

Table 1. Germination assay of *alix* mutants

	Phenotype of progeny				
Genotype of parental line	Wild type	Seedling lethal	Ungerminated	Seedling lethal+ ungerminated	*n*
WT (Columbia-0)	100%	0%	0%	0%	424
alix-2$^{+/-}$ (het)	83.2%	11.9%	4.9%	16.8%	405
alix-4$^{+/-}$ (het)	77%	9.5%	13.5%	23%	400

on Z-stack images of BCECF-AM-stained wild-type, *alix*, and *amsh3* vacuoles. Surface rendering revealed similar higher surface area-to-volume ratios for *alix-4* and *amsh3-1* in comparison with the wild type, reflecting the tubular interconnected vacuolar structures in these mutants (Fig. 3 *C* and *D* and Fig. S5*B*). In addition, the presence of 1 μm vacuolar or provacuolar profiles was confirmed by electron microscopy of high-pressure frozen/freeze substituted roots. These vacuolar structures contained membrane and cytoplasmic materials in their lumen and were abundant in *alix* root cells, but not in the wild-type (Fig. 3 *E* and *F*). In contrast, the morphology of other organelles such as the Golgi apparatus, endoplasmic reticulum (ER), nucleus, plastids, and mitochondria did not seem to be affected in *alix-2* (Fig. 3 *E* and *F* and Fig. S5 *C*–*H*).

AMSH3 Shows Colocalization with Late Endosomal Markers. Human ALIX and yeast Bro1p were reported to localize on endosomes and to be involved in intracellular trafficking (28). To investigate whether AMSH3 and ALIX localize on the same cellular compartment and function in intracellular transport, we expressed an *AMSH3pro:AMSH3-YFP* construct in plants. *AMSH3pro:AMSH3-YFP* complemented the seedling lethal phenotype of *amsh3-1*, indicating that AMSH3-YFP is a functional fusion protein (Fig. S6 *A* and *B*).

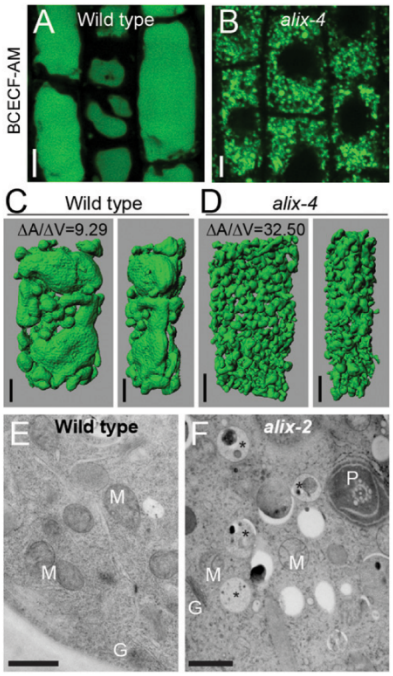

Fig. 3. *alix* shows aberrant vacuole morphology. (*A* and *B*) Vacuole morphology of wild-type and *alix* mutants. Vacuoles of 2-d-old wild-type (*A*) and 7-d-old *alix-4* (*B*) were stained with BCECF-AM and analyzed under a confocal microscope. Vacuoles in the root epidermis cells are shown. (Scale bars, 5 μm.) (*C* and *D*) 3D surface renderings of vacuoles from a representative root epidermal cell of 2-d-old wild-type (*C*) and 7-d-old *alix-4* (*D*) seedlings. Z-stack images were processed to generate 3D reconstruction pictures of vacuoles. Views from the front (*Left*) and the side (*Right*) are shown. Note the tubular appearance of mutant vacuoles. (Scale bars, 5 μm.) ΔA/ΔV: surface area to volume ratio. (*E* and *F*) Overview of WT (*E*) and *alix-2* (*F*) root cells from 5-d-old seedlings. Note the presence of vacuolar/provacuolar compartments with membranes and cytoplasmic contents (asterisks). G, Golgi; M, mitochondria; P, plastid. (Scale bars, 1 μm.)

AMSH3-YFP showed strong cytosolic signals similar to the previously published N-terminal YFP fusion YFP-AMSH3 (26), but localized also on intracellular foci. To investigate the nature of these foci, we performed colocalization studies using trans-Golgi network (TGN)/early endosome (EE) markers monomeric red fluorescent protein (mRFP)-syntaxin of plants 43 (SYP43) and mRFP-SYP61 (38, 39), as well as late endosome (LE) markers arabidopsis rat sarcoma-related proteins in brain GTPase6 (ARA6)-mRFP and mRFP-ARA7 (40, 41). AMSH3-YFP signals did not show frequent colocalization with the TGN/EE markers (Fig. 4 *A*, *B*, and *E*). In contrast, 62.8% (n = 368) and 74.8% (n = 306) of AMSH3-YFP-positive vesicles showed colocalization with ARA6- and ARA7-labeled vesicles, respectively, indicating that the AMSH3-YFP foci represent mostly late endosomes (Fig. 4 *C*, *D*, and *E*).

To further establish the endosome localization of AMSH3, we treated the AMSH3-YFP/mRFP-SYP43 coexpressing line with the ADP ribosylation factor-GTP exchange factor (ARF-GEF) inhibitor brefeldin A (BFA) and the AMSH3-YFP/mRFP-ARA7 coexpressing line with the PI3K/PI4K inhibitor wortmannin (WM). Although mRFP-SYP43 localized to the so-called BFA bodies on 60-min BFA treatment, AMSH3-YFP signals were not found in the BFA-induced compartments (Fig. 4*F*). On treatment with WM, both mRFP-ARA7 and AMSH3-YFP localized to the surface of the swollen MVBs that appeared as ring-like structures (Fig. 4*G*). These results corroborate that AMSH3-YFP does not stably associate with TGN/EE but localizes together with LE markers on vesicles sensitive to WM.

AMSH3 and ALIX Colocalize on Late Endosomes. If ALIX functions together with AMSH3, they should show overlapping intracellular localizations. We thus examined the localization of GFP-ALIX with the late endosome marker mRFP-ARA7. Similar to AMSH3-YFP, GFP-ALIX signals showed cytosolic distribution but also localized on punctuate structures: 32.8% ALIX-positive vesicles (n = 283) colocalized with the LE-marker ARA7 (Fig. 5*A*), indicating that part of the ALIX pool localizes to late endosomes. Similar to AMSH3-YFP, GFP-ALIX relocalized to WM-induced compartments together with mRFP-ARA7 (Fig. 5*B*). Similar to AMSH3-YFP, GFP-ALIX-labeled vesicles did not efficiently colocalize with the TGN/EE-endosome marker mRFP-SYP43 (9.96%, n = 280) and did not react to BFA-treatment (Fig. S7 *A* and *B*). We next wanted to investigate whether AMSH3 and ALIX localize to the same cellular compartment and generated an RFP-fused AMSH3 construct, *AMSH3pro:AMSH3-TagRFP*. Similar to the YFP-tagged AMSH3, AMSH3-TagRFP showed both cytosolic and endosomal localization: 68.7% (n = 282) of AMSH3-positive compartments showed colocalization with GFP-ALIX (Fig. 5*C*). Compartments positive for both GFP-ALIX and AMSH3-TagRFP were sensitive to WM treatment (Fig. 5*D*), suggesting both proteins colocalize on late endosomes.

A systematic YTH analysis of *Arabidopsis* ESCRT-related proteins has shown that ALIX interacts with the ESCRT-III subunit SNF7 (35). ESCRT-III components accumulate in aberrant late endosomal structures on inhibition of ESCRT-III disassembly by inactivation of the ATPases associated with diverse cellular activities (AAA)-ATPase suppressor of K+ transport growth defect 1(SKD1)/Vps4p (26, 41, 42). In *Arabidopsis*, the overexpression of ATPase-inactive SKD1(EQ) was shown to induce aggregation of endosomes (26, 41) that were labeled with the late endosome marker ARA7, but not those labeled with the early endosome marker SYP41 or clathrin light chain (43). In accordance with the previously reported interaction with SNF7 (35) and its partially late-endosomal localization, GFP-ALIX accumulated in the SKD1 (EQ)-induced enlarged vesicular compartments together with the ESCRT-III subunit VPS2.1 and AMSH3-TagRFP (Fig. 5 *E* and *F*). Altogether these results show that ALIX and AMSH3 colocalize on

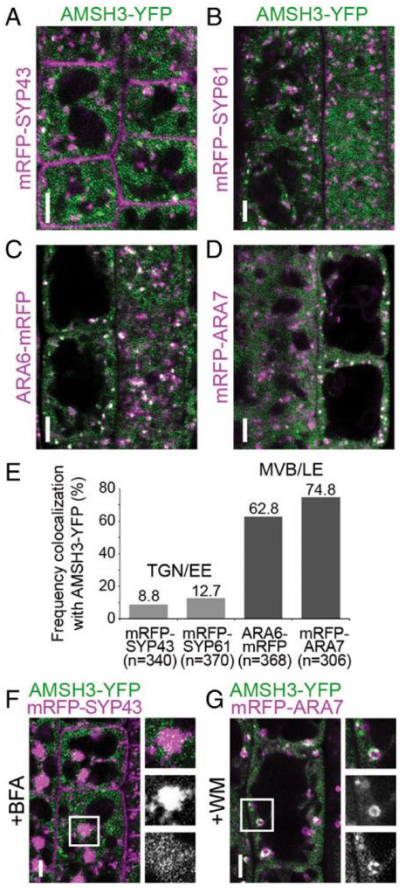

Fig. 4. AMSH3 localizes to ARA6- and ARA7-labeled late endosomes. (*A* to *D*) Seedlings expressing *AMSH3pro:AMSH3-YFP* were crossed with *SYP43pro:mRFP-SYP43* (*A*), *SYP61pro:mRFP-SYP61* (*B*), *ARA6pro:ARA6-mRFP* (*C*), and *ARA7pro:mRFP-ARA7* (*D*) expressing plants and colocalization was examined under a confocal microscope. (Scale bars, 5 μm.) SYP43 and SYP61 are markers for TGN or EE, and ARA6 and ARA7 are markers for MVB or LE. (*E*) Numbers of AMSH3-YFP-positive vesicles that colocalize with the mRFP-tagged markers in *A*–*D* were counted to calculate the colocalization frequency. (*F*) An *AMSH3-YFP* and *mRFP-SYP43* expressing seedling as in *A* was treated with 50 μM brefeldin A (BFA) for 60 min. Note that although mRFP-SYP43 relocalized to the BFA bodies, AMSH3-YFP did not. A magnification of the area indicated with the white rectangle is shown on the right side (from top to bottom: merged, mRFP-ARA7, and AMSH3-YFP). (Scale bars, 5 μm.) (*G*) An *AMSH3-YFP* and *mRFP-ARA7* expressing seedling as in *D* was treated with 33 μM WM for 120 min. Both AMSH3-YFP and mRFP-ARA7 localize to WM-induced compartments. A magnification of the area indicated with the white rectangle is shown on the right side (from top to bottom: merged, mRFP-ARA7, and AMSH3-YFP). (Scale bars, 5 μm.)

late endosomal compartments that are sensitive to WM and SKD1 ATPase activity.

ALIX Binds Ubiquitin and Is Involved in Ubiquitin-Dependent Protein Degradation. AMSH proteins were implicated in the degradation of ubiquitinated membrane proteins in both mammals and plants (22, 27). We reasoned that if ALIX functions in the same pathway as AMSH3, *alix* mutants would also show similar defects in the degradation of ubiquitinated cargos. Indeed, when we analyzed total extracts from seedlings using an anti-ubiquitin antibody, *alix* mutants showed high levels of high-molecular weight ubiquitinated proteins (Fig. 6*A*), suggesting ALIX plays a role in the removal of ubiquitin conjugates.

The V-domain of both Bro1p and human ALIX was shown to mediate the interaction with ubiquitin in intracellular trafficking (29, 31, 44). Because the amino acid sequence homology in the

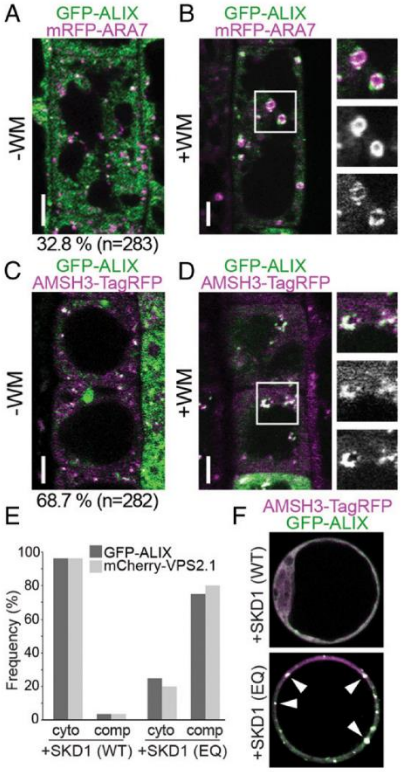

Fig. 5. AMSH3 and ALIX colocalize on late endosomes. (*A* and *B*) ALIX localizes to ARA7-labeled late endosomes. Seedlings expressing *ALIXpro:GFP-ALIX* and *ARA7pro:mRFP-ARA7* were examined with a confocal microscope without (*A*) or with (*B*) 120 min treatment with 33 μM WM. Percentage of GFP-ALIX vesicles colocalizing with mRFP-ARA7 vesicles is indicated below the panel in *A*. (Scale bars, 5 μm.) (*C* and *D*) Seedlings coexpressing *ALIXpro:GFP-ALIX* and *AMSH3pro:AMSH3-TagRFP* were analyzed without (*C*) or with 120 min treatment with 33 μM WM. (*D*) Percentage of GFP-ALIX vesicles colocalizing with AMSH3-TagRFP vesicles is indicated below the panel in *C*. (Scale bars, 5 μm.) (*E*) *ALIXpro:GFP-ALIX* was cotransformed with *UBQ10pro:mCherry-VPS2.1* and either *35Spro:HA-SKD1(WT)* or *35Spro:HA-SKD1(EQ)* in *Arabidopsis* cell culture-derived protoplasts. Percentages of cells with cytosolic localization (cyto) or SKD1(EQ)-induced compartments (comp) of GFP-ALIX and mCherry-VPS2.1 are indicated. (*F*) AMSH3 and ALIX localize to SKD(EQ)-induced compartments. *ALIXpro:GFP-ALIX* and *35Spro:AMSH3-TagRFP* were cotransformed with either *35Spro:HA-SKD1(WT)* or *35Spro:HA-SKD1(EQ)* in *Arabidopsis* cell culture-derived protoplasts. Representative cells are shown. Note that on coexpression of SKD1(EQ), both AMSH3-TagRFP and GFP-ALIX relocalize to enlarged endosomal compartments (arrowheads).

Arabidopsis ALIX V-domain is relatively moderate (25% amino acid identity with human ALIX and 17% with Bro1p), we tested whether it could bind ubiquitin. In a ubiquitin binding assay using ubiquitin agarose, recombinant His-ALIX(V) interacted with ubiquitin, whereas the negative control His-SKD1 did not (Fig. 6*B*), suggesting the ubiquitin-binding ability of the ALIX V-domain is conserved in *Arabidopsis*. Because K63-linked ubiquitin chains are implicated in endocytic degradation, we tested whether His-ALIX(V) can interact with this type of linkage. We analyzed the interaction of His-ALIX(V) with linear and K63-linked diubiquitin, using the MicroScale Thermophoresis technique that enables affinity measurements without the immobilization of either of the proteins (45). The results showed that His-ALIX(V) bound K63-linked diubiquitin, but not linear diubiquitin, implying that ALIX is involved in pathways mediated by K63-ubiquitin linkages (Fig. 6*C*).

DUB-interacting proteins can affect the activity of DUBs, as shown for the case of human AMSH and its binding partner STAM, which activates AMSH (46, 47). To establish whether ALIX can influence the enzymatic activity of AMSH3, we performed DUB assays with AMSH3 in the presence or absence of ALIX, using the fluorescent substrate diubiquitin-carboxytetramethylrhodamine (TAMRA). The cleavage of diubiquitin to monoubiquitin separates the quencher from the fluorophore, which can be measured as an increase in fluorescence. AMSH3 readily catalyzed this reaction; however, preincubation with equimolar amount of ALIX did not change the AMSH3 enzyme kinetics (Fig. S8), suggesting ALIX does not influence the DUB activity of AMSH3.

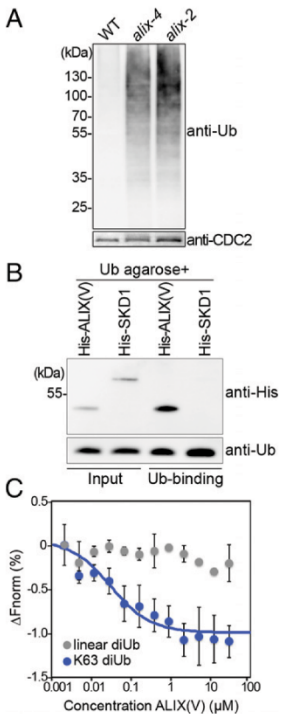

Fig. 6. ALIX binds ubiquitin. (*A*) *alix* mutants accumulate ubiquitin conjugates. Total extracts of wild-type (WT), *alix-2*, and *alix-4* were subjected to immunoblot analysis using an anti-ubiquitin antibody. CDC2 was used as loading control. (*B*) ALIX binds monoubiquitin. A recombinant His-ALIX fragment containing the V-domain (His-ALIX(V): amino acids 393–734), and His-SKD1 were incubated with ubiquitin agarose. After extensive washing, the eluate was analyzed by immunoblotting using an anti-His tag and an anti-Ub antibody. (*C*) MicroScale Thermophoresis assays show that recombinant His-ALIX(V) binds K63-linked diubiquitin, but not linear diubiquitin. The average of three experiments are shown. ΔFnorm, normalized fluorescence. Blue, K63-lilnked diubiquitin; gray, linear diubiquitin. Error bars, SEM.

ALIX Is Important for Localization of AMSH3 on ARA7-Labeled Vesicles. To investigate whether the *ALIX* null mutation affects MVB formation, we analyzed MVBs in wild-type and *alix-2* roots by transmission electron microscopy. *alix-2* mutants were able to form MVBs (Fig. 7 *A* and *B*); however, we also occasionally observed clustering of MVBs in *alix-2* cells (Fig. 7*C*), implying a function of ALIX in MVB formation. The size of MVBs was significantly reduced in *alix-2* cells compared with that of wild-type cells (Fig. 7*D*), supporting the idea that ALIX is involved in MVB formation. In contrast, there was no significant difference in the size of ILVs between wild-type and *alix-2* (Fig. 7*E*).

Yeast Bro1p interacts with Doa4p, a UBP-class DUB unrelated to AMSH, and recruits it to endosomes (36, 48). To test whether loss of ALIX function affects association of AMSH3 to endosomes, we analyzed the localization of AMSH3-YFP together with the late-endosomal marker mRFP-ARA7 in *alix-2*. Whereas AMSH3-YFP and mRFP-ARA7 endosomes showed colocalization with high frequency in a wild-type background (Fig. 4 *D* and *E*), AMSH3-YFP signals were dispersed in the cytosol and did not colocalize with mRFP-ARA7 in *alix-2* (Fig. 7*F*). The numbers of both mRFP-ARA7 and AMSH3-YFP-positive vesicles were decreased in the *alix-2* mutant, among which AMSH-YFP signals were more affected (Fig. 7*H*). When treated with WM for 120 min, mRFP-ARA7 appeared in enlarged WM compartments, as it did in the wild type (Fig. 7*G*). In contrast, AMSH3-YFP showed reduced sensitivity toward WM and localized less frequently in ARA7-labeled WM compartments (structures with a diameter larger than 1.5 μm) in the *alix-2* mutant background (Fig. 7 *G* and *I*). Together, these results indicate that the localization of AMSH3-YFP to mRFP-ARA7-labeled late endosomes requires intact ALIX function *in planta* (Fig. 7*J*).

Discussion

Our data show that *Arabidopsis* ALIX interacts directly with the late-endosome localized metalloprotease DUB AMSH3 and is important for its localization to late endosomes. Mutant analyses support a functional relationship between ALIX and AMSH3, as phenotypic alterations of *amsh3* and *alix* mutants are strikingly similar in regard to seedling lethality, vacuole morphology, and accumulation of ubiquitinated proteins.

Class-E *vps* mutants in budding yeast, to which mutants of ESCRT-III and *BRO1* belong, do not show apparent alterations in central vacuole morphology (49). In contrast, *Arabidopsis alix* mutants have abnormal vacuoles, suggesting that the function of ALIX homolog differs in this regard in yeast and plants. Vacuoles are essential organelles in plants (50), have developmental stage- or organelle-specific functions (51, 52), and as recently reported, can be also regulated by the phytohormone auxin (53). Thus, the underlying mechanisms of vacuole biogenesis might be more complex in plants than in yeast.

siRNA-mediated gene silencing of human *ALIX* in HeLa cells was shown to decrease the number of multivesicular endosomes (34). Our ultrastructural analysis of *alix-2* mutant cells showed smaller MVBs that are occasionally found forming clusters, which indicates that the function of *Arabidopsis* ALIX is also important for proper MVB biogenesis. However, in contrast to the membranous aggregates that are observed in typical class-E mutants of budding yeast (54), defects in *Arabidopsis* class-E genes seem to affect MVB biogenesis in a different manner.

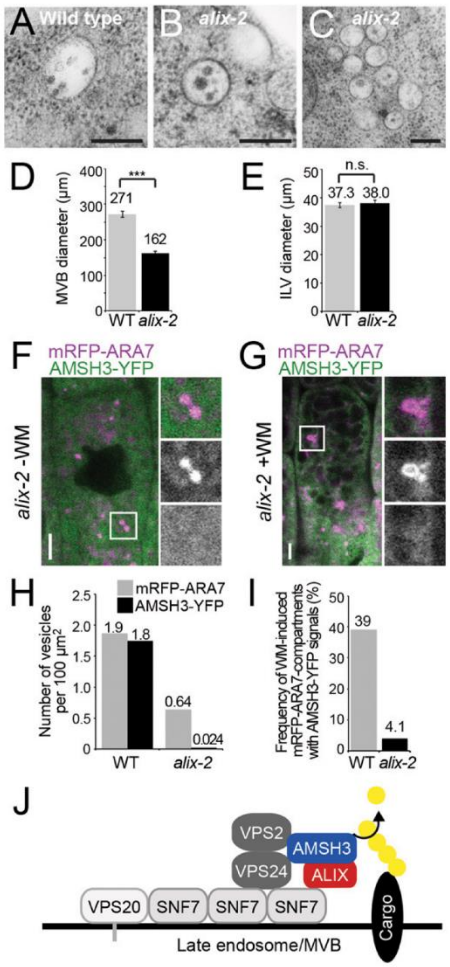

Fig. 7. AMSH3 does not localize on late ARA7-labeled vesicles in the *alix* mutant. (*A* and *B*) Electron micrographs of MVBs from wild-type (*A*) and *alix-2* (*B*) cells. (Scale bars, 200 µm.) (*C*) Electron micrographs showing clustered MVBs in *alix-2*. (Scale bar, 200 µm.) (*D*) Diameter of MVBs in wild-type (light gray, $n = 61$) and *alix-2* (dark gray, $n = 50$). Error bars, SEM. The difference between wild-type (WT) and *alix-2* is highly significant, with $P < 0.001$ (***). (*E*) Diameter of ILVs in wild-type (WT; light gray, $n = 28$) and *alix-2* (dark gray, $n = 42$). Error bars, SEM. The difference between WT and *alix-2* is not significant (n.s.) ($P > 0.05$). (*F* and *G*) Localization of AMSH3-YFP and mRFP-ARA7 in root epidermis cells of *alix-2* without (*F*) or with (*G*) 120 min WM treatment. Note that AMSH3-YFP localize neither on mRFP-ARA7-labeled vesicles nor on WM-enlarged late endosomes. Magnifications of the area indicated with white rectangles are shown on the right side (from top to bottom: merged, mRFP-ARA7, and AMSH3-YFP). (Scale bars, 5 µm.) (*H*) Number of mRFP-ARA7 and AMSH3-YFP vesicles per 100 µm² in wild-type (WT) and *alix-2*. Note that reduction of the number of AMSH3-YFP vesicles is stronger than of mRFP-ARA7 vesicles in *alix-2*. (*I*) Number of WM-induced mRFP-ARA7 compartments containing AMSH3-YFP signals in wild-type (WT) and *alix-2*. (*J*) Predicted model for ALIX interaction with AMSH3 and ESCRT-III. AMSH3 associates with ESCRT-III subunits VPS2 and VPS24 through its MIT domain and with ALIX through the middle domain. ALIX binds to ESCRT-III component SNF7 via the BRO1 domain and to AMSH3 through the V-domain. ALIX does not influence AMSH3 DUB activity, but might function to stabilize the interaction of AMSH3 with ESCRT-III-positive MVBs.

A *Xenopus* ALIX homolog was shown to interact with AMSH in cell lysates (55); however, neither the nature of this interaction nor the functional relationship between ALIX and AMSH has been established. Our analysis demonstrated that AMSH3 and ALIX interact directly in vitro and coimmunoprecipitate in vivo, suggesting these two proteins function together. They colocalize on WM-sensitive late endosomes, and *ALIX* is necessary for the endosomal localization of AMSH3. Furthermore, mutant analyses revealed phenotypic similarities between null mutants of *ALIX* and *AMSH3*, indicating they play a role in the same biological pathways.

Yeast Bro1p and a human ALIX-related protein HD-PTP were shown to recruit UBPs Doa4p and UBPY, respectively, to endosomes (36, 56). In contrast to Doa4p, and similarly to UBPY (57), AMSH3 interacts directly with ESCRT-III subunits through its MIT domain (26). Interaction between AMSH3 and ALIX alone is probably not enough for proper AMSH3 function, as the deletion of the MIT domain of AMSH3 renders it nonfunctional (27). Thus, ALIX may function to stabilize the interaction of AMSH3 with ESCRT-III. Alternatively, defects in degradation of ubiquitinated cargos or possible AMSH3 substrates in the *alix* mutants might also affect the localization of AMSH3 to endosomes.

In addition to the localization to vesicles, AMSH3-YFP signals were also observed dispersed in the cytosol. Differential regulation of AMSH3 activity in the cytosol and on endosomes could therefore be important to guarantee deconjugation of ubiquitin chains only on endosome-associated substrates. Human AMSH was shown to be activated by the binding of STAM (47). The *Arabidopsis* genome does not contain a sequence-homolog of STAM (9), and although *Arabidopsis* AMSH3 interacts with ESCRT-III subunits (26) and ALIX, none of them was shown to influence its DUB activity. Future research should identify factors that may inhibit AMSH3 activity before its recruitment to endosomes or enhance its activity on endosomal membranes.

Despite its relatively low conservation among the different kingdoms, *Arabidopsis* ALIX also interacted with ubiquitin through its V-domain, similar to its homologs (29, 31, 44). The V-domain was also reported to serve as a dimerization domain (58) and clathrin-binding domain (44). Whereas Bro1p interacts with the DUB Doa4p through its C-terminal proline-rich motif (59), our experiments identified a subregion in the V-domain of *Arabidopsis* ALIX to be sufficient for the interaction with AMSH3. How the binding of different proteins is coordinated within this domain is an intriguing question.

In addition to ALIX, the *Arabidopsis* genome encodes for four additional Bro1 domain-containing proteins (AT1G13310, AT1G17940, AT1G73990, and AT5g14020). These proteins are shorter than ALIX and lack other recognizable functional domains. Because the Bro1 domain is characterized as the interaction domain for ESCRT-III (60), these proteins might also play a role in ESCRT-mediated processes. The moderate frequency of colocalization of GFP-ALIX with both the early endosomal marker SYP43 and the late endosomal marker ARA7 suggests *Arabidopsis* ALIX, as its homologs, could play a broad role in membrane trafficking events, which will be an interesting topic for future studies.

Methods

Cloning Procedure. Details of the cloning procedure and primers used for cloning are described in *SI Methods* and Table S1, respectively.

Biological Material. All experiments were performed with *A. thaliana* (Columbia-0 ecotype). The T-DNA insertion lines of ALIX were obtained from the Genomanalyse im biologischen System Pflanze-Kolner Arabidopsis T-DNA (GABI-Kat) collection (*alix-2*, GABI 83711) (61) and from the Nottingham *Arabidopsis* Stock Centre (*alix-4*, SALK 063124). *alix-2* mutants were genotyped

using primers KK94 and KK95 for wild-type and KK94 and o8409 for T-DNA insertion. *alix-4* mutants were genotyped with primers KK72 and KK73 for the wild-type and KK72 and LBb1.3 for the T-DNA insertion.

Plant transformations were carried out using the floral dip method (62). Seedlings were grown in continuous light at 110 μmol $m^{-2} \cdot s^{-1}$ light intensity. Standard Murashige & Skoog growth medium (Duchefa Biochemie) supplemented with 1% sucrose was used to grow seedlings. Adult plants were grown on soil. *Arabidopsis* root epidermis cell culture was used to produce protoplasts for transient transformation and localization analysis, as described previously (26).

Immunoblotting, Antibodies, and Immunoprecipitation. To prepare total protein extracts from *Arabidopsis* seedlings, frozen seedlings were homogenized with the TissueLyser-II (Qiagen), using glass beads, and the pulverized tissue was mixed with the extraction buffer [50 mM Tris·HCl at pH 7.5, 150 mM NaCl, 0.5% Triton X-100, and protease inhibitor mixture (Roche)]. The mixture was centrifuged 10 min at 13,000 × *g*, and the supernatant was used for further experiments. Immunoprecipitation of GFP-ALIX from plant total extracts was performed as described in ref. 63, using GFP-Trap_A (Chromotek). Protein purification from *Escherichia coli* and in vitro binding assays were performed as described previously (26). SDS/PAGE and immunoblotting were performed according to standard methods. An anti-ALIX antibody was raised in rabbits using a total amount of 800 μg of recombinant 6xHis-ALIX(V) as antigen (Eurogentec). The serum was used at a 1:1,000 dilution, and the specificity of the antibody was verified using total extracts from *alix* null mutants. Additional primary antibodies used were anti-AMSH3 (20), anti-CDC2 (Santa Cruz), anti-GAL4 DNA binding domain (Santa Cruz), anti-His (Sigma-Aldrich), anti-UB(P4D1) (Santa Cruz), and horseradish peroxidase conjugated anti-HA (Sigma-Aldrich).

Ub-Binding Assay. The ub-binding assay was performed using ubiquitin agarose (Enzo Life Sciences), as described in ref. 64. For MicroScale Thermophoresis, His-ALIX(V) was labeled with Monolith Protein Labeling Kit RED-NHS (NanoTemper). Next, 50 nM labeled His-ALIX(V) was mixed with a twofold dilution series of K48- and K63- linked diubiquitin (Enzo Life Sciences), starting with a concentration of 37 μM. Themophoresis was measured in standard treated capillaries (NanoTemper) with a monolith NT.115 instrument (NanoTemper), as described in ref. 65.

Microscopy. For the visualization of vacuoles in the root epidermis cells, seedlings were incubated in liquid Murashige and Skoog (MS) supplemented with 5 μM BCECF-AM (Molecular Probes) and 0.02% Pluronic F-127 (Molecular Probes, Invitrogen) for 1 h at room temperature in the dark. Brefeldin A (BFA) (Sigma Aldrich) and WM (Applichem) treatments were performed at a concentration of 50 and 33 μM, respectively, for 60 min for BFA and 120 min for WM at room temperature. GFP-, YFP-, or TagRFP/mRFP-fusion proteins as well as BCECF-AM staining were analyzed with an FV-1000/IX81 confocal laser scanning microscope (Olympus) equipped with GaAsP detectors (Olympus) and a UPlanSApo ×60/1.20 (Olympus) objective, using the 488-, 515-, and 559-nm laser line, respectively. Images were subsequently processed using FluoView (Olympus) and Photoshop CS6 (Adobe). For 3D-reconstruction and surface rendering of BCECF-stained vacuoles, 90 Z-stacks images with 0.2-μm step size were obtained and subsequently processed, using Imaris 8 (Bitplane) with the following parameters: surface area detail level, 0.12 μm; diameter of largest sphere, 1.00 μm; background subtraction, enabled. The area/volume ratio was calculated using the following formula: ΔA/ΔV = area (μm^2)/[volume (μm^3)]^(1/3)^2. For the analysis of AMSH3-YFP signals on ARA7-positive WM compartments, ARA7-labeled structures with a minimal diameter of 1.5 μm were identified using Imaris 8 (Bitplane).

Transmission Electron Microscopy. Root tips from 5-d-old wild-type and *alix-2* seedlings were high-pressure frozen in a Baltec HP010, substituted in an AFS Leica device for 5 d at −90 °C in acetone containing 0.2% (wt/vol) uranyl acetate and 0.2% (vol/vol) glutaraldehyde, and embedded in Lowicryl HM20 resin (Electron Microscopy Sciences). Samples were sectioned and stained with 2% (wt/vol) uranyl acetate in 70% methanol and lead citrate [2.6% (wt/vol) lead nitrate and 3.5% (wt/vol) sodium citrate, pH12].

Note Added in Proof. While this paper was in production, a paper by Cardona-López et al. entitled "ESCRT-III-associated protein AtALIX mediates high affinity phosphate transporter trafficking to maintain phosphate homeostasis in Arabidopsis" has been accepted for publication in *The Plant Cell*. In this paper, the authors also reported that ALIX is essential in *Arabidopsis* and involved in intracellular trafficking and vacuole biogenesis.

ACKNOWLEDGMENTS. We thank Tomohiro Uemura, Takashi Ueda, and Akihiko Nakano (University of Tokyo) for kindly sharing published materials and for discussion; Yasushi Saeki, Yoko Kimura, and Keiji Tanaka for the pMal-p2p vector; and Genomanalyse im biologischen System Pflanze-Kolner Arabidopsis T-DNA and Nottingham *Arabidopsis* Stock Centre for providing *alix* mutant seeds. We are also grateful to Kamyar Hadian and Kenji Schorpp (Helmholtzzenrum München) for help with the MicroScale Thermophoresis measurement. This work was supported by grants from the Deutsche Forschungsgemeinschaft SFB924 (A10, to P.B.), the Spanish Ministry of Research, Development and Innovation BIO2013-46539-R (to V.R.), the National Science Foundation MCB1157824 (to M.S.O.), and the Deutsche Forschungsgemeinschaft IS221/4-1 and SFB924 (A06, to E.I.).

1. Kerscher O, Felberbaum R, Hochstrasser M (2006) Modification of proteins by ubiquitin and ubiquitin-like proteins. *Annu Rev Cell Dev Biol* 22:159–180.
2. Vierstra RD (2009) The ubiquitin-26S proteasome system at the nexus of plant biology. *Nat Rev Mol Cell Biol* 10(6):385–397.
3. Komander D, Rape M (2012) The ubiquitin code. *Annu Rev Biochem* 81:203–229.
4. Platta HW, Stenmark H (2011) Endocytosis and signaling. *Curr Opin Cell Biol* 23(4): 393–403.
5. Haglund K, Dikic I (2012) The role of ubiquitylation in receptor endocytosis and endosomal sorting. *J Cell Sci* 125(Pt 2):265–275.
6. Shields SB, Piper RC (2011) How ubiquitin functions with ESCRTs. *Traffic* 12(10): 1306–1317.
7. Henne WM, Stenmark H, Emr SD (2013) Molecular mechanisms of the membrane sculpting ESCRT pathway. *Cold Spring Harb Perspect Biol* 5(9):a016766.
8. Reyes FC, Buono R, Otegui MS (2011) Plant endosomal trafficking pathways. *Curr Opin Plant Biol* 14(6):666–673.
9. Winter V, Hauser MT (2006) Exploring the ESCRTing machinery in eukaryotes. *Trends Plant Sci* 11(3):115–123.
10. Korbei B, et al. (2013) Arabidopsis TOL proteins act as gatekeepers for vacuolar sorting of PIN2 plasma membrane protein. *Curr Biol* 23(24):2500–2505.
11. Hershko A, Ciechanover A (1998) The ubiquitin system. *Annu Rev Biochem* 67: 425–479.
12. Komander D, Clague MJ, Urbé S (2009) Breaking the chains: Structure and function of the deubiquitinases. *Nat Rev Mol Cell Biol* 10(8):550–563.
13. Clague MJ, Coulson JM, Urbé S (2012) Cellular functions of the DUBs. *J Cell Sci* 125(Pt 2):277–286.
14. Isono E, Nagel MK (2014) Deubiquitylating enzymes and their emerging role in plant biology. *Front Plant Sci* 5:56.
15. Amerik AY, Hochstrasser M (2004) Mechanism and function of deubiquitinating enzymes. *Biochim Biophys Acta* 1695(1-3):189–207.
16. Tanaka N, et al. (1999) Possible involvement of a novel STAM-associated molecule "AMSH" in intracellular signal transduction mediated by cytokines. *J Biol Chem* 274(27):19129–19135.
17. Ishii N, et al. (2001) Loss of neurons in the hippocampus and cerebral cortex of AMSH-deficient mice. *Mol Cell Biol* 21(24):8626–8637.
18. McDonell LM, et al.; FORGE Canada Consortium (2013) Mutations in STAMBP, encoding a deubiquitinating enzyme, cause microcephaly-capillary malformation syndrome. *Nat Genet* 45(5):556–562.
19. Maytal-Kivity V, Reis N, Hofmann K, Glickman MH (2002) MPN+, a putative catalytic motif found in a subset of MPN domain proteins from eukaryotes and prokaryotes, is critical for Rpn11 function. *BMC Biochem* 3:28.
20. Isono E, et al. (2010) The deubiquitinating enzyme AMSH3 is required for intracellular trafficking and vacuole biogenesis in Arabidopsis thaliana. *Plant Cell* 22(6):1826–1837.
21. Katsiarimpa A, et al. (2013) The deubiquitinating enzyme AMSH1 and the ESCRT-III subunit VPS2.1 are required for autophagic degradation in Arabidopsis. *Plant Cell* 25(6):2236–2252.
22. McCullough J, Clague MJ, Urbé S (2004) AMSH is an endosome-associated ubiquitin isopeptidase. *J Cell Biol* 166(4):487–492.
23. Agromayor M, Martin-Serrano J (2006) Interaction of AMSH with ESCRT-III and deubiquitination of endosomal cargo. *J Biol Chem* 281(32):23083–23091.
24. Kyuuma M, et al. (2007) AMSH, an ESCRT-III associated enzyme, deubiquitinates cargo on MVB/late endosomes. *Cell Struct Funct* 31(2):159–172.
25. Ma YM, et al. (2007) Targeting of AMSH to endosomes is required for epidermal growth factor receptor degradation. *J Biol Chem* 282(13):9805–9812.
26. Katsiarimpa A, et al. (2011) The Arabidopsis deubiquitinating enzyme AMSH3 interacts with ESCRT-III subunits and regulates their localization. *Plant Cell* 23(8): 3026–3040.
27. Katsiarimpa A, et al. (2014) The ESCRT-III-interacting deubiquitinating enzyme AMSH3 is essential for degradation of ubiquitinated membrane proteins in Arabidopsis thaliana. *Plant Cell Physiol* 55(4):727–736.
28. Bissig C, Gruenberg J (2014) ALIX and the multivesicular endosome: ALIX in Wonderland. *Trends Cell Biol* 24(1):19–25.
29. Dowlatshahi DP, et al. (2012) ALIX is a Lys63-specific polyubiquitin binding protein that functions in retrovirus budding. *Dev Cell* 23(6):1247–1254.
30. Bissig C, et al. (2013) Viral infection controlled by a calcium-dependent lipid-binding module in ALIX. *Dev Cell* 25(4):364–373.
31. Keren-Kaplan T, et al. (2013) Structure-based in silico identification of ubiquitin-binding domains provides insights into the ALIX-V:ubiquitin complex and retrovirus budding. *EMBO J* 32(4):538–551.

32. Nikko E, Marini AM, André B (2003) Permease recycling and ubiquitination status reveal a particular role for Bro1 in the multivesicular body pathway. *J Biol Chem* 278(50):50732–50743.
33. Katoh K, et al. (2003) The ALG-2-interacting protein Alix associates with CHMP4b, a human homologue of yeast Snf7 that is involved in multivesicular body sorting. *J Biol Chem* 278(40):39104–39113.
34. Matsuo H, et al. (2004) Role of LBPA and Alix in multivesicular liposome formation and endosome organization. *Science* 303(5657):531–534.
35. Richardson LG, et al. (2011) Protein-Protein Interaction Network and Subcellular Localization of the Arabidopsis Thaliana ESCRT Machinery. *Front Plant Sci* 2:20.
36. Luhtala N, Odorizzi G (2004) Bro1 coordinates deubiquitination in the multivesicular body pathway by recruiting Doa4 to endosomes. *J Cell Biol* 166(5):717–729.
37. Finn RD, et al. (2014) Pfam: The protein families database. *Nucleic Acids Res* 42(Database issue):D222–D230.
38. Uemura T, et al. (2004) Systematic analysis of SNARE molecules in Arabidopsis: Dissection of the post-Golgi network in plant cells. *Cell Struct Funct* 29(2):49–65.
39. Uemura T, et al. (2012) Qa-SNAREs localized to the trans-Golgi network regulate multiple transport pathways and extracellular disease resistance in plants. *Proc Natl Acad Sci USA* 109(5):1784–1789.
40. Ueda T, Uemura T, Sato MH, Nakano A (2004) Functional differentiation of endosomes in Arabidopsis cells. *Plant J* 40(5):783–789.
41. Haas TJ, et al. (2007) The Arabidopsis AAA ATPase SKD1 is involved in multivesicular endosome function and interacts with its positive regulator LYST-INTERACTING PROTEIN5. *Plant Cell* 19(4):1295–1312.
42. Babst M, Wendland B, Estepa EJ, Emr SD (1998) The Vps4p AAA ATPase regulates membrane association of a Vps protein complex required for normal endosome function. *EMBO J* 17(11):2982–2993.
43. Kolb C, et al. (2015) FYVE1 is essential for vacuole biogenesis and intracellular trafficking in Arabidopsis. *Plant Physiol* 167(4):1361–1373.
44. Pashkova N, et al. (2013) The yeast Alix homolog Bro1 functions as a ubiquitin receptor for protein sorting into multivesicular endosomes. *Dev Cell* 25(5):520–533.
45. Wienken CJ, Baaske P, Rothbauer U, Braun D, Duhr S (2010) Protein-binding assays in biological liquids using microscale thermophoresis. *Nat Commun* 1:100.
46. Kim MS, Kim JA, Song HK, Jeon H (2006) STAM-AMSH interaction facilitates the deubiquitination activity in the C-terminal AMSH. *Biochem Biophys Res Commun* 351(3):612–618.
47. McCullough J, et al. (2006) Activation of the endosome-associated ubiquitin isopeptidase AMSH by STAM, a component of the multivesicular body-sorting machinery. *Curr Biol* 16(2):160–165.
48. Nikko E, André B (2007) Split-ubiquitin two-hybrid assay to analyze protein-protein interactions at the endosome: Application to Saccharomyces cerevisiae Bro1 interacting with ESCRT complexes, the Doa4 ubiquitin hydrolase, and the Rsp5 ubiquitin ligase. *Eukaryot Cell* 6(8):1266–1277.
49. Raymond CK, Howald-Stevenson I, Vater CA, Stevens TH (1992) Morphological classification of the yeast vacuolar protein sorting mutants: Evidence for a prevacuolar compartment in class E vps mutants. *Mol Biol Cell* 3(12):1389–1402.
50. Rojo E, Gillmor CS, Kovaleva V, Somerville CR, Raikhel NV (2001) VACUOLELESS1 is an essential gene required for vacuole formation and morphogenesis in Arabidopsis. *Dev Cell* 1(2):303–310.
51. Frigerio L, Hinz G, Robinson DG (2008) Multiple vacuoles in plant cells: Rule or exception? *Traffic* 9(10):1564–1570.
52. Zouhar J, Rojo E (2009) Plant vacuoles: Where did they come from and where are they heading? *Curr Opin Plant Biol* 12(6):677–684.
53. Löfke C, Dünser K, Scheuring D, Kleine-Vehn J (2015) Auxin regulates SNARE-dependent vacuolar morphology restricting cell size. *Elife* 4:e05868.
54. Babst M, Katzmann DJ, Estepa-Sabal EJ, Meerloo T, Emr SD (2002) Escrt-III: An endosome-associated heterooligomeric protein complex required for mvb sorting. *Dev Cell* 3(2):271–282.
55. Dejournett RE, et al. (2007) Phosphorylation of the proline-rich domain of Xp95 modulates Xp95 interaction with partner proteins. *Biochem J* 401(2):521–531.
56. Ali N, et al. (2013) Recruitment of UBPY and ESCRT exchange drive HD-PTP-dependent sorting of EGFR to the MVB. *Curr Biol* 23(6):453–461.
57. Row PE, et al. (2007) The MIT domain of UBPY constitutes a CHMP binding and endosomal localization signal required for efficient epidermal growth factor receptor degradation. *J Biol Chem* 282(42):30929–30937.
58. Pires R, et al. (2009) A crescent-shaped ALIX dimer targets ESCRT-III CHMP4 filaments. *Structure* 17(6):843–856.
59. Richter C, West M, Odorizzi G (2007) Dual mechanisms specify Doa4-mediated deubiquitination at multivesicular bodies. *EMBO J* 26(10):2454–2464.
60. Kim J, et al. (2005) Structural basis for endosomal targeting by the Bro1 domain. *Dev Cell* 8(6):937–947.
61. Rosso MG, et al. (2003) An *Arabidopsis thaliana* T-DNA mutagenized population (GABI-Kat) for flanking sequence tag-based reverse genetics. *Plant Mol Biol* 53(1-2):247–259.
62. Clough SJ, Bent AF (1998) Floral dip: A simplified method for Agrobacterium-mediated transformation of *Arabidopsis thaliana*. *Plant J* 16(6):735–743.
63. Isono E, Schwechheimer C (2010) Co-immunoprecipitation and protein blots. *Methods Mol Biol* 655:377–387.
64. Kalinowska K, Isono E (2014) Analysis of global ubiquitylation and ubiquitin-binding domains involved in endosomal trafficking. *Methods Mol Biol* 1209:189–202.
65. Hadian K, et al. (2011) NF-κB essential modulator (NEMO) interaction with linear and lys-63 ubiquitin chains contributes to NF-κB activation. *J Biol Chem* 286(29):26107–26117.
66. Dreze M, et al. (2010) High-quality binary interactome mapping. *Methods Enzymol* 470:281–315.
67. Shimada TL, Shimada T, Hara-Nishimura I (2010) A rapid and non-destructive screenable marker, FAST, for identifying transformed seeds of Arabidopsis thaliana. *Plant J* 61(3):519–528.

The Plant Cell, Vol. 25: 2236–2252, June 2013, www.plantcell.org

The Deubiquitinating Enzyme AMSH1 and the ESCRT-III Subunit VPS2.1 Are Required for Autophagic Degradation in *Arabidopsis*[C][W][OPEN]

Anthi Katsiarimpa,[a,1] Kamila Kalinowska,[a,1] Franziska Anzenberger,[a] Corina Weis,[b] Maya Ostertag,[b] Chie Tsutsumi,[c] Claus Schwechheimer,[a] Frédéric Brunner,[d] Ralph Hückelhoven,[b] and Erika Isono[a,2]

[a] Department of Plant Systems Biology, Technische Universität München, 85354 Freising, Germany
[b] Department of Phytopathology, Technische Universität München, 85354 Freising, Germany
[c] Department of Botany, National Museum of Nature and Science, Tsukuba 305-0005, Japan
[d] Department of Plant Biochemistry, Center for Plant Molecular Biology, Tübingen University, 72076 Tuebingen, Germany

In eukaryotes, posttranslational modification by ubiquitin regulates the activity and stability of many proteins and thus influences a variety of developmental processes as well as environmental responses. Ubiquitination also plays a critical role in intracellular trafficking by serving as a signal for endocytosis. We have previously shown that the *Arabidopsis thaliana* ASSOCIATED MOLECULE WITH THE SH3 DOMAIN OF STAM3 (AMSH3) is a deubiquitinating enzyme (DUB) that interacts with ENDOSOMAL COMPLEX REQUIRED FOR TRANSPORT-III (ESCRT-III) and is essential for intracellular transport and vacuole biogenesis. However, physiological functions of AMSH3 in the context of its ESCRT-III interaction are not well understood due to the severe seedling lethal phenotype of its null mutant. In this article, we show that *Arabidopsis* AMSH1, an AMSH3-related DUB, interacts with the ESCRT-III subunit VACUOLAR PROTEIN SORTING2.1 (VPS2.1) and that impairment of both AMSH1 and VPS2.1 causes early senescence and hypersensitivity to artificial carbon starvation in the dark similar to previously reported autophagy mutants. Consistent with this, both mutants accumulate autophagosome markers and accumulate less autophagic bodies in the vacuole. Taken together, our results demonstrate that AMSH1 and the ESCRT-III-subunit VPS2.1 are important for autophagic degradation and autophagy-mediated physiological processes.

INTRODUCTION

Reversible posttranslational modification by the small modifier protein ubiquitin is a critical step for regulating protein activities and abundance in many plant signaling pathways and cellular processes (reviewed in Vierstra, 2009). Thus, ubiquitinating as well as deubiquitinating enzymes (DUBs) play key roles in diverse cellular functions. Whereas soluble proteins can be degraded by the 26S proteasome upon polyubiquitination, plasma membrane–bound proteins are degraded by vacuolar proteases following ubiquitin-dependent endocytosis (reviewed in Zelazny et al., 2011). In plants, the auxin efflux facilitator PIN-FORMED2 (PIN2), the flagellin receptor FLAGELLIN-SENSITIVE2, the water channel PLASMA MEMBRANE INTRINSIC PROTEIN2, the iron transporter IRON-REGULATED TRANSPORTER1, and the boron transporter REQUIRES HIGH BORON1 have been shown to be ubiquitinated prior to endocytosis (Abas et al., 2006; Göhre et al., 2008; Lee et al., 2009; Barberon et al., 2011; Kasai et al., 2011). Furthermore, translational fusion of monoubiquitin to PLASMA MEMBRANE PROTON ATPASE (PMA) was shown to be sufficient for triggering endocytosis and vacuolar transport via multivesicular bodies (MVBs) (Herberth et al., 2012). However, how exactly ubiquitin-dependent endocytosis is regulated at the molecular level in plants and contributes to different physiological processes remains to be elucidated.

We have recently shown that the *Arabidopsis thaliana* DUB, ASSOCIATED MOLECULE WITH THE SH3 DOMAIN OF STAM3 (AMSH3), interacts with the endocytosis machinery and is essential for plant development (Isono et al., 2010; Katsiarimpa et al., 2011). AMSH3 is closely related to the human DUBs AMSH and AMSH-LP, which belong to the class of eukaryotic DUBs and metalloproteases with an MPR1, PAD1 N-terminal+ (MPN+) domain (Tanaka et al., 1999; Maytal-Kivity et al., 2002; Komander et al., 2009). Two MPN+ domain proteins, namely, REGULATORY PARTICLE NON-ATPASE11 (RPN11) (Glickman et al., 1998; Verma et al., 2002) and COP9 SIGNALOSOME5 (CSN5) (Chamovitz et al., 1996; Cope et al., 2002), are subunits of stable multiprotein complexes. By contrast, *Arabidopsis* AMSH3 is not part of a stable higher molecular weight complex (Isono et al., 2010), and, in contrast with RPN11 and CSN5, AMSH proteins are active as monomers (McCullough et al., 2004). AMSH proteins have essential functions in the development of animals and plants, since AMSH-deficient mice die postnatum with loss of neurons in the hippocampus (Ishii et al., 2001), and *Arabidopsis amsh3* null mutations are seedling lethal and cause a number of intracellular trafficking defects (Isono et al., 2010).

[1] These authors contributed equally to this work.
[2] Address correspondence to erika.isono@wzw.tum.de.
The author responsible for distribution of materials integral to the findings presented in this article in accordance with the policy described in the Instructions for Authors (www.plantcell.org) is: Erika Isono (erika.isono@wzw.tum.de).
[C] Some figures in this article are displayed in color online but in black and white in the print edition.
[W] Online version contains Web-only data.
[OPEN] Articles can be viewed online without a subscription.
www.plantcell.org/cgi/doi/10.1105/tpc.113.113399

Autophagy (macroautophagy) is another vacuolar degradation pathway, by which cytosolic components or organelles are selectively or nonselectively transported to the vacuole/lysosome for degradation (reviewed in Klionsky and Ohsumi, 1999). Since the discovery of *AUTOPHAGY-RELATED* (*ATG*) genes from yeast in the 1990s, intensive genetic and molecular analyses have identified over 30 autophagy-related genes. Autophagy is also implicated in a diverse array of physiological and pathological effects in mammals (reviewed in Mizushima and Levine, 2010). *ATG* genes are highly conserved also in plants, and mutant analyses have shown them to have central functions in nutrient remobilization during starvation and senescence (Doelling et al., 2002; Yoshimoto et al., 2004, 2009; Sláviková et al., 2005; Thompson et al., 2005; Inoue et al., 2006; Phillips et al., 2008; Chung et al., 2009).

The individual steps of autophagosome formation have been revealed by ultrastructural and biochemical studies (reviewed in Klionsky and Ohsumi, 1999). First, isolation membranes or phagophores are formed, probably from the endoplasmic reticulum, which will then engulf parts of the cytosol in autophagosomes with characteristic double-membrane structures. Autophagosomes are then targeted to vacuoles or lysosomes in which their contents are degraded by resident proteases. Alternatively, depending on organism and cell type, autophagosomes may undergo fusion with late endosomes or MVBs to form amphisomes. Amphisomes can then fuse to vacuoles/lysosomes to become autolysosomes, in which the autophagosomal contents are degraded. In mammals and flies, several studies have reported that intact MVBs as well as a functional ENDOSOMAL COMPLEX REQUIRED FOR TRANSPORT-III (ESCRT-III), a core complex in MVB sorting, are necessary for proper autophagosomal degradation (Filimonenko et al., 2007; Lee et al., 2007; Rusten et al., 2007; Han et al., 2012). However, a role for ESCRT-III in the plant autophagy pathway has not been demonstrated yet.

We have previously shown that *Arabidopsis* AMSH3 interacts with the ESCRT-III subunits VACUOLAR PROTEIN SORTING2.1 (VPS2.1) and VPS24.1 (Katsiarimpa et al., 2011). The embryo- and seedling-lethal phenotypes of *vps2.1* and *amsh3* mutations, respectively, have prevented us so far from analyzing the physiological functions of VPS2.1 and AMSH3. In this study, we characterize the *Arabidopsis amsh1-1* mutant, which has reduced levels of the *AMSH3*-related gene, *AMSH1*.

Unlike the *amsh3* null mutants, the *amsh1-1* knockdown mutant does not have an apparent growth defect. However, *amsh1-1* accumulates ubiquitinated proteins and shows chlorosis when transferred to the dark, a phenotype reminiscent of autophagy mutants. Furthermore, *amsh1-1* accumulates ATG8 in the dark and accumulates less autophagic bodies in the vacuole. AMSH1, like AMSH3, directly interacts with the ESCRT-III subunit VPS2.1. Plants that overexpress a dominant-negative form of *VPS2.1* are deficient in endocytosis, accumulate ATG8, and show hypersensitivity to dark treatment. Similar to previously identified autophagy-defective *atg* mutants from *Arabidopsis*, *amsh1-1* shows also altered susceptibility toward pathogen infection. Together, the results presented here demonstrate the importance of AMSH1 and VPS2.1 in autophagic degradation and in the physiological processes related to it.

RESULTS

Arabidopsis AMSH Genes Are Evolutionary Conserved and Belong to Independent Clades within the *AMSH* Gene Family

AMSH proteins are widely conserved in eukaryotes. In the *Arabidopsis* genome, three *AMSH* genes can be found according to sequence similarity in the catalytic domain (Maytal-Kivity et al., 2002; Isono et al., 2010). To understand the evolutionary origin of the three *Arabidopsis AMSH* genes, we identified sequences related to *Arabidopsis AMSHs* in the genomes of 10 fully sequenced plant species (*Physcomitrella patens*, *Selaginella moellendorffii*, maize [*Zea mays*], sorghum [*Sorghum bicolor*], rice [*Oryza sativa*], *Populus trichocarpa*, castor bean [*Ricinus communis*], soybean [*Glycine max*], grape [*Vitis vinifera*], and *Arabidopsis lyrata*). Phylogenic analysis based on nucleotide sequences of the resulting 37 genes showed that each of the three *Arabidopsis AMSH* genes is part of an independent clade with other eudicot homologs, suggesting an evolutionary conservation of the three genes in eudicot species (Figure 1; see Supplemental Data Set 1 online).

The monophyly of *AMSH2* with high support allowed us to infer that the hitherto uncharacterized *AMSH2* genes have been conserved at least from ancestral angiosperms. By contrast, *AMSH1* and *AMSH3* may have originated from a eudicot-specific gene duplication event after the separation from monocots. Alternatively, *AMSH1* and *AMSH3* may have already been present before the separation of monocots and eudicots, and monocots may have lost their copy of the *AMSH1* gene and gone through an independent gene duplication event in the course of evolution.

AMSH1 and *AMSH3* Show Synergistic Interaction

We next wanted to establish whether the three *Arabidopsis AMSH* genes have redundant functions. We previously identified two *amsh3* mutant null alleles (Isono et al., 2010) and now investigated additional T-DNA insertion lines of *AMSH1* and *AMSH2*. For *AMSH1*, we identified one T-DNA insertion line, which we named *amsh1-1*, with reduced *AMSH1* transcript level. *amsh1-1* carried an insertion in the 5′-untranslated region of the gene (Figure 2A), and the transcript level of *AMSH1* was reduced more than 10-fold compared with the wild type (see Supplemental Figure 1A online). AMSH1 protein levels were also strongly decreased in this mutant (Figure 2F). Since *AMSH1* transcripts were still detectable, and since immunoblotting with the anti-AMSH1 antibody showed a weak band in *amsh1-1*, it is likely that *amsh1-1* is not a complete loss-of-function mutant but rather a weak mutant allele with compromised AMSH1 function. By contrast, we found that the available T-DNA insertion line of *AMSH2* did not have significantly reduced *AMSH2* transcript levels (data not shown).

When grown in continuous light, homozygous *amsh1-1* plants did not show obvious developmental phenotypes (Figure 2B). However, when we introduced the *amsh3-2* allele into *amsh1-1*, the resulting *amsh1-1/amsh1-1 AMSH3/amsh3-2* mutant (*a1/a1 A3/a3*) showed severe growth defects and early senescence (Figures 2B to 2D), indicating a synergistic interaction between *AMSH1* and *AMSH3*.

AMSH1 is an active enzyme and its catalytic MPN+ domain possesses DUB activity toward K63-linked, but not K48-linked, ubiquitin chains. The activity of the AMSH1 MPN+ domain was

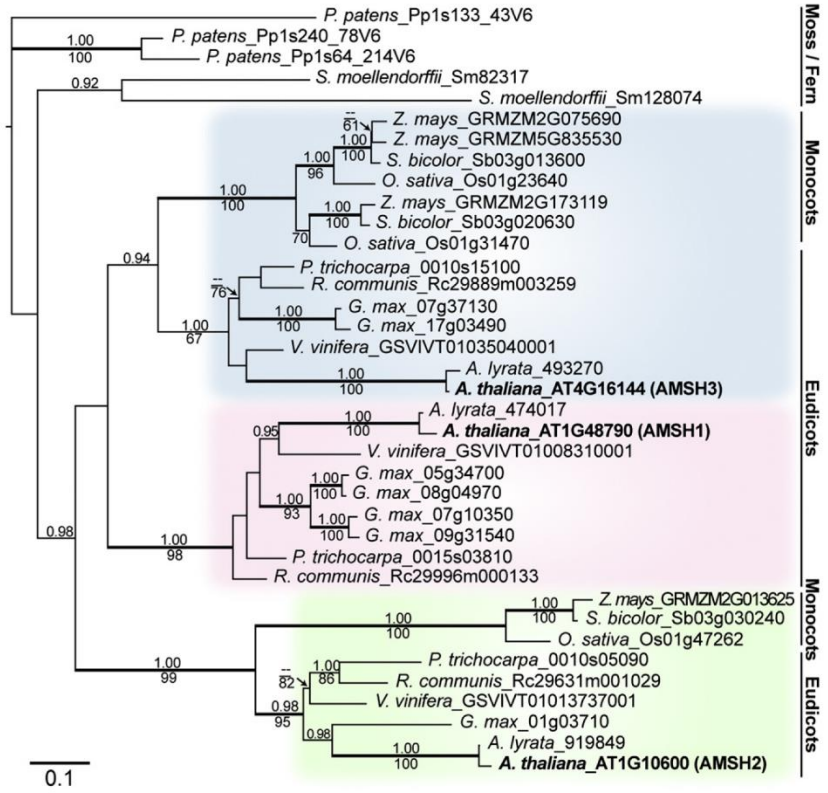

Figure 1. AMSH1, AMSH2, and AMSH3 Belong to Independent Clades.

Phylogenetic analysis of AMSH genes from *P. patens*, *S. moellendorffii*, maize, sorghum, rice, *P. trichocarpa*, castor bean, soybean, grape, *A. lyrata*, and *Arabidopsis* using P. patens_Pp133_43V6 as an outgroup. A maximum likelihood tree (-ln L = 9462.34) based on the region surrounding the MPN+ domain (549 bp) is shown. The alignment used for generating the phylogenic tree is available as Supplemental Data Set 1 online. Values above branches indicate posterior probabilities (>0.9) calculated by Bayesian analysis, and those below branches indicate maximum parsimony bootstrap values (>60). Thick branches are highly supported (posterior probabilities P > 0.95 and bootstrap values >90). Bar = 0.1 amino acid substitutions per site.
[See online article for color version of this figure.]

inhibited by the metalloprotease inhibitor 1,10-phenanthroline (Figure 2E), indicating that like other MPN+ domain proteins, AMSH1 activity is also dependent on metal ions coordinated in the MPN+ domain. Molecular analysis showed that the *amsh1-1* homozygous mutants, in spite of their normal growth, accumulated ubiquitinated proteins at a higher level than the wild type, and *amsh1-1/amsh1-1 AMSH3/amsh3-2* accumulated ubiquitin conjugates at an even higher level (Figure 2F). Interestingly, *amsh1-1* did not show obvious decreases in its monoubiquitin levels (see Supplemental Figure 1B online), suggesting that the depletion of free ubiquitin molecules is probably not the cause of its phenotype, in contrast with the yeast DUB mutant *doa4* (Swaminathan et al., 1999).

AMSH1 and *AMSH3* Have Distinct Expression Patterns

To test whether *AMSH1* and *AMSH3* are expressed in the same tissues, we generated promoter–β-glucuronidase (GUS) fusions for both genes and analyzed the expression patterns. During seedling development, the expression of both *AMSH1* and *AMSH3* could be observed in leaves and hypocotyls as well as in roots, though their expression patterns overlapped only partially (Figures 3A to 3F). Furthermore, *AMSH3* was strongly expressed in emerging lateral roots, whereas *AMSH1* expression seemed to be excluded from this region (Figures 3G to 3L). The largely differential expression pattern of *AMSH1* and *AMSH3* implies that the two genes might be under different spatio-temporal regulation and that AMSH1 and AMSH3 functions are not interdependent.

amsh1-1 Shows Hypersensitivity to Dark Treatment

The senescence phenotype of *amsh1/amsh1 AMSH3/amsh3* caught our attention since we observed that *amsh1-1* also showed early senescence when grown under short-day conditions with 8 h light (110 to 120 μmol m^{-2} s^{-1} light) and 16 h

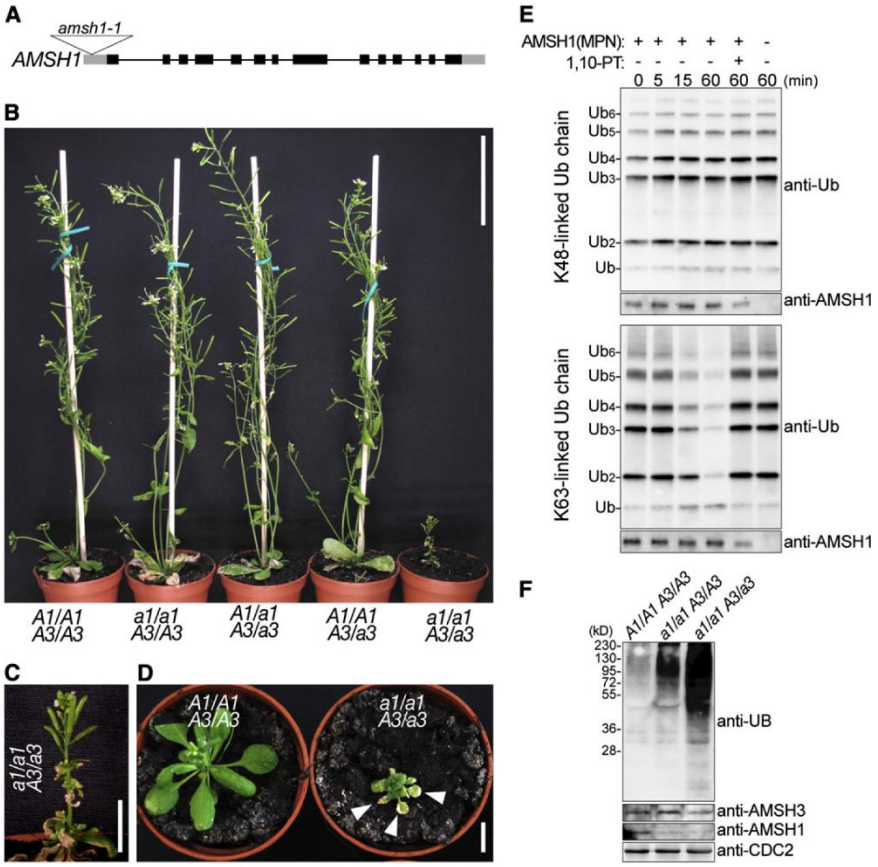

Figure 2. *amsh1/amsh1 AMSH3/amsh3* Is Dwarf and Accumulates Ubiquitinated Proteins.

(A) T-DNA insertion site of *amsh1-1*. Lines indicate introns and boxes indicate exons (black boxes, coding region; gray boxes, untranslated regions). The triangle indicates the site of T-DNA insertion.

(B) Phenotypes of progeny from an *amsh1-1 amsh3-2* double heterozygous (*A1/a1 A3/a3*) plant. The *amsh1-1* homozygous mutant in an *amsh3-2* heterozygous background (*a1/a1 A3/a3*) shows dwarfism. Bar = 6 cm.

(C) Magnification of the *a1/a1 A3/a3* plant shown in **(B)**. Bar = 1 cm.

(D) Photographs of an *a1/a1 A3/a3* plant in comparison with a wild-type (*A1/A1 A3/A3*) plant of the same age. Note that the *a1/a1 A3/a3* mutant plant exhibits early senescence, indicated by arrowheads. Bar = 1 cm.

(E) DUB assay with K48- or K63-linked ubiquitin chains. The MPN+ domain of AMSH1 was incubated with or without the metalloprotease inhibitor 1,10-phenanthroline (1,10-PT). The reactions were terminated at the indicated time points, and hydrolysis of ubiquitin chains was detected by immunoblotting using an anti-UB antibody. The amount of AMSH1 (MPN+) in each reaction was verified by immunoblotting with an anti-AMSH1 antibody.

(F) Immunoblots with anti-UB, anti-AMSH3, and anti-AMSH1 antibodies on total protein extracts from the wild type (*A1/A1 A3/A3*), homozygous *amsh1-1* (*a1/a1 A3/A3*), and *a1/a1 A3/a3*. CDC2 is used as a loading control.

dark. This phenotype was not apparent in *amsh1-1* plants that had been grown in 10 h light/14 h dark (see Supplemental Figure 1E online), indicating that daylength has a critical effect on the physiology of *amsh1-1*.

Early senescence is, among others, a hallmark of autophagy mutants (Doelling et al., 2002; Thompson et al., 2005; Xiong et al., 2005; Yoshimoto et al., 2009). Since autophagy is also associated with intracellular trafficking and protein degradation (Rojo et al., 2001; Surpin et al., 2003; Zouhar et al., 2009), a function associated with AMSH3 (Isono et al., 2010; Katsiarimpa et al., 2011), we examined the autophagy pathway in *amsh1-1* in more detail.

We first analyzed the response of *amsh1-1* to artificial carbon starvation upon transfer to the dark. Wild-type seedlings normally survive the prolonged dark treatment, probably due to a functional autophagic nutrient recycling pathway, whereas

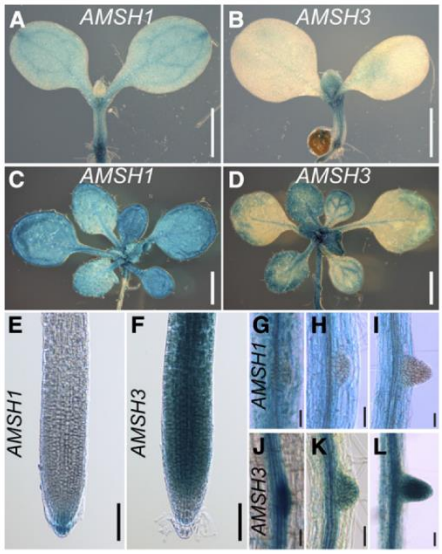

Figure 3. *AMSH1* and *AMSH3* Are Differentially Expressed during Plant Development.

Histochemical assay showing expression patterns of *AMSH1pro*:*GUS* (**[A]**, **[C]**, **[E]**, and **[G]** to **[I]**) and *AMSH3pro*:*AMSH3-GUS* (**[B]**, **[D]**, **[F]**, and **[J]** to **[L]**).
(A) and **(B)** Seven-day-old seedlings. Bars = 0.5 mm.
(C) and **(D)** Fourteen-day-old seedlings. Bars = 1 mm.
(E) and **(F)** Root tips of 7-d-old seedlings. Bars = 0.1 mm.
(G) to **(L)** Emerging lateral roots of 14-d-old seedlings.

mutants of autophagic components show chlorosis upon prolonged dark treatment (Doelling et al., 2002; Thompson et al., 2005; Xiong et al., 2005; Phillips et al., 2008; Yoshimoto et al., 2009; Chung et al., 2010). To investigate whether *amsh1-1* also has altered response to dark treatment, we transferred wild-type and *amsh1-1* seedlings for 5 d to the dark. Indeed, while wild-type seedlings were still green after 5 d of dark treatment, *amsh1-1* seedlings became yellowish and had reduced chlorophyll content (51.7% in comparison with the wild type) (Figures 4A and 4B). This result suggests that *amsh1-1*, like previously reported *atg* mutants, may have also defects in the autophagic pathway. The dark-induced chlorosis and the accumulation of ubiquitinated proteins in *amsh1-1* could be complemented by a genomic fragment of *AMSH1*, indicating that the down-regulation of *AMSH1* in *amsh1-1* is indeed the cause of these phenotypes (see Supplemental Figures 1C and 1D online).

amsh1-1 Is Defective in Autophagic Degradation

To further assess the autophagy pathway in *amsh1-1*, we monitored the abundance of ATG8, which is a structural component of autophagosomes (Yoshimoto et al., 2004). ATG8 can be used as an autophagy marker, since its accumulation implies defect in the autophagy pathway. ATG8 accumulates either upon inhibition of degradation by the application of protease inhibitors like E-64d (Inoue et al., 2006) or in mutants defective in autophagosome formation (Yoshimoto et al., 2004; Thompson et al., 2005; Phillips et al., 2008; Chung et al., 2010). Indeed, when wild-type and *atg7-2* (Hofius et al., 2009) seedlings were incubated with E-64d, E64-d–induced accumulation of ATG8 was observed in the wild type, while *atg7-2* accumulated ATG8 without E-64d (see Supplemental Figure 2C online).

The amount of ATG8 was comparable in light-grown wild type and *amsh1-1* (Figure 4C, top panel). However, when the seedlings were grown in the dark for 5 d to induce autophagy, high amounts of ATG8 accumulated in *amsh1-1* in comparison with the wild type (Figure 4C, bottom panel), suggesting that *amsh1-1* is less efficient in autophagic degradation. The accumulation of ATG8 was enhanced in both genotypes upon E-64d treatment, indicating that even in *amsh1-1*, autophagic degradation was not completely inhibited. Transcript levels of all *ATG8* isoforms in *amsh1-1* were comparable to the wild type under this condition (see Supplemental Figure 2E online), inferring that the accumulation of ATG8 is not a consequence of transcriptional misregulation in *amsh1-1*.

We next wanted to examine whether selective autophagy is also impaired in *amsh1-1*. As opposed to bulk autophagy, during selective autophagy, specific cargo proteins are recognized by cargo adaptors and degraded via the autophagy pathway. NEIGHBOR of BRCA1 GENE1 (NBR1) is a cargo receptor and substrate of selective autophagy (Svenning et al., 2011). NBR1 accumulated in *atg7-2* as previously reported, but not in *amsh1-1* (Figure 4D; see Supplemental Figure 2D online), suggesting that NBR1-mediated selective autophagy is not defective in *amsh1-1*. The fact that *amsh1-1* does not show bulk and selective autophagic degradation defects in light suggests that residual AMSH1 in *amsh1-1* is sufficient for both processes in light. However, the low amount of AMSH1 probably becomes limiting in the dark, where bulk autophagy, but not NBR1-mediated selective autophagy, is highly activated.

To distinguish between the defects in autophagic protein degradation and autophagosome formation, we made use of the dye monodansylcadaverine (MDC), which stains autophagic bodies (Contento et al., 2005) upon treatment with the vacuolar protease inhibitor E-64d. E-64d inhibits the degradation of autophagic bodies in the vacuole and thus causes accumulation of MDC-stained autophagic bodies in the vacuoles stained with 2′,7′-bis-(2-carboxyethyl)-5-(and 6)carboxyfluorescein acetoxymethyl ester (BCECF-AM) (Figure 4E). The accumulation of MDC-positive aggregates was not detected in *atg7-2* (see Supplemental Figure 2A online), indicating that although it accumulates ATG8, the formation of autophagosomes is not visible in this mutant. Furthermore, E-64d–induced MDC-positive vacuolar aggregates colocalized with the autophagosome marker GFP-ATG8e (Contento et al., 2005) (Figure 4F), but not with the late-endosome marker YFP-ARA7 (Geldner et al., 2009) (see Supplemental Figure 2B online), corroborating the specificity of MDC staining under our experimental conditions.

amsh1-1, in contrast with *atg7-2*, is not impaired in the formation of autophagosomes, since MDC-stained compartments were visible in *amsh1-1*. However, accumulation of E-64d–induced aggregates was less apparent in *amsh1-1* compared with the wild type when maximal projection images of z-stacks obtained

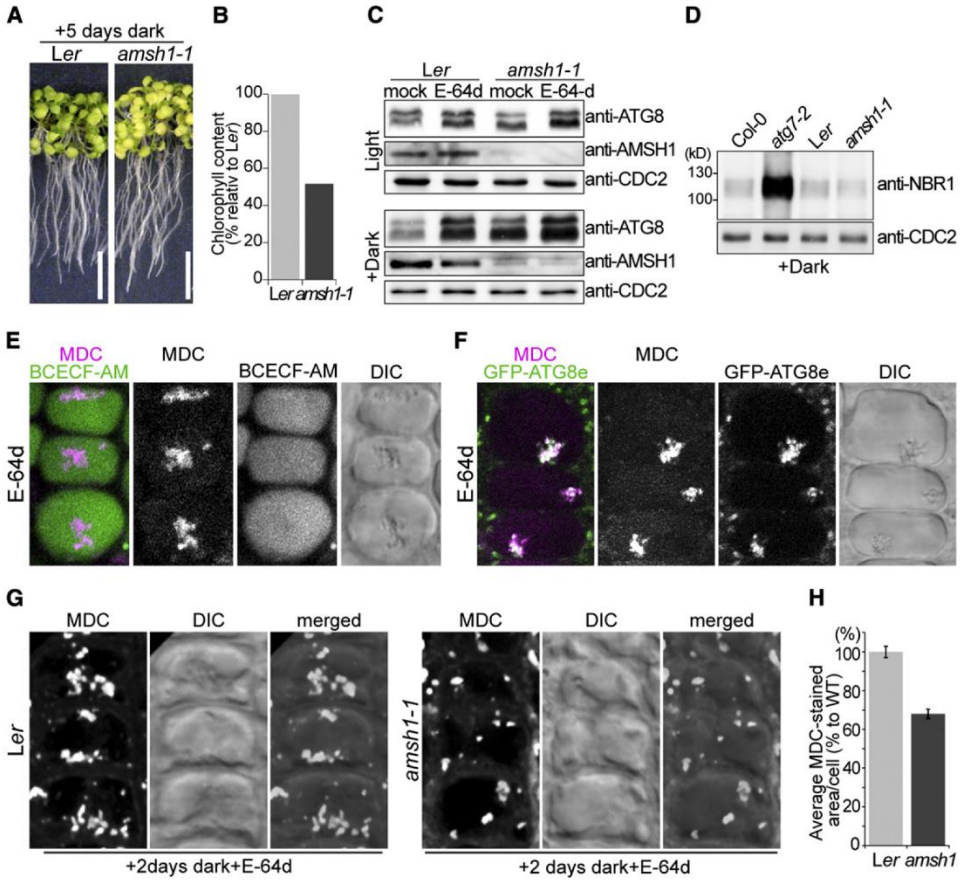

Figure 4. *amsh1-1* Is Deficient in Autophagic Degradation.

(A) Photographs of wild-type (*Ler*) and *amsh1-1* seedlings after 5 d in the dark (left panel). Seedlings were grown 7 d on half-strength MS under long-day conditions before transfer to dark. Note that starvation-induced chlorosis is enhanced in *amsh1-1* compared with the wild type. Bars = 1 cm.
(B) Total chlorophyll content of seedlings in **(A)**. Value of the wild type was set to 100%.
(C) Immunoblot with an anti-ATG8 antibody. Total proteins were extracted from seedlings grown in light for 12 d (Light, top panel) or as in **(A)** (Dark, bottom panel) before treatment with either DMSO (mock) or E-64d.
(D) Total proteins were extracted from seedlings grown as in **(A)** and subjected to immunoblot with an anti-NBR1 antibody. *atg7-2* is used as a positive control and CDC2 is used as loading control.
(E) Confocal images of MDC-stained wild-type root epidermal cells. BCECF-AM was used to visualize the vacuoles. Seedlings were grown as in **(A)** and treated with E-64d for 1 h before staining with MDC. Note that upon E-64d treatment, MDC positive autophagic bodies accumulate in the BCECF-AM–stained vacuole.
(F) Confocal images of MDC-stained GFP-ATG8e–expressing root epidermal cells. Seedlings were grown as in **(A)** and treated 6 h with E-64d before staining with MDC.
(G) Wild-type (*Ler*) and *amsh1-1* seedlings were grown as in **(A)**. Seedlings were subsequently treated with E-64d for 1 h and stained with MDC. Confocal images (maximal projection) of MDC-stained root epidermal cells of the wild type (*Ler*, left panel) and *amsh1-1* (right panel) are shown.
(H) Quantification of MDC-staining positive area per cell in the wild type (*Ler*) and *amsh1-1* ($n = 831$ for *Ler* and $n = 749$ for *amsh1-1*). Photographs taken in **(G)** were analyzed by the FluoView software, and the values of the wild type were set to 100%. Error bars indicate SE.

by confocal microscopy were analyzed (Figure 4G). Subsequent quantification of the thus imaged MDC-positive signal area in individual cells (n = 831 for the wild type, and n = 749 for *amsh1-1*) showed that *amsh1-1* had reduced accumulation of autophagic bodies in the vacuole when compared with the wild type (68% of average MDC-stained area per cell compared with the wild type) (Figure 4H). This result indicates that autophagosomes are less efficiently targeted to the vacuole in *amsh1-1*.

AMSH1 Interacts with the ESCRT-III Subunit VPS2.1 through Its MIT Domain

We next investigated whether the inhibition of bulk autophagic degradation in *amsh1-1* is a consequence of altered intracellular trafficking. For this purpose, we examined the interaction of AMSH1 with the endocytosis machinery. AMSH1, like AMSH3, contains an N-terminal microtubule interacting and trafficking (MIT) domain, which we had previously shown to be important for the interaction with the MIT interacting motif (MIM) present in ESCRT-III subunits (Katsiarimpa et al., 2011). We therefore tested in a directed yeast two-hybrid (Y2H) assay whether AMSH1 can also interact with the ESCRT-III core subunits VPS2.1, VPS20.1, VPS24.1, and SUCROSE NON-FERMENTING7.1 (SNF7.1) (Winter and Hauser, 2006; Richardson et al., 2011; Shahriari et al., 2011). Among the four tested subunits, AMSH1 interacted only with VPS2.1 (Figure 5A; see Supplemental Figure 3A online).

The MIT domain is necessary for the interaction of AMSH1 with VPS2.1 since deletion of this domain led to loss of interaction (Figure 5B; see Supplemental Figure 3B online). Moreover, AMSH1 and VPS2.1 interact directly through the 154–amino acid MIT and 17–amino acid MIM region, respectively, as shown by an in vitro binding assay (Figure 5C). Altogether, these data indicate that AMSH1, like AMSH3, may play a role in ESCRT-III-mediated intracellular trafficking pathway by interacting with VPS2.1.

Overexpression of VPS2.1-GFP Causes Inhibition of Endocytosis

To investigate whether VPS2.1 is also involved in the same physiological pathway as AMSH1, we generated transgenic plants that express VPS2.1 as a C-terminal fusion with green fluorescent protein (*35Spro*:*VPS2.1-GFP*). C-terminal fusions of ESCRT-III subunits, including VPS2.1, with large proteins, such as GFP, have been shown to disturb ESCRT-III function in other organisms due to their aggregation in class-E compartments (Howard et al., 2001; Teis et al., 2008; Teis et al., 2010). Indeed, we found that *35Spro*:*VPS2.1-GFP* plants occasionally showed abnormal growth already at the seedling stage (see Supplemental Figure 4A online) and that part of the overexpressed VPS2.1-GFP localized to large aggregates in the cytosol that may represent class-E compartments (see Supplemental Figure 4B online). After transfer to soil, adult *35Spro*:*VPS2.1-GFP* plants, similarly to *amsh1-1*/*amsh1-1 amsh3-2*/*AMSH3* plants, showed early leaf senescence and a severe dwarf phenotype (Figure 6A) and were mostly sterile (data not shown).

We then tested whether the expression of *VPS2.1-GFP* has an inhibitory effect on endocytosis of plasma membrane cargo. For this purpose, we examined the endocytosis of an artificial MVB cargo PMA-GFP-UB (Herberth et al., 2012) upon coexpression with *35Spro*:*VPS2.1-TagRFP*, a construct expressing *VPS2.1* with a C-terminal *TagRFP* in *Arabidopsis* cell culture–derived protoplasts. Fusion of monoubiquitin to PMA-GFP alters the intracellular distribution of this normally plasma membrane–localized protein, which then becomes visible in vesicles and in the vacuolar lumen (Figure 6B). SKD1/Vps4p is an AAA-ATPase required for the disassembly of ESCRT-III (Babst et al., 1997). As

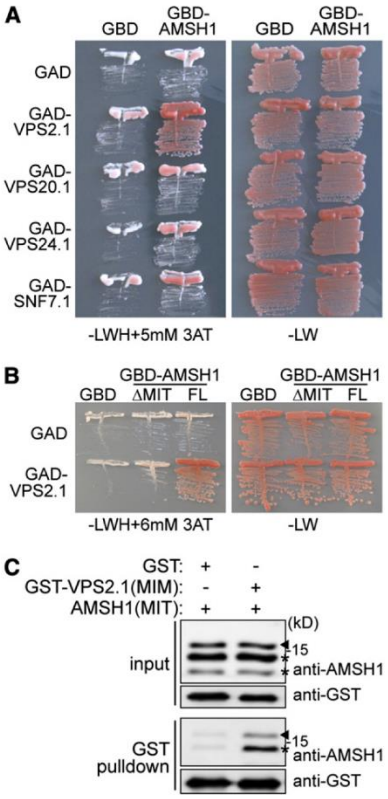

Figure 5. AMSH1 Interacts with ESCRT-III Subunit VPS2.1 through the MIT Domain.

(A) Y2H analysis of GBD-AMSH1 with GAD-fused ESCRT-III subunits VPS2.1, VPS20.1, VPS24.1, and SNF7.1. Transformants were plated on medium lacking Leu, Trp, and His (-LWH) supplemented with 5 mM 3-Amino-1,2,4-triazole (3-AT) (left panel) to test for their auxotrophic growth or on medium lacking Leu and Trp (-LW) (right panel).
(B) Y2H analysis of GBD-AMSH1 (FL; full-length) and GBD-AMSH1(ΔMIT) with GAD-VPS2.1. Transformants were grown on –LWH+6 mM 3-AT (left panel) or -LW (right panel) medium to test for their auxotrophic growth.
(C) In vitro binding assay of the MIT domain of AMSH1 with GST or GST-fused MIM domain of VPS2.1. After GST pulldown, bead-bound proteins were analyzed by immunoblotting using anti-AMSH1 and anti-GST antibodies. Arrowheads indicate the positions of AMSH1(MIT), and asterisks indicate degradation products.
[See online article for color version of this figure.]

previously reported, coexpression of an inactive SKD1(EQ), but not that of wild-type SKD1(WT), results in the inhibition of vacuolar targeting of PMA-GFP-UB (Figure 6C). Similarly, we found PMA-GFP-UB signals to be excluded from the vacuolar lumen upon coexpression with *35Spro*:*VPS2.1-TagRFP*, suggesting that the C-terminal fluorophore fusion of VPS2.1 has an inhibitory effect similar to SKD1(EQ) (Figure 6C).

We next analyzed the vacuolar degradation of the auxin efflux facilitator PIN2, a well-characterized cargo of the MVB pathway (Abas et al., 2006; Spitzer et al., 2009). While no apparent accumulation of PIN2 was observed in *amsh1-1* (see Supplemental Figure 4C online), ubiquitinated proteins as well as PIN2 accumulated in *35Spro*:*VPS2.1-GFP* seedlings at a higher level compared with wild-type seedlings (Figures 6D and 6E). Since the transcript levels of *PIN2* were not consistently and strongly upregulated in *35Spro*:*VPS2.1-GFP* seedlings (see Supplemental Figure 4D online), accumulation of PIN2 is probably a consequence of a posttranscriptional mechanism. Together, these results indicate that the overexpression of the dominant-negative *VPS2.1-GFP* has an inhibitory effect on the degradation of (ubiquitinated) MVB cargo, probably due to impaired ESCRT-III and MVB function.

VPS2.1-GFP–Overexpressing Plants Are Defective in Autophagic Degradation

Since our studies had implicated the VPS2.1-interactor AMSH1 in autophagy, we examined the response of *VPS2.1-GFP*–overexpressing plants to dark treatment. After 5 d in the dark, *35Spro*:*VPS2.1-GFP* seedlings, like *amsh1-1* seedlings, showed strong chlorosis and reduction in chlorophyll content (39 and 32% compared with the wild type) (Figures 7A and 7B).

When we analyzed ATG8 protein abundance in *35Spro*:*VPS2.1-GFP* seedlings, more ATG8 was detected even under normal growth conditions and a further increase was observed after transfer to the dark (Figure 7C). Expression of *ATG8a-i* was not increased in these lines, indicating that the accumulation of

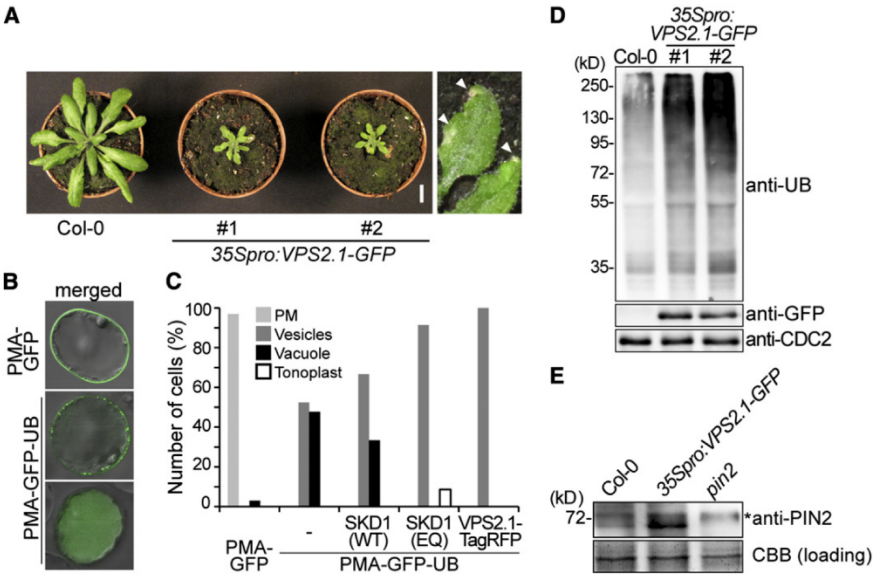

Figure 6. *VPS2.1-GFP*–Overexpressing Seedlings Are Deficient in Endocytosis and Accumulate PIN2.

(A) *VPS2.1-GFP*–overexpressing plants are dwarf and exhibit an early senescence phenotype. Plants of two independent transgenic lines (#1 and #2) are shown together with a wild-type plant (Col-0) of the same age. Magnification of senescing leaves (arrowheads) is shown on the far right. Bar = 1cm.

(B) Analysis of the differential intracellular distribution of PMA-GFP and PMA-GFP-UB. PMA-GFP shows predominantly plasma membrane localization (top panel), while PMA-GFP-UB signals are found in vesicles and the vacuolar lumen (middle and bottom panels, respectively). Photographs are merged with differential interference contrast pictures of the corresponding cell.

(C) Localization of PMA-GFP and PMA-GFP-UB upon coexpression with *SKD1* and *VSP2.1* constructs. Cell culture–derived protoplasts expressing *PMA-GFP* alone (n = 33), *PMA-GFP-UB* (n = 128) alone or with *35Spro:HA-SKD1(WT)* (n = 21), *35Spro:HA-SKD1(EQ)* (n = 116), and *35Spro:VPS2.1-TagRFP* (n = 40) were analyzed by confocal microscopy. Relative number of cells showing each localization was scored. Light-gray bars, plasma membrane; dark-gray bars, vesicles; solid bars, vacuole lumen; and open bars, tonoplast.

(D) *VPS2.1-GFP*–overexpressing plants accumulate ubiquitinated proteins. Total extract of wild-type (Col-0) and *35Spro*:*VPS2.1-GFP* seedlings were subjected to immunoblotting using anti-UB, anti-GFP, and anti-CDC2 antibodies. CDC2 was used as a loading control.

(E) *35Spro*:*VPS2.1-GFP* seedlings accumulate PIN2. Membrane protein extract from the roots of wild-type (Col-0), *35Spro*:*VPS2.1-GFP*, and *pin2* seedlings were subjected to immunoblotting using an anti-PIN2 antibody. A representative immunoblot is shown. Coomassie blue (CBB)–stained protein bands were used as a loading control. The asterisk indicates an unspecific band.

ATG8 is not a consequence of transcriptional misregulation of *ATG8* genes (see Supplemental Figure 4F online).

Next, we examined the protein level of NBR1 in *VPS2.1-GFP*–overexpressing plants. In contrast with *amsh1-1*, in which NBR1 accumulation was not observed, NBR1 accumulated at high levels in *35Spro*:*VPS2.1-GFP* plants (Figure 7D), while its transcript level remained unchanged (see Supplemental Figure 4E online). In contrast with ATG8, however, the amount of accumulated NBR1 remained unaltered after dark treatment, suggesting that NBR1-dependent selective autophagy is not dark induced. Treatment with E-64d did not enhance the accumulation of either NBR1 or ATG8 (Figure 7E), indicating that *35Spro*:*VPS2.1-GFP* is severely impaired in autophagic degradation. Since, in contrast with *amsh1-1*, *35Spro*:*VPS2.1-GFP* plants are incapable of dealing

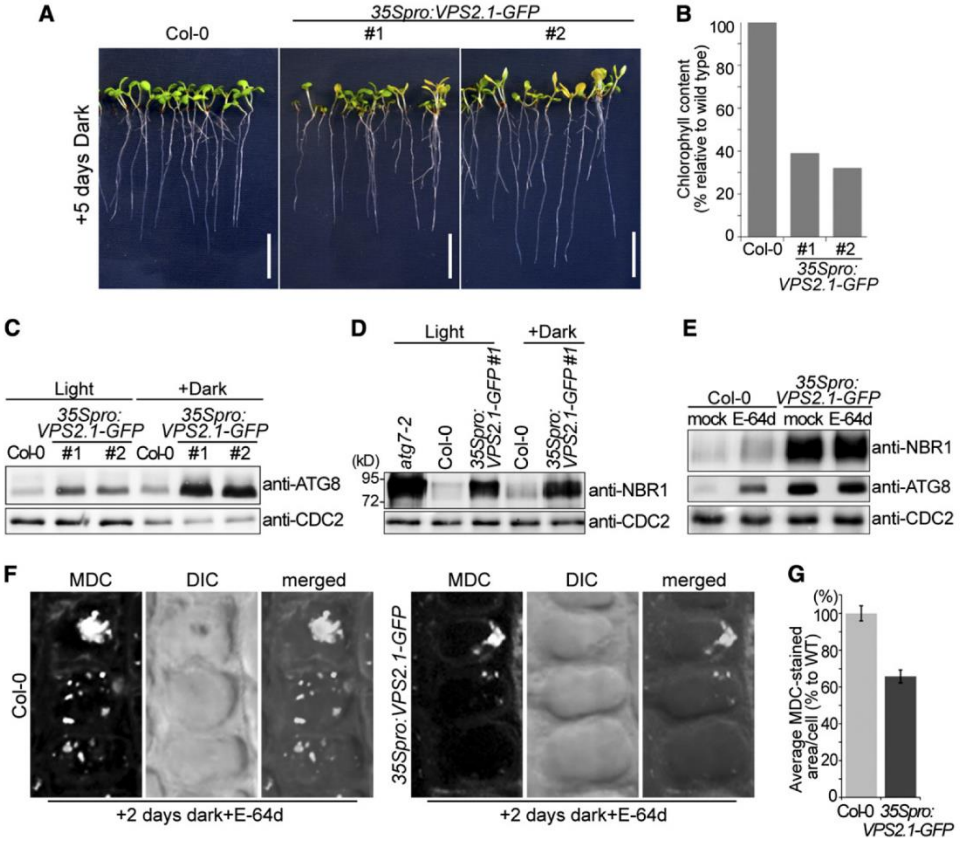

Figure 7. *VPS2.1-GFP*–Overexpressing Seedlings Have Defects in Both Nonselective and Selective Autophagy.

(A) *35Spro*:*VPS2.1-GFP* seedlings exhibit starvation-induced chlorosis after dark treatment. Long-day-grown wild-type (Col-0) and *35Spro*:*VPS2.1-GFP* seedlings were transferred to the dark for 5 d. Note that the *35Spro*:*VPS2.1-GFP* lines segregate for the transgene. Bars = 1 cm.

(B) Chlorophyll content of seedlings shown in **(A)**.

(C) *35Spro*:*VPS2.1-GFP* seedlings accumulate ATG8. Immunoblot using an anti-ATG8 antibody on total protein extract from wild-type (Col-0) and *35Spro*:*VPS2.1-GFP* seedlings grown under long-day conditions for 12 d (Light) or transferred to dark after 7 d for 5 d (Dark). CDC2 was used as loading control.

(D) NBR1 accumulates in *35Spro*:*VPS2.1-GFP* seedlings. Total protein extracts of *atg7-2*, the wild type (Col-0), and *35Spro*:*VPS2.1-GFP* grown as in **(C)** were analyzed by immunoblotting using an anti-NBR1 antibody. CDC2 was used as loading control.

(E) E-64d does not enhance the accumulation of NBR1 and ATG8 in *35Spro*:*VPS2.1-GFP*. Seedlings grown in the dark for 5 d were treated with E-64d for 6 h, and total extracts were submitted to immunoblotting with anti-NBR1 and anti-ATG8 antibodies. CDC2 was used as loading control. Note that E-64d enhances the accumulation of NBR1 and ATG8 only in the wild type (Col-0).

(F) Wild-type (Col-0) and *35Spro*:*VPS2.1-GFP* seedlings were grown for 7 d in long days and subsequently 2 d in the dark. Seedlings were then treated with E-64d for 1 h and stained with MDC. Confocal images (maximal projection) of MDC-stained root epidermal cells of the wild type (Col-0, left panel) and *35Spro*:*VPS2.1-GFP* (right panel) are shown. DIC, differential interference contrast.

(G) Quantification of MDC-stained area per cell in the wild type (WT; Col-0) and *35Spro*:*VPS2.1-GFP* (n = 547 for Col-0, and n = 376 for *35Spro*:*VPS2.1-GFP*). Photographs taken in **(F)** were analyzed by the FluoView software and the value of wild type was set to 100%. Error bars indicate SE.

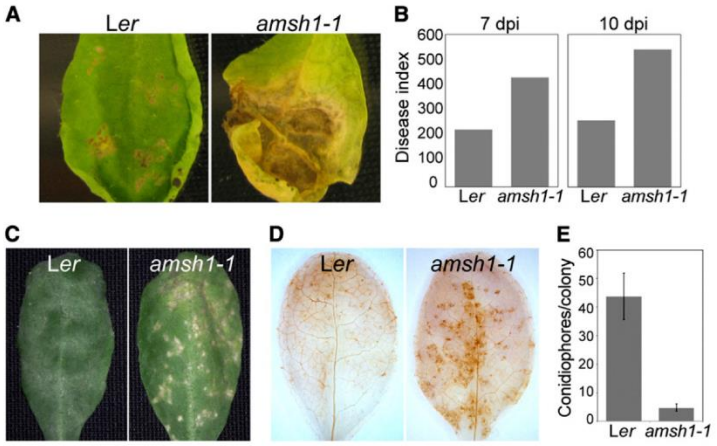

Figure 8. *amsh1-1* Displays Altered Susceptibility to Mildew Infection.

(A) Wild-type (L*er*) and *amsh1-1* plants were grown under short-day conditions (10 h light/14 h dark). Rosetta leaves of 5.5-week-old plants were drop-inoculated with 10^6 spores/mL *A. brassicicola*, and a representative leaf was photographed after 11 d of inoculation.
(B) Disease indices from experiments shown in **(A)** were calculated 7 d (7 dpi) and 10 d (10 dpi) after inoculation with *A. brassicicola* spores.
(C) Disease symptoms of wild-type (L*er*) and *amsh1-1* plants upon infection with *E. cruciferarum* spores. Plants were grown as in **(A)**, and 6-week-old plants were inoculated with *E. cruciferarum* spores. A representative leaf was photographed 7 d after inoculation.
(D) *amsh1-1* plants accumulate hydrogen peroxide. Leaves of wild-type (L*er*) and *amsh1-1* plants 2 d after infection with *E. cruciferarum* spores were stained with DAB for hydrogen peroxide accumulation, which is indicated by brown stain.
(E) Quantification of conidiophores per spore. Leaves were stained with trypan blue 6 d after inoculation with *E. cruciferarum* spores, and the number of conidiophores per colony was counted. Error bars indicate SE.

with basal levels of bulk and selective autophagic degradation in the light, we can conclude that overexpression of *VPS2.1-GFP* has a much stronger inhibitory effect on autophagic degradation than does the knockdown of *AMSH1*.

A report on *Caenorhabditis elegans* ESCRT-III RNAi mutants suggests that the accumulation of autophagosomes in ESCRT-III mutants is a consequence of the activation of autophagy due to a protective mechanism (Djeddi et al., 2012). In *Arabidopsis*, activation of autophagy, for example, after dark treatment, was shown to be coupled with transcriptional upregulation of *ATG8* (Doelling et al., 2002; Thompson et al., 2005). Thus, the comparable transcript levels of *ATG8* isoforms in *amsh1-1* and *35Spro*:*VPS2.1-GFP* with their corresponding wild types imply that autophagic flux is not increased in these mutants.

To examine the behavior of autophagosomes in dark-treated *35Spro*:*VPS2.1-GFP*, we stained E-64d–treated seedlings with MDC. We reasoned that if VPS2.1 function is necessary for the autophagic degradation, cells should accumulate less MDC-stained autophagic bodies in the vacuoles of *35Spro*:*VPS2.1-GFP*. MDC-stained vacuolar aggregates were observed in *35Spro*:*VPS2.1-GFP*, indicating that autophagosomes formation is not inhibited (Figure 7F). Further quantification showed that the area of MDC-stained autophagic bodies per cell was smaller in *35Spro*:*VPS2.1-GFP* cells (65.8% of average MDC-stained area per cell compared with the wild type; $n = 547$ for the wild type and $n = 376$ for *35Spro*:*VPS2.1-GFP*) (Figure 7G), implying that *VPS2.1-GFP* overexpression and the partial loss of AMSH1 function lead to similar defects in autophagic degradation.

amsh1-1 Displays Altered Pathogen Susceptibility

Recent studies on *atg* mutants showed the involvement of autophagy in plant innate immunity and pathogen defense (Liu et al., 2005; Patel and Dinesh-Kumar, 2008; Hofius et al., 2009; Yoshimoto et al., 2009; Lai et al., 2011; Lenz et al., 2011; Wang

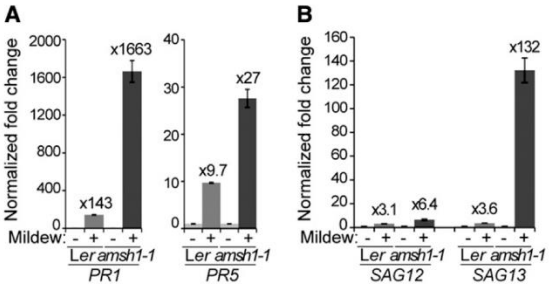

Figure 9. Transcript Levels of Pathogen- and Senescence-Related Genes Are Highly Upregulated in *amsh1-1* after Mildew Infection.

(A) and **(B)** Relative gene expression of pathogen-related genes *PR1* and *PR5* **(A)** and senescence-related genes *SAG12* and *SAG13* **(B)** in wild-type (L*er*) and *amsh1-1* plants uninfected or infected with *E. cruciferarum* spores. Total RNA was extracted from plants 2 d after infection. Expression levels were normalized to the reference gene *ACT8* and the expression levels in mock-treated L*er* and *amsh1-1* plants were set to 1 in each experiment. Error bars indicate SE.

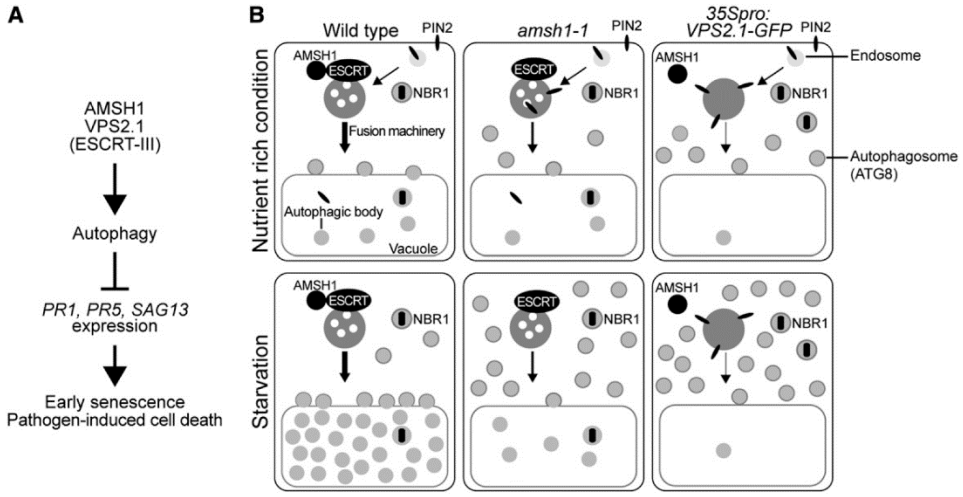

Figure 10. AMSH1 and ESCRT-III Are Important for Autophagy and Autophagy-Mediated Physiological Responses in Plants.

(A) AMSH1 and VPS2.1 functions are important for autophagic degradation. As previously reported, functional autophagy represses *PR* and *SAG* gene expression, induction of which causes early senescence and pathogen-induced cell death.

(B) *amsh1-1* and *35Spro*:*VPS2.1-GFP* are impaired in the degradation of autophagosomes to different extents. In wild-type cells, plasma membrane–localized PIN2 is endocytosed via the MVB pathway. The selective autophagy cargo receptor and substrate NBR1 is delivered to the vacuole via autophagosomes. Autophagosomes fuse with the vacuole in order to degrade its contents. Factors required for the recognition and fusion of autophagosomes with the vacuolar membrane as well as proteases responsible for the degradation of autophagic bodies may be transported via an MVB-dependent pathway. Upon carbon deprivation in the dark, autophagic recycling is highly upregulated. The weak *amsh1-1* knockdown mutant is still capable of endocytic and autophagic degradation under optimal growth condition. However, when bulk autophagy is highly activated upon dark-induced carbon starvation, *amsh1-1* accumulates ATG8 and shows less autophagic bodies in the vacuole, indicative for impaired autophagic degradation. When ESCRT-III function is disturbed by overexpressing *VPS2.1-GFP*, both endocytosis and autophagic recycling is strongly inhibited even under optimal growth conditions, leading to the accumulation of ATG8, NBR1, and PIN2. Accumulation of ATG8 increases when bulk autophagy is activated in the dark. Taken together, intact AMSH1 and ESCRT-III (VPS2.1) are essential for proper autophagic degradation.

et al., 2011). As *amsh1-1* and *35Spro*:*VPS2.1-GFP* showed impaired autophagic degradation, we hypothesized that these mutants may also exhibit altered pathogen response. Since *VPS2.1-GFP*–overexpressing plants were dwarf and had altered leaf size and morphology, we decided to conduct the pathogen assays only with *amsh1-1*. We used 5- to 6-week-old *amsh1-1* plants grown under 10-h-light/14-h-dark conditions because under this condition *amsh1-1* did not show early senescence (see Supplemental Figure 1E online).

Wild-type and *amsh1-1* plants were inoculated with the *Arabidopsis* pathogens *Alternaria brassicicola* or *Erysiphe cruciferarum*. *A. brassicicola* is a necrotrophic fungus that induces cell death upon infection. In comparison with the wild type, in which cell lesion was restricted to the inoculation spots, *amsh1-1* showed increased susceptibility, visible by the complete wilting and spreading necrosis along the entire leaf 10 to 11 d after infection (Figures 8A and 8B). Thus, similarly to previously characterized *atg* mutants, *amsh1-1* is also hypersensitive to *A. brassicicola* infection.

E. cruciferarum is an obligate biotroph that requires living cells for growth. In the wild type, *E. cruciferarum* infection did not cause visible cell lesions on leaves 5 d after infection (Figure 8C, left panel). However, at the same stage, *amsh1-1* showed spontaneous cell death on leaves (Figure 8C, right panel). This pathogen-induced cell death in *amsh1-1* was accompanied by an increased production of reactive oxygen species (Figure 8D). We also counted fewer conidiophores per spores on *amsh1-1* leaves when compared with the wild type (Figure 8E; see Supplemental Figures 5A to 5C online), indicating that *amsh1-1* is more resistant against *E. cruciferarum* as an indirect consequence of programmed cell death, which is triggered in the mutant.

Transcriptional Upregulation of Defense-Related Genes May Be Responsible for the Early Senescence of *amsh1-1* and 35Spro:VPS2.1-GFP

To further investigate the molecular mechanism underlying the *amsh1-1* pathogen response phenotype, we examined the expression of defense-related genes in wild-type and *amsh1-1* plants after infection with *E. cruciferarum*. Upon pathogen infection, basal immune responses, which are dependent on salicylic acid (SA), are upregulated and the expression of typical SA marker genes, such as *PATHOGENE-RELATED GENE1* (*PR1*) and *PR5* (Ward et al., 1991) as well as *SENESCENCE ASSOCIATED GENE12* (*SAG12*) and *SAG13* (Morris et al., 2000; Brodersen et al., 2002), is induced (reviewed in Wiermer et al., 2005).

Two days after infection with *E. cruciferarum* spores, a strong induction of *PR1*, *PR5*, *SAG12*, and *SAG13* was detected both in the wild type and in *amsh1-1* (Figures 9A and 9B). However, the induction of *PR1*, *PR5*, and *SAG13* was much stronger in *amsh1-1* (Figures 9A and 9B), suggesting that the SA signaling pathway is hyperactivated in *amsh1-1*. High *PR* gene transcript accumulation in association with programmed cell death may be the cause for the enhanced resistance phenotype toward *E. cruciferarum* while conferring enhanced susceptibility to a necrotrophic pathogen such as *A. brassicicola*.

We then tested the possibility that the early senescence phenotype of *amsh1-1* under short-day conditions (8 h light/16 h dark) is also a consequence of the upregulation of SA-induced genes. Indeed, a strong upregulation of *PR1*, *PR5*, and *SAG13* was observed in 8-week-old *amsh1-1*, specifically when grown under 8 h light/16 h dark, but not under 10 h light/14 h dark (see Supplemental Figures 6A and 6B online). This suggests a correlation of the photoperiod-dependent early senescence phenotype (see Supplemental Figure 1D online) with the hyperactivated SA signaling in *amsh1-1*. Similar transcriptional upregulation of *PR* genes and *SAG13* was also found in the *35Spro*:*VPS2.1-GFP* seedlings (see Supplemental Figure 6C online).

Altogether, these results suggest that AMSH1 and VPS2.1 are necessary for proper autophagy in plants and, thus, for physiological processes depending on an intact autophagy pathway (Figures 10A and 10B).

DISCUSSION

In this study, we showed that AMSH1, an AMSH3-related DUB, interacts with the endocytosis machinery through the ESCRT-III subunit VPS2.1. AMSH1 and AMSH3 possess an N-terminal MIT domain and a C-terminal MPN domain (Isono et al., 2010) but share only 47% overall amino acid identity, suggesting that the two proteins might have similar biochemical properties but also specific physiological functions. The fact that *AMSH1* and *AMSH3* are not products of a recent duplication event in *Arabidopsis*, that they show in part mutually exclusive expression patterns, and that in contrast with AMSH3, AMSH1 does not interact with VPS24.1 in Y2H interaction studies might further support this hypothesis.

Mutant analyses showed that AMSH1 and VPS2.1 are part of the autophagic degradation pathway and are important for plant survival in the dark, regulation of senescence, and pathogen defense. Phenotypes of *amsh1-1* and *35Spro*:*VPS2.1-GFP* include early senescence and chlorosis in the dark. At the molecular level, they both accumulate ubiquitinated proteins, and though to different degrees, both accumulate ATG8 and show defects in autophagosome delivery to the vacuole, indicating the involvement of AMSH1 and VPS2.1 in autophagic degradation. However, in contrast with *35Spro*:*VPS2.1-GFP*, *amsh1-1* does not show accumulation of PIN2. This might be due to the nature of the *amsh1-1* allele, which allows a residual amount of AMSH1 to still exist. It is a future challenge to investigate whether AMSH1 directly targets ubiquitinated MVB cargos or rather components of the trafficking machinery. Taken together, our results imply that an intact MVB pathway with its associated DUB AMSH1 is also essential for autophagy in plants and, hence, for autophagy-mediated physiological processes.

Although there is a strong indication that SA-dependent basal immunity and cell death are indirectly deregulated in *amsh1-1*, we cannot exclude the possibility that AMSH1 and also VPS2.1 may directly affect plant defense. Receptor-mediated endocytosis and exocytosis are known to play important roles in plant immune response, and many specific and general players involved in this pathway have been identified. For example, PENETRATION1 (PEN1)/SYNTAXIN OF PLANTS121 (SYP121) is a SNARE protein that contributes to the delivery of antimicrobial compounds to the infection site (Collins et al., 2003). PEN1 and multiple other components of the intracellular trafficking pathway, including VAMP72 proteins, GNOM, an ESCRT-I subunit VPS28, and MVBs, have been shown to relocate to pathogen infection sites (Assaad et al., 2004; An et al., 2006; Kwon et al., 2008; Lu et al., 2012; Nielsen et al., 2012).

In contrast with *syp122*, *syp42/syp43*, which is defective in *trans*-Golgi dependent intracellular trafficking, shows increased susceptibility to the obligate biotroph *Golovinomyces orontii* (Zhang et al., 2007; Uemura et al., 2012). Similarly, ESCRT-I mutants are also more susceptible to infection with the obligate biotrophic oomycete *Hyaloperonospora arabidopsidis* (Lu et al., 2012), in contrast with *amsh1-1*, which is more resistant to the obligate biotroph *E. cruciferarum.* These apparently conflicting results might reflect the complexity of regulatory mechanisms with a different outcome depending on the mutant-pathogen combination.

Dysfunction of AMSH1 and VPS2.1 may inhibit trafficking of autophagosomes to the vacuole. The process of heterotypic membrane fusion by which autophagosome membranes are combined with other membranes is not yet well understood. One group of proteins important for proper and efficient fusion between membranes is the SNAREs, which reside on membranes and form heteromeric complexes. A recent article reported the identification of human Syntaxin 7 as an autophagosomal SNARE, essential for autophagosome fusion to endosomes and lysosomes (Itakura et al., 2012). Similar fusion mechanisms involving SNAREs might also take place in plants. A family of Rab GTPases, Ypt7p/Rab7/RAB7, was also shown to affect fusion of autophagosomes with endosomes and vacuoles in yeast (Balderhaar et al., 2010), human cell culture (Gutierrez et al., 2004; Jäger et al., 2004), and plants (Kwon et al., 2010). In *amsh1-1* and *VPS2.1-GFP*–overexpressing plants, proteins required for docking and/or fusion between autophagosomes and the target membrane might be mistargeted or reduced, leading to fusion defects. Alternatively, the ESCRT machinery and AMSH1 may be directly involved in the heterotypic fusion event. Future experiments are needed to identify and reveal the identity of the factors involved in this process and elucidate the molecular mechanism of their regulation.

METHODS

Biological Material

All experiments were performed with *Arabidopsis thaliana* (Columbia-0 [Col-0] or Landsberg *erecta* [L*er*] background). T-DNA insertion lines of *AMSH1*, designated *amsh1-1* (CSHL_ET8678; L*er* ecotype) and *AMSH2* (CSHL_ET4018; L*er* ecotype) were obtained from the Martienssen Lab (Cold Spring Harbor Laboratory). The T-DNA insertion site of *amsh1-1* was identified using the specific T-DNA primer DS3.1 in combination with

the gene-specific AMSH1 reverse primer and the wild type with the combination of AMSH1 forward and AMSH1 reverse primers. T-DNA insertion mutants *atg7-2* (Hofius et al., 2009) and *pin2* (Willige et al., 2011) in the Col-0 background were described previously.

Plant transformations were performed using the floral dip method (Clough and Bent, 1998). Seedlings were grown in continuous light, long-day (16 h light and 8 h dark), or short-day (8 h light and 16 h dark or 10 h light and 14 h dark) conditions, as indicated for each experiment, at 110 to 120 μmol m^{-2} s^{-1} light intensity. Standard Murashige and Skoog (MS) growth medium (Duchefa Biochemie) supplemented with 1% Suc or half-strength MS (2.15 g/L MS and 2.3 mM MES, pH 5.7) was used to grow seedlings, and adult plants were grown in soil.

For exposure to artificial starvation or carbon deprivation, 7-d-old seedlings grown on half-strength MS or 3-week-old plants grown on soil under long-day (16 h daylight/8 h dark) conditions were transferred to the dark for 2 or 5 d as indicated for each experiment.

Cloning Procedures

All primers used for cloning and subcloning are listed in Supplemental Table 1 online. Detailed cloning procedures are described in Supplemental Methods 1 online.

Molecular Phylogeny

The nucleotide sequences from various species were identified in Phytozome (http://www.phytozome.net) according to their similarity to *Arabidopsis* AMSH genes, aligned with ClustalX (Thompson et al., 1997), and then improved manually. Phylogenetic analyses were performed by maximum likelihood with PAUP using the sequence from *Physcomitrella patens* (Pp1s133_43V6) as an outgroup. All characters were equally weighted, and gaps were treated as missing data. The nucleotide substitution model was set as GTR + I + G by MrModeltest 2.2 (Nylander, 2004), and a heuristic search was implemented with 100 random addition sequence replicates involving TBR branch swapping.

To estimate clade credibility, bootstrap values by maximum parsimony method, and posterior probabilities by Bayesian analysis were calculated. Bootstrap values were calculated from 1000 pseudo-replicates, each with 100 random additions. For posterior probabilities, the Bayesian search was conducted by MCMC with two independent sets of four chains, each run for 10 million generations, sampling every 100 generations by MrBayes 3.1.2 (Ronquist and Huelsenbeck, 2003). The nucleotide substitution model was set as GTR + I + G. The program Tracer (Tracer v1.4; available from http://beast.bio.ed.ac.uk/Tracer) was used to check the runs had reached stationarity and effective sample size of all the parameters was high (>100). The first 2.5 million generations before sufficient stationary generations were discarded as burn-in periods and the rest of trees were used to calculate posterior probabilities.

GUS Assay

Excised mature embryos from seeds as well as 7- and 14-d-old seedlings were treated with heptan (Roth) for 15 min. After removing heptan, the embryos and seedlings were incubated in GUS substrate solution (50 mM sodium phosphate, pH 7, 10 mM EDTA, 0.5 mM $K_4[Fe(CN)_6]$, 0.5 mM $K_3[Fe(CN)_6]$, 0.5 mM X-Gluc, and 0.02% Silvett) at 37°C. Tissues were cleared with an ethanol:acetic acid solution (6:1) at 37°C for 1 h and subsequently with a series of decreasing percentage of ethanol. Photographs were taken using a MZ16 (Leica) or BX61 (Olympus) microscope equipped with a charge-coupled device camera.

Chlorophyll Content Measurement

Twenty seedlings were weighed and immediately incubated in 1 mL *N*,*N*-dimethylformamide at 4°C under agitation in dark. After 48 h, the absorbance of the supernatant was measured at 664 and 647 nm. Subsequently, total chlorophyll content was determined according to total chlorophyll = [(OD664*7.04) + (OD647*20.27)]/fresh weight (Porra et al., 1998).

Quantitative RT-PCR

All primers used for quantitative RT-PCR are listed in Supplemental Table 2 online. Total RNA was extracted with a NucleoSpin RNA plant kit (Machery-Nagel), and 1 μg of total RNA was reverse transcribed with an oligo(dT) primer and M-MulV reverse transcriptase (Fermentas) following the manufacturer's instructions. Quantitative real-time PCR was performed using iQ SYBR Green Supermix (Bio-Rad) in a CFX96 real-time system cycler (Bio-Rad). A 45-cycle two-step amplification protocol (10 s at 95°C, 25 s at 60°C) was used for all measurements.

Protein Extraction, Immunoblotting, and Antibodies

Yeast total proteins were extracted as described previously (Kushnirov, 2000). SDS-PAGE and immunoblotting were performed according to standard methods.

Total protein extracts were prepared in extraction buffer (50 mM Tris-HCl, pH 7.5, 150 mM NaCl, 0.5% Triton X-100, and protease inhibitor cocktail [Roche]). For PIN2 immunoblot analysis, roots of 10-d-old seedlings were homogenized in extraction buffer. Extracts were centrifuged for 20 min at 9000*g*, and the supernatant was further centrifuged for 1 h at 100,000*g* in a Sorvall MTX 500 benchtop centrifuge (Thermo-Scientific), and the P100 fraction was subjected to immunoblotting.

An anti-AMSH1 antibody was raised against the full-length protein 6xHis-AMSH1 expressed and purified from *Escherichia coli* Rosetta(DE3) strain (Novagen). Six hundred micrograms of purified protein was used to raise antibodies in rabbits (Eurogentec). The serum was used at a 1:1000 dilution. The specificity of the antibody was verified using total extracts from *amsh1-1*.

Additional antibodies used were as follows: anti-AMSH3 (Isono et al., 2010), anti-ATG8 (Thompson et al., 2005), anti-GFP (Invitrogen), anti-CDC2 (Santa Cruz), anti-GAL4BD (Santa Cruz), anti-PIN2 (Agrisera), anti-NBR1 (Svenning et al., 2011), anti-UB(P4D1) (Santa Cruz), and horseradish peroxidase–conjugated anti-HA (Sigma-Aldrich).

In Vitro DUB Assay, Glutathione *S*-Transferase Pulldown, and Y2H Analysis

Glutathione *S*-transferase (GST), GST-VPS2.1(MIM), GST-AMSH1(MPN), and GST-AMSH1(MIT) were expressed in *E. coli* Rosetta(DE3) cells (Merck) and purified with Glutathione Sepharose 4B (GE Healthcare). After purification, the GST moiety of GST-AMSH1(MPN) and GST-AMSH1(MIT) was removed by digestion with PreScission Protease (GE Healthcare). DUB assays and GST pull-down assays were performed as described previously (Isono et al., 2010; Katsiarimpa et al., 2011). Y2H analysis was performed as described previously (Katsiarimpa et al., 2011).

MDC and BCECF-AM Staining and E-64d Treatment

Arabidopsis seedlings were stained with 50 μM MDC (Sigma-Aldrich) in PBS for 10 min at room temperature to visualize autophagosomes. Subsequently, the seedlings were washed twice with PBS to remove excess stain. To visualize the vacuole, seedlings were incubated with 5 μM BCECF-AM (Molecular Probes) for 1 h. To inhibit vacuolar proteases, seedlings were incubated with 100 μM E-64d (Santa Cruz) for 1, 6, or 12 h as indicated for each experiment.

Microscopy

GFP-fused proteins, BCECF staining and MDC staining were analyzed with an FV-1000/IX81 confocal laser scanning microscope (Olympus) with

a UPlanSApo ×60/1.20 (Olympus) objective using the 488- and 405-nm laser line, respectively. For maximal projection images of MDC-stained root cells, sequential Z-stack images were collected with 0.48-µm plane distance. Images were subsequently processed using FluoView (Olympus) and Photoshop CS6 (Adobe).

Pathogen Assays

For *Alternaria brassicicola* infection, 5.5-week-old plants grown under short-day conditions (10 h light/14 h dark) were drop inoculated with 10^6 spores/mL of *A. brassicicola*. Disease indices were calculated 7 and 10 d after inoculation according to Epple et al. (1997).

For the *Erysiphe cruciferarum* assay, 6-week-old plants grown under short-day conditions (10 h light/14 h dark) were inoculated with a density of 3 to 5 spores per mm^2. Susceptibility of plants to mildew was scored by visual examination after 5 and 7 d of inoculation. To quantify fungal growth, the number of hyphae and of conidiophores per spore was counted under the microscope 5 and 7 d after inoculation, respectively, after staining the leaves with trypan blue (Pelikan).

Accession Numbers

Sequence data from this article can be found in the Arabidopsis Genome Initiative database under the following accession numbers: *AMSH1* (AT1G48790), *AMSH2* (AT1G10600), *AMSH3* (AT4G16144), *CDC2* (AT3G48750), *SKD1* (AT2G27600), *VPS2*.1 (AT2G06530), *VPS20.1* (AT5G63880), *VPS24.1* (AT5G22950), *SNF7.1* (AT4G29160), *ATG8a* (AT4G21980), *ATG8b* (AT4G04620), *ATG8c* (AT1G62040), *ATG8d* (AT2G05630), *ATG8e* (AT2G45170), *ATG8f* (AT4G16520), *ATG8g* (AT3G60640), *ATG8h* (AT3G06420), *ATG8i* (AT3G15580), *PR1* (AT2G14610), *PR5* (AT1G75040), *SAG12* (AT5G45890), *SAG13* (AT2G29350), *ACT8* (AT1G49240), *PIN2* (AT5G57090), and *NBR1* (AT4G24690). Sequence accession numbers (Phytozome) for *AMSH* homologs are as follows: *P. patens* (Pp1s133_43V6, Pp1s240_78V6, and Pp1s64_214V6), *Selaginella moellendorffii* (Sm82317 and Sm128074), *Zea mays* (GRMZM2g075690, GRMZM5g835530, and GRMZM2g173119), *Sorghum bicolor* (Sb13g013600 and Sb3g020630), *Oryza sativa* (Os1g23640 and Os1g31470), *Populus trichocarpa* (0010s15100, 0015s03810, and 0010s05090), *Ricinus communis* (Rc29889m003259, Rc29996m000133, and Rc29631m001029), *Glycine max* (07g37130, 17g03490, 05g34700, 08g04970, 07g10350, 09g31540, and 01g03710), *Vitis vinifera* (GSVIVT01035040001, GSVIVT010083100001, and GSVIVT01013737001), and *Arabidopsis lyrata* (493270, 474017, and 919849).

Supplemental Data

The following materials are available in the online version of this article.

Supplemental Figure 1. *amsh1-1* Shows Early Senescence under 8-h Daylight Short-Day Conditions.

Supplemental Figure 2. Autophagosomes Accumulate in Wild-Type Plants after Dark Treatment.

Supplemental Figure 3. Expression of Y2H Constructs.

Supplemental Figure 4. Phenotypes of *VPS2.1-GFP*–Overexpressing Plants.

Supplemental Figure 5. *E. cruciferarum* Growth Is Restricted in *amsh1-1* Plants.

Supplemental Figure 6. *PR1*, *PR5*, and *SAG13* Are Upregulated in *35Spro*:*VPS2.1-GFP* Plants under 8-h Daylight Conditions in *amsh1-1* Plants.

Supplemental Table 1. List of Primers Used for Cloning.

Supplemental Table 2. List of Primers Used for qRT-PCR.

Supplemental Data Set 1. Nucleotide Sequence Alignment of *Arabidopsis AMSH1*, *AMSH2*, and *AMSH3* with Their Counterparts from Other Plant Species.

Supplemental Methods 1. Cloning Procedure.

ACKNOWLEDGMENTS

We thank Richard Vierstra (University of Wisconsin–Madison) for the anti-ATG8 antibody, Swen Schellmann (University of Cologne) for the PMA-GFP and PMA-GFP-UB constructs, Diane Bassham (Iowa State University) for the GFP-ATG8e line, Niko Geldner (University of Lausanne) for the YFP-ARA7 (Wave2y) line, Tsuyoshi Nakagawa (Shimane University) for the pGWB vectors, and the Martienssen lab (Cold Spring Harbor Laboratory) and Nottingham Arabidopsis Stock Centre for providing seeds. We also thank Natsumaro Kutsuna (University of Tokyo), Melina Zourelidou and Björn Willige (Technische Universität München) for technical advice and Marie-Kristin Nagel (Technische Universität München) for critical reading of the article. This work was supported by the following grants from the Deutsche Forschungsgemeinschaft: SCHW 751/7-1 to C.S., BR 3875/1-1 to F.B., SFB924 (B08) to R.H., and IS 221/2-2 (SPP1365/2) to E.I.

AUTHOR CONTRIBUTIONS

A.K., K.K., C.S., F.B., R.H., and E.I. designed the experiments. A.K., K.K., F.A., C.W., M.O., C.T., F.B., and E.I. performed the experiments. A.K., K.K., C.T., F.B., R.H., and E.I. analyzed the experiments. E.I. wrote the article.

Received May 3, 2013; revised May 3, 2013; accepted June 10, 2013; published June 25, 2013.

REFERENCES

Abas, L., Benjamins, R., Malenica, N., Paciorek, T., Wiśniewska, J., Moulinier-Anzola, J.C., Sieberer, T., Friml, J., and Luschnig, C. (2006). Intracellular trafficking and proteolysis of the *Arabidopsis* auxin-efflux facilitator PIN2 are involved in root gravitropism. Nat. Cell Biol. **8:** 249–256. Erratum. Nat. Cell Biol. **8:** 424.

An, Q., Ehlers, K., Kogel, K.H., van Bel, A.J., and Hückelhoven, R. (2006). Multivesicular compartments proliferate in susceptible and resistant MLA12-barley leaves in response to infection by the biotrophic powdery mildew fungus. New Phytol. **172:** 563–576.

Assaad, F.F., Qiu, J.L., Youngs, H., Ehrhardt, D., Zimmerli, L., Kalde, M., Wanner, G., Peck, S.C., Edwards, H., Ramonell, K., Somerville, C.R., and Thordal-Christensen, H. (2004). The PEN1 syntaxin defines a novel cellular compartment upon fungal attack and is required for the timely assembly of papillae. Mol. Biol. Cell **15:** 5118–5129.

Babst, M., Sato, T.K., Banta, L.M., and Emr, S.D. (1997). Endosomal transport function in yeast requires a novel AAA-type ATPase, Vps4p. EMBO J. **16:** 1820–1831.

Balderhaar, H.J., Arlt, H., Ostrowicz, C., Bröcker, C., Sündermann, F., Brandt, R., Babst, M., and Ungermann, C. (2010). The Rab GTPase Ypt7 is linked to retromer-mediated receptor recycling and fusion at the yeast late endosome. J. Cell Sci. **123:** 4085–4094.

Barberon, M., Zelazny, E., Robert, S., Conéjéro, G., Curie, C., Friml, J., and Vert, G. (2011). Monoubiquitin-dependent endocytosis of the

iron-regulated transporter 1 (IRT1) transporter controls iron uptake in plants. Proc. Natl. Acad. Sci. USA **108:** E450–E458.

Brodersen, P., Petersen, M., Pike, H.M., Olszak, B., Skov, S., Odum, N., Jørgensen, L.B., Brown, R.E., and Mundy, J. (2002). Knockout of *Arabidopsis* accelerated-cell-death11 encoding a sphingosine transfer protein causes activation of programmed cell death and defense. Genes Dev. **16:** 490–502.

Chamovitz, D.A., Wei, N., Osterlund, M.T., von Arnim, A.G., Staub, J.M., Matsui, M., and Deng, X.W. (1996). The COP9 complex, a novel multisubunit nuclear regulator involved in light control of a plant developmental switch. Cell **86:** 115–121.

Chung, T., Phillips, A.R., and Vierstra, R.D. (2010). ATG8 lipidation and ATG8-mediated autophagy in *Arabidopsis* require ATG12 expressed from the differentially controlled ATG12A AND ATG12B loci. Plant J. **62:** 483–493.

Chung, T., Suttangkakul, A., and Vierstra, R.D. (2009). The ATG autophagic conjugation system in maize: ATG transcripts and abundance of the ATG8-lipid adduct are regulated by development and nutrient availability. Plant Physiol. **149:** 220–234.

Clough, S.J., and Bent, A.F. (1998). Floral dip: A simplified method for Agrobacterium-mediated transformation of *Arabidopsis thaliana*. Plant J. **16:** 735–743.

Collins, N.C., Thordal-Christensen, H., Lipka, V., Bau, S., Kombrink, E., Qiu, J.L., Hückelhoven, R., Stein, M., Freialdenhoven, A., Somerville, S.C., and Schulze-Lefert, P. (2003). SNARE-protein-mediated disease resistance at the plant cell wall. Nature **425:** 973–977.

Contento, A.L., Xiong, Y., and Bassham, D.C. (2005). Visualization of autophagy in *Arabidopsis* using the fluorescent dye monodansylcadaverine and a GFP-AtATG8e fusion protein. Plant J. **42:** 598–608.

Cope, G.A., Suh, G.S., Aravind, L., Schwarz, S.E., Zipursky, S.L., Koonin, E.V., and Deshaies, R.J. (2002). Role of predicted metalloprotease motif of Jab1/Csn5 in cleavage of Nedd8 from Cul1. Science **298:** 608–611.

Djeddi, A., Michelet, X., Culetto, E., Alberti, A., Barois, N., and Legouis, R. (2012). Induction of autophagy in ESCRT mutants is an adaptive response for cell survival in *C. elegans*. J. Cell Sci. **125:** 685–694.

Doelling, J.H., Walker, J.M., Friedman, E.M., Thompson, A.R., and Vierstra, R.D. (2002). The APG8/12-activating enzyme APG7 is required for proper nutrient recycling and senescence in *Arabidopsis thaliana*. J. Biol. Chem. **277:** 33105–33114.

Epple, P., Apel, K., and Bohlmann, H. (1997). Overexpression of an endogenous thionin enhances resistance of *Arabidopsis* against *Fusarium oxysporum*. Plant Cell **9:** 509–520.

Filimonenko, M., Stuffers, S., Raiborg, C., Yamamoto, A., Malerød, L., Fisher, E.M., Isaacs, A., Brech, A., Stenmark, H., and Simonsen, A. (2007). Functional multivesicular bodies are required for autophagic clearance of protein aggregates associated with neurodegenerative disease. J. Cell Biol. **179:** 485–500.

Geldner, N., Dénervaud-Tendon, V., Hyman, D.L., Mayer, U., Stierhof, Y.-D., and Chory, J. (2009). Rapid, combinatorial analysis of membrane compartments in intact plants with a multicolor marker set. Plant J. **59:** 169–178.

Glickman, M.H., Rubin, D.M., Coux, O., Wefes, I., Pfeifer, G., Cjeka, Z., Baumeister, W., Fried, V.A., and Finley, D. (1998). A subcomplex of the proteasome regulatory particle required for ubiquitin-conjugate degradation and related to the COP9-signalosome and eIF3. Cell **94:** 615–623.

Göhre, V., Spallek, T., Häweker, H., Mersmann, S., Mentzel, T., Boller, T., de Torres, M., Mansfield, J.W., and Robatzek, S. (2008). Plant pattern-recognition receptor FLS2 is directed for degradation by the bacterial ubiquitin ligase AvrPtoB. Curr. Biol. **18:** 1824–1832.

Gutierrez, M.G., Munafó, D.B., Berón, W., and Colombo, M.I. (2004). Rab7 is required for the normal progression of the autophagic pathway in mammalian cells. J. Cell Sci. **117:** 2687–2697.

Han, J.H., Ryu, H.H., Jun, M.H., Jang, D.J., and Lee, J.A. (2012). The functional analysis of the CHMP2B missense mutation associated with neurodegenerative diseases in the endo-lysosomal pathway. Biochem. Biophys. Res. Commun. **421:** 544–549.

Herberth, S., Shahriari, M., Bruderek, M., Hessner, F., Müller, B., Hülskamp, M., and Schellmann, S. (2012). Artificial ubiquitylation is sufficient for sorting of a plasma membrane ATPase to the vacuolar lumen of *Arabidopsis* cells. Planta **236:** 63–77.

Hofius, D., Schultz-Larsen, T., Joensen, J., Tsitsigiannis, D.I., Petersen, N.H., Mattsson, O., Jørgensen, L.B., Jones, J.D., Mundy, J., and Petersen, M. (2009). Autophagic components contribute to hypersensitive cell death in *Arabidopsis*. Cell **137:** 773–783.

Howard, T.L., Stauffer, D.R., Degnin, C.R., and Hollenberg, S.M. (2001). CHMP1 functions as a member of a newly defined family of vesicle trafficking proteins. J. Cell Sci. **114:** 2395–2404.

Inoue, Y., Suzuki, T., Hattori, M., Yoshimoto, K., Ohsumi, Y., and Moriyasu, Y. (2006). AtATG genes, homologs of yeast autophagy genes, are involved in constitutive autophagy in *Arabidopsis* root tip cells. Plant Cell Physiol. **47:** 1641–1652.

Ishii, N., Owada, Y., Yamada, M., Miura, S., Murata, K., Asao, H., Kondo, H., and Sugamura, K. (2001). Loss of neurons in the hippocampus and cerebral cortex of AMSH-deficient mice. Mol. Cell. Biol. **21:** 8626–8637.

Isono, E., Katsiarimpa, A., Müller, I.K., Anzenberger, F., Stierhof, Y.D., Geldner, N., Chory, J., and Schwechheimer, C. (2010). The deubiquitinating enzyme AMSH3 is required for intracellular trafficking and vacuole biogenesis in *Arabidopsis thaliana*. Plant Cell **22:** 1826–1837.

Itakura, E., Kishi-Itakura, C., and Mizushima, N. (2012). The hairpin-type tail-anchored SNARE syntaxin 17 targets to autophagosomes for fusion with endosomes/lysosomes. Cell **151:** 1256–1269.

Jäger, S., Bucci, C., Tanida, I., Ueno, T., Kominami, E., Saftig, P., and Eskelinen, E.L. (2004). Role for Rab7 in maturation of late autophagic vacuoles. J. Cell Sci. **117:** 4837–4848.

Kasai, K., Takano, J., Miwa, K., Toyoda, A., and Fujiwara, T. (2011). High boron-induced ubiquitination regulates vacuolar sorting of the BOR1 borate transporter in *Arabidopsis thaliana*. J. Biol. Chem. **286:** 6175–6183.

Katsiarimpa, A., Anzenberger, F., Schlager, N., Neubert, S., Hauser, M.T., Schwechheimer, C., and Isono, E. (2011). The *Arabidopsis* deubiquitinating enzyme AMSH3 interacts with ESCRT-III subunits and regulates their localization. Plant Cell **23:** 3026–3040.

Klionsky, D.J., and Ohsumi, Y. (1999). Vacuolar import of proteins and organelles from the cytoplasm. Annu. Rev. Cell Dev. Biol. **15:** 1–32.

Komander, D., Clague, M.J., and Urbé, S. (2009). Breaking the chains: Structure and function of the deubiquitinases. Nat. Rev. Mol. Cell Biol. **10:** 550–563.

Kushnirov, V.V. (2000). Rapid and reliable protein extraction from yeast. Yeast **16:** 857–860.

Kwon, C., et al. (2008). Co-option of a default secretory pathway for plant immune responses. Nature **451:** 835–840.

Kwon, S.I., Cho, H.J., Jung, J.H., Yoshimoto, K., Shirasu, K., and Park, O.K. (2010). The Rab GTPase RabG3b functions in autophagy and contributes to tracheary element differentiation in *Arabidopsis*. Plant J. **64:** 151–164.

Lai, Z., Wang, F., Zheng, Z., Fan, B., and Chen, Z. (2011). A critical role of autophagy in plant resistance to necrotrophic fungal pathogens. Plant J. **66:** 953–968.

Lee, H.K., Cho, S.K., Son, O., Xu, Z., Hwang, I., and Kim, W.T. (2009). Drought stress-induced Rma1H1, a RING membrane-anchor

E3 ubiquitin ligase homolog, regulates aquaporin levels via ubiquitination in transgenic *Arabidopsis* plants. Plant Cell **21:** 622–641.

Lee, J.A., Beigneux, A., Ahmad, S.T., Young, S.G., and Gao, F.B. (2007). ESCRT-III dysfunction causes autophagosome accumulation and neurodegeneration. Curr. Biol. **17:** 1561–1567.

Lenz, H.D., et al. (2011). Autophagy differentially controls plant basal immunity to biotrophic and necrotrophic pathogens. Plant J. **66:** 818–830.

Liu, Y., Schiff, M., Czymmek, K., Tallóczy, Z., Levine, B., and Dinesh-Kumar, S.P. (2005). Autophagy regulates programmed cell death during the plant innate immune response. Cell **121:** 567–577.

Lu, Y.J., Schornack, S., Spallek, T., Geldner, N., Chory, J., Schellmann, S., Schumacher, K., Kamoun, S., and Robatzek, S. (2012). Patterns of plant subcellular responses to successful oomycete infections reveal differences in host cell reprogramming and endocytic trafficking. Cell. Microbiol. **14:** 682–697.

Maytal-Kivity, V., Reis, N., Hofmann, K., and Glickman, M.H. (2002). MPN+, a putative catalytic motif found in a subset of MPN domain proteins from eukaryotes and prokaryotes, is critical for Rpn11 function. BMC Biochem. **3:** 28.

McCullough, J., Clague, M.J., and Urbé, S. (2004). AMSH is an endosome-associated ubiquitin isopeptidase. J. Cell Biol. **166:** 487–492.

Mizushima, N., and Levine, B. (2010). Autophagy in mammalian development and differentiation. Nat. Cell Biol. **12:** 823–830.

Morris, K., MacKerness, S.A., Page, T., John, C.F., Murphy, A.M., Carr, J.P., and Buchanan-Wollaston, V. (2000). Salicylic acid has a role in regulating gene expression during leaf senescence. Plant J. **23:** 677–685.

Nielsen, M.E., Feechan, A., Böhlenius, H., Ueda, T., and Thordal-Christensen, H. (2012). *Arabidopsis* ARF-GTP exchange factor, GNOM, mediates transport required for innate immunity and focal accumulation of syntaxin PEN1. Proc. Natl. Acad. Sci. USA **109:** 11443–11448.

Nylander, J.A. (2004). MrModeltest 2.0. (Uppsala, Sweden: Uppsala University).

Patel, S., and Dinesh-Kumar, S.P. (2008). *Arabidopsis* ATG6 is required to limit the pathogen-associated cell death response. Autophagy **4:** 20–27.

Phillips, A.R., Suttangkakul, A., and Vierstra, R.D. (2008). The ATG12-conjugating enzyme ATG10 Is essential for autophagic vesicle formation in *Arabidopsis thaliana*. Genetics **178:** 1339–1353.

Porra, R.J., Urzinger, M., Winkler, J., Bubenzer, C., and Scheer, H. (1998). Biosynthesis of the 3-acetyl and 13(1)-oxo groups of bacteriochlorophyll a in the facultative aerobic bacterium, *Rhodovulum sulfidophilum*—The presence of both oxygenase and hydratase pathways for isocyclic ring formation. Eur. J. Biochem. **257:** 185–191.

Richardson, L.G., Howard, A.S., Khuu, N., Gidda, S.K., McCartney, A., Morphy, B.J., and Mullen, R.T. (2011). Protein-protein interaction network and subcellular localization of the *Arabidopsis thaliana* ESCRT machinery. Front. Plant Sci. **2:** 20.

Rojo, E., Gillmor, C.S., Kovaleva, V., Somerville, C.R., and Raikhel, N.V. (2001). VACUOLELESS1 is an essential gene required for vacuole formation and morphogenesis in *Arabidopsis*. Dev. Cell **1:** 303–310.

Ronquist, F., and Huelsenbeck, J.P. (2003). MrBayes 3: Bayesian phylogenetic inference under mixed models. Bioinformatics **19:** 1572–1574.

Rusten, T.E., Vaccari, T., Lindmo, K., Rodahl, L.M., Nezis, I.P., Sem-Jacobsen, C., Wendler, F., Vincent, J.P., Brech, A., Bilder, D., and Stenmark, H. (2007). ESCRTs and Fab1 regulate distinct steps of autophagy. Curr. Biol. **17:** 1817–1825.

Shahriari, M., Richter, K., Keshavaiah, C., Sabovljevic, A., Huelskamp, M., and Schellmann, S. (2011). The *Arabidopsis* ESCRT protein-protein interaction network. Plant Mol. Biol. **76:** 85–96.

Sláviková, S., Shy, G., Yao, Y., Glozman, R., Levanony, H., Pietrokovski, S., Elazar, Z., and Galili, G. (2005). The autophagy-associated Atg8 gene family operates both under favourable growth conditions and under starvation stresses in *Arabidopsis* plants. J. Exp. Bot. **56:** 2839–2849.

Spitzer, C., Reyes, F.C., Buono, R., Sliwinski, M.K., Haas, T.J., and Otegui, M.S. (2009). The ESCRT-related CHMP1A and B proteins mediate multivesicular body sorting of auxin carriers in *Arabidopsis* and are required for plant development. Plant Cell **21:** 749–766.

Surpin, M., Zheng, H., Morita, M.T., Saito, C., Avila, E., Blakeslee, J.J., Bandyopadhyay, A., Kovaleva, V., Carter, D., Murphy, A., Tasaka, M., and Raikhel, N. (2003). The VTI family of SNARE proteins is necessary for plant viability and mediates different protein transport pathways. Plant Cell **15:** 2885–2899.

Svenning, S., Lamark, T., Krause, K., and Johansen, T. (2011). Plant NBR1 is a selective autophagy substrate and a functional hybrid of the mammalian autophagic adapters NBR1 and p62/SQSTM1. Autophagy **7:** 993–1010.

Swaminathan, S., Amerik, A.Y., and Hochstrasser, M. (1999). The Doa4 deubiquitinating enzyme is required for ubiquitin homeostasis in yeast. Mol. Biol. Cell **10:** 2583–2594.

Tanaka, N., Kaneko, K., Asao, H., Kasai, H., Endo, Y., Fujita, T., Takeshita, T., and Sugamura, K. (1999). Possible involvement of a novel STAM-associated molecule "AMSH" in intracellular signal transduction mediated by cytokines. J. Biol. Chem. **274:** 19129–19135.

Teis, D., Saksena, S., and Emr, S.D. (2008). Ordered assembly of the ESCRT-III complex on endosomes is required to sequester cargo during MVB formation. Dev. Cell **15:** 578–589.

Teis, D., Saksena, S., Judson, B.L., and Emr, S.D. (2010). ESCRT-II coordinates the assembly of ESCRT-III filaments for cargo sorting and multivesicular body vesicle formation. EMBO J. **29:** 871–883.

Thompson, A.R., Doelling, J.H., Suttangkakul, A., and Vierstra, R.D. (2005). Autophagic nutrient recycling in *Arabidopsis* directed by the ATG8 and ATG12 conjugation pathways. Plant Physiol. **138:** 2097–2110.

Thompson, J.D., Gibson, T.J., Plewniak, F., Jeanmougin, F., and Higgins, D.G. (1997). The CLUSTAL_X windows interface: Flexible strategies for multiple sequence alignment aided by quality analysis tools. Nucleic Acids Res. **25:** 4876–4882.

Uemura, T., Kim, H., Saito, C., Ebine, K., Ueda, T., Schulze-Lefert, P., and Nakano, A. (2012). Qa-SNAREs localized to the trans-Golgi network regulate multiple transport pathways and extracellular disease resistance in plants. Proc. Natl. Acad. Sci. USA **109:** 1784–1789.

Verma, R., Aravind, L., Oania, R., McDonald, W.H., Yates, J.R., III., Koonin, E.V., and Deshaies, R.J. (2002). Role of Rpn11 metalloprotease in deubiquitination and degradation by the 26S proteasome. Science **298:** 611–615.

Vierstra, R.D. (2009). The ubiquitin-26S proteasome system at the nexus of plant biology. Nat. Rev. Mol. Cell Biol. **10:** 385–397.

Wang, Y., Nishimura, M.T., Zhao, T., and Tang, D. (2011). ATG2, an autophagy-related protein, negatively affects powdery mildew resistance and mildew-induced cell death in *Arabidopsis*. Plant J. **68:** 74–87.

Ward, E.R., Uknes, S.J., Williams, S.C., Dincher, S.S., Wiederhold, D.L., Alexander, D.C., Ahl-Goy, P., Metraux, J.P., and Ryals, J.A. (1991). Coordinate gene activity in response to agents that induce systemic acquired resistance. Plant Cell **3:** 1085–1094.

Wiermer, M., Feys, B.J., and Parker, J.E. (2005). Plant immunity: The EDS1 regulatory node. Curr. Opin. Plant Biol. **8:** 383–389.

Willige, B.C., Isono, E., Richter, R., Zourelidou, M., and Schwechheimer, C. (2011). Gibberellin regulates PIN-FORMED abundance and is required for auxin transport-dependent growth and development in *Arabidopsis thaliana*. Plant Cell **23:** 2184–2195.

Winter, V., and Hauser, M.T. (2006). Exploring the ESCRTing machinery in eukaryotes. Trends Plant Sci. **11:** 115–123.

Xiong, Y., Contento, A.L., and Bassham, D.C. (2005). AtATG18a is required for the formation of autophagosomes during nutrient stress and senescence in *Arabidopsis thaliana*. Plant J. **42:** 535–546.

Yoshimoto, K., Hanaoka, H., Sato, S., Kato, T., Tabata, S., Noda, T., and Ohsumi, Y. (2004). Processing of ATG8s, ubiquitin-like proteins, and their deconjugation by ATG4s are essential for plant autophagy. Plant Cell **16:** 2967–2983.

Yoshimoto, K., Jikumaru, Y., Kamiya, Y., Kusano, M., Consonni, C., Panstruga, R., Ohsumi, Y., and Shirasu, K. (2009). Autophagy negatively regulates cell death by controlling NPR1-dependent salicylic acid signaling during senescence and the innate immune response in *Arabidopsis*. Plant Cell **21:** 2914–2927.

Zelazny, E., Barberon, M., Curie, C., and Vert, G. (2011). Ubiquitination of transporters at the forefront of plant nutrition. Plant Signal. Behav. **6:** 1597–1599.

Zhang, Z., Feechan, A., Pedersen, C., Newman, M.A., Qiu, J.L., Olesen, K.L., and Thordal-Christensen, H. (2007). A SNARE-protein has opposing functions in penetration resistance and defence signalling pathways. Plant J. **49:** 302–312.

Zouhar, J., Rojo, E., and Bassham, D.C. (2009). AtVPS45 is a positive regulator of the SYP41/SYP61/VTI12 SNARE complex involved in trafficking of vacuolar cargo. Plant Physiol. **149:** 1668–1678.